



**HAL**  
open science

# Reliability analysis of a reinforced concrete deck slab supported on steel girders

David Ferrand

► **To cite this version:**

David Ferrand. Reliability analysis of a reinforced concrete deck slab supported on steel girders. Materials. University of Michigan, 2005. English. NNT: . tel-00474728

**HAL Id: tel-00474728**

**<https://theses.hal.science/tel-00474728>**

Submitted on 5 May 2010

**HAL** is a multi-disciplinary open access archive for the deposit and dissemination of scientific research documents, whether they are published or not. The documents may come from teaching and research institutions in France or abroad, or from public or private research centers.

L'archive ouverte pluridisciplinaire **HAL**, est destinée au dépôt et à la diffusion de documents scientifiques de niveau recherche, publiés ou non, émanant des établissements d'enseignement et de recherche français ou étrangers, des laboratoires publics ou privés.

**RELIABILITY ANALYSIS OF A REINFORCED CONCRETE DECK SLAB SUPPORTED  
ON STEEL GIRDERS**

**by**

**David Ferrand**

A dissertation submitted in partial fulfillment  
of the requirements for the degree of  
Doctor of Philosophy  
(Civil Engineering)  
in The University of Michigan

date of defence: April 15th, 2005

Doctoral Committee:

Professor Andrzej S. Nowak, Co-chair  
Assistant Research Scientist Maria M. Szerszen, Co-chair  
Professor Jwo Pan Assistant  
Professor Gustavo J. Parra-Montesinos

© David Ferrand 2005  
All Rights Reserved

## **ACKNOWLEDGMENTS**

I wish to express my gratitude to Professor Andrzej S. Nowak and Doctor Maria M. Szerszen, co-chairs of my doctoral committee, for their instructions, continuous guidance, and kindness throughout this study. I would also like to express my special thanks to Professors Gustavo J. Parra-Montesinos, and Jwo Pan, members of the doctoral committee, for their helpful suggestions and valuable advice on this dissertation.

I would like to acknowledge the help and friendship of my fellow colleagues and friends throughout the various phase of this study. Special thanks to my wife Kulsiri for her understanding, continuous help, and encouragement. I would also like to thank the Civil Engineering Department administrative staff for their help in administrative matters as well as the technicians for their technical support.

Finally, I would like to express my sincere gratitude and appreciation to my parents, and my sisters for their love, continuous support, and encouragement in every step of my life.

## TABLE OF CONTENTS

<b>ACKNOWLEDGMENTS .....</b>	<b>ii</b>
<b>LIST OF TABLES .....</b>	<b>vii</b>
<b>LIST OF FIGURES .....</b>	<b>ix</b>
<b>LIST OF APPENDICES .....</b>	<b>xix</b>
<b>CHAPTER</b>	
<b>1. INTRODUCTION.....</b>	<b>1</b>
1.1. Problem Statement.....	1
1.2. Objectives and Scope of this Dissertation .....	3
1.3. Structure of the Dissertation .....	5
<b>2. LITERATURE REVIEW .....</b>	<b>10</b>
2.1. Behavior and Performance of Deck Slab.....	10
2.1.1. Historical Review.....	10
2.1.2. Behavior of Deck Slabs and Their Serviceability.....	12
2.2. Design and Analysis of Bridge Deck.....	15
2.3. Reliability of Bridge Structure.....	18
<b>3. FIELD TESTING PROCEDURE .....</b>	<b>22</b>
3.1. Introduction.....	22
3.2. Description of the Selected Bridge Structure.....	22
3.3. Instrumentation and Data Acquisition .....	23
3.3.1. Strain Measurement .....	24
3.3.2. Data Acquisition System.....	24
3.4. Live Load for Field Testing .....	26

<b>4. ANALYTICAL MODEL FOR BRIDGE STRUCTURES .....</b>	<b>35</b>
4.1. General.....	35
4.2. Introduction to ABAQUS .....	36
4.3. Description of Available Elements .....	36
4.4. Finite Element Analysis Methods for Bridges.....	39
4.5. Material Models.....	39
4.5.1. Material Model for Concrete .....	41
4.5.2. Modeling of Reinforcement in FEM.....	45
4.5.3. Material Model for Steel.....	46
4.6. Solution Methods.....	47
4.6.1. The Newton-Raphson Method.....	48
4.6.2. Steps, Increments and Iterations .....	49
4.6.3. Convergence and Increments .....	49
4.7. Material Model Verification .....	51
4.7.1. Example 1: One Way Reinforced Concrete Slab.....	51
4.7.2. Two Way Reinforced Concrete Slab .....	54
4.7.3. Composite Bridge .....	55
4.8. Parameters Influencing Bridge Analysis .....	57
4.8.1. Boundary Conditions .....	57
4.8.2. Composite Action .....	58
4.8.3. Effect of Non Structural Members.....	59
4.9. Calibration of the finite Element Models.....	60
<b>5. STRUCTURAL RELIABILITY .....</b>	<b>101</b>
5.1. Introduction.....	101
5.2. Fundamental Concepts.....	101
5.3. Reliability Analysis Method .....	103
5.3.1. Limit State.....	103
5.3.2. Reliability Index.....	105
5.3.3. First Order Second Moment Methods (FOSM) .....	106
5.3.4. Hasofer-Lind Reliability Index .....	109

5.3.5. Rackwitz-Fiessler Procedure .....	111
5.4. Simulation Techniques.....	113
5.4.1. Monte Carlo Simulation.....	113
5.4.2. Rosenblueth's 2K + 1 Point Estimate Method.....	116
5.5. Bridge Load Model.....	118
5.5.1. Introduction.....	118
5.5.2. Dead Load.....	119
5.5.3. Live Load.....	119
5.5.4. Dynamic Live Load .....	121
5.6. Bridge Resistance Model.....	121
<b>6. RESULTS OF RELIABILITY ANALYSIS.....</b>	<b>129</b>
6.1. Considered Parameters and Configuration of the Studied Bridges .....	129
6.1.1. Empirical and Traditional Design Method for Bridge Decks.....	130
6.1.2. Girder Spacing .....	133
6.1.3. Span Length .....	133
6.1.4. Boundary Conditions .....	134
6.1.5. Live Load Position.....	135
6.2. Limit State Function .....	136
6.3. Load Model.....	137
6.4. Resistance Model.....	138
6.4.1. Parameters Used in Finite Element Model .....	138
6.4.2. Procedure to Obtain Resistance Parameters .....	139
6.5. Reliability Analysis Procedure and Results.....	141
6.5.1. Reliability Analysis Procedure .....	141
6.5.2. Results of the Reliability Analysis.....	142
<b>7. SUMMARY AND CONCLUSIONS.....</b>	<b>180</b>
7.1. Summary .....	180
7.2. Conclusions.....	183

7.2.1. General Conclusions .....	183
7.2.2. Conclusions for Cracking Limit State.....	184
7.2.3. Conclusions for Crack Opening Limit State.....	185
7.3. Suggestions for Future Research .....	186
<b>APPENDICES.....</b>	<b>188</b>
<b>BIBLIOGRAPHY .....</b>	<b>238</b>

## LIST OF TABLES

### Table

3.1. Sequence of test runs .....	28
5.1. Reliability index versus probability of failure.....	124
5.2. Statistical paramaters of dead load.....	124
5.3. Statistical parameters of resistance.....	124
6.1. Factored moments computed using the traditional method for the three different spacing.....	148
6.2. Summary of rebars quantity using the traditional method for the three different spacing.....	148
6.3. Summary of rebars quantity using the empirical method.....	149
6.4. Factored moments computed for the design of the bridges.....	149
6.5. Factored shear computed for the design of the bridges.....	149
6.6. Summary of the girder section used in this research.....	149
6.7. Summary of the different bridge configuration studied .....	150
6.8. Value of $f_{sa}$ for negative moment section.....	150
6.9. Value of $f_{sa}$ for positive moment section.....	150
6.10. Random variables parameters used in the 2K+1 point estimate method.....	151
6.11. Moment due to live load for different bridge configuration.....	151
6.12. Example of calculation of the reliability index for the empirical design, 60 FT span bridge, 10 FT girder spacing, negative moment (top of the slab) – cracking limit state. ....	152

6.13. Example of calculation of the reliability index for the empirical design, 60 FT span bridge, 10 FT girder spacing, negative moment (top of the slab) – crack opening limit state. ....	153
6.14. Summary of reliability indices for all configurations investigated - cracking .	154
6.15. Summary of reliability indices for all configurations investigated – crack opening .....	155
A.1. Unfactored moments and shears for an interior girder .....	209
A.2. Unfactored moments and shears for an exterior girder .....	209
A.3. Composite section properties .....	209

## LIST OF FIGURES

### Figure

1.1. Typical cross sections of a reinforced concrete deck slab supported by steel or prestressed concrete girders.....	7
1.2. Deck cross section showing typical bar placement .....	7
1.3. Examples of extensive cracking and potholes in concrete bridge deck .....	8
1.4. Flowchart of this research project .....	9
2.1. Grillage model .....	20
2.2. Actual composite girder and corresponding Finite Element used by Burns et al. ....	20
2.3. Typical section of the model by Tarhini and Frederic .....	21
3.1. Cross section of the tested steel girder bridge .....	29
3.2. Strain transducers location on the tested bridge .....	29
3.3. A typical strain transducer.....	30
3.4. Wheatstone full bridge circuit configuration.....	30
3.5. Removable Strain Transducer attached to the botttom flange.....	31
3.6. Strain transducer attached near support.....	31
3.7. Data acquisition system connected to the PC notebook computer.....	32
3.8. General data acquisition system .....	32
3.9. SCXI Data Acquisition System Setup.....	33
3.10. Three-unit 11-axle truck used in the field tests .....	34
3.11. Axle weight and axle spacing configuration .....	34

4.1. Commonly used element families .....	63
4.2. Linear and quadratic brick.....	63
4.3. Model detailing.....	64
4.4. Stress-strain response of concrete to uniaxial loading in tension.....	64
4.5. Stress-strain response of concrete to uniaxial loading in tension with ABAQUS .....	65
4.6. Illustration of the definition of the cracking strain $\varepsilon_t^{ck}$ used to describe the tension stiffening .....	65
4.7. Concrete tension stiffening defined as a function of cracking displacement .....	66
4.8. Concrete tension stiffening defined as a linear function of the cracking energy 66	
4.9. Tension stiffening model used in this study .....	67
4.10. Compressive stress-strain curve of concrete .....	67
4.11. Compressive stress-strain curve of concrete proposed by Honegstad.....	68
4.12. Definition of the compressive inelastic strain $\varepsilon_c^{in}$ .....	68
4.13. Mohr-Coulomb and Drucker-Prager yield surfaces in principal stress space ....	69
4.14. Yield surface in the deviatoric plane, corresponding to different value of $K_c$ .....	69
4.15. Yield surface in plane stress.....	70
4.16. Embedded rebars element.....	70
4.17. Stress-strain characteristics of reinforcement in uniaxial tension .....	71
4.18. Perfect plastic idealization of steel reinforcement.....	71
4.19. Von Mises yield surface in principal stress space .....	72
4.20. Nonlinear load-displacement curve.....	72
4.21. Graphic representation of the Newton-Raphson method .....	73
4.22. Internal and external loads on a body.....	73
4.23. First iteration in an increment.....	74

4.24. Second iteration in an increment .....	74
4.25. Configuration of the one way slab tested by Jain and Kennedy.....	75
4.26. General view of the one way slab FE Model .....	75
4.27. Modeling of the reinforcement in the one way slab FE Model.....	76
4.28. Compressive stress-strain curve of concrete used in the one way slab example	76
4.29. Comparison between experimental results and FE results of the one way example.....	77
4.30. View of the deformed shape of the FE model of the one way slab example .....	77
4.31. Configuration of the two way slab tested by McNeice .....	78
4.32. General view of the two way slab FE Model .....	79
4.33. Modeling of the reinforcement in the two way slab FE Model.....	80
4.34. Comparison between experimental results and FE results of the two way slab example at point “a” .....	80
4.35. Comparison between experimental results and FE results of the two way slab example at point “b” .....	81
4.36. Comparison between experimental results and FE results of the two way slab example at point “c” .....	81
4.37. Comparison between experimental results and FE results of the two way slab example at point “d” .....	82
4.38. View of the deformed shape of the FE model of the two way slab example .....	82
4.39. Cross section of the Newmark bridge .....	83
4.40. General view of the Mewmark bridge FE Model.....	83
4.41. Modeling of the reinforcement in the Newmark bridge FE Model – Top longitudinal reinforcement .....	84
4.42. Comparison between experimental results and FE results of the Newmark bridge at girder A.....	84
4.43. Comparison between experimental results and FE results of the Newmark bridge at girder B.....	85

4.44. Comparison between experimental results and FE results of the Newmark bridge at girder C .....	85
4.45. Comparison between experimental results and FE results of the Newmark bridge at girder D.....	86
4.46. Comparison between experimental results and FE results of the Newmark bridge at girder E .....	86
4.47. View of the deformed shape of the FE Model of the Newmark bridge .....	87
4.48. The three cases of boundary conditions used in the Finite Element Analysis: (a) Simply supported, hinge-roller; (b) Hinge at both end of the girder, (c) Partially fixed support.....	87
4.49. General view of the tested bridge FE Model.....	88
4.50. View of the girder and cross frame of the FE Model .....	88
4.51. View of the bottom longitudinal reinforcement in the FE Model .....	89
4.52. View of the bottom transversal reinforcement in the FE Model .....	89
4.53. View of the top longitudinal reinforcement in the FE Model .....	90
4.54. View of the top transversal reinforcement in the FE Model .....	90
4.55. Close view of the tire pressure applied on the deck .....	91
4.56. General view of the 11-axle truck applied on the FE Model .....	91
4.57. View of the spring used in the FE Model to simulate partial fixity .....	92
4.58. Comparison of test results with analytical results at third span – Truck in the center of north lane.....	92
4.59. Comparison of test results with analytical results near support – Truck in the center of north lane.....	93
4.60. Displaced shape of the bridge model – Truck in the center of north lane.....	93
4.61. Comparison of test results with analytical results at third span – Truck in the center of south lane.....	94
4.62. Comparison of test results with analytical results near support – Truck in the center of south lane.....	94
4.63. Displaced shape of the bridge model – Truck in the center of south lane.....	95

4.64. Comparison of test results with analytical results at third span – Truck close to the curb of north lane.....	95
4.65. Comparison of test results with analytical results near support – Truck close to the curb of north lane.....	96
4.66. Displaced shape of the bridge model – Truck close to curb of north lane .....	96
4.67. Comparison of test results with analytical results at third span – Truck close to the curb of south lane .....	97
4.68. Comparison of test results with analytical results near support – Truck close to the curb of south lane .....	97
4.69. Displaced shape of the bridge model – Truck close to the curb of south lane ...	98
4.70. Comparison of test results with analytical results at third span – Truck in the center of the bridge.....	98
4.71. Comparison of test results with analytical results near support – Truck in the center of the bridge.....	99
4.72. Displaced shape of the bridge model – Truck in the center of the bridge.....	99
4.73. Comparison of test results with analytical results at third span – Simulation of two trucks in the center of south and north lane.....	100
4.74. Comparison of test results with analytical results near support – Simulation of two trucks in the center of south and north lane.....	100
5.1. PDF $\phi(z)$ and CDF $\Phi(z)$ for a standard normal random variable.....	125
5.2. Probability Density Function of load, resistance, and safety margin.....	125
5.3. Reliability index as shortest distance to origin.....	126
5.4. Hasofer-Lind reliability index .....	126
5.5. HL-93 loading specified by AASHTO LRFD 1998 – Truck and uniform load .....	127
5.6. HL-93 loading specified by AASHTO LRFD 1998 – Tandem and uniform load .....	127
5.7. Gross vehicle weight (GVW) of trucks surveyed on I-94 over M-10 in the Greater Detroit area (Michigan).....	128

5.8. Axle weight (GVW) of trucks surveyed on I-94 over M-10 in the Greater Detroit area (Michigan) .....	128
6.1. (a) Idealized strip design, (b) transverse section under load, (c) rigid girder model, and (d) displacement due to girder translation. ....	156
6.2. Layout of the deck reinforcement for the three girders spacing according the traditional method.....	157
6.3. Layout of the deck reinforcement according the empirical method.....	158
6.4. View of the Empirical reinforcement modeled in the Finite Element Model ..	158
6.5. View of the Traditional reinforcement modeled in the Finite Element Model	159
6.6. View of the 60 FT span Finite Element Model with 6 FT girder spacing.....	159
6.7. View of the 60 FT span Finite Element Model with 8 FT girder spacing.....	160
6.8. View of the 60 FT span Finite Element Model with 10 FT girder spacing.....	160
6.9. View of the 120 FT span Finite Element Model with 10 FT girder spacing....	161
6.10. Boundary conditions used in the reliability analysis .....	161
6.11. Characteristics of the design truck .....	162
6.12. General view of the HS-20 load applied on the FE model.....	162
6.13. First investigated truck position – maximum negative moment .....	163
6.14. Detail of the first investigated position – longitudinal crack at the top of the deck .....	163
6.15. Second investigated truck position – maximum positive moment.....	164
6.16. Detail of the second investigated position – longitudinal crack at the bottom of the deck.....	164
6.17. Third investigated truck position – maximum positive moment at midspan ...	165
6.18. Detail of the third investigated position – longitudinal and transversal crack at the bottom of the deck .....	165
6.19. Histogram of number of axles for citation trucks.....	166
6.20. Histogram of Gross Vehicle Weight for citation trucks.....	166

6.21. Cumulative Distribution Function of axle load for a year, citation data .....	167
6.22. Tension stiffening used in the Finite Element Program .....	167
6.23. Compressive stress-strain of concrete implemented in the FEM .....	168
6.24. Tensile stress in concrete versus applied load .....	168
6.25. Tensile stress in reinforcement versus applied load .....	169
6.26. Comparison of reliability indices between the two design methods as a function of the girder spacing for the longitudinal cracking, negative moment at the support (top of the slab).....	169
6.27. Comparison of reliability indices between the two design methods as a function of the girder spacing for the longitudinal cracking, positive moment at the support (bottom of the slab) .....	170
6.28. Comparison of reliability indices between the two design methods as a function of the girder spacing for the longitudinal cracking, positive moment at midspan (bottom of the slab) .....	170
6.29. Comparison of reliability indices between the two design methods as a function of the span length for the longitudinal cracking, negative moment at the support (top of the slab).....	171
6.30. Comparison of reliability indices between the two design methods as a function of the span length for the longitudinal cracking, positive moment at the support (bottom of the slab) .....	171
6.31. Comparison of reliability indices between the two design methods as a function of the span length for the longitudinal cracking, positive moment at midspan (bottom of the slab) .....	172
6.32. Comparison of reliability indices between the two boundary conditions as a function of the girder spacing for the longitudinal cracking, negative moment at support (top of the slab).....	172
6.33. Comparison of reliability indices between the two boundary conditions as a function of the girder spacing for the longitudinal cracking, positive moment at midspan (bottom of the slab).....	173
6.34. Comparison of reliability indices between the two boundary conditions as a function of the girder spacing for the transverse cracking, positive moment at midspan (bottom of the slab).....	173

6.35. Comparison of reliability indices between the two design methods as a function of the girder spacing for the longitudinal crack opening, negative moment at the support (top of the slab).....	174
6.36. Comparison of reliability indices between the two design methods as a function of the girder spacing for the longitudinal crack opening, positive moment at the support (bottom of the slab) .....	174
6.37. Comparison of reliability indices between the two design methods as a function of the girder spacing for the longitudinal crack opening, positive moment at midspan (bottom of the slab) .....	175
6.38. Comparison of reliability indices between the two design methods as a function of the span length for the longitudinal crack opening, negative moment at the support (top of the slab).....	175
6.39. Comparison of reliability indices between the two design methods as a function of the span length for the longitudinal crack opening, positive moment at the support (bottom of the slab) .....	176
6.40. Comparison of reliability indices between the two design methods as a function of the span length for the longitudinal crack opening, positive moment at midspan (bottom of the slab).....	176
6.41. Comparison of reliability indices between the two boundary conditions as a function of the girder spacing for the longitudinal cracking, positive moment at the support (bottom of the slab).....	177
6.42. Comparison of reliability indices between the two boundary conditions as a function of the girder spacing for the longitudinal cracking, positive moment at midspan (bottom of the slab).....	177
6.43. Comparison of reliability indices between the two design methods as a function of the annual mean maximum axle weight for the longitudinal cracking, negative moment at midspan (top of the slab) – span = 60 FT, Girder spacing = 10 FT	178
6.44. Comparison of reliability indices between the two design methods as a function of the annual mean maximum axle weight for the longitudinal crack opening, negative moment at midspan (top of the slab) – span = 60 FT, Girder spacing = 10 FT .....	178
6.45. Comparison of reliability indices between the two design methods as a function of the annual mean maximum axle weight for the longitudinal cracking, negative moment at midspan (top of the slab) – span = 120 FT, Girder spacing = 10 FT .....	179

6.46. Comparison of reliability indices between the two design methods as a function of the annual mean maximum axle weight for the longitudinal crack opening, negative moment at midspan (top of the slab) – span = 120 FT, Girder spacing = 10 FT .....	179
A.1. Elevation of the bridge. ....	210
A.2. Plan view of the bridge.....	210
A.3. Cross section of the bridge .....	211
A.4. Lever rule.....	211
A.5. Truck placement for maximum moment plus lane load. ....	212
A.6. Tandem placement for maximum moment plus lane load .....	212
A.7. Truck placement for the maximum shear .....	213
A.8. Tandem placement for the maximum shear .....	213
A.9. Lane loading. ....	213
A.10. Steel section at midspan .....	214
A.11. Composite section at midspan .....	214
A.12. Computation of plastic moment .....	215
A.13. Deflection due to load P. ....	215
A.14. Truck placement for maximum deflection .....	216
A.15. Flow chart for the plastic moment of compact section for flexural members, computation of $y$ and $M_p$ for positive bending sections .....	217
A.16. Position of the neutral axis for the five different cases .....	218
A.17. Flow chart for the computation of shear resistance, nominal resistance of unstiffened webs. ....	219
B.1. Bridge deck cross section .....	234
B.2. Deck slab dead load.....	234
B.3. Overhang dead load.....	234

B.4. Barrier dead load (15 IN from the edge of the bridge).....	235
B.5. Wearing surface dead load .....	235
B.6. Live load, maximum positive moment one lane loaded.....	235
B.7. Live load, maximum positive moment two lanes loaded.....	236
B.8. Live load, maximum negative moment .....	236
B.9. Concrete cover.....	236
B.10. Deck slab reinforcement according the Traditional Method.....	237
B.11. Deck slab reinforcement according the Empirical Method.....	237

## LIST OF APPENDICES

### Appendix

- A. EXAMPLE OF DESIGN OF A COMPOSITE STEEL BRIDGE .....189
- B. EXAMPLE OF DECK SLAB DESIGN .....220

# CHAPTER 1

## INTRODUCTION

### 1.1. Problem Statement

The premature deterioration of concrete bridge decks is a multi-billion dollar problem in the United States. In December 2003, the Federal Highway Administration estimated that approximately 27 percent of the 592,000 nation's bridges are considered structurally deficient or functionally obsolete. It would cost about 80 billion dollars to bring all of the nation's bridges to an acceptable and safe standard by either rehabilitation or replacement. Moreover, according to the data of the "national bridge inventory" obtained from the U.S. Department of Transportation, it is estimated that deficiencies occur mostly in the decks in more than half of the bridges in United States.

Not only bridge deck deterioration is an economic problem; it is also a risk to those who traverse the structure. Forms of deterioration can range from slightly damaged deck surfaces, causing unpleasant sights and decreasing bridge deck serviceability, up to spalling of large pieces of concrete that reduces the structural integrity and it can be a danger for the public. Therefore, there is a compelling need to understand the behavior of bridge decks under service load and develop a reliable procedure to assess the serviceability of the deck, which will then serve as a decision-making tool for the rehabilitation or the replacement of the decks.

In the United States, most of the bridge decks are constructed as reinforced concrete slabs supported by steel or precast prestressed girders, as shown in Figure 1.1. Such decks have traditionally been designed using the "strip method", based on a

conventional beam theory, which assumes that the slab is continuous over fixed supports. As a result, the top part of the slab is reinforced with steel bars to resist the negative moments, and the bottom part of the slab is reinforced with steel bars to resist the positive moments. Temperature and shrinkage reinforcement is added orthogonally at the top and at the bottom. An example of bar placement is shown in Figure 1.2. When cracks occur in concrete, the top reinforcement can be subjected to environmental agents and aggressive chemicals; such as deicing salt, and it can start to corrode. The corrosion can result in a lateral expansion of the steel bars, leading to spalling of concrete cover and subsequent formation of potholes, as shown in Figure 1.3.

Previous research in the United States and mainly in Canada showed that the flexural capacity of bridge decks can be increased by the presence of in-plane compressive forces, created when the deck is restrained by supports that cannot move laterally. This phenomenon is referred as “arching action” and is the basis of the empirical design provisions of the Ontario (Canada) Bridge Design Code (1993). This empirical method has been adopted in the current AASHTO LRFD code (2005), and it is referred to as isotropic reinforcement. According to the empirical method, arching action requires less steel reinforcement than that required by the strip method of AASHTO LRFD code (2005). Therefore, it is believed that the decks designed by empirical method are more resistant to deterioration due to fewer sources of corrosion (fewer steel rebars).

At the present, there is no assessment method available to evaluate the serviceability and durability of bridge decks. Therefore, in this dissertation, a procedure for bridge decks evaluation is developed, which is focused on evaluation and comparison of bridge decks performance for the two aforementioned design procedures. A reliability based method associated with a state of the art nonlinear finite element analysis, calibrated using field tests, is developed in order to understand the structural behavior of the deck and to assess its performance.

## 1.2. Objectives and Scope of this Dissertation

The main objective of this research is to develop a model that predicts the behavior of a reinforced concrete bridge deck subjected to live load using an advanced Finite Element program and assess its performance at the serviceability level. Comparison is made for the two design methods specified by the AASHTO LRFD code.

This study is focused on reinforced concrete deck slab-on-girders with beam spacing up to 3 m. (10 ft) designed according to the two design methods specified by the AASHTO LRFD code. The design is also carried out for different girder spacing as well as different span length.

The specific objectives of this thesis include:

1. To develop an analytical model for the behavior of bridge decks, using Finite Element non-linear procedure, calibrated with the field test results including the actual support conditions. The developed procedure will be applied to determine the actual stress/strain distribution in the concrete deck slab due to trucks placed at different positions, and to evaluate the performance of bridge decks at the serviceability limit states.

In this dissertation, two serviceability limit states are considered, and are defined as 1) cracking of reinforced concrete deck slab when stress in the deck exceeds tensile strength of concrete; and 2) control of crack opening which is based on the tensile stress in the reinforcement, as specified in AASHTO LRFD code (2005). Definitions of these serviceability limit states are explained in details in Chapter 6.

2. To develop a reliability procedure for the analysis of the deck. Reliability indices are computed for the serviceability limit states for a wide range of girder spacings, span lengths, boundary conditions, and more significantly for both design methods specified by AASHTO LRFD code. The results of the reliability analysis will serve as a basis for a critical evaluation of the code provisions, proposed modifications and recommendations.

The research involves an experimental and analytical program. Figure 1.4 presents a flowchart of this study and the performed tasks.

The field tests were carried out on a steel girder bridge, with the girders spaced at 3 m (10 ft). The results were used to quantify the level of fixity at the supports and to calibrate the FEM model.

A non-linear finite element model for reinforced concrete was developed using the commercial software ABAQUS. Results of available laboratory experiments on slabs were compared with the analytical results in order to validate the developed material behavior model. The tested bridge was also analyzed using the same material model in order to investigate the effect of observed partial fixity of the boundary conditions.

After the FEM model was validated and refined, several bridges with a reinforced concrete deck slab supported on steel girders were designed according to the two different design methods specified by the AASHTO LRFD code (2004); the traditional strip method and empirical design. The design was carried out for several girder spacings as well as different span lengths. These designed bridges were then modeled using the finite element program and the calibrated material behavior model. The results from the FEM program for each studied bridge configuration will serve in the calculation of resistance parameters in the reliability analysis.

A reliability analysis at serviceability limit state was carried out for each considered bridge deck configuration. Two limit states were considered in this study, 1) cracking of concrete and 2) crack opening of concrete. Load parameters were calculated from live load data obtained from previous studies by Nowak and Kim (1997). Resistance parameters were formulated using the Rosenblueth's  $2K + 1$  point estimate method, combined with FEM calculation for aforementioned designed bridge deck configurations. The computed resistance parameters were then applied along with live load parameters, available from previous research conducted at the University of Michigan, to obtain reliability indices. The serviceability of wide-spaced girder bridge decks was assessed

comparing the calculated reliabilities with the targeted reliability index. Finally, conclusions and recommendations were formulated.

### **1.3. Structure of the Dissertation**

This dissertation is divided into 7 chapters as follows:

Chapter 1: Introduction. A general overview of the problem is presented. The objective and scope of this study are given. An introduction to other chapters is presented.

Chapter 2: Literature review. This chapter serves as a review of the work done by others on bridge deck behavior and analytical methods used to predict their response under different load cases. A review of research works in the area of reliability of bridges is also summarized.

Chapter 3: Field testing procedure. This chapter presents the bridge testing program and describes the equipment and procedures used. Technical drawings and details of the tested bridge are presented for reference.

Chapter 4: Analytical model for bridge structures. An introduction to the Finite Element Method is presented; the material model used in this research is described along with the modeling method. The validation of the material model using experimental results by other researchers is explained. In addition, calibration of the boundary conditions using the results from field tests is also discussed.

Chapter 5: Structural Reliability. This chapter summarizes the reliability theory and methods of reliability calculations with the emphasis on the Rosenblueth's  $2K + 1$  point estimate method. In addition, load and resistance models used in common practice are also explained.

Chapter 6: Analytical results of reliability analysis. This chapter explains load and resistance models as well as the limit state functions developed and used in this study.

Parameters used in the Rosenblueth's  $2K + 1$  point estimate method are also presented. In addition, the two code-specified design methods for bridge decks used in this study are presented. Finally, the results of the reliability analysis for the studied bridge deck configurations are discussed. The serviceability of wide-spaced girder bridge decks is assessed and the obtained reliability indices are compared.

Chapter 7: Summary and conclusions. This chapter summarizes the performed research and highlights the main findings. Conclusions are drawn and recommendations for future work are proposed.

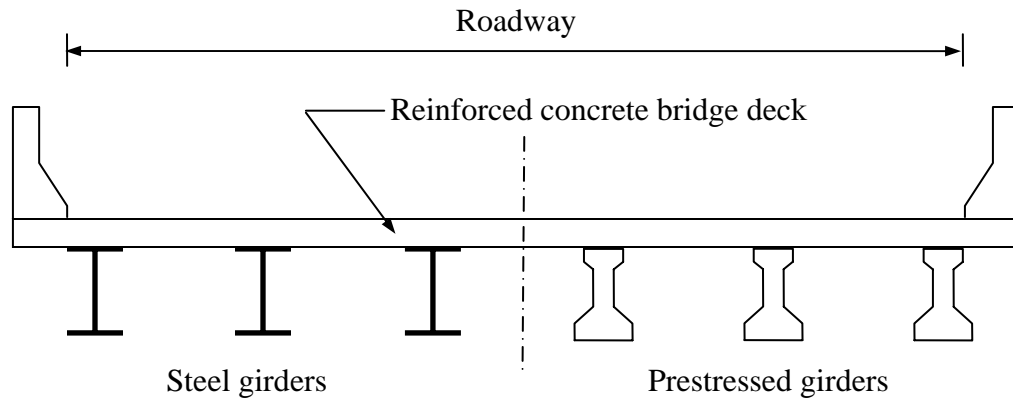


Figure 1.1 Typical cross sections of a reinforced concrete deck slab supported by steel or prestressed concrete girders

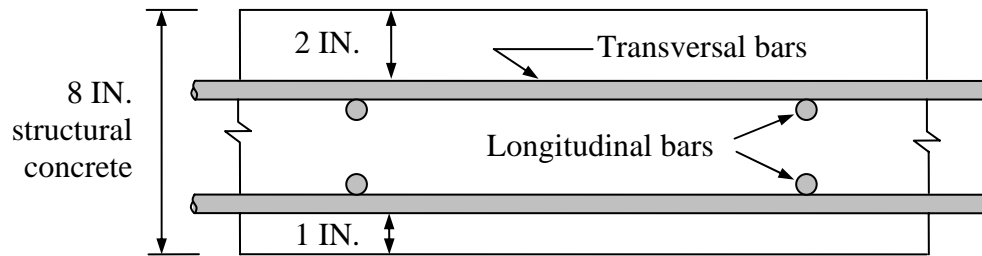


Figure 1.2 Deck cross section showing typical bar placement



Figure 1.3 Examples of extensive cracking and potholes in concrete bridge deck

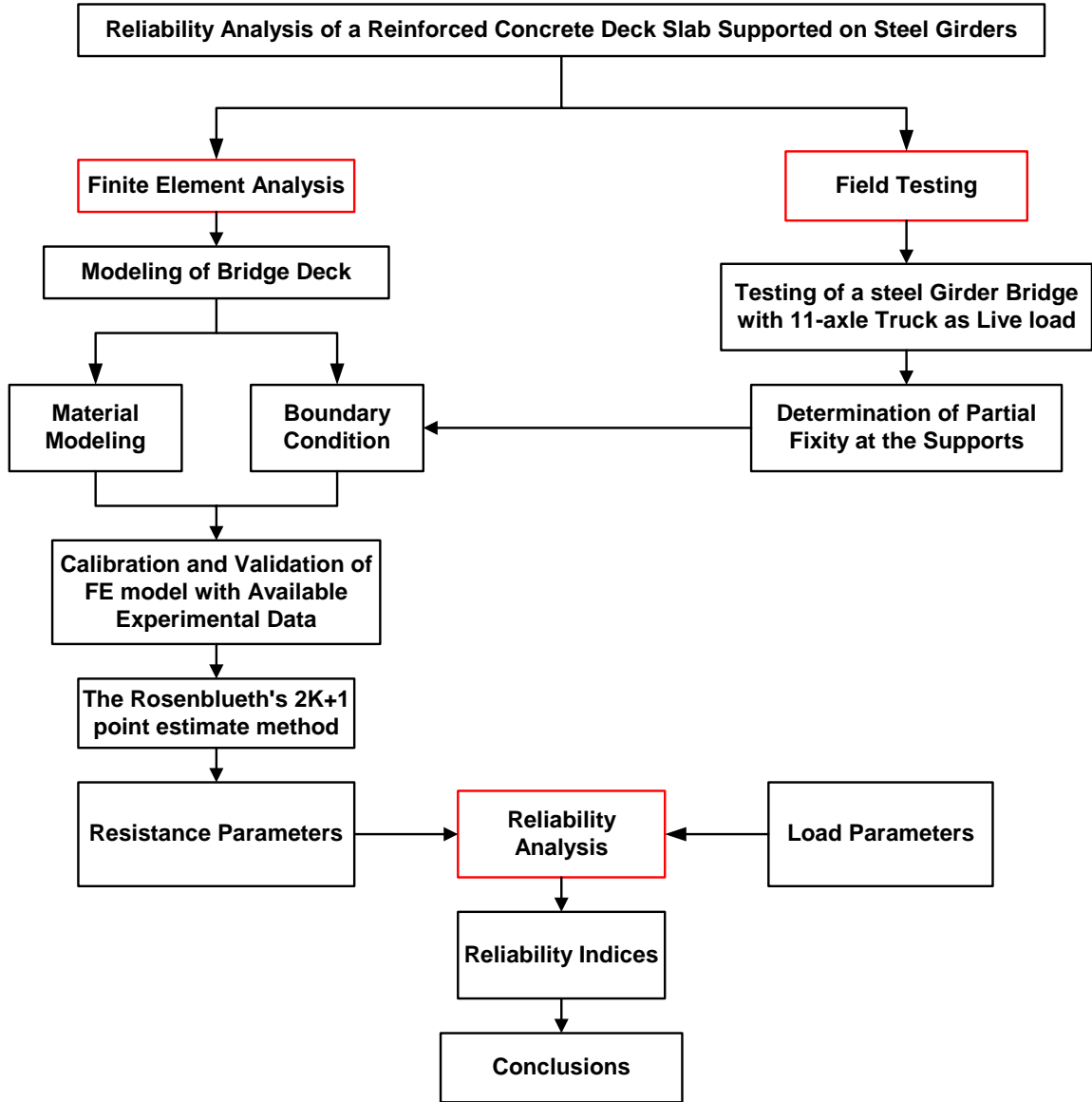


Figure 1.4 Flow-chart of the research

## **CHAPTER 2**

### **LITERATURE REVIEW**

#### **2.1. Behavior and Performance of Deck Slab**

##### **2.1.1. Historical Review**

The effect of in-plane forces on the load carrying capacity of reinforced concrete slabs has been an active field of structural engineering research for several decades. In 1956, Ockleston tested a three-story reinforced concrete building in Johannesburg, South Africa, and recorded collapse load three or four times the capacities predicted by yield-line theory. Ockleston also identified this phenomenon as the effect of compressive membrane forces. After a study of the behavior of continuous prestressed concrete slabs, Guyon suggested that arching action should be taken into account in designing such slab to resist concentrated out-of-plane loads. Other experimental verifications of this effect were also carried out by Christiansen, Fredericksen and Park.

In the late 1950's, tests were conducted on single panels by Sozen and Gamble at the University of Illinois. When bounded by element which could develop horizontal reaction, such reinforced concrete panels were found to have flexural capacities considerably in excess of the load calculated by Johanson's yield line theory. The additional capacity was attributed primarily to the effect of in-planes forces. Likewise, Newmark, in his famous 1948 paper on I-beam bridges, recommends using slab design moments which are 30% lower than the theoretical design moment calculated in his research because of this additional reserve of strength. He recognized that the strength

enhancement due to compression membrane action occurred only after yield and that eventual collapse took the form of punch-out shear.

Research in this field originally concentrated on the behavior of building floor systems, and most tests were conducted using small-scale models. At the end of 1975, the Ontario Ministry of Transportation and Communications decided to develop a code for designing highway bridges. A series of tests were undertaken by academic researchers and the Ministry's Research and Development Division. Results showed that large reserves of strength existed in deck slabs under static and fatigue loading. This research work was supplemented by field tests of actual bridges. It was concluded that a slab's load carrying capacity was increased by in-plane restraints.

Based on these findings, an empirical design method was proposed, involving an isotropic reinforcement layout in the deck. Required reinforcement is considerably less than that specified by the AASHTO Code. Some bridge decks in Ontario have been designed using the proposed empirical method. Field tests have been conducted in Canada on a composite prestressed concrete girder bridge with a deck detailed in accordance with the empirical method. The load-deflection curve at the loaded point was linear up to about 100 KIPS wheel load level.

The convenience in construction of such decks, and the savings in the amount of reinforcement required, has attracted the attention of researchers in the United State. The New York Highway Department conducted a study of the strength of highway bridges decks. Under design loads, the stress in reinforcement was found not to exceed 12 KSI. When loaded to ultimate, all locations bounded by longitudinal girders failed by punching shear. Regardless of the reinforcing pattern used, failure loads always exceeded six times the design wheel load for slab bounds by girders.

### **2.1.2. Behavior of Deck Slabs and their Serviceability**

In most of the available literature, the analytical models do not take into account the deflection of the girders and the transverse deck slab behavior is analyzed using classical beam theory, assuming that the girders provide a rigid support. However, because of the girder flexibility, the maximum stresses in a bridge deck can vary significantly from the design values. Fang et al. (1988) showed that the negative bending moment in bridge decks and the resulting top tensile stresses are very low, much less than the positive bending moments and the bottom tensile stress. Their work indicates that, in general, the tensile strength of a concrete deck considerably exceeds the top tensile stress induced by traffic loads due to the deflection of girders.

Cao et al. (1996 and 1999) developed a simplified analytical method for the slab-on-girder bridge deck, and analyzed the behavior of a reinforced concrete bridge deck with flexible girders. The analysis was based on the plate theory and was validated using the results of the finite-element computations conducted on two different bridge decks. They concluded that the design formula in the AASHTO specification overestimates the negative bending moments in a slab-on-girder deck. They developed an analytical procedure for the evaluation of the maximum negative bending moments in a bridge deck by the superposition of the negative bending moment in a deck slab on rigid girders and the positive bending moment in a deck slab induced by girder deflection. They found that the reduction of the maximum negative bending moment in a deck slab due to girder deflection depends on the stiffness ratio of the deck to girder, and the ratio of the girder spacing to the span length of the bridge. The maximum negative moment decreases with an increase in span length and stiffness of the supporting girders.

Cao et al. (1996) suggested eliminating most of the top reinforcing bars in a deck. They conducted a test to assess the maximum tensile stress, as well as the durability of the deck slab in the absence of a top reinforcement. For all considered truck-load

positions, the transverse tensile strains at the top of the deck were less than 30% of the expected cracking strain of the concrete. However, even though top transverse reinforcement is not required to carry traffic loads, they recommended further research on the control of temperature and shrinkage cracks.

In general, the top reinforcing bars are most susceptible to corrosion. Therefore, the reduction of the amount of top reinforcement can slow down the deck deterioration. Mufti et al. (1999) suggested to simply eliminate the reinforcement in concrete bridge decks as one solution for corrosion. A number of tests were conducted to show that the behavior of such a deck slab is acceptable, providing a number of ties are installed to connect top flanges of adjacent girders. Extra shear studs are necessary in order to insure arching action without reinforcement. So far, several bridge decks without reinforcement were built. However, an extensive longitudinal cracking was observed between the girders.

The performance of bridge decks is often attributed to serviceability limit state. Deck deterioration starts with corrosion of reinforcement when deck is subjected to sodium chloride deicers. The process speeds up in a presence of shrinkage cracks. It has been reported that the limitation or elimination of these cracks at early stages of deck construction significantly increases deck durability. In fact, the deck performance can be improved by a better design. The story of the construction of the New Jersey Turnpike (Riley 1993) is a good example of such improvement. Originally, bridges were opened to traffic in 1951 and after 8 years about 10 percent of slabs had to be replaced, and so far about 38 percent of the slabs were replaced. Originally designed deck slabs were 6 ½ IN. thick reinforced with bars #5 @ 7-1/2 IN. at the top and bottom in transversal direction and bars #4 @ 12 IN. at the top and #5 @ 10 IN. at the bottom in the longitudinal direction. After design revision in 1960's, the replaced new decks have thickness close to 1 FT (with latex modified concrete wearing surface) and they are reinforced with bars #6 @ 6 IN. at the top and bottom in transversal direction, and bars #5 @ 6 IN. at the top and

the bottom in the longitudinal direction. These new deck slabs with an increased thickness and area of reinforcement do not show any deterioration signs after 25 years in service. As a result, it was concluded that the increased deck stiffness helps to limit restrained shrinkage cracking, and increased percentage of reinforcement can even eliminate these cracks.

Some researchers have suggested that the other way to improve the durability of bridge decks can be by using better materials, for example higher strength concrete. However, greater compressive strength is not always better or necessary. Mistakes and misconceptions concerning structural concrete are discussed by Schrader (1993) in articles presented at the ACI seminars on "Repairing Concrete Bridges". If extra strength is gained by adding cement, the cost will increase with only a negligible increase in load-carrying capacity for reinforced concrete flexural designs. More importantly, there will be more shrinkage, especially if there also is an increase in water (even when water/cement ratio is kept constant). In addition, higher strength mixes generally become more brittle because they have higher modulus of elasticity and produce more hydration heat; thus resulting in more cracking and internally developed stress. Such characteristics as flexural strength, thermal shock, and impact resistance, or fatigue strength will also be worse for high strength concrete than for ordinary one. From the aforementioned reasons, it can be stated that the idea of increasing slab stiffness by using higher strength concrete with higher modulus of elasticity is not a good one.

Allen (1991) made an intensive investigation on the cracking and serviceability of reinforced concrete bridge deck. After observation of deck slab designed with the empirical method, he outlined some very important facts in the behavior of bridge deck which have been very often neglected when considering serviceability. Cracking strength of typical bridge decks is an important parameter in the performance of deck, compression membrane action is a post-yield phenomenon and strength enhancement due to compression membrane action adversely affects the serviceability of decks. Allen

visited at least 20 experimental isotropic decks built in North America. Nearly every isotropic bridge exhibited more cracking than a typical AASHTO LRFD reinforced deck, especially longitudinal crack in positive moment area.

## **2.2. Design and Analysis of Bridge Deck**

Techniques used in the analysis and the design of slab-on-girder bridges have improved in the last years. Available theoretical methods are varied in their approaches as well as their accuracy and assumptions. Bridge superstructure can be idealized for theoretical analysis in many different ways. The different assumptions used in the formulation and calculations can lead to significant differences in the accuracy of the results. The major numerical approaches reported in the literature are:

1. The orthotropic plate theory; the bridge superstructure is replaced with an equivalent plate having different elastic properties in two orthogonal directions.
2. The Grillage analysis; the bridge is modeled by longitudinal grillage beam elements whose constants are usually calculated based on the composite girder-slab properties, and by transverse beam elements, based on the slab properties.
3. Combination of plate and grid analysis.
4. Finite Element Method. The structure is idealized by continuum elements such as shell, plate or solids elements. The different possible combinations of elements used in Finite Element have improved. In the past, the first 2-dimensional approaches were using shell elements for slab and beam elements for girders. Currently, with 3-dimensional approaches, shell elements are used for the girders and solid elements are used to model the slab.

The plane grillage models (Cusens 1975 and Bhatt 1986) shown in Figure 2.1 are the most commonly used, particularly in design practice. The bridge deck slab is divided into a number of longitudinal and transverse beams lying in the same plane. Each

longitudinal beam represents a girder and part of the slab. The properties of such beams are determined by the position of the neutral axis, which is dependent on the composite or non-composite behavior of the bridge. A transverse grillage beam represents a strip of slab and makes the connection between longitudinal elements. Detailed recommendations on the implementation of a grillage analysis for slab bridges can be found in West (1973), Hambly (1991), and Zhang and Aktan (1997). Such simple FEM models allow only for a global evaluation of bridge behavior. The accuracy of these calculations depends on the assumed location of the neutral axis in bending elements (O'Brien and Keogh 1998). The determination of this location is difficult, especially in bridges where wide cantilevers, barriers, or sidewalks cause the neutral axis to change position across the bridge width. In such cases, a more complex, 3-dimensional grillage model can be used (O'Brien and Keogh 1998 and Zhang and Aktan 1997). In these models, grid beams placed on two levels are connected using rigid vertical links. Although both grillage analyses represent a simple geometry that is easy to model, they require an elaborate determination of beam properties, often based on questionable assumptions.

For the case of finite element method, in some cases, the slab is divided using shell elements and girders are represented using beam elements (Mabsout et al. 1999 and Hays et al. 1997). Diaphragms (if considered) are also represented by beam elements. In such plane models (Mabsout et al. 1999), centroid of beams coincides with the centroid of the slab. To determine the cross-section properties of the beam, the actual distance between its neutral axis and the middle plane of the slab must be taken into account. Ebeido and Kennedy (1996) performed intensive finite element analysis on skew-composite girder bridges. They use linear shell element with six degree of freedom at each node to model the concrete deck slab. Girders were modeled using three dimensional linear beam elements with also six degree of freedoms at each node. These beam elements were also used to model diaphragm and cross frame bracing. The nonlinear material model allowed for cracking of concrete in tension. The concrete under

compression was modeled by an elastic-plastic theory, using yield surfaces based on the equivalent pressure stress and the Von-Mises equivalent stress. Constraints were applied between the shell node of the concrete deck slab and the beam node of the longitudinal steel girders to ensure full interaction. They performed nonlinear analysis using ABAQUS by applying incremental load and used the Newton-Raphson procedure to achieve convergence. Fang, Worley and Burns (1986) performed testing on bridge deck slab designed with the empirical method. They used linear and quadratic thick shell elements with three degree of freedom at each nodes to model the slab and three dimensional beam elements with six degree of freedom at each nodes located at the girder mid-height as shown in Figure 2.2. No slip was assumed between the slab and the girder. The effect of concrete cracking was included in the modeling of the deck slab by the mean of the smeared cracking approach. A sequential linear approach was used as solving method.

Despite the use of rigid link to connect space frame elements and shell elements, and to account for the eccentricity of the girders, it is still difficult with this method to include a precise composite action when determining beam stiffness.

To overcome this problem, shell elements can be used to model the girders (Alaylioglu 1997 and Tarhini and Frederic 1992). This seems to be a better solution, especially for elements such as steel girders consisting of thin parts. Sometimes, the bridge behavior can be strongly affected by the structural components such as sidewalks, curbs, and barriers. In such cases, it can be incorrect to model them only by changing the thickness of shell elements. Tarhini and Frederic (1992) developed this 3-dimensional finite element analysis to study wheel load distribution shown in Figure 2.3. The concrete slab was modeled with a linear brick element, with three degree of freedom at each node. Linear shell element with six degree of freedom at each node was used to model the web and the flanges of the girders. Cross bracing and diaphragm are modeled with three-dimensional beam element.

The application of solid elements also allows for a more detailed investigation of local stress and strain distribution. Modeling the slab with solid elements, and the girders and diaphragms with shell elements, seems to describe most adequately the bridge geometry and physical properties.

The evaluation of FEM models for bridges shows a tendency towards more complex model geometries with a larger number of elements. At the same time, the determination of element properties is clearer and stands closer to reality.

### **2.3. Reliability of Bridge Structure**

The older bridge code was based on the selection of reasonable upper-bound estimate of normal working loads, the use of elastic methods of structural analysis, and the provision of some margins in strength. These margins was chosen by the selection of allowable working stresses separated by a factor of safety from critical stress, such as the yield stress or ultimate stress of the material. These factors were not the same for all materials. In 1971, O'Connor expresses the possibility that statistical method of design may be adopted in which the emphasis is on probability of failure. This method has been adopted now in most bridge design codes and has two basic characteristics:

1. It attempts to consider all possible limit state and,
2. It is based on probabilistic methods

The simplest limit state is the failure of a component under a particular applied load. This depends on two parameters: the magnitude of the load as in the sense of how it affects the structure, here called the load effect, and the resistance or the strength of the component. If the load effect exceeds the resistance, then the component will fail. However, both the magnitude of the load effect and the resistance may be subject to statistical variation. By knowing the statistical distribution of the load effect and resistance, it is then possible to calculate numerically a probability of failure. This

method allows for more efficient design and bridge test data can be used to improve the accuracy of load and resistance models by reducing the uncertainty caused by the idealized assumptions used in analysis.

Live Load covers the forces produced by vehicles moving on the bridge. What is of interest for the designer is the effect of the live load. These effects depends on many parameters such as the span length, the truck weight, the axle weight and spacing, the position of the truck on the bridge, the volume of traffic (ADTT), girder spacing, and the stiffness of structural members. Agarwal and Wolkowicz (1976) and Nowak (1993) developed live load model for the AASHTO LRFD which provides an appropriate model at the stage of design. Live load models reflecting the actual traffic can be derived using Weigh In Motion measurement for a specific site (Nowak et al. 1994, Kim at al. 1996).

The resistance of a bridge is also a random variable. Tantawi (1986) and Tabsh and Nowak (1991) studied the behavior of steel-concrete composite cross section. Nowak (1995) also derived statistical parameters for composite and noncomposite steel girder, prestressed concrete girder, and reinforced concrete T-beams.

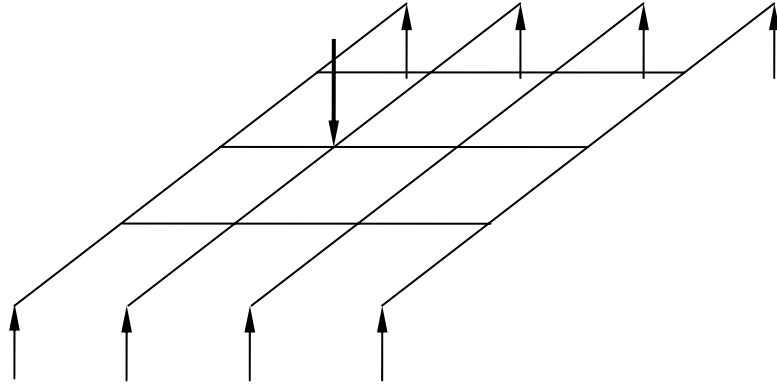


Figure 2.1 Grillage model

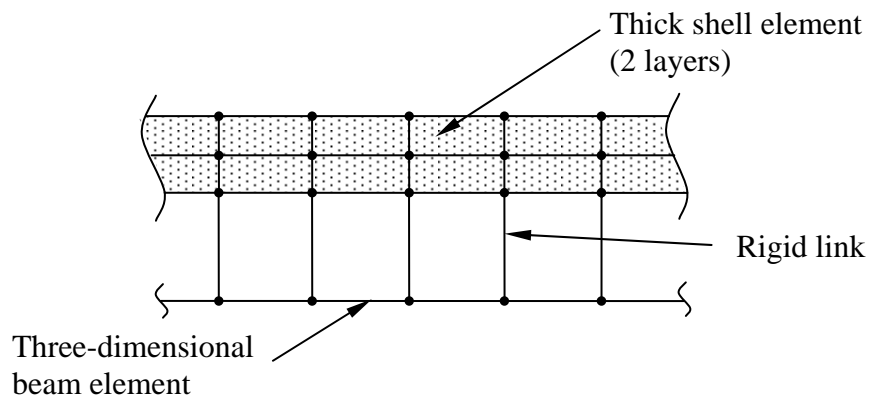
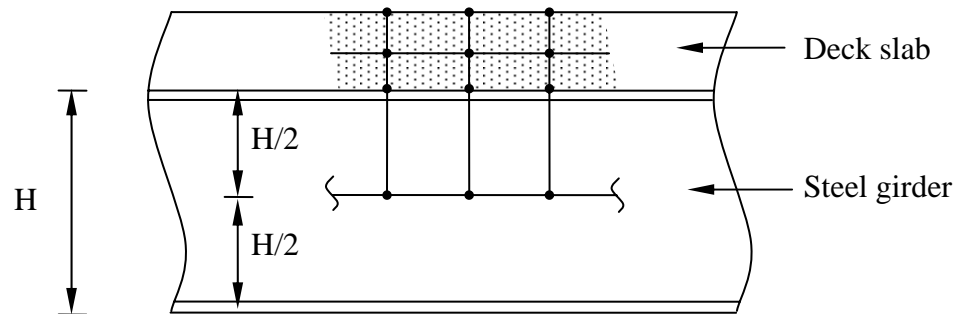


Figure 2.2 Actual composite girder and corresponding finite element model used by Burns et al.

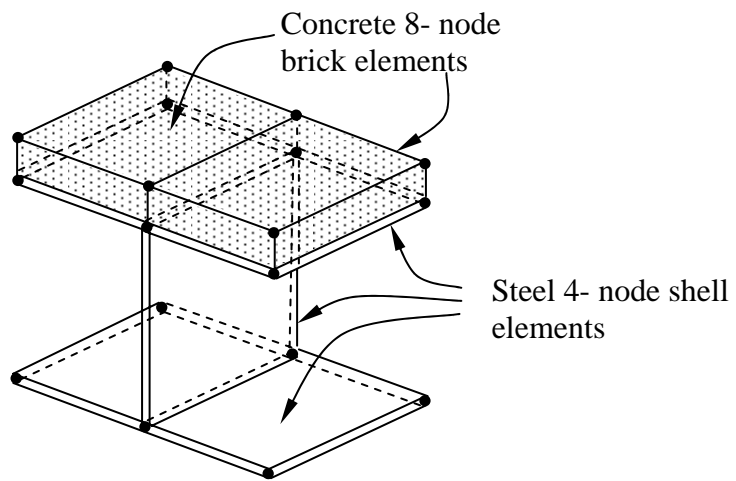


Figure 2.3 Typical section of the model by Tarhini and Frederic

## **CHAPTER 3**

### **FIELD TESTING PROCEDURE**

#### **3.1. Introduction**

From a list of bridges with large spacing between girders, provided by the Michigan Department of Transportation, a bridge suitable for field testing was selected. The main objective of the field tests was to determine the actual behavior of bridge superstructure supported by steel girders spaced at more than 10 FT. The selected bridge was tested using a three-unit 11-axles truck as live load (the largest live load legally permitted in the State of Michigan). The test results were used to calibrate the Finite Element Model and to analyze the effect of partial fixity of the support on the behavior of reinforced concrete bridge decks.

#### **3.2. Description of the Selected Bridge Structure**

The selected bridge, S06 of 82291, was built in 1974 and it is located on Pennsylvania Road over I-275, near New Boston, Michigan. It is a two span structure with a span length of 144 FT, and a cantilever of 12 FT. The total bridge length is 288 FT, without any skew. The bridge has five steel girders spaced at 10 FT 3 IN, and the deck is 9 ½ IN thick (see Figure 3.1 and Figure 3.2). The depth of the steel girders is 60 IN. The reinforced concrete deck carries one lane in each direction.

### 3.3. Instrumentation and Data Acquisition

Measurements of mechanical, thermal, electrical, and chemical quantities are made by devices called sensors and transducers. The sensor is responsive to changes in the quantity to be measured, for example, stress, temperature, position, or displacement. The transducer converts such measurements into electrical signals, which, usually amplified, can be fed to the data acquisition for the readout and recording of the measured quantities. Some devices act as both sensor and transducer.

#### 3.3.1. Strain Measurement

While there are several methods of measuring strain, the most common is with a strain gauge, a device whose electrical resistance varies in proportion to the amount of strain in the device. The most widely used gauge is the bonded metallic strain gauge. It consists of a very fine wire or, more commonly, metallic foil arranged in a grid pattern. The grid pattern maximizes the amount of metallic wire or foil subject to strain in the parallel direction. The cross sectional area of the grid is minimized to reduce the effect of shear strain and Poisson strain. The grid is bonded to a thin backing, called the carrier, which is embedded between two plastic strips. The separate layers of the gage are bonded together; therefore, the strain experienced by the test specimen is transferred directly to the strain gauge, which responds with a linear change in electrical resistance.

Strain transducers are the essential component of the electrical measurement technique applied to the measurement of mechanical quantities, usually calibrated in shop; they have a high level of accuracy, and they are easy to install in the field. Figure 3.3 shows a typical transducer.

In practice, the strain measurements rarely involve quantities larger than a few millistrain ( $\epsilon \times 10^{-3}$ ). Therefore, there is a need to measure very small changes in resistance. As a result, in most cases, strain gages have bridge configuration with a

voltage excitation source. The general Wheatstone bridge, developed by Sir Charles Wheatstone in 1843, allows the measurement of electrical resistance; it consists of four resistive arms with an excitation voltage applied across the bridge and an output voltage. The Wheatstone bridge is well suited for the measurement of resistance change in a strain gage, particularly, the full bridge circuit configuration, shown in Figure 3.4, which can eliminate temperature effects.

In this study, the strain transducers were attached to the bottom flanges of the girders at a distance of 26 FT (Figure 3.5) from the support on the west span (it was not possible to install them closer to the midspan because it would have required closure of a traffic lane on I-275), and close to support (Figure 3.6) to measure the moment restraint provided by the support. Strain transducers were connected to the SCXI data acquisition system by the National Instruments (Figure 3.7).

### **3.3.2. Data Acquisition System**

Strain transducers and LVDT's are connected to the SCXI data acquisition system (manufactured by National Instruments). The data acquisition mode is controlled from the external PC notebook computer, and collected data are processed and directly saved in the PC's hard drive. The data acquisition system connected to the PC notebook computer is shown in Figure 3.7.

The data acquisition system consists of a four slot SCXI-1000 chassis, one SCXI-1200 data acquisition module, two SCXI-1100 multiplexer modules, and one notebook computer with Labview software. A multiplexer is a switch arrangement that allows many input channels to share one amplifier and one analog-digital converter (Figure 3.8). The power for all components is provided by an electric generator. The generator also supplies excitation for strain transducers through the AC to DC converter.

The SCXI-1000 chassis integrates the operation of multiple SCXI modules with a SCXI-1200 module. The chassis bus includes guarded analog buses for signal routing and digital buses for transferring data and timing signals.

The SCXI-1200 data acquisition module is a multifunction analog, digital, and timing module. It is connected directly to the standard PC parallel printer port. The module has a 12-bit analog to digital converter (ADC) and a sustained sampling rate of 20 kHz in the Standard Parallel Port (SPP) mode. It acquires data from and controls several SCXI signal conditioning modules installed in the same chassis.

The SCXI-1100 is a 32 differential channel multiplexer amplifier module. It can be configured to sample a variety of millivolt and volt signals by using the selectable gain and bandwidth settings. The signals from the strain transducers are connected to the SCXI-1100 module. Each SCXI-1100 module multiplexes the 32 channels into a single channel of the SCXI-1200 module. Several SCXI-1100 modules can be added to multiplex hundreds of signals into a single channel on a SCXI-1200 module. Conditioned signals from SCXI-1100 are passed along the SCXIbus in the backplane of the chassis to the SCXI-1200 data acquisition module. LabView was used to control the SCXI-1200 module and signal conditioning functions on the SCXI modules.

LabView is the data acquisition and control programming language installed in the PC. It has necessary library functions for data acquisition, analysis, and presentation. The data acquisition process, such as a sampling rate and data acquisition mode, is controlled with options in LabView. After the data acquisition, the voltage data can be converted into strains by using the data analysis routines in LabView. The results are displayed on the computer screen in real time and saved in the PC's hard drive. With LabView, the SCXI system can be controlled according to the user's needs, objectives, and routines.

The current system is capable of handling 64 channels of strain or deflection inputs. Up to 32 additional channels can be added if required. A portable field computer

is used to store, process and display the data on site. A typical data acquisition setup is shown in Figure 3.9. The data from all instruments is collected after placing the trucks in desired positions or while trucks are passing on the bridge. For the normal speed tests, a sampling rate of 300 per second was used for calculation of dynamic effects. This is equivalent to 11.4 samples per meter at a truck speed of 95 km/h. The real time responses of all transducers are displayed on the monitor during all stages of testing, assuring safety of the bridge load test.

### **3.4. Live Load for Field Testing**

Over the years, live loads on bridges have considerably increased. For example, in 1950 the maximum observed gross vehicle weight (GVW) of a truck recorded in Michigan was approximately 110 KIP (Michigan Bridge Analysis Guide 1983); in 1995, in the weigh-in-motion study carried out by Nowak and Laman at the University of Michigan on several highway bridges in southeast Michigan, the maximum GVW of 250 KIP was recorded. While in most states the maximum legal gross vehicle weight for commercial trucks is 80 KIP, in Michigan the maximum legal gross vehicle weight can exceed 170 KIP. There are more than 100,000 registered commercial trucks in Michigan; approximately 15% of these can carry more than 80 KIP and approximately 1% can carry over 170 KIP (Michigan Department of Transportation Position Paper on Trucks and Transportation, 1998), but since these trucks represent only a third of the 300,000 trucks operating in Michigan, it is estimated that less than 5% of all trucks in Michigan are over 80 KIP.

In the field tests, the measurements were taken using a three-unit 11-axle truck with known weight and axle configuration. The actual axle weights of the test trucks were measured at a weight station prior to the test. Figure 3.10 shows the three-unit 11-

axle truck used in the test and Figure 3.11 shows its actual axle weight and axle spacing configuration.

The truck was driven over the bridge at crawling speed to simulate static loading. For each run, the strain measurement was recorded simultaneously using all 10 strain transducers. Table 3.1 shows the sequence of test runs.

Table 3.1 Sequence of test runs

Run #	Loaded Lane	Truck Position
1	North	Center
2	South	Center
3	North	Curb
4	South	Curb
5	Center	Center

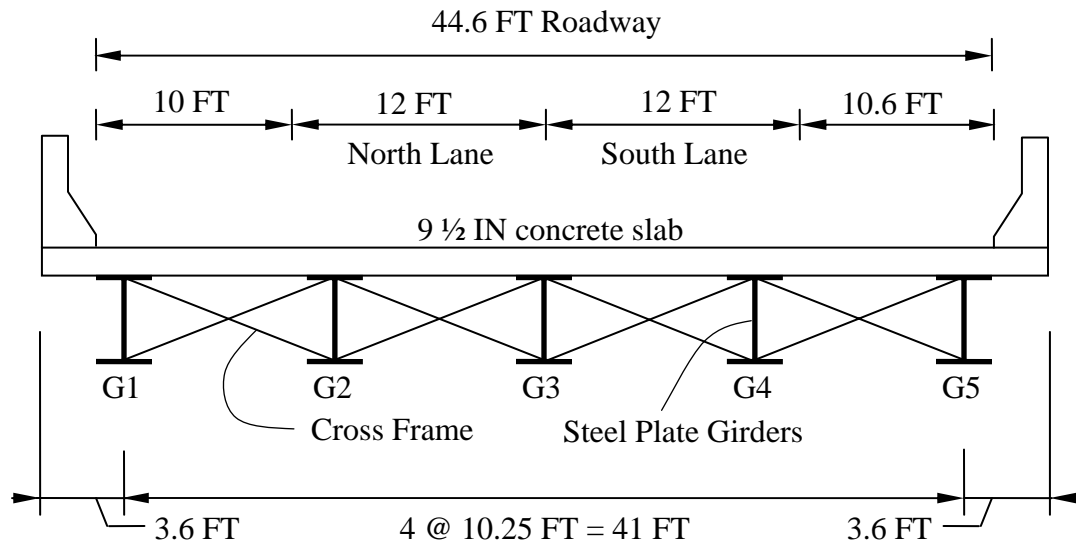


Figure 3.1 Cross section of the tested steel girder bridge

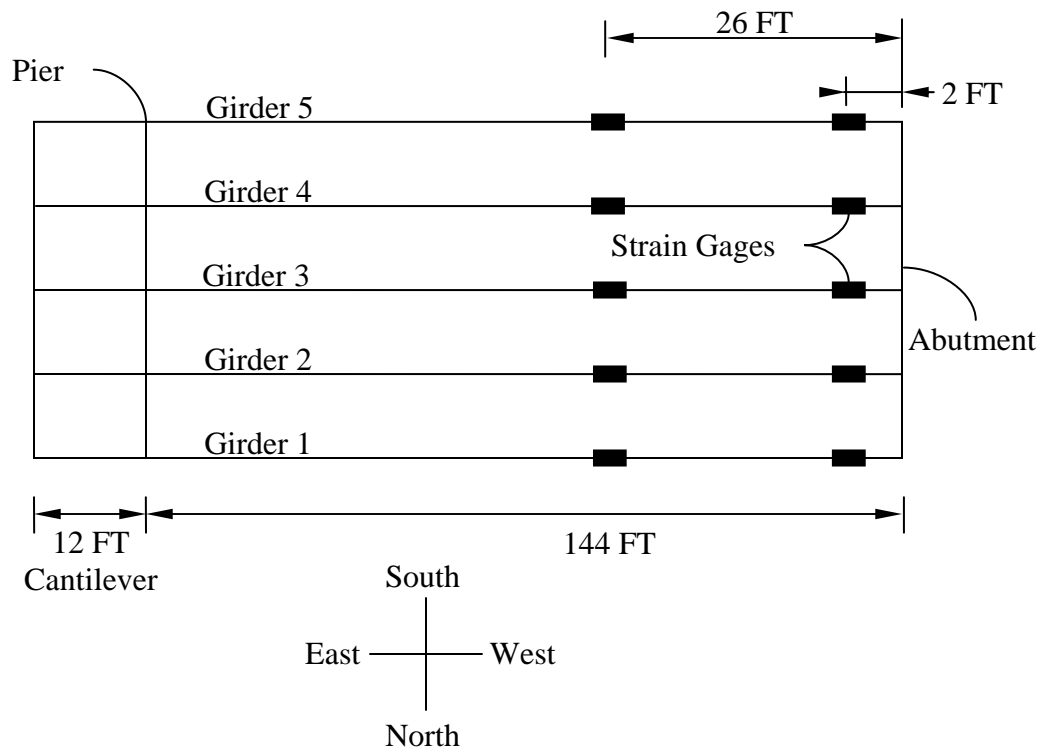


Figure 3.2 Strain transducers location on the tested bridge

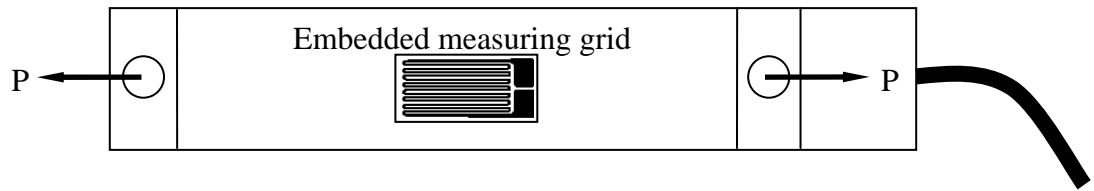


Figure 3.3 A typical strain transducer

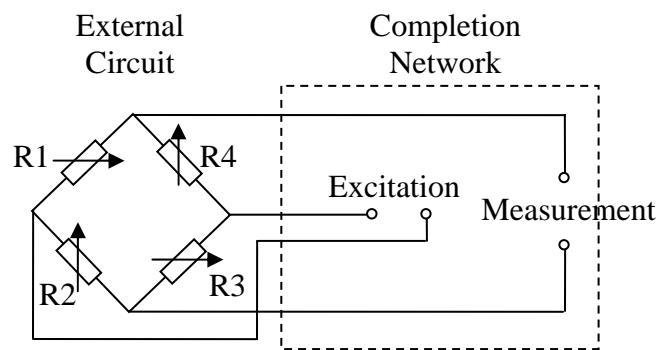


Figure 3.4 Wheatstone full bridge circuit configuration



Figure 3.5 Removable Strain Transducer attached to the bottom flange



Figure 3.6 Strain transducer attached near support



Figure 3.7 Data acquisition system connected to the PC notebook computer

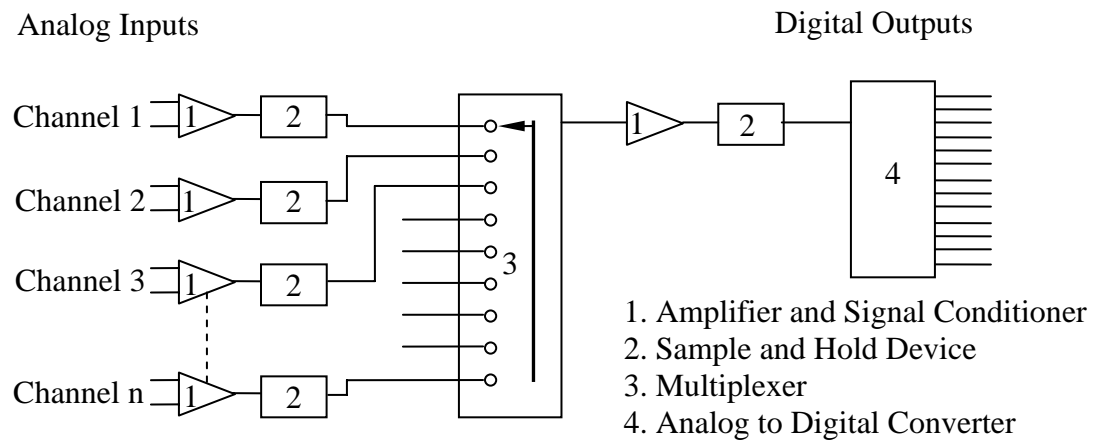


Figure 3.8 General data acquisition system

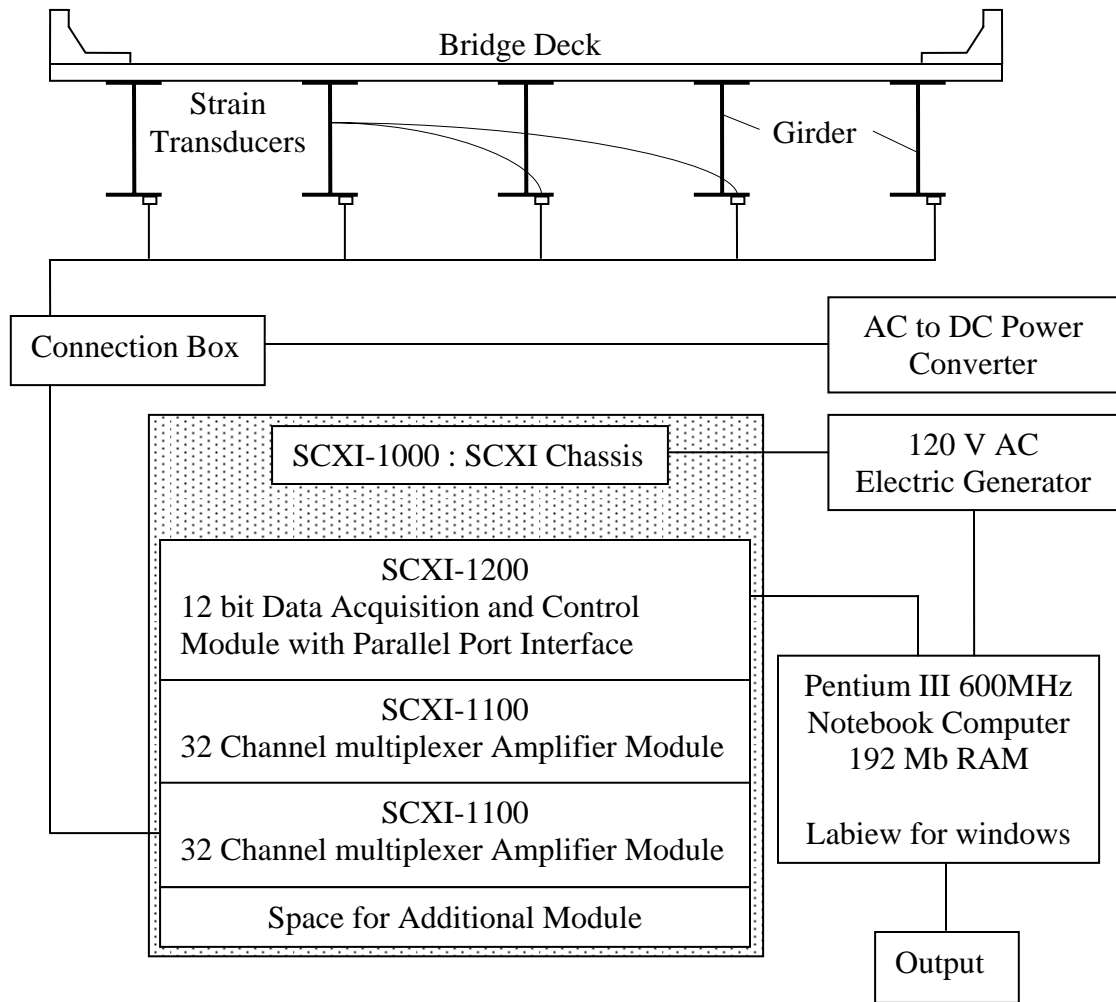


Figure 3.9 SCXI Data Acquisition System Setup



Figure 3.11 Three-unit 11-axle truck used in the field tests

Front

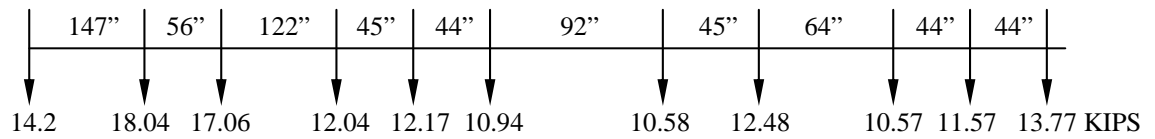


Figure 3.12 Axle weight and axle spacing configuration

## **CHAPTER 4**

### **ANALYTICAL MODEL FOR BRIDGE STRUCTURES**

#### **4.1. General**

One of the main objectives of the study was to develop a numerical model which would accurately predict the behavior of bridge structures, more particularly the behavior of reinforced concrete deck slab, and would be easily applicable for a wide range of highway bridges.

To analyze a bridge superstructure, several methods can be used, depending on the bridge's structural characteristics, geometric configuration, and support conditions. The conventional methods include orthotropic plate theory, plane grillage model, space frame method, finite strip method, and finite element method. The finite element method was implemented for analysis in this study because of its power and versatility. However, since one of the primary objectives of this research is to study the deck behavior, the modeling of the deck slab becomes more significant. Hence, the difficulty was to select a finite element model that can predict the behavior of the entire superstructure and can be at the same time sufficiently accurate to model the response of a reinforced concrete deck slab.

This study was focused on bridges supported by steel girders, therefore, concrete and steel (structural steel and reinforcing steel) are two materials of importance in the analytical program. A conventional linear elastic analysis is insufficient, because it cannot predict the effect of concrete cracking and steel yielding in the structural behavior. As a result, material nonlinearity was included for both steel and concrete. Because the

expected bridge deflections could be large, geometrical nonlinearity was also included into the model.

In order to validate the accuracy of the nonlinear material model for steel and concrete used in this study, results from three laboratory tests of slabs published in the literature as well as the field test data from the actual bridge described in Chapter 3 were used and compared with the finite element model calculations. The analysis was performed using ABAQUS finite element program available at the University of Michigan.

## **4.2. Introduction to ABAQUS**

ABAQUS, Inc. is one of the world leading providers of software for advanced finite element analysis. It has been adopted by many major corporations across different engineering disciplines. ABAQUS, Inc. can provide solutions for linear, non-linear, and explicit problems. Their powerful graphic interface allows accuracy to define the model and is particularly useful to visualize and present analytical results. However, the easier finite element software is to use, the more careful the user has to be when interpreting the results. Indeed, it is always easier to obtain results from a finite element program than to prove their validity. Finite element software is a powerful tool, but it has to be used with caution.

## **4.3. Description of Available Elements**

ABAQUS has an extensive element library to provide a powerful set of tools for solving various problems. All these elements are divided into different categories according to five main characteristics: their family, their degrees of freedom, their number of nodes, their formulation and finally their integration. The elements are given names that identify each of these five very important aspects.

Figure 4.1 shows the element families that are most commonly used in a stress analysis. The main difference between the element families is the geometry type that each element family represents.

The most important degrees of freedom for a stress/displacement simulation are translations, and for shell and beam elements, rotations at each node. They are the fundamental variables calculated in the analysis. Some additional degrees of freedom can exist in addition to displacement degrees of freedom at each node, as, for example, temperatures degree of freedom for thermal-stress analysis.

Displacement or other degrees of freedom are calculated at the nodes. At any other point in the element, the displacements are obtained by interpolating from the nodal displacements. Usually, the interpolation order is determined by the number of node used in the element. For example, elements which have nodes only at their corners, such as a 8-node brick shown in Figure 4.2(a), use a linear interpolation and are often called linear element or first-order elements. Elements with midside nodes, such as a 20-node brick shown in Figure 4.2(b), use quadratic interpolation and are often called quadratic elements or second-order elements.

An element's formulation refers to the mathematical theory used to define the element's behavior. The most common formulations provided by ABAQUS are the Lagrangian formulation, mainly used in stress/displacement analysis, and the Eulerian formulations, mainly used in fluid mechanics simulations. In addition to these standard formulations, ABAQUS has also alternative formulations such as, for example, a hybrid formulation to deal with almost incompressible or inextensible behavior.

ABAQUS uses numerical techniques to integrate various quantities over the volume of each element, such as for instance the displacement. The Gaussian quadrature is used for most elements; therefore, material responses are evaluated at each integration point in each element. Reduced or full integration can be chosen for most of the continuum elements.

Despite the fact that they provide less accuracy than the second order elements, first order elements were selected in this research because they require less computational time and more importantly, they seem to be more stable when used with the concrete damaged plasticity model. Reduced integration scheme was also used. Reduced integration uses a lower order integration to form the element stiffness. It reduces running time, especially for three dimensions. For example, 20-node brick fully integrated element has 27 integrations points ( $3 \times 3 \times 3$ ), while 20-node brick with reduced integration has only 8 ( $2 \times 2 \times 2$ ); therefore, element assembly is roughly 3.5 times more costly for the fully integrated element.

When using the first order, reduced integration elements, hourglassing can be a problem. Since the elements have only one integration point, it is possible for them to distort in such way that the strains calculated at the integration point are all zero, which, in turn, leads to uncontrolled distortion of the mesh. To overcome this problem, the enhanced hourglassing control option was enabled, concentrated load were avoided and boundary conditions were distributed over a number of adjacent nodes.

Finally, elements using hybrid formulation were found to give a more stable response than non-hybrid elements. Usually hybrid elements are intended for use with almost incompressible material behavior when a very small displacement produces extremely large changes in pressure. In this situation, a purely displacement-based solution is too sensitive to be used numerically. With the hybrid formulation, this singularity is removed from the system by treating the pressure stress independently. Hybrid element have more internal variables and are slightly more expensive but they showed better results when used with the concrete material model as shown later in this chapter.

#### **4.4. Finite Element Analysis Methods for Bridges**

There are different analytical methods to analyze bridge superstructure. In the past decade, with the increase of computational power, these methods have improved in accuracy and computation time; however, each theoretical method varies with regard to approach, assumptions and limitations and therefore varies a lot in their applicability. While some methods focus on the overall behavior of the structure, others concentrate on the modeling of parts of the bridge, such as a girder, etc. These different methods have been presented in details in chapter 2.

In this study, a three-dimensional model was selected to investigate the behavior of the considered bridges. As shown in Figure 4.3, the web and flanges of steel girders are modeled with 4-node shell elements. Each node has six degrees of freedom (three in translation and three in rotation). The reinforced concrete deck slab is modeled using 8-node brick element, each node having three degree of freedom. Each reinforcing rebar is modeled by means of truss elements embedded into the deck slab at their exact depth and with accurate spacing. Since this study concentrated on stress distribution within the reinforced concrete deck slab, special attention was paid to the meshing process. As shown later in this chapter, it was observed that with this particular type of element, in a nonlinear analysis, four layers of elements were giving good results in terms of stress/strain distribution and load/deflection behavior. The structural effects of the secondary members such as sidewalk and parapet were also taken into account in the finite element model of the tested bridge. As shown in Figure 4.3, transverse bracing and cross framed diaphragms were also modeled using truss elements.

#### **4.5. Material Models**

The two materials used in this research are concrete and steel; reinforcing steel is used for the rebars and structural steel is used for the girders. Rather than attempting to

develop complicated material models with a complete mechanical description of the behavior of concrete, reinforcement, as well as their interaction, the built-in material models available in ABAQUS were used in this study. These models efficiently represent the main parameters governing the response of structural concrete.

#### 4.5.1. Material Model for Concrete

The concrete model used in this study is the concrete damaged plasticity model available in ABAQUS. This model is based on the assumption of isotropic damage and is designed for applications in which concrete is subjected to arbitrary loading conditions. The model takes into consideration the degradation of the elastic stiffness induced by plastic straining both in tension and compression.

The model assumes that the main two failure mechanisms are tensile cracking and compressive crushing of concrete. The evolution of the failure surface is controlled by two variables,  $\varepsilon_t^{pl}$  and  $\varepsilon_c^{pl}$ , which are referred to as tensile and compressive equivalent plastic strains, respectively.

In this study, the Poisson coefficient ( $\nu$ ) of 0.15 was used for concrete and the concrete density of 150 PCF was used in the computation of the dead load.

##### 4.5.1.1 Uniaxial Tension Behavior

Tensile behavior of concrete is a key factor in serviceability considerations such as the assessment of crack spacing and crack width, concrete and reinforcement stresses and deformations. The stress-strain response of a concrete member in uniaxial tension, Figure 4.4, is initially almost linear elastic. Near the peak load, the response softens due to microcracking, and, as the tensile strength is reached, a crack forms. However, the tensile stress does not instantly drop to zero; instead the carrying capacity decreases with increasing deformation, i.e. a strain-softening or quasi brittle behavior can be observed.

Hillerborg (1976) introduced the “fictitious crack model” after which the ABAQUS model is developed. Under uniaxial tension the stress-strain response follows a linear elastic relationship until value of the failure stress,  $\sigma_{t0}$ , is reached. The postfailure behavior is modeled with the “tension stiffening” option available in ABAQUS which allows the user to define the strain-softening behavior for cracked concrete (See Figure 4.5).

The tension stiffening is very important not only to define the postcracked behavior of concrete, but also to model its interaction with the reinforcing rebars in a simple manner. Tension stiffening can be specified by means of postfailure stress-strain relation or by applying a fracture energy cracking criterion, as discussed below.

In reinforced concrete, the postfailure behavior is described by the postfailure stress expressed as a function of the cracking strain,  $\varepsilon_t^{ck}$ . The cracking strain, as illustrated in Figure 4.6, is defined as the total strain minus the elastic strain; that is  $\varepsilon_t^{ck} = \varepsilon_t - \varepsilon_t^{el}$ , where  $\varepsilon_t^{el} = \sigma_t / E$ . Estimation of the needed tension stiffening depends of several factors such as the density of reinforcement, quality of the bond between rebar and concrete, relative size of concrete aggregate compared to the rebar diameter, and the mesh. A reasonable starting point for a typical reinforced concrete structure modeled with a fairly detailed mesh is to assume that the strain softening after failure reduces the stress linearly to zero at a total strain of about 10 times the strain at failure. However, the ABAQUS manual advices that this parameter should be calibrated for each particular case and moreover that, in some cases, the specification of a postfailure stress-strain relationship introduces unreasonable mesh sensitivity in the results, especially if cracking occurs in localized regions. Therefore, a second approach is available, the fracture energy cracking criterion first defined by Hilleborg (1976). Hilleborg defined the energy required to open a unit area of crack,  $G_f$ , as a material parameter using brittle mechanics concepts. With this approach the concrete behavior is described by a stress-displacement response rather than a stress-strain response. Under tension, a concrete specimen cracks across some

section. After it has been pulled apart sufficiently for most of the stress to disappear, its length is determined primarily by opening of the crack. The opening does not depend on the specimen length. In this model, the postfailure stress is specified as a tabular function of cracking displacement, as shown in Figure 4.7. Alternatively, the fracture energy can be specified directly as a material property, but then a linear loss of strength after cracking, as shown in Figure 4.8, is assumed. The cracking displacement at which complete loss of strength takes place is, therefore,  $u_{t0} = 2G_f / \sigma_{t0}$ . Recommended values of fracture energy  $G_f$  range from 0.22 LB/IN to 0.67 LB/IN.

The ABAQUS manual (2004) stresses the importance of the tension stiffening parameters since, generally, more tension stiffening makes it easier to obtain numerical solutions. Too little tension stiffening will cause the local cracking failure in concrete to introduce temporarily unstable behavior in the overall response of the model.

In this study, the tension stiffening was modeled using the stress-displacement approach proposed by Hillerborg. The postfailure stress was defined as a bilinear function of cracking displacement as shown in Figure 4.9. As a first approximation, the cracking displacement of point  $b$ ,  $u_b$  in Figure 4.9, is obtained using the fracture energy cracking criterion described by the equation  $u_b = 2G_f / \sigma_{t0}$ . Instead of defining the stress value of point  $b$ ,  $\sigma_b$ , equal to zero, as it would be the case in the traditional fracture energy cracking criterion,  $\sigma_b$  is set equal to a percentage of the cracking stress,  $\sigma_{t0}$  (between 10 to 20%). Then, a third point, point  $c$  in Figure 4.9, is defined to complete the bilinear tension stiffening. Usually, cracking displacement of point  $c$ ,  $u_c$ , is set as twice the cracking displacement  $u_b$ , and the stress value of point  $c$ ,  $\sigma_c$  is set at 1% of  $\sigma_{t0}$  (minimum stress value that can be input in this model). If numerical solutions cannot be obtained with these parameters,  $u_b$  and  $u_c$  can be increased as shown in Figure 4.9.

#### 4.5.1.2 Uniaxial Compression Behavior

Under uniaxial compression concrete has a linear response until the value of initial yield is reached,  $\sigma_{c0}$ . In the plastic regime, the response is typically characterized by stress hardening up to,  $\sigma_{cu}$ , followed by a decrease of the carrying capacity with an increase of deformation, i.e. strain softening in compression, as shown in Figure 4.10.

In this study, the compressive stress-strain curve was based on the model proposed by Hognestad (1951). The ascending branch is modeled with a parabolic function and the descending branch is modeled with a linear function. Figure 4.11 shows the stress-strain relationship of the conventional concrete by Hognestad. The following equations represent the model:

$$\text{For } 0 \leq \varepsilon_c < \varepsilon_0 \quad f_c = f'_c \left[ 2 \left( \frac{\varepsilon_c}{\varepsilon_0} \right) - \left( \frac{\varepsilon_c}{\varepsilon_0} \right)^2 \right] \quad (4.1)$$

$$\text{For } \varepsilon_0 \leq \varepsilon_c < \varepsilon_0 \quad f_c = f'_c [1 - Z(\varepsilon_c - \varepsilon_0)] \quad (4.2)$$

where  $\varepsilon_c$  = strain in concrete at any particular point,  $f_c$  = stress in concrete corresponding to  $\varepsilon_c$ ,  $f'_c$  = maximum compressive stress,  $\varepsilon_0$  = strain corresponding to  $f'_c$ , taken as  $2f'_c/E_c$ , and  $Z$  = slope of the descending branch. The values of constants [ $f'_c$ ,  $\varepsilon_0$ ,  $Z$ ] in Eqs. (4.1) and (4.2) used in this research are listed in Chapter 5.

To define the stress-strain behavior of plain concrete in uniaxial compression outside the elastic range, ABAQUS requires the user to input a tabular data of the compressive stress as a function of the inelastic strain,  $\varepsilon_c^{in}$ . As illustrated in Figure 4.12, the compressive inelastic strain is defined as the total strain minus the elastic strain, that is  $\varepsilon_c^{in} = \varepsilon_c - \varepsilon_c^{el}$ , where  $\varepsilon_c^{el} = \sigma_c / E$  and the elastic modulus  $E$  is calculated using the following equation:

$$E = 57,000 \sqrt{f'_c} = 3605 \text{ KSI} \quad (4.3).$$

#### 4.5.1.3 Concrete Plasticity

One of the main parameters which define the concrete damaged plasticity model of ABAQUS is the yield function. The yield surface makes use of two stress invariants of the effective stress tensor, the hydrostatic pressure stress.

$$\bar{p} = -\frac{1}{3} \text{trace}(\bar{\sigma}) \quad (4.4)$$

where the effective stress tensor is defined as:

$$\bar{\sigma} = D : (\varepsilon - \varepsilon^{pl}) \quad (4.5)$$

and the Huber-Mises equivalent effective stress.

$$\bar{q} = \sqrt{\frac{3}{2} (\bar{S} : \bar{S})} \quad (4.6)$$

where  $\bar{S}$  is the effective stress deviator, defined as  $\bar{S} = \bar{\sigma} + \bar{p}I$

The model makes use of the yield function of Lubliner et al. (1989), with the modifications proposed by Lee and Fenves (1998) to account for different evolution of strength under tension and compression. This yield criterion based on the Mohr-Coulomb and Drucker-Prager yield criterion presented in Figure 4.13 take into account the fact that an increase in hydrostatic compressive stress produces an increased ability of concrete to resist yield. Also, concrete exhibits different yield stresses in tension and compression. The Mohr-Coulomb and the Drucker-Prager yield criteria are a generalization of the Tresca and Huber-Von Mises criteria respectively that accounts for the influence of hydrostatic stress.

In terms of effective stresses (Equation 4.5), the yield function takes the form

$$F = \frac{1}{1-\alpha} \left( \bar{q} - 3\alpha \bar{p} + \beta \left( \varepsilon_t^{ck} \right) \left( \bar{\sigma}_{\max} \right) - \gamma \left( -\bar{\sigma}_{\max} \right) \right) - \bar{\sigma}_c \left( \varepsilon_c^{in} \right) = 0 \quad (4.7)$$

with

$$\alpha = \frac{(\sigma_b / \sigma_c) - 1}{2(\sigma_b / \sigma_c) - 1}; 0 \leq \alpha < 0.5$$

$$\beta = \frac{\bar{\sigma}_c \left( \varepsilon_c^{in} \right)}{\bar{\sigma}_t \left( \varepsilon_t^{ck} \right)} (1 - \alpha) - (1 + \alpha)$$

$$\gamma = \frac{3(1 - K_c)}{2K_c - 1}$$

Here,  $\bar{\sigma}_{\max}$  is the maximum principal effective stress,  $\sigma_b / \sigma_c$  is the ratio of equibiaxial compressive yield stress to uniaxial compressive yield stress, and  $K_c$  is the ratio of the second stress invariant on the tensile meridian ( $q_{(T.M.)}$  on Figure 4.14) to that on the compression meridian ( $q_{(C.M.)}$  on Figure 4.14), at initial yield for any given value of the pressure invariant  $p$  such that the maximum principal stress is negative; it must satisfy the condition  $0.5 < K_c \leq 1$ . Typical yield surfaces are shown in Figure 4.14 for the deviatoric plane and Figure 4.15 for plane stress conditions.

#### 4.5.2. Modeling of Reinforcement in FEM

In order to correctly analyze the behavior of reinforced concrete deck slab, it was very important to properly and accurately represent the different reinforcement configurations of each different deck such as, rebar diameter, rebar spacing and rebar depth. Up until now, most of the Finite Element softwares were modeling rebar by means of “layer” whose thickness,  $t$ , was calculated as a function of the rebar cross section area,  $A$ , and rebar spacing,  $s$ , using the equation  $t = A/s$ . These layers were then integrated in the stiffness matrix of the model to represent the effect of reinforcement on the structure behavior. This method was proved to be accurate to describe the overall behavior of the

structure but was not precise enough to accurately measure the stresses in the rebar. Since it is significant for this research to be able to read precisely these stresses, a new approach is proposed. Each individual rebar is modeled using a one dimensional truss element with a circular cross section area equal to the area of each rebar. They are defined with the metal plasticity model presented in the next paragraph to describe the behavior of the rebar material and are embedded in the mesh of a 8-node brick element used to model the concrete. With this modeling approach, the concrete behavior is considered independently of the rebar. The embedded element technique in ABAQUS is used to specify that an element or group of elements, the steel rebars, lies embedded in the host element, the concrete deck slab as shown in Figure 4.16. ABAQUS will search for the geometric relationships between nodes of the embedded elements and the host elements; if a node of an embedded element lies within a host element, the degree of freedom of that node is eliminated and the node becomes an embedded node. The degrees of freedom of the embedded node are constrained to the interpolated values of the degrees of freedom of the host element.

Effects associated with the rebar/concrete interface, such as bond slip, are modeled approximately by introducing some tension stiffening into the concrete modeling, as presented earlier, to simulate load transfer across cracks through the rebar. Defining rebar as element by itself is a tedious and complex job but essential to correctly capture the behavior of the concrete deck slab.

### **4.5.3. Material Model for Steel**

#### **4.5.3.1 Steel in Tension**

The stress-strain characteristics of reinforcing steel used as reinforcing steel (hot-rolled low-carbon steel bar), in tension, Figure 4.17, exhibits an initial linear elastic

portion,  $\sigma_s = E_s \varepsilon_s$ , a yield plateau at  $\sigma_s = f_y$  beyond which the strain increases with little or no change in stress, and a strain-hardening range until rupture occurs at the tensile strength,  $\sigma_s = f_{su}$ . Various steel grades are usually defined in terms of yield strength  $f_y$ . The extension of the yield plateau depends on the steel grade; its length generally decreases with increasing strength. In the present work, since the behavior of the reinforced concrete deck slab is not studied after yielding of the rebar, a perfect plastic idealization of the stress-strain response of reinforcement is sufficient for this study (Figure 4.18). Therefore, only the Young modulus  $E_s$ , whose nominal value is taken as 29,000 KSI, and the yielding stress, whose nominal value is equal to 60 KSI, need to be inputted into ABAQUS.

#### 4.5.3.2 Plasticity and Yield Surface

Perfect plasticity means that the yield stress does not change with plastic strain. The Von Mises yield surfaces are used in the model. As shown in Figure 4.19 it assumes that yielding of the metal is independent of the equivalent pressure stress, observation which is confirmed experimentally for most metals. This model, although quite simple is accurate enough for the present, as shown in the material verification part below.

### 4.6. Solution Methods

ABAQUS combines incremental and iterative procedures for solving nonlinear problems. These procedures involve the following principles:

- The Newton-Raphson method to solve nonlinear equations
- The determination of convergence
- The definition of loads as a function of time
- The automatic choice of time increment

The objective of the analysis is to determine the nonlinear load-displacement curve for a structure as shown in Figure 4.20. In a nonlinear analysis the solution cannot be calculated by solving a single system of linear equations, as it would be done in a linear problem. Instead, the solution is found by specifying the loading as a function of time and incrementing time to obtain the nonlinear response. Therefore, the simulation is divided into a number of time increments and finds the approximate equilibrium configuration at the end of each time increment. Using the Newton-Raphson method, it often takes ABAQUS several iterations to find an acceptable solution for each time increment.

#### 4.6.1. The Newton-Raphson Method

Newton and Raphson used ideas of the calculus to generalize an ancient method to find the zeros of an arbitrary equation  $f(x) = 0$ . The underlying idea is the approximation of the function  $f(x)$  by the tangent lines as shown in Figure 4.21. Let  $r$  be a root (also called a "zero") of  $f(x)$ , that is  $f(r) = 0$ . Assume that  $f'(r) \neq 0$ . Let  $x_1$  be a number close to  $r$  (which may be obtained by looking at the graph of  $f(x)$ ). The tangent line to the graph of  $f(x)$  at  $(x_1, f(x_1))$  has  $x_2$  as its  $x$ -intercept. From Figure 4.21, we see that  $x_2$  is getting closer to  $r$ . Easy calculations give

$$x_2 = x_1 - \frac{f(x_1)}{f'(x_1)} \quad (4.8)$$

Since we assumed  $f'(r) \neq 0$ , we will not have problems with the denominator being equal to 0. We continue this process and find  $x_3$  from the equation

$$x_3 = x_2 - \frac{f(x_2)}{f'(x_2)} \quad (4.9)$$

This process generates a sequence of numbers  $\{x_n\}$  that approximate  $r$ . This technique of successive approximations of real zeros is called Newton-Raphson Method.

#### **4.6.2. Steps, Increments and Iterations**

Since these terms will be used often in the next paragraph, it is important for the reader to understand the differences between a step, an increment and an iteration. A step is a subdivision of the time history of a simulation. Each step, defined by the user, consists of an analysis procedure options, loading options, etc... Different loads, boundary conditions, analysis procedures can be defined in each step. An increment is a subdivision of a step. In nonlinear analysis each step is divided in increments so that a nonlinear solution can be calculated. The user suggests to the software the size of the first increment, and ABAQUS automatically chooses the size of the subsequent increments. The user can also define a maximum and a minimum for the size of increments. An iteration is an attempt at finding an equilibrium solution within an increment. If the model is not in equilibrium at the end of the iteration, ABAQUS tries another iteration. If after a given number of iterations equilibrium is not reached, the software may reduce the increment size and try to find a solution.

#### **4.6.3. Convergence and increments**

Consider the external forces,  $P$ , and the internal (nodal) forces,  $I$ , acting on a body as shown in Figure 4.22. The internal loads acting on a node are caused by stresses in the elements that are attached to that node. The body is in equilibrium if and only if the summation of forces at each node is equal to zero, therefore the basic equation of equilibrium is  $P-I = 0$ .

In the analysis, the load is increased by a small increment  $\Delta P$  and a correction displacement,  $c_a$ , is calculated for the structure using  $\Delta P$  and the structure's tangent stiffness,  $K_0$ , which is based on the structure configuration at  $u_0$  (see Figure 4.23), in the equilibrium equation:

$$[K]\{u\} = \{F\} \quad (4.10)$$

Where  $[K]$  is the overall stiffness matrix,  $\{u\}$  is the vector of unknown nodal displacements, and  $\{F\}$  is the vector of applied equivalent forces on the system. Using  $c_a$ , the structure configuration is updated to  $u_a$  ( $u_a = u_0 + c_a$ ). Then, the software computes the structure's internal forces,  $I_a$ , for this new configuration. The difference between the applied load and  $P$ , and  $I_a$  is calculated as,  $R_a = P - I_a$  where  $R_a$  is the residual force for this iteration. If  $R_a$  is zero at every degree of freedom in the model, point a in Figure 4.23 would be on the load deflection curve and the structure would be in equilibrium. In a nonlinear problem,  $R_a$  will never be exactly zero, so it is compared to a tolerance value specified by the user. If  $R_a$  is less than this residual tolerance at all nodes, the solution is accepted as being in equilibrium. In this study the tolerance was set at 0.5% of the average force in the structure as recommended by the ABAQUS manual.

If  $R_a$  is less than the current tolerance value,  $P$  and  $I_a$  are considered to be in equilibrium and  $u_a$  is a valid equilibrium configuration for the structure. However, before ABAQUS accepts the solution, it also checks that the last displacement correction,  $c_a$ , is small relative (less than 1% in this study) to the total incremental displacement. Both convergence checks must be satisfied before a solution is said to have converged.

If one of the checks does not converge, ABAQUS performs another iteration to try to bring the internal and external forces into balance. First, a new stiffness matrix,  $K_a$ , is computed for the structure based on the updated configuration,  $u_a$ . Using this new stiffness with the residual  $R_a$  in the equation 4.9 above, we obtain another displacement

correction,  $c_b$  that brings the system closer to equilibrium as shown in Figure 4.24. A new force residual,  $R_b$ , is calculated using the internal forces from the structure's new configuration,  $u_b$ . Again, the largest force residual at any degree freedom is compared against the force residual tolerance, and the displacement correction for the second iteration,  $c_b$ , is compared to the increment of displacement. If necessary, further iterations are performed.

For each iteration, ABAQUS forms the stiffness matrix of the structure and solves the system of equations  $[K]\{u\} = \{F\}$  as it would do for a linear analysis. Therefore, the computational cost of each iteration is very similar to the cost of a complete linear analysis; and since numerous iterations are needed to obtain a solution, computational time for a nonlinear analysis can be many times greater than the computational time of a linear analysis. For example in this study, some analysis took as long as 24 hours of computational time. The number of iterations needed to find a converged solution for a time increment will vary depending on the degree of nonlinearity of the problem. With the default incrementation control, if the solution has not converged after 16 iterations or if the solution appears to diverge, the program stops the increment and starts again with a new increment size set to 25 % of its previous value. If the solution still fails to converge, the increment size is reduced again. This process is continued until a solution is found. If the time increment becomes smaller than the minimum defined by the user or more than 5 attempts are needed, the program stops the analysis. If two consecutive increments converge in less than 5 iterations, the program automatically increases the increment size by 50%. Those default automatic incrementation controls were used for this study but could be adjusted for a given problem.

## **4.7. Material Model Verification**

### **4.7.1. Example 1: One Way Reinforced Concrete Slab**

#### 4.7.1.1 Problem Description

Jain and Kennedy (1974) performed an extensive test program on reinforced concrete slab. Their research was aimed to develop a precise knowledge of the yield criterion for slab. One of the specimens they tested is a 30 IN long by 18 IN wide slab as shown in Figure 4.25. The specimen is 1.5 IN thick. The reinforcement consist of plain mild steel BB rods with an  $3/16$  IN diameter spaced at 2.57 IN longitudinally and spaced at 2.15 IN transversely. The first layer of steel (longitudinal steel) was placed at  $3/16$  IN clear cover, and the second layer (transversal steel), orthogonal to the first, was placed directly over the first. Both ends of each reinforcing bar were hooked as a safeguard against bond failure. The slab was loaded with an uniaxial moment generated by means of two uniformly distributed line loads across the slab width and symmetrically placed about the middle line of the slab at 6 IN of each support.

#### 4.7.1.2 Modeling and Material Properties

The symmetry of the slab problem suggests that only half of the slab needs to be modeled. 8-nodes linear brick elements with reduced integration are used to model the concrete. As described earlier in this chapter, the enhanced hourglass control and hybrid formulation are used for this element. Because bending is the primary mode of deformation, a minimum of four elements are needed through the thickness of the model to capture the response adequately and to have enough stress calculations points so that the response is reasonably smooth. 21 elements are used along the half slab and 26 elements are used transversely (Figure 4.26). In order to avoid stress concentration at the support, an additional row of element is added behind the support. As shown in picture Figure 4.27, the reinforcing bars were modeled using truss element and were embedded into the slab elements. Perfect bond between concrete and the rebars was assumed.

The concrete damaged plasticity described earlier was used to implement the material properties into the Finite Element Program. The compressive strength of concrete,  $f'_c$ , was 4700 PSI, and the stress-strain curve was modeled using the Honegstad model described earlier (Figure 4.28). The postfailure stress was defined as a bilinear function of the cracking displacement curved with  $\sigma_t = 300$  PSI,  $\sigma_b = 50$  PSI,  $u_b = 0.01$  IN,  $\sigma_c = 3$  PSI and  $u_c = 0.1$  IN. The steel was modeled with a perfect plastic curve.

#### 4.7.1.3 Solution Control Parameters and Loading

Reinforced concrete solutions involve regimes where the load displacement response is unstable. The Riks procedure available in ABAQUS is designed to overcome difficulties associated with obtaining solution during the unstable phases of the response. It assumes proportional loading and develops the solution by stepping along the load-displacement equilibrium line with the load magnitude included as an unknown. In this particular example, the analysis was run in displacement control. The total imposed displacement was equal to 0.3 IN and the first increment was set at 0.1% of this total displacement. The load was measured at the support and the deflection was measured at midspan.

#### 4.7.1.4 Analysis Results

As we can see in the Figure 4.29, the results between the experiment and the Finite Element Model are in very good agreement in term of moment versus deflection. The Finite Element Model exhibits a slightly stiffer behavior in the post-cracking portion of the curve, but despite this, the program is still able to accurately capture the cracking and yielding load. The deformed shape of the slab is shown in Figure 4.30.

## 4.7.2. Two Way Reinforced Concrete Slab

### 4.7.2.1 Problem Description

McNeice (1967) carried out a number of tests on two way slab. The modeled slab was 36 IN square by 1.75 IN thick with an isotropic mesh of 0.85% placed at a depth of 1.31 IN. The slab was supported at four corners and tested under a central load. The deflection was measured at several points at the edge of the slab and close to the center of the slab shown as points a, b, c, and d in Figure 4.31.

### 4.7.2.2 Modeling and Material Properties

The symmetry of the slab suggests that only a quarter of the slab needs to be modeled. As in the one way slab, 4 layers of 8-nodes linear brick elements with reduced integration are used to model the concrete. The enhanced hourglass control and the hybrid formulation are also used in this problem. In order to avoid stress concentration, one more row of element was added on the two external edges, behind the support, and rather than using a concentrated load, a pressure load was applied on a circular surface element of 1.5 IN diameter as shown on Figure 4.32. As shown in Figure 4.33 the reinforcing bars were modeled using truss element and were embedded into the slab elements. Perfect bond between concrete and the rebars was assumed.

The concrete damaged plasticity described earlier was used to implement the material properties into the Finite Element Program. The compressive strength of concrete,  $f'_c$ , was 5500 PSI, and the stress-strain curve was modeled using the Honegstad model described earlier. The postfailure stress was defined as a bilinear function of the cracking displacement curved with  $\sigma_t = 250$  PSI,  $\sigma_b = 25$  PSI,  $u_b = 0.005$  IN,  $\sigma_c = 3$  PSI and  $u_c = 0.1$  IN. The steel was modeled with a perfect plastic curve.

#### 4.7.2.3 Solution Control Parameters and Loading.

Again in this example the solution involves regimes where the load displacement response is unstable. Therefore The Riks procedure available in ABAQUS is applied as well in this example to overcome difficulties associated with obtaining solution during the unstable phases of the response. In this particular example, the analysis was run in load control. A 3.2 KIP load was applied on the circular element described earlier and the first increment was set at 0.5 % of this total load. Deflections were measured at the four locations shown in Figure 4.31.

#### 4.7.2.4 Analysis Results

Results obtained from each measured point, listed as points a, b, c, and d are shown in Figure 4.34, Figure 4.35, Figure 4.36, and Figure 4.37, respectively. The results between the experiment and the Finite Element Model are in very good agreement in terms of load versus deflection. Again, the Finite Element Model exhibits a slightly stiffer behavior in the cracked part of the curved, but despite this, the program is still able to accurately capture the behavior of the slab. The deformed shape of the slab is shown in Figure 4.38.

### **4.7.3. Composite Bridge**

#### 4.7.3.1 Problem Description

This model test bridge was studied experimentally by Newmark et al (1946) and his results have been used by numerous authors to verify their model. The structure is a quarter scale model of a 15 FT simply supported steel I-beam bridge with five girders spaced at 18 IN. The girders are 8 IN- 6.5 LB Junior beam, the slab is 1 3/4 IN thick and made composite with the girder. The slab was reinforced with four layers of 1/8 IN

diameter rebars; two orthogonal layers at the top and two orthogonal at the bottom with a clear cover of 1/3 IN. The top longitudinal rebars are spaced at 6 IN, the top transversal at 1.9 IN, the bottom longitudinal at 2 IN and the bottom transversal at 1.25 IN. In this example, the test was carried out into the post-elastic range as well, thus, providing a means of comparison for the proposed Finite Element Model with experimental results. The bridge was loaded with four concentrated loads simulating the rear wheel of two trucks, as shown in Figure 4.39, placed at midspan. These four loads were applied by means of a crew-jack bearing against a steel frame which was anchored to the floor. Deflections were recorded at each girder at the same transverse section at which the loads were applied.

#### 4.7.3.2 Modeling and Material Properties

In this example, three layers of 8-node linear brick elements with reduced integration are used to model the concrete. The enhanced hourglass control and the hybrid formulation are also used in this problem. The girders were modeled with 4-node linear shell elements using reduced integration scheme. The enhanced hourglass control was enabled for these elements as well. The girders are modeled fully composite with the deck. In order to avoid stress concentration, one more row of element was added behind the support, and rather than using concentrated loads, a pressure load was applied on circular surface elements of 3.75 IN diameter as shown on Figure 4.40. As shown in Figure 4.41 the reinforcing bars were modeled using truss element and were embedded into the slab elements. Perfect bond between concrete and the rebars was assumed.

The concrete damaged plasticity described earlier was used to implement the material properties into the Finite Element Program. The compressive strength of concrete,  $f'_c$ , was 3000 PSI, and the stress-strain curve was modeled using the Honegstad model described earlier. The postfailure stress was defined as a bilinear function of the

cracking displacement curved with  $\sigma_t = 400$  PSI,  $\sigma_b = 100$  PSI,  $u_b = 0.0035$  IN,  $\sigma_c = 4$  PSI and  $u_c = 0.1$  IN. The steel was modeled with a perfect plastic curve. The yield stress was 45 KSI for the rebars and 41 KSI for the beams.

#### 4.7.3.3 Solution Control Parameters and Loading.

Again in this example the solution involves regimes where the load displacement response is unstable. Therefore The Riks procedure available in ABAQUS is applied as well in this example to overcome difficulties associated with obtaining solution during the unstable phases of the response. In this example, the analysis was run in load control. A 11 KIP load was applied on each of the four the circular element described earlier and the first increment was set at 0.1 % of this total load. Deflections at midspan of each girder were measured.

#### 4.7.3.4 Analysis Results

As we can see in Figure 4.42 to Figure 4.46 for girder A to girder E respectively, the results between the experiment and the Finite Element Model are in very good agreement in term of load versus deflection. This example proves that the modeling technique and the material model used in this study are accurate and efficient enough to precisely predict the reinforced concrete deck slab behavior. The deformed shape of the slab is shown in Figure 4.47

## **4.8. Parameters Influencing Bridge Analysis**

### **4.8.1. Boundary Conditions**

Only simply supported bridges were considered in this study. However in older bridges, especially steel girder bridges, corrosion of the bearings usually causes

additional constraints for both rotations and longitudinal displacements. The effect of boundary conditions on the structure behavior were observed and reported by numerous authors (Bakht and Jaeger 1988, 1992, Schultz et al. 1995). They reported that small modifications in the boundary conditions have considerable effect in the bridge behavior. During field test conducted at the University of Michigan by Nowak et al. (1998, 2000, 2001, 2002) large amount of compressive strain were observed and recorded near support of simply supported bridge. This partial fixity has an effect to significantly reduce the moment at midspan. Huria et al. (1993) even concluded that model parameters describing the boundary conditions are observed as more critical than material parameters.

Therefore, it is important in this research to take in consideration the effect of the boundary conditions and try to estimate its effects on the reliability of the reinforced concrete bridge deck. The results obtained during the field test described in chapter 3 were used to calibrate these boundary conditions. Three cases of boundary condition were considered in the Finite Element Model of the tested bridge as shown in Figure 4.48. In Figure 4.48 (a), the supports are modeled with a hinge and a roller. In Figure 4.48 (b), both supports are hinged. In Figure 4.48 (c), in order to model the support conditions of the in-situ bridge, a simple modification of support condition is proposed. This was done by assuming the rotational friction at the supports of the target bridge to be small enough and by attaching a horizontal spring, of stiffness  $k$ , to the roller supports of the bridge. The magnitude of stiffness  $k$  was calibrated using field measurement. Details of the calibration are explained in Section 4.9.

#### **4.8.2. Composite Action**

In composite section, both the concrete section and the steel section acts together to resist moments due to live load whereas in non-composite section, only the girders are taken into account to estimate the maximum stress induced by bending. In reinforced

concrete deck bridges supported by steel girder, composite action is present when there is no slippage between the bottom face of the slab and the top flange of the girder.

Composite action changes the position of the neutral axis of the section and increases its moment of inertia; therefore it increases the stiffness and decreases the maximum compression bridge. In modern bridge, shear stud are used to guarantee the composite action, but it was observed during field test (Schultz, 1995; Nowak, 1998) that even in older bridges, designed as non-composite, the bond between concrete and steel is usually enough to carry shear forces induced by dead load and live loads. Consequently, full composite action was assumed in the Finite Element Analysis.

#### **4.8.3. Effect of non structural members**

Sidewalks, railing, parapet and diaphragm are considered as non-structural member. Their influence on girder distribution was first investigated by Mabsout, Tarhini, and Kobrosly (1997). They concluded that the presence of sidewalks and railings could increase the load carrying capacity by as much as 30% if included in the strength evaluation of bridges. Eamon (2000), found that in terms of load distribution, when considering bridges with barrier plus diaphragms and barrier plus sidewalk plus diaphragm, girder distribution is decreased at ultimate capacity from 5%-20% in most cases. Eom (2001) observed that the contribution of bending moment from the concrete slab can increase from 4% to 16% if sidewalks are included on both side of the bridge deck.

Therefore, in this study, when calibrating the Finite Element Model to the field test results, the effect of parapet was included as shown in Figure 4.3. Barriers were not included because they were not continuous with the slab. However in the Finite Element Analysis used for the reliability study and presented in the next chapter, sidewalk, parapet and barrier were not modeled to try to reduce computational time of the simulations.

#### 4.9. Calibration of the Finite Element Models

The calibration process is used to determine unknown model parameters, by comparing calculated data with available field test data. In this study, the calibration process was used mainly to evaluate the boundary conditions. The tested bridge, presented in chapter 3, was modeled using 4-node linear shell element for the girders and 8-node linear brick element for the deck as described earlier (Figure 4.49). Full composite action was assumed. Reinforcement was precisely included in the model according to the information obtained from the drawings of the bridge as shown in Figure 4.51 to Figure 4.54. Total bond is assumed between the rebars and the concrete. The material models for concrete and steel described earlier were also applied. As shown in Figure 4.49 and Figure 4.50, the parapet and the cross frame bracing were modeled using brick and truss elements respectively. Full composite action between the girder and the concrete deck was assumed.

The load was applied in form of one 11-axle, three-unit truck, the same as the one used during the field test and described in Chapter 3. The input data included axle loads and axle spacings. Instead of using concentrated load for the axle, each tire contact area is modeled by a rectangle of 20 IN by 10 IN as shown in Figure 4.55 and the load due to each axle is modeled as a pressure, applied on the contact area, and equal to the axle load divided by two, to obtain the wheel load, and then divided by the area of the contact area ( $200 \text{ IN}^2$ ). These rectangles are modeled using surface elements, which have the particularity to not have any cross section property therefore they do not contribute to the total stiffness of the bridge. Moreover, by using this method, stress concentrations are avoided which was a recurrent problem when using concentrated load. A general view of the truck load applied in the model is shown in Figure 4.55.

The trucks were positioned as in the field test. The transverse position of the trucks was as measured during the actual test. The longitudinal position of the truck was

calculated as the position producing the maximum bending moment where the strain transducers were located.

The stiffness of the spring used to model partial fixity of the support, as shown in Figure 4.48 (c), was calibrated by comparing the strain value measured during field test to the strain value calculated by the Finite Element Analysis. Figure 4.57 shows the spring used in the FE Model. In the case of a truck in the center of north lane, strain values obtained from FE model for the bottom flanges of a girder at approximately one third of the span as well as near support, are presented in Figure 4.58 and Figure 4.59, respectively. A view of the corresponding displaced shape of the bridge is shown in Figure 4.60. These obtained strains were then compared with the field test results. This comparison is made for each of the five transversal positions of the truck investigated during the field test and results are shown in Figure 4.61 to Figure 4.72. In each case, the upper curve represents the calculated values for a simple support with free longitudinal displacement at one end. The simple support condition is usually assumed by designers in the design process. Comparison with test results shows that for such boundary conditions, the resulting strains values were much greater than the actual measured strains. In the case where the longitudinal displacement is completely restrained at the bottom flange, calculated strains are lower than the actual measured strains (lower curve in Figure 4.61 to Figure 4.72). Therefore, the boundary condition of the actual bridge is, as expected, in between these two boundary conditions. It was very difficult to find a configuration satisfying both the data near support and the data close to third span; however, after several trials, a stiffness  $k = 2000 \text{ KIP/IN}$  was found to be an acceptable value to model the partial fixity of the boundary conditions, as can be seen in Figure 4.61 to Figure 4.72.

A sixth fictitious position was also created by superposing the results of the truck on the north lane plus the results of the truck on the south lane. Since previous field test conducted with two trucks (Nowak et al. 1998, 2000, 2001, 2002) showed that the response of most bridges is still elastic at such load, these results are assumed to be

equivalent to those which would have been obtained with two trucks placed in the center of the two traffic lanes simultaneously. Results of this fictitious position are shown in Figure 4.73 and Figure 4.74. This also confirmed the accuracy of the selected stiffness value.

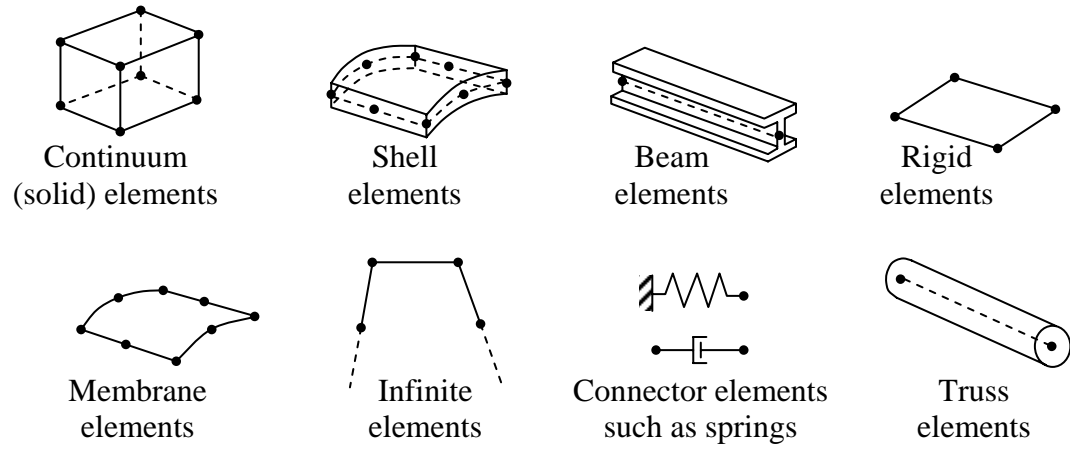


Figure 4.1 Commonly used element families

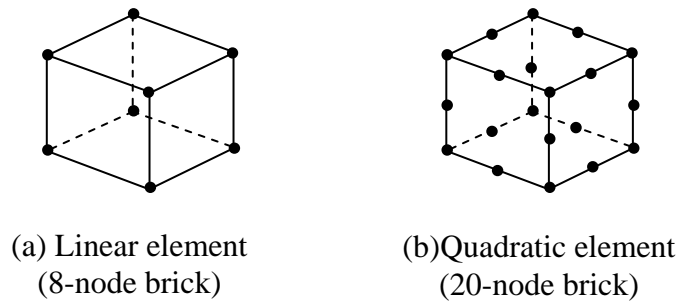


Figure 4.2 Linear and quadratic brick

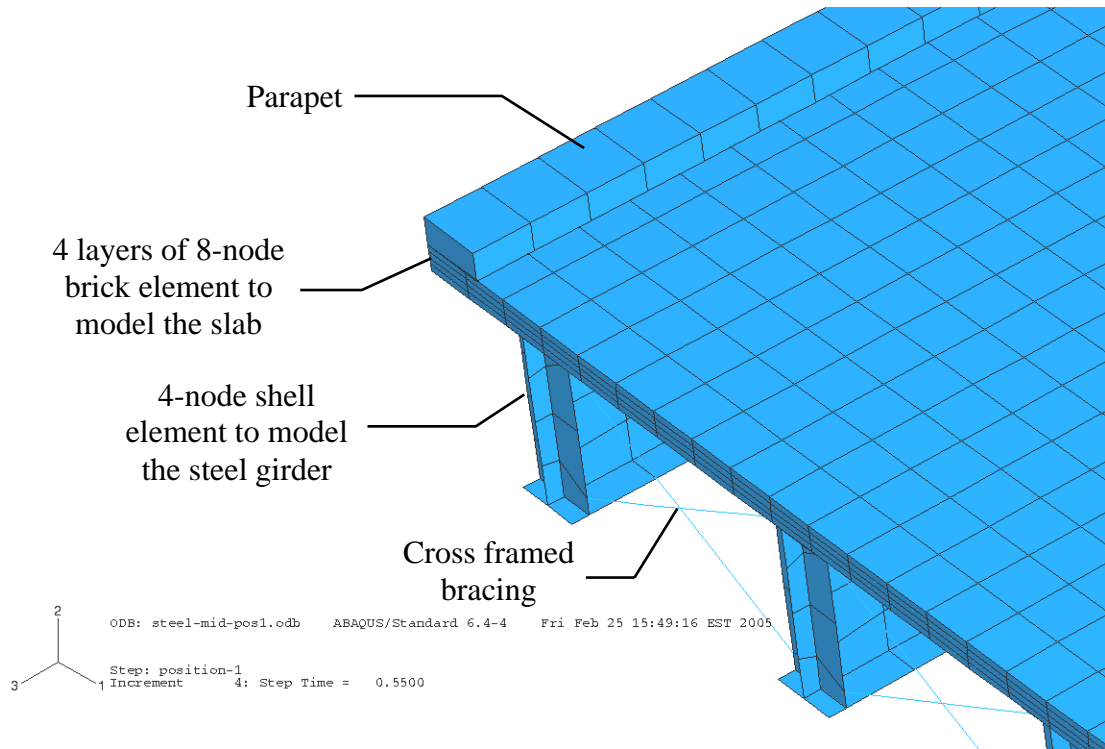


Figure 4.3 Model detailing

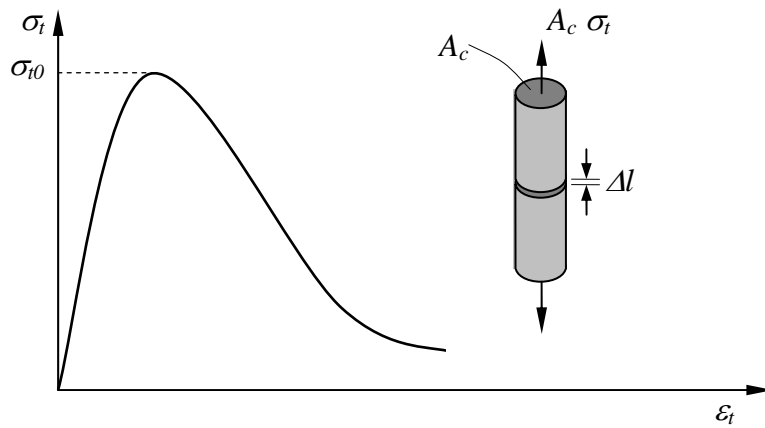


Figure 4.4 Stress-strain response of concrete to uniaxial loading in tension

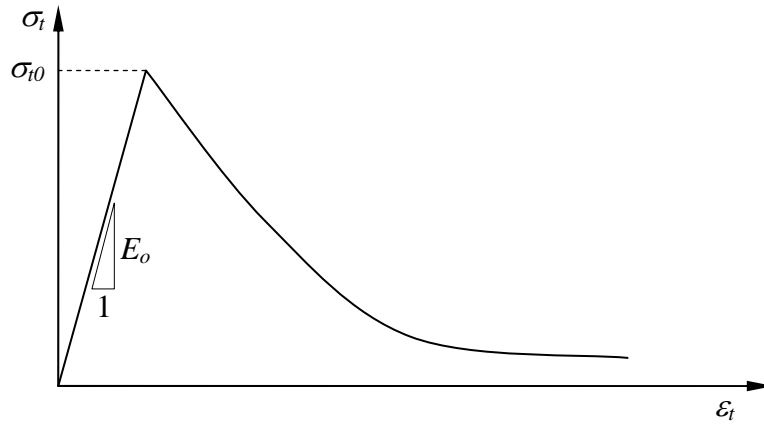


Figure 4.5 Stress-strain response of concrete to uniaxial loading in tension with ABAQUS

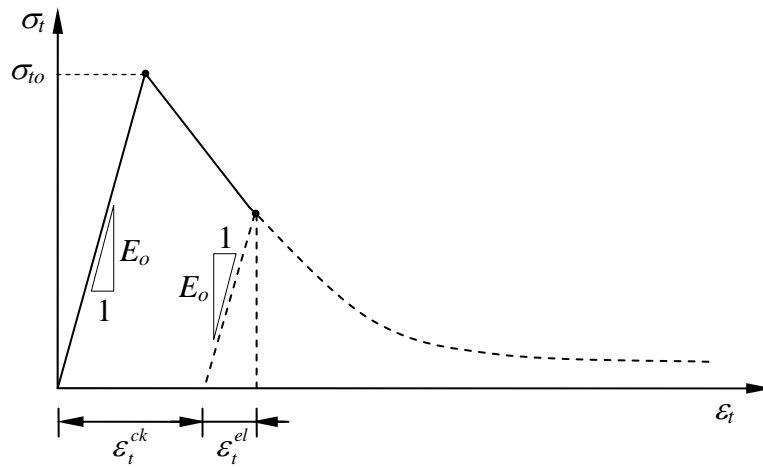


Figure 4.6 Illustration of the definition of the cracking strain  $\varepsilon_t^{ck}$  used to describe the tension stiffening

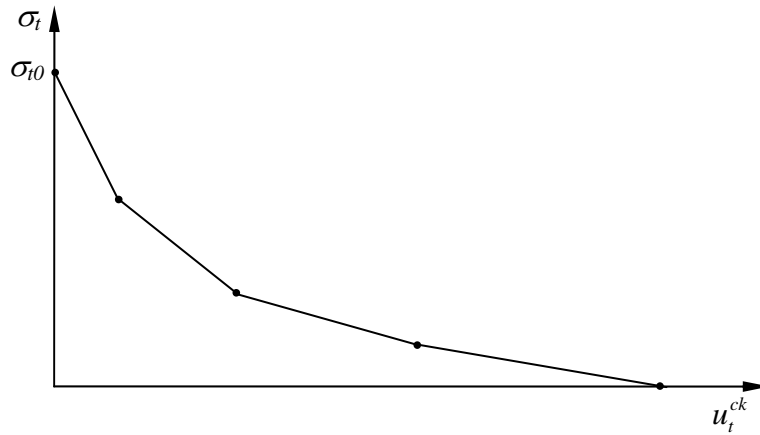


Figure 4.7 Concrete tension stiffening defined as a function of cracking displacement

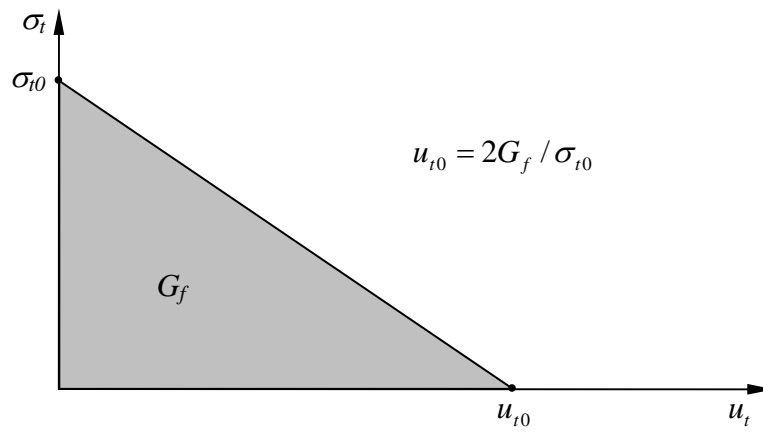


Figure 4.8 Concrete tension stiffening defined as a linear function of the cracking energy

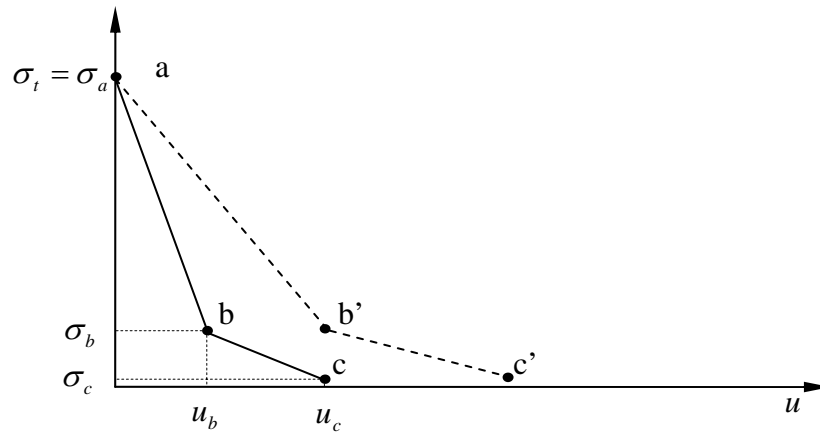


Figure 4.9 Tension stiffening model used in this study

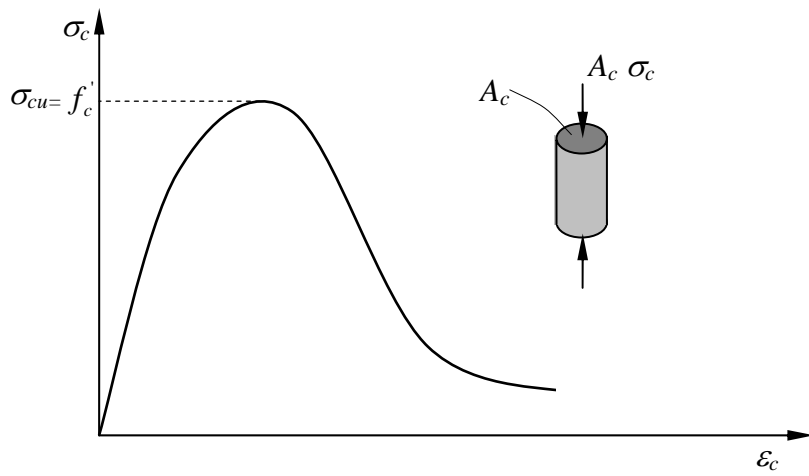


Figure 4.10 Compressive stress-strain curve of concrete

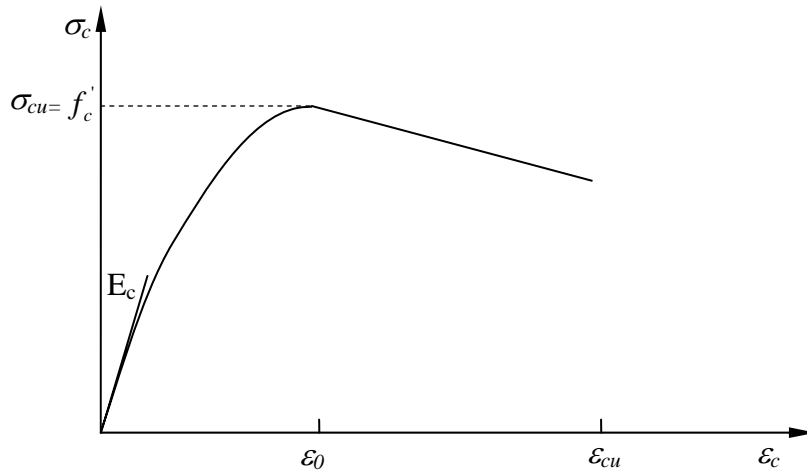


Figure 4.11 Compressive stress-strain curve of concrete proposed by Honegstad

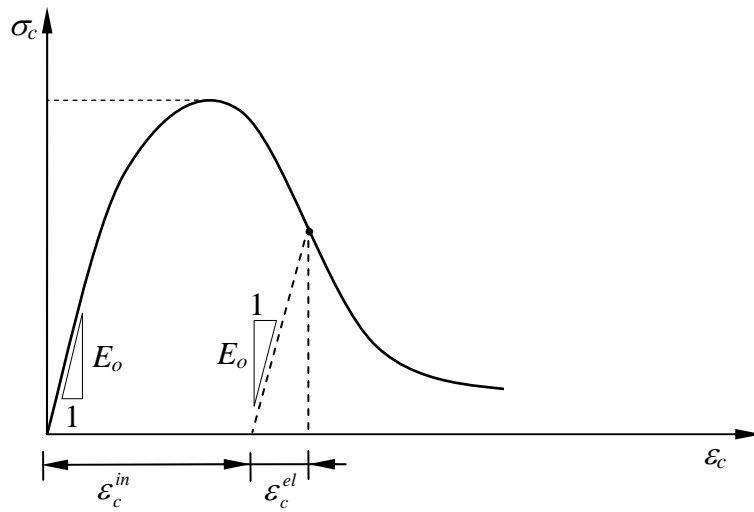


Figure 4.12 Definition of the compressive inelastic strain  $\epsilon_c^{in}$

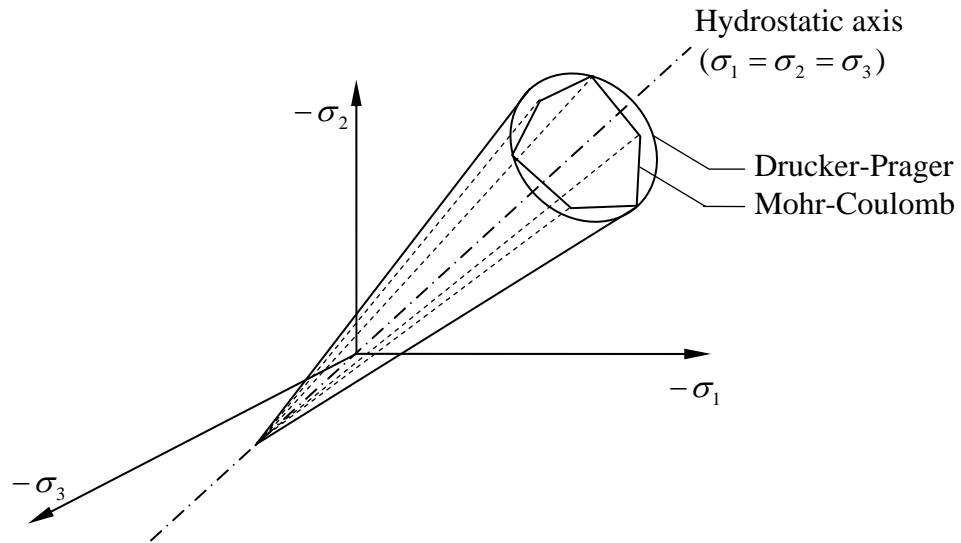


Figure 4.13 Mohr-Coulomb and Drucker-Prager yield surfaces in principal stress space

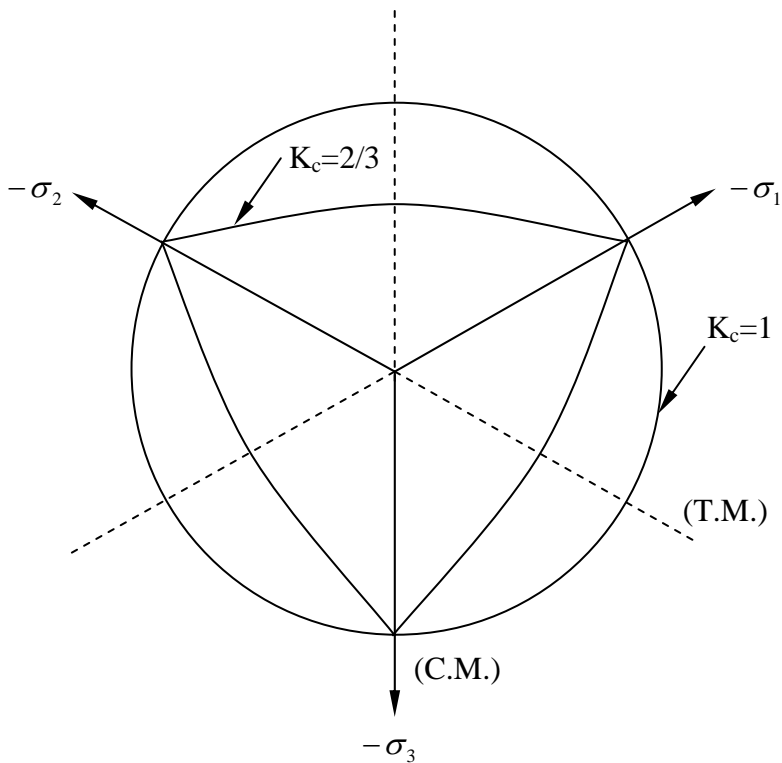


Figure 4.14 Yield surface in the deviatoric plane, corresponding to different value of  $K_c$

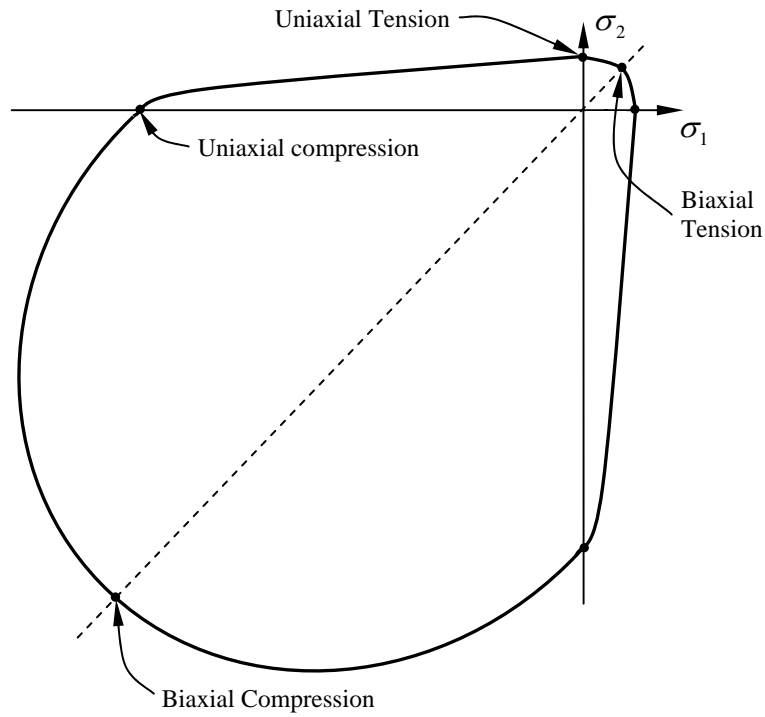


Figure 4.15 Yield surface in plane stress

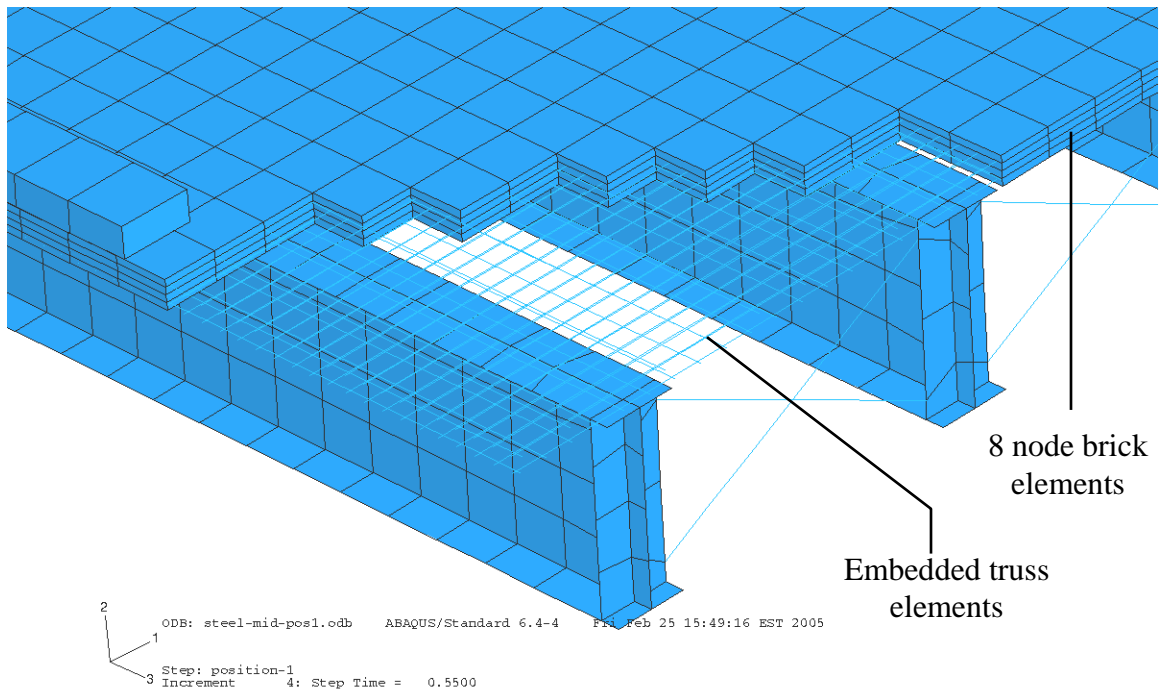


Figure 4.16 Embedded rebar element

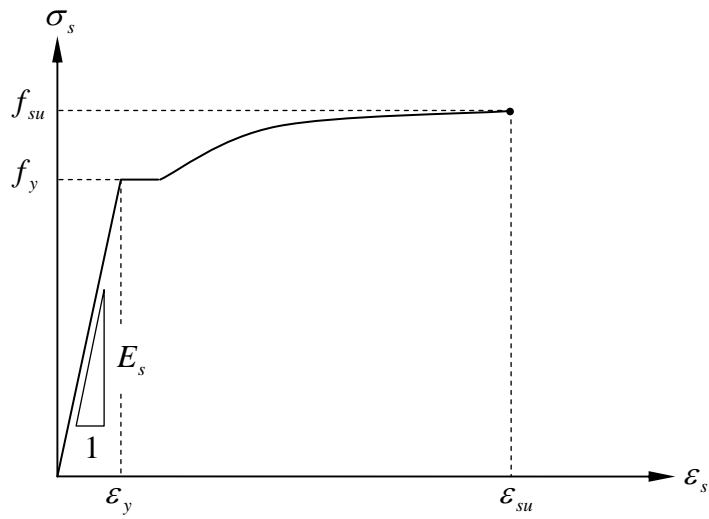


Figure 4.17 Stress-strain characteristics of reinforcement in uniaxial tension

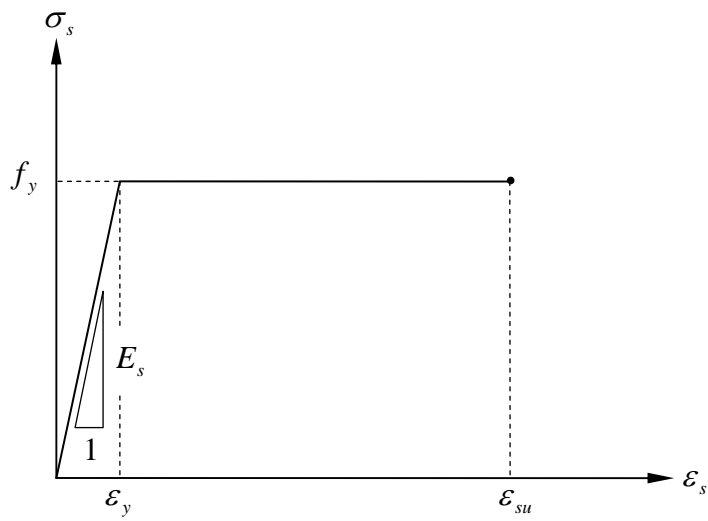


Figure 4.18 Perfect-plastic idealization of steel reinforcement

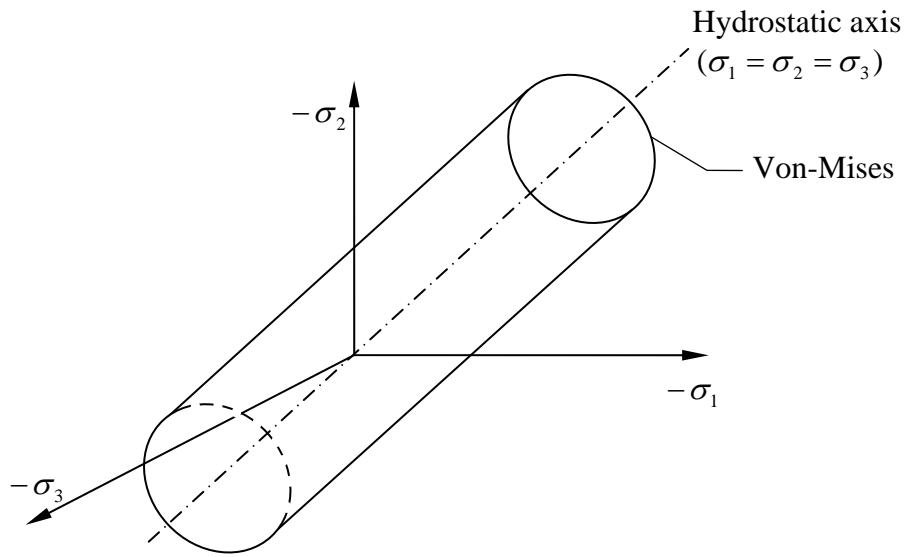


Figure 4.19 Von Mises yield surface in principal stress space

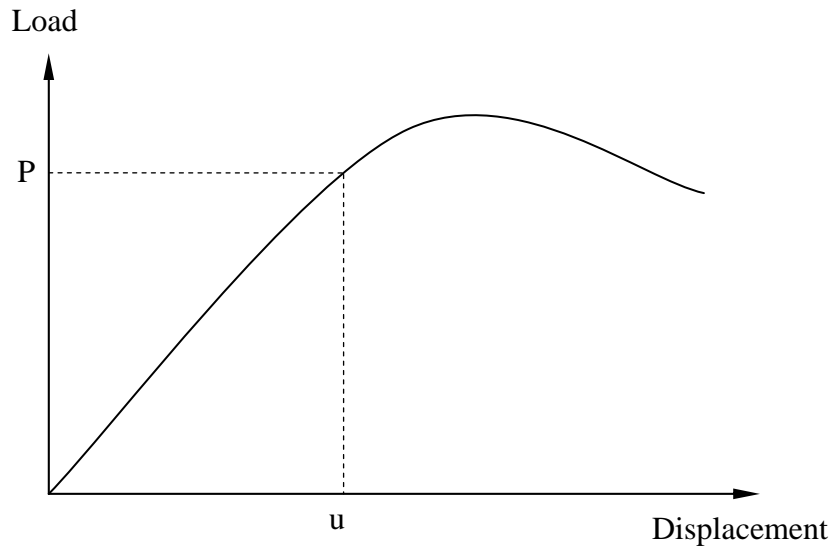


Figure 4.20 Nonlinear load-displacement curve

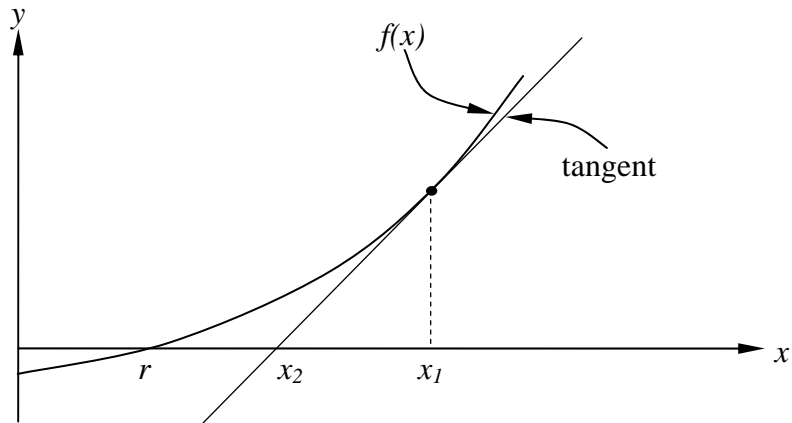
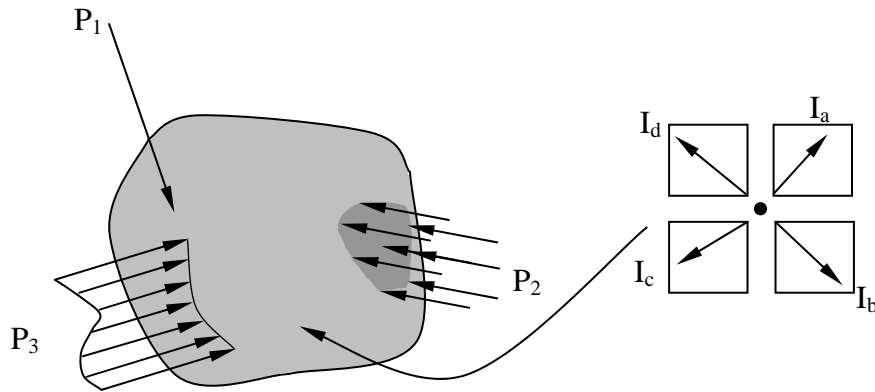


Figure 4.21 Graphic representation of the Newton-Raphson method



(a) external loads acting on a body      (b) internal forces acting at a node

Figure 4.22 Internal and external loads on a body

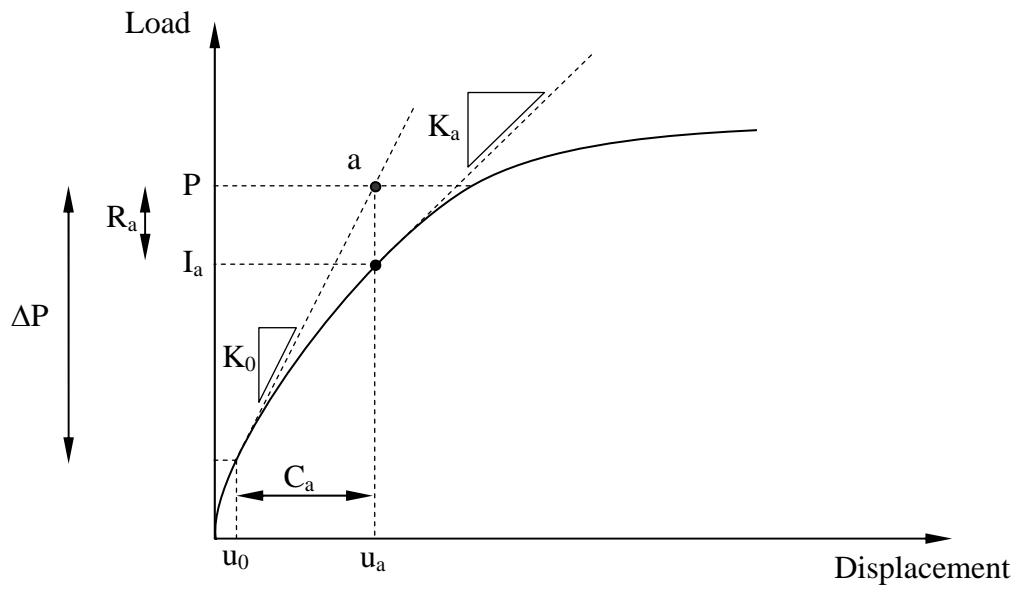


Figure 4.23 First iteration in an increment

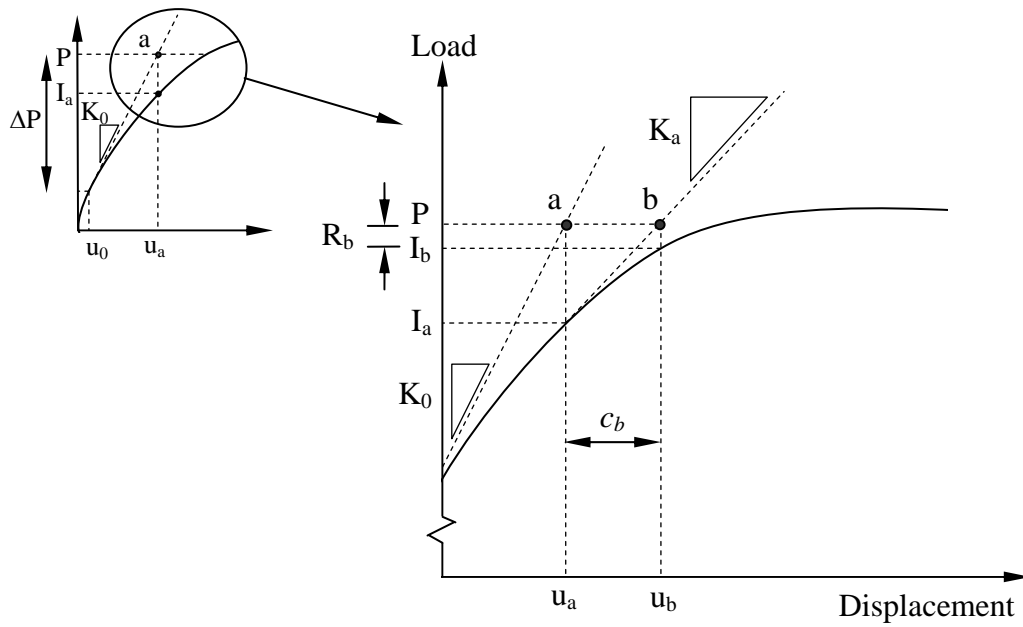


Figure 4.24 Second iteration in an increment

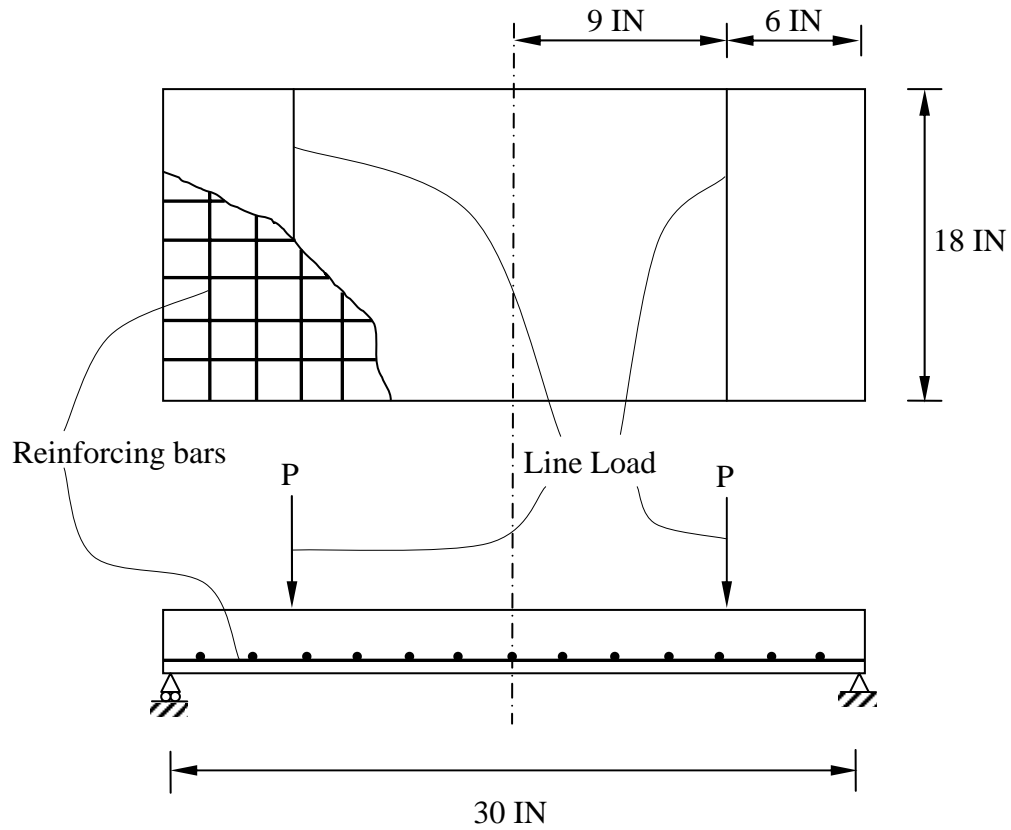


Figure 4.25 Configuration of the one way slab tested by Jain and Kennedy

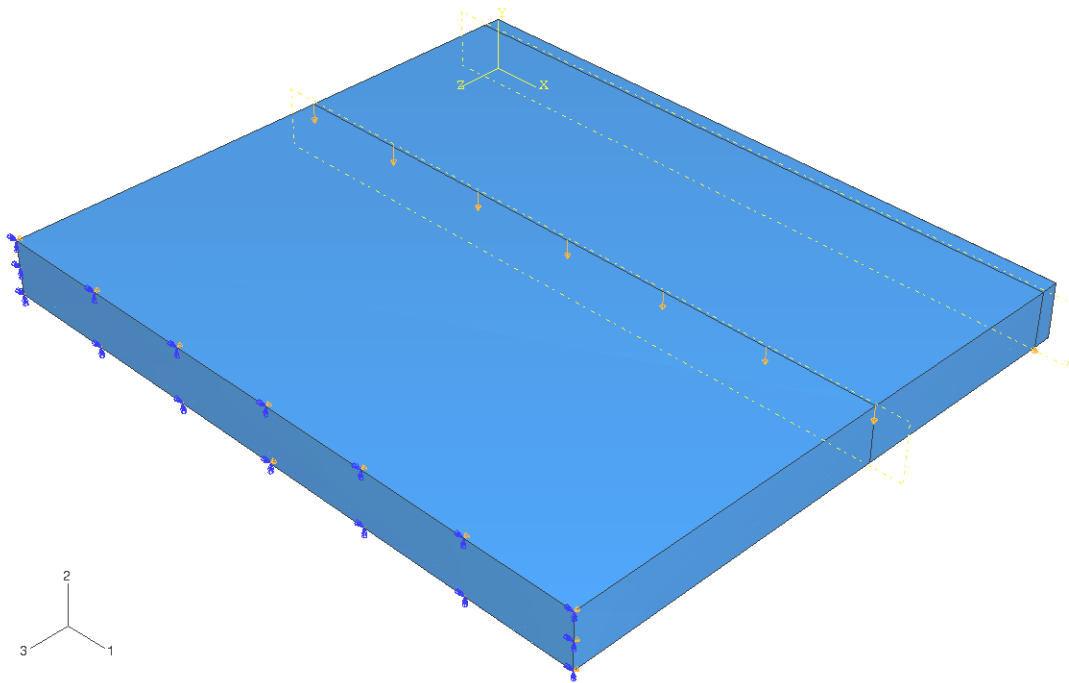


Figure 4.26 General view of the one way slab FE model

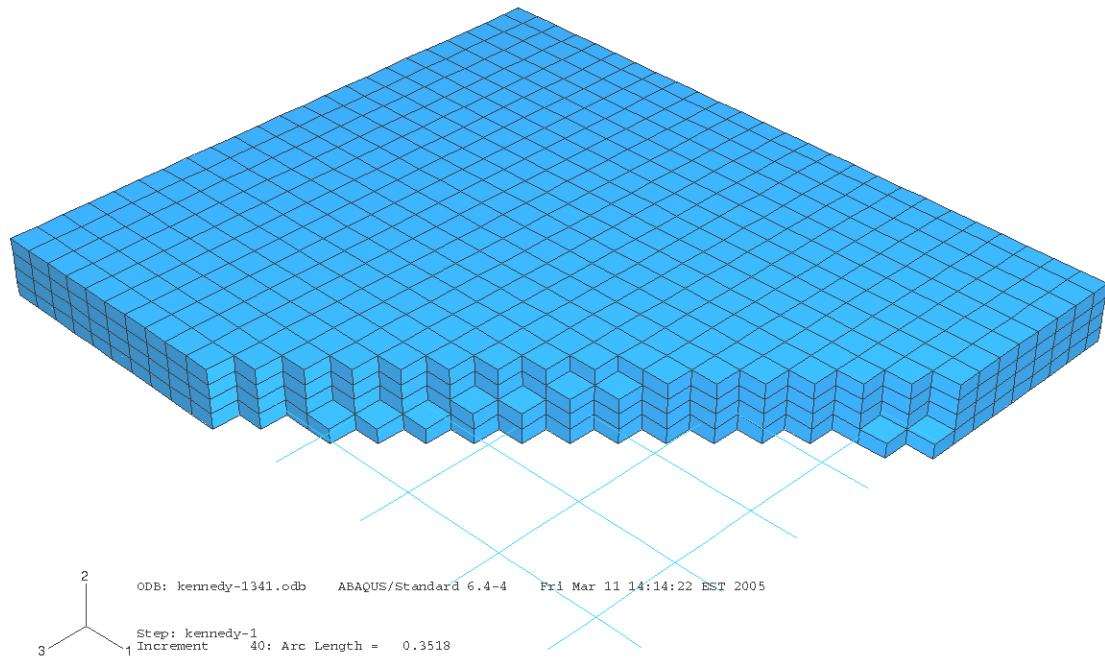


Figure 4.27 Modeling of the reinforcement in the one way slab FE Model

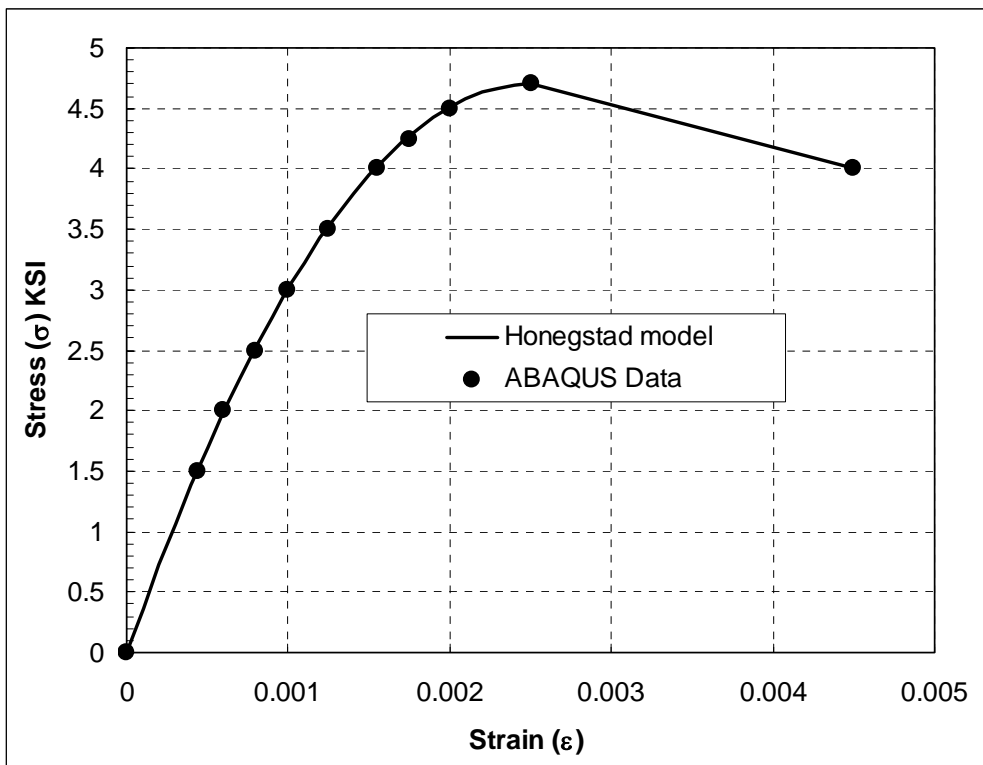


Figure 4.28 Compressive stress-strain curve of concrete used in the one way slab example

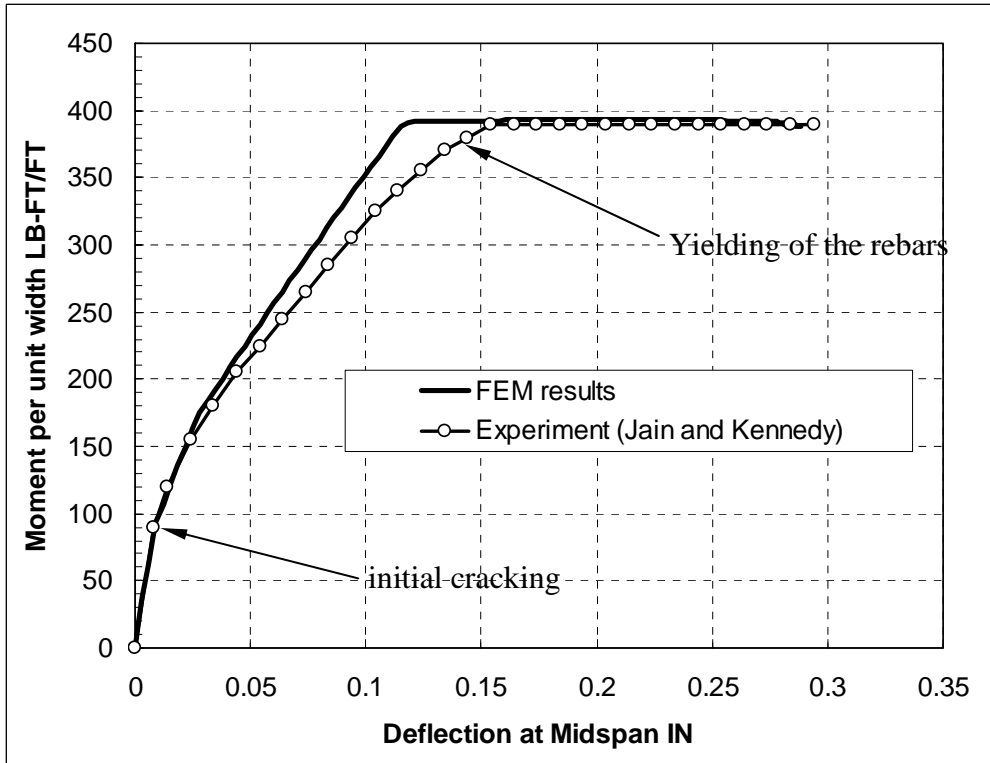


Figure 4.29 Comparison between experimental results and FE results of the one way slab example

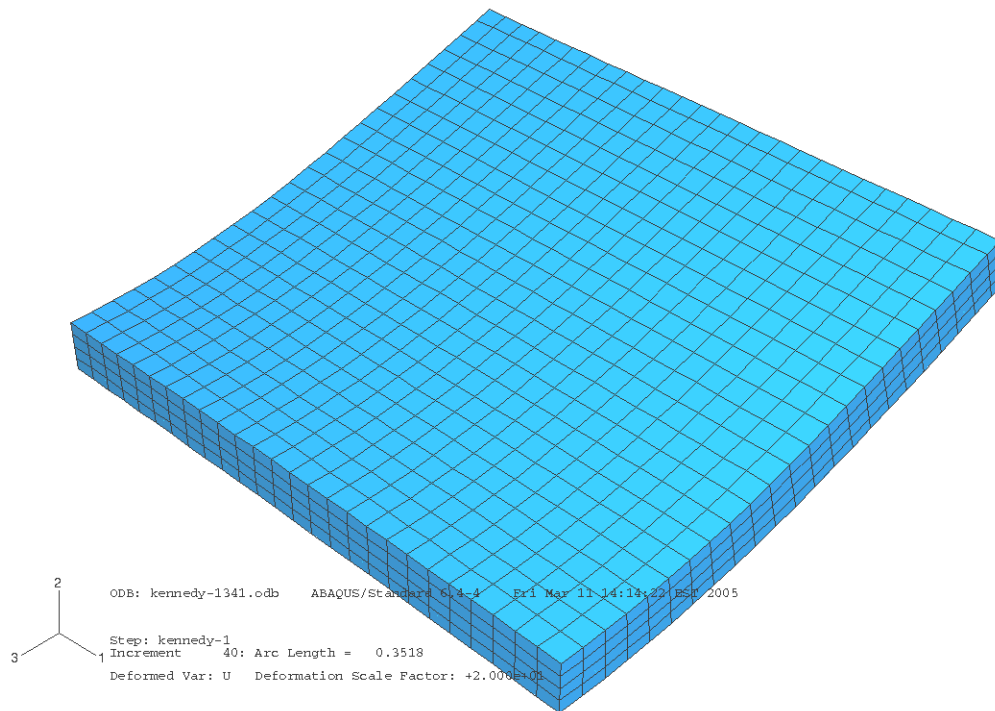


Figure 4.30 View of the deformed shape of the FE model of the one way slab example

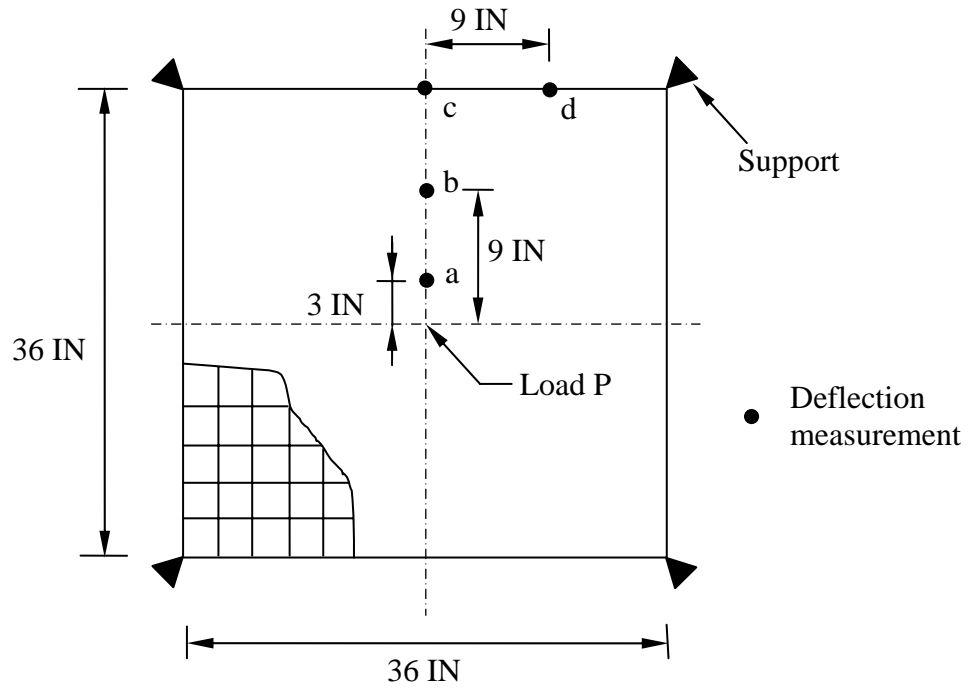


Figure 4.31 Configuration of the two way slab tested by McNeice

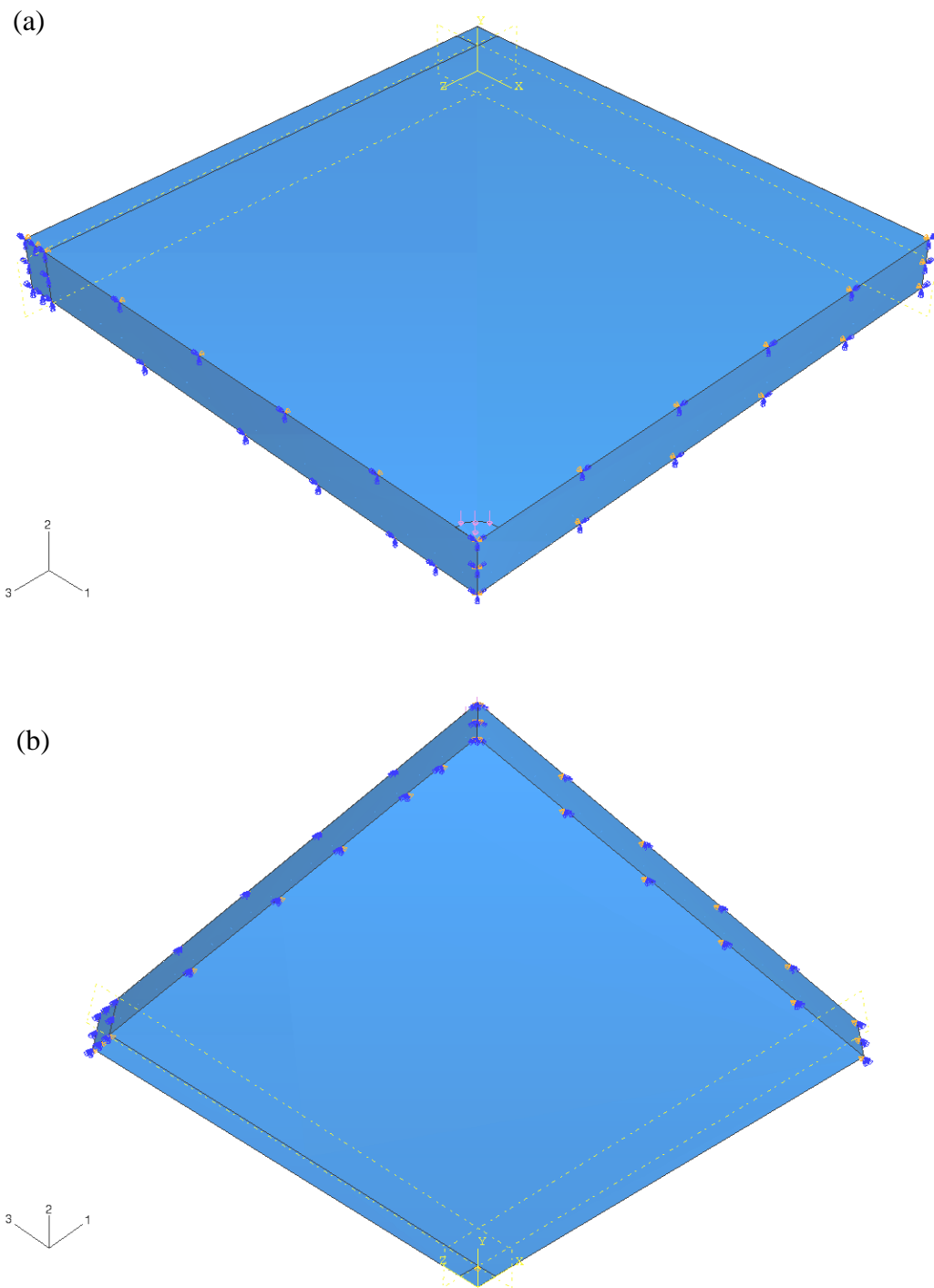


Figure 4.32 General view of the two way slab FE Model, top view (a) and bottom view (b).

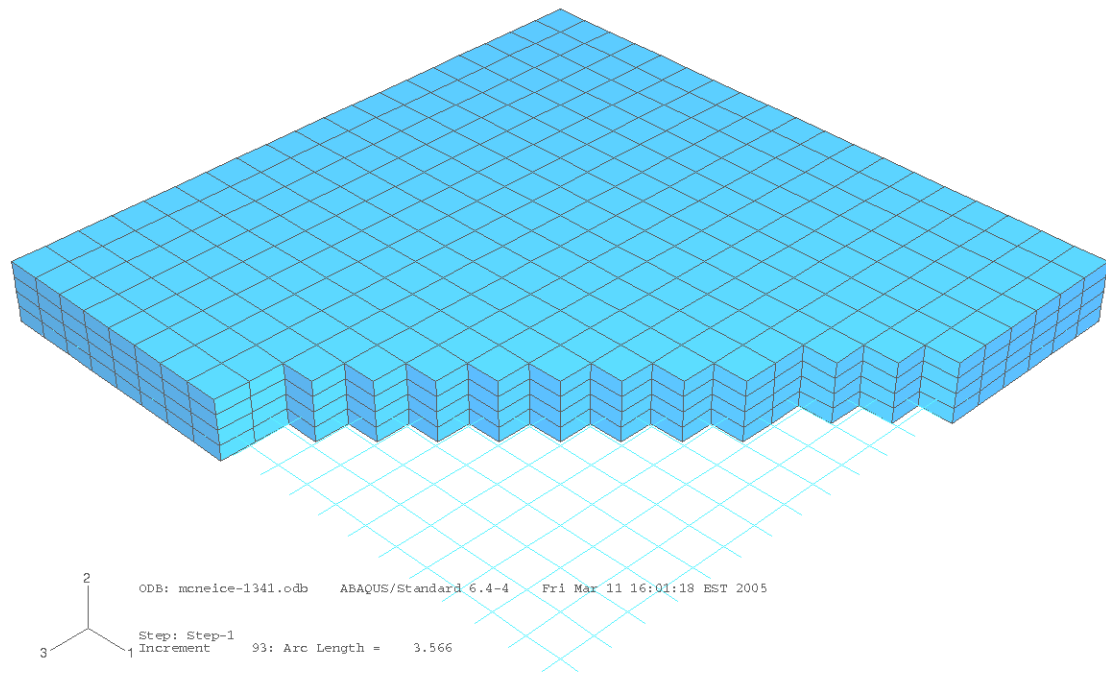


Figure 4.33 Modeling of the reinforcement in the two way slab FE Model

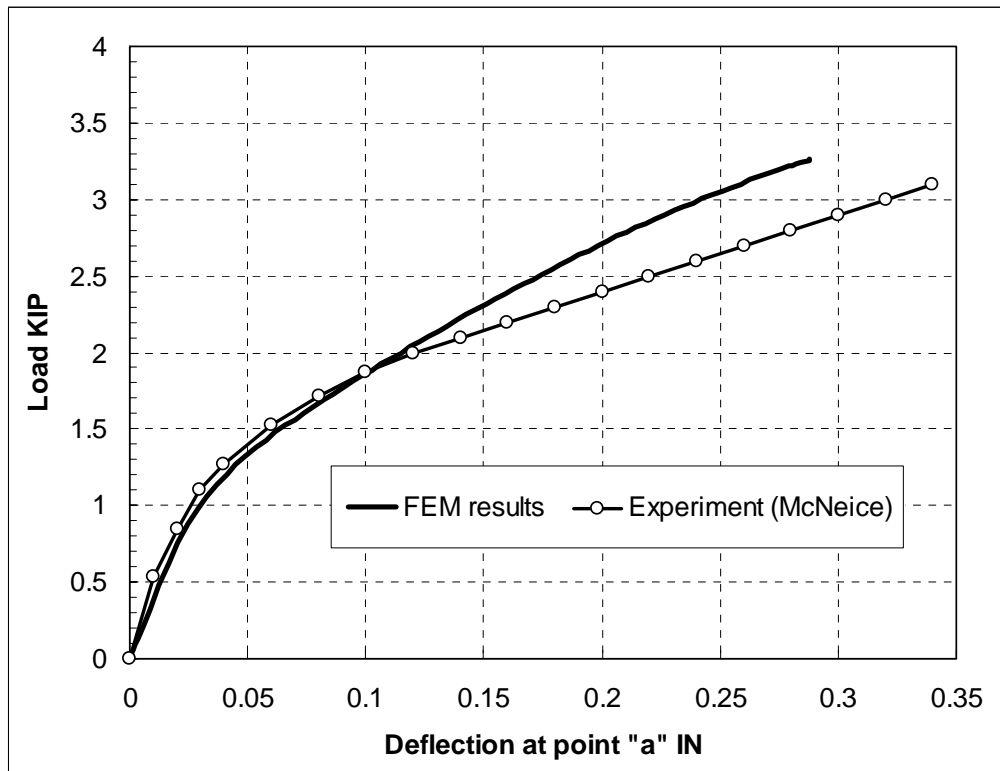


Figure 4.34 Comparison between experimental results and FE results of the two way slab example at point "a"

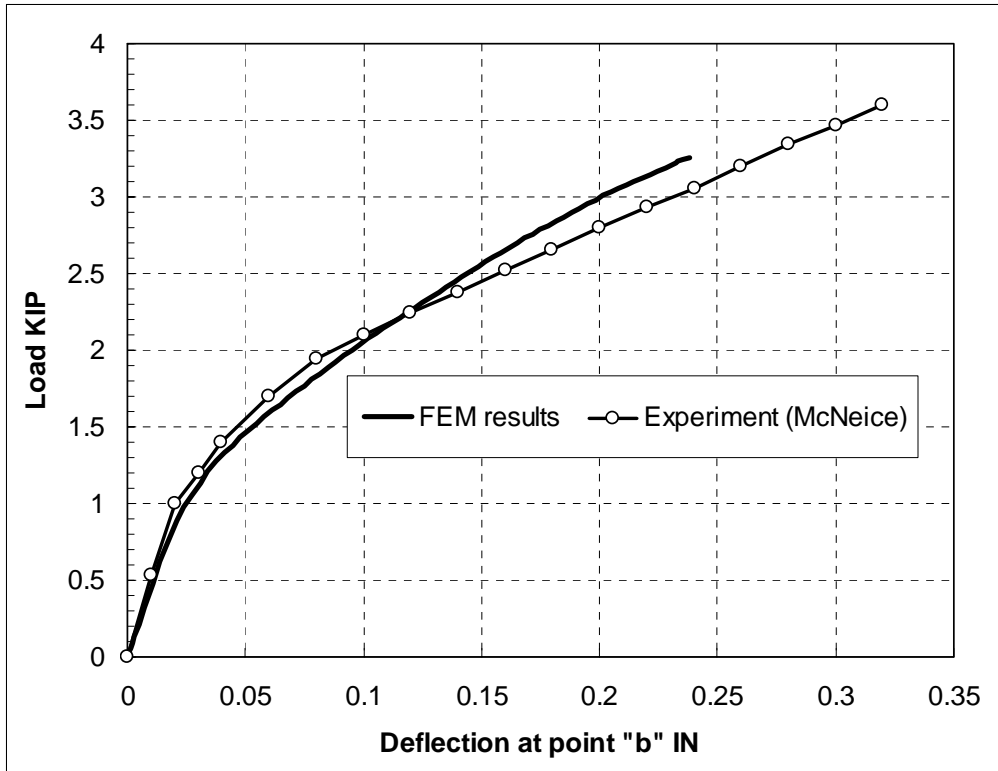


Figure 4.35 Comparison between experimental results and FE results of the two way slab example at point "b"

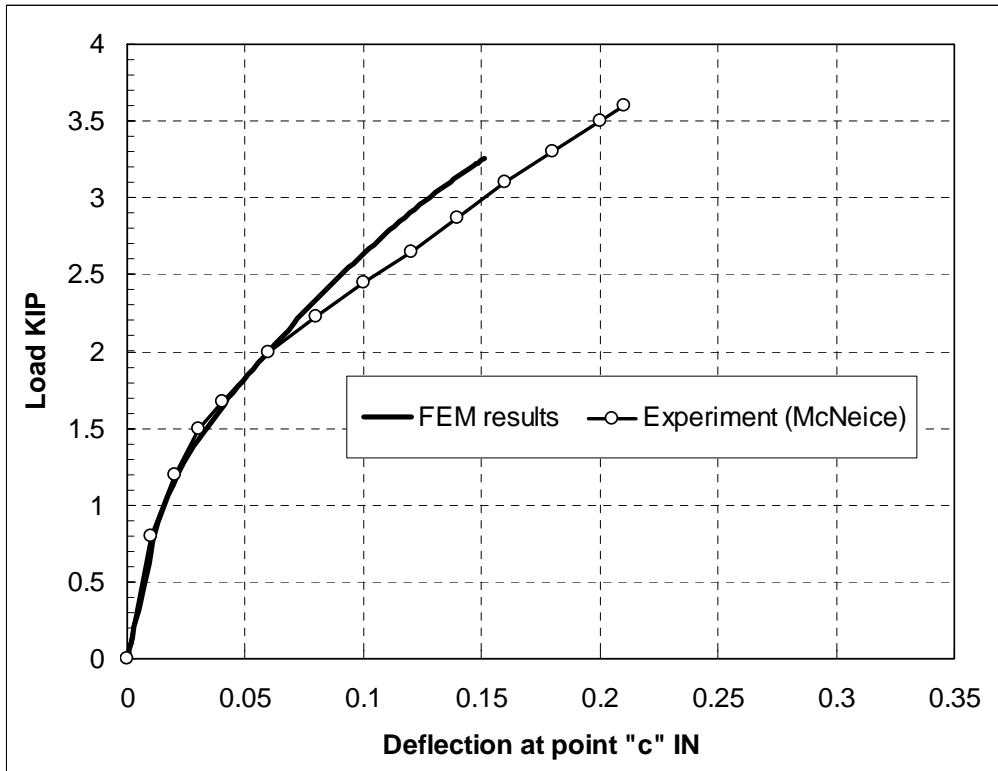


Figure 4.36 Comparison between experimental results and FE results of the two way slab example at point "c"

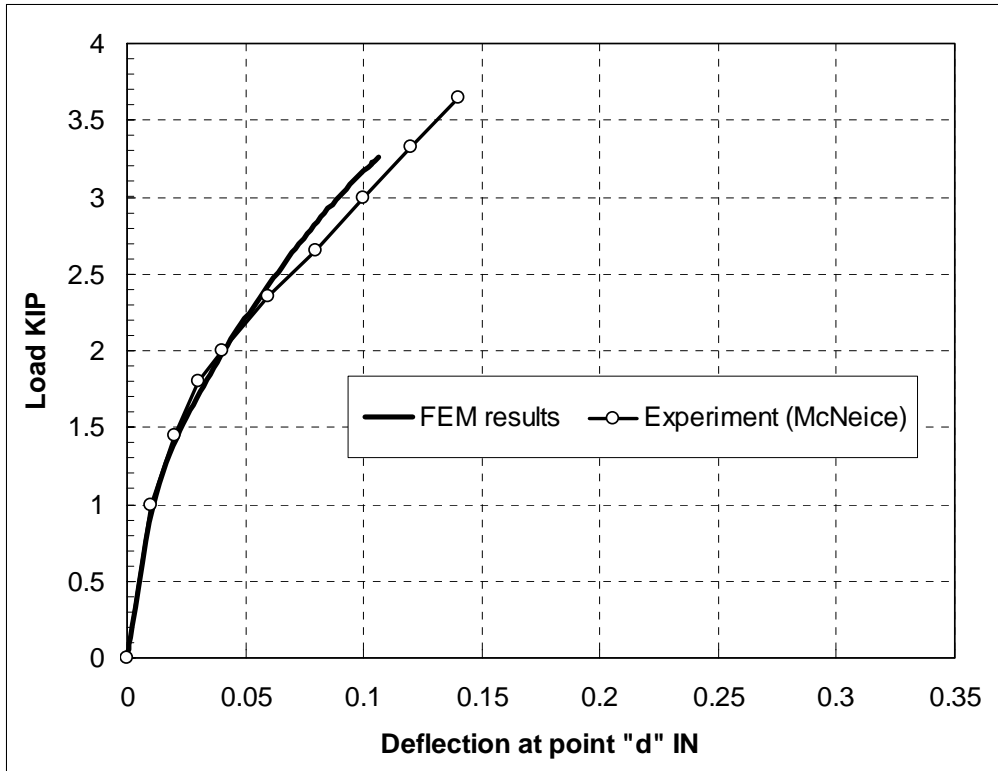


Figure 4.37 Comparison between experimental results and FE results of the two way slab example at point "d"

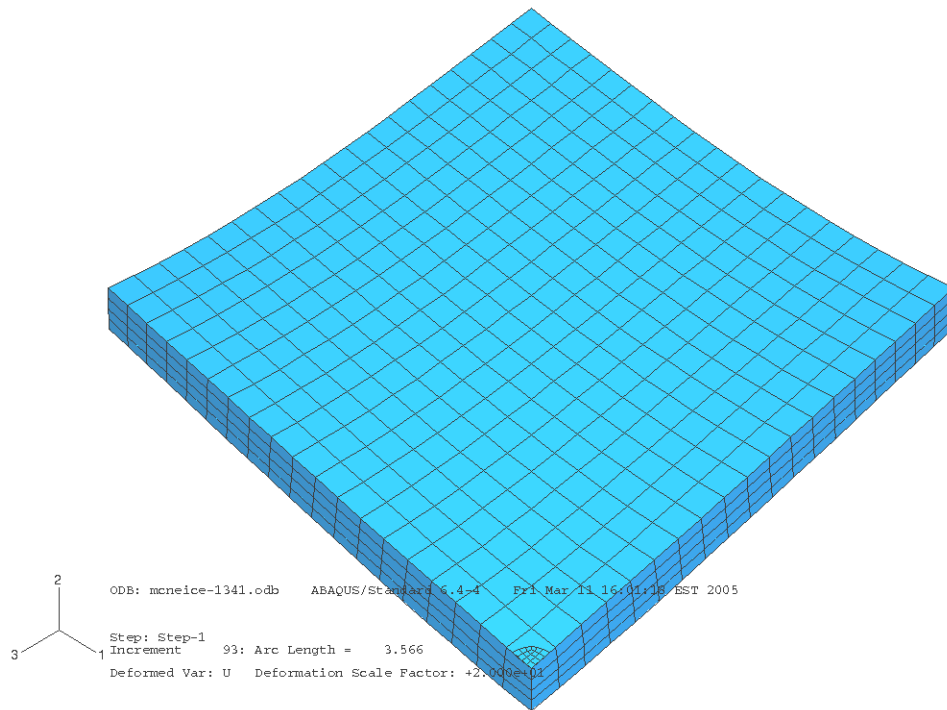


Figure 4.38 View of the deformed shape of the FE model of the two way slab example

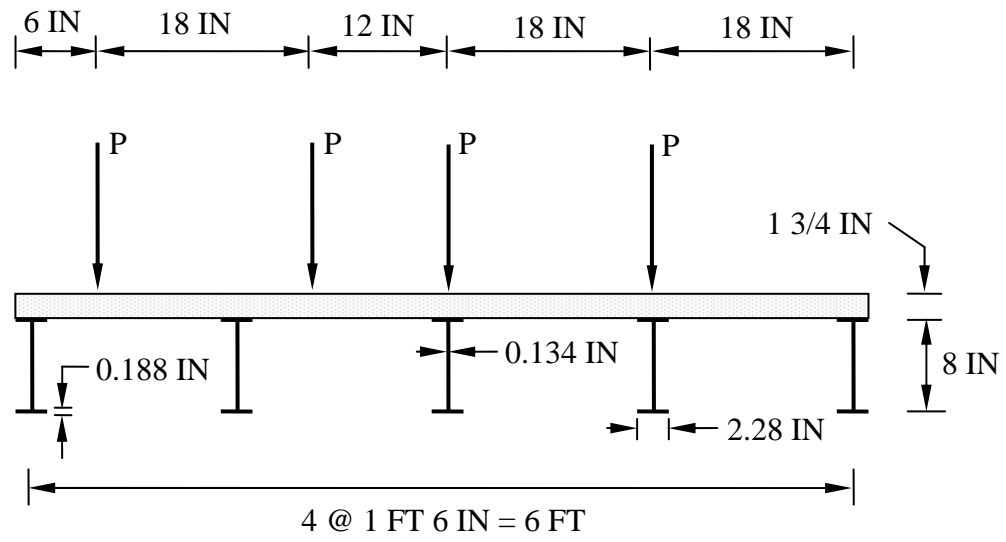


Figure 4.39 Cross section of the Newmark bridge

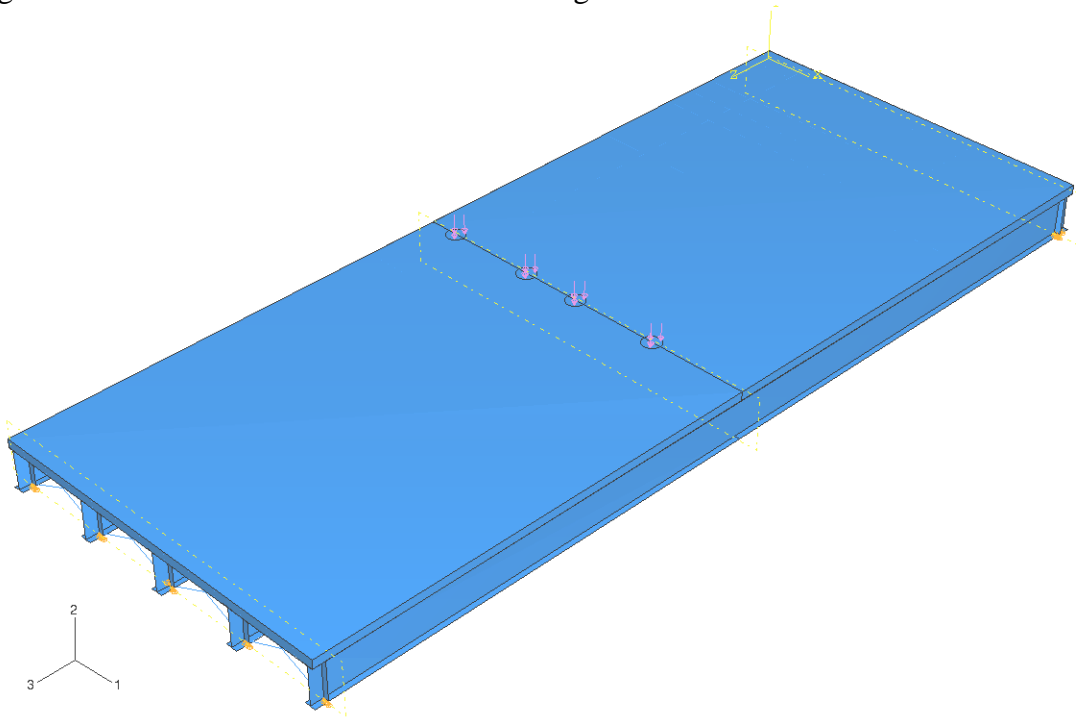


Figure 4.40 General view of the Newmark bridge FE Model

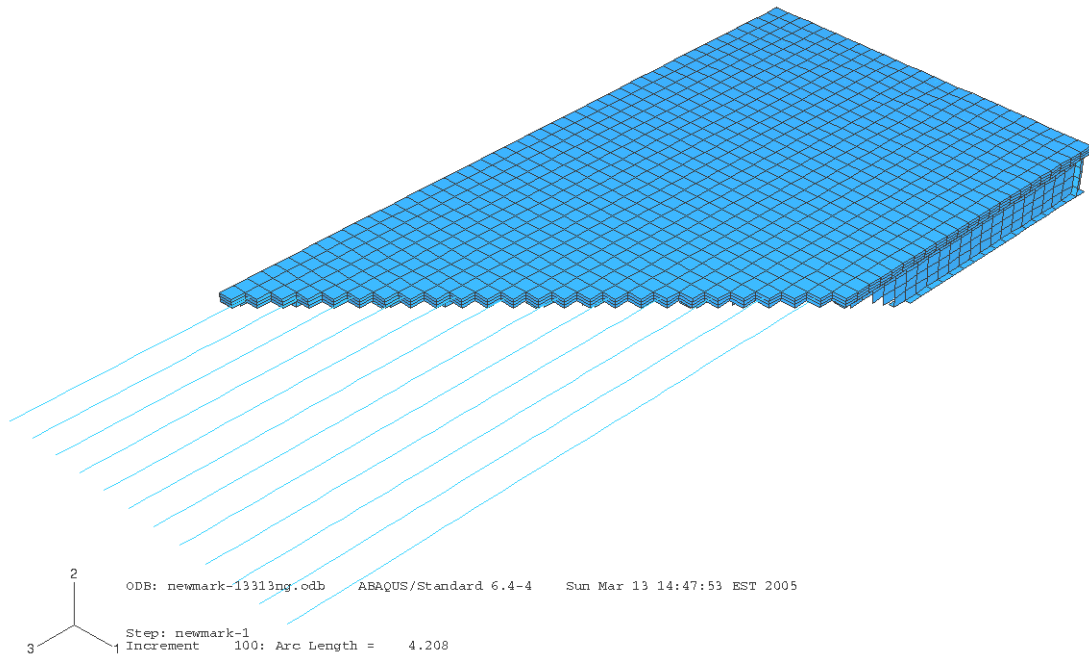


Figure 4.41 Modeling of the reinforcement in the Newmark bridge FE Model – Top longitudinal reinforcement

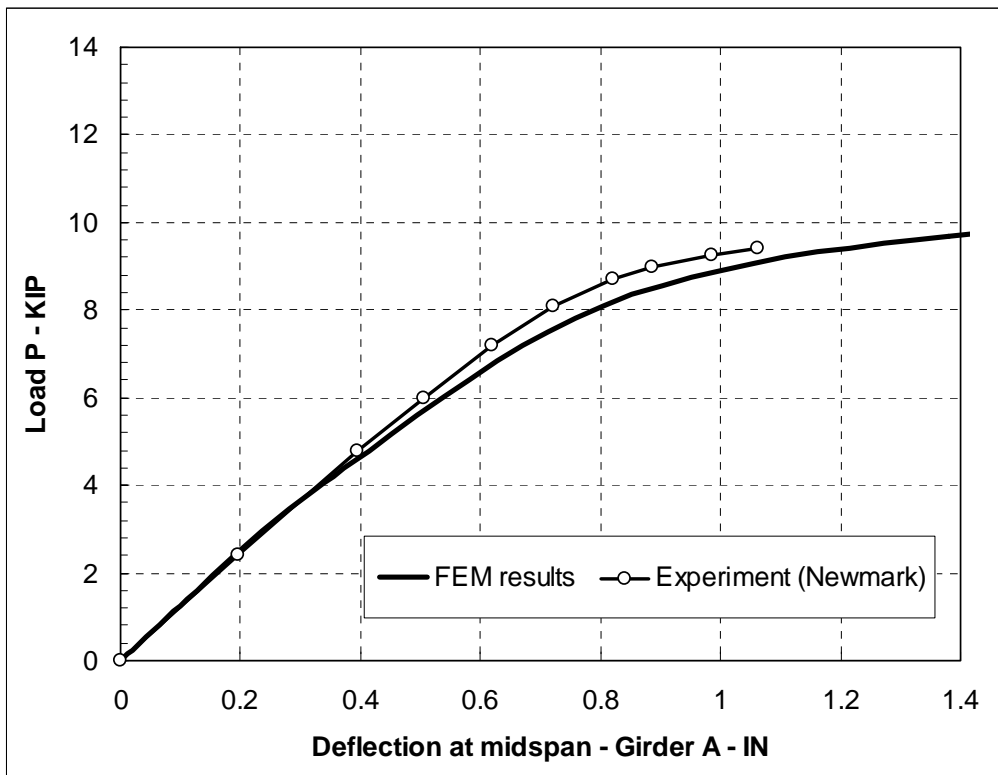


Figure 4.42 Comparison between experimental results and FE results of the Newmark bridge at girder A

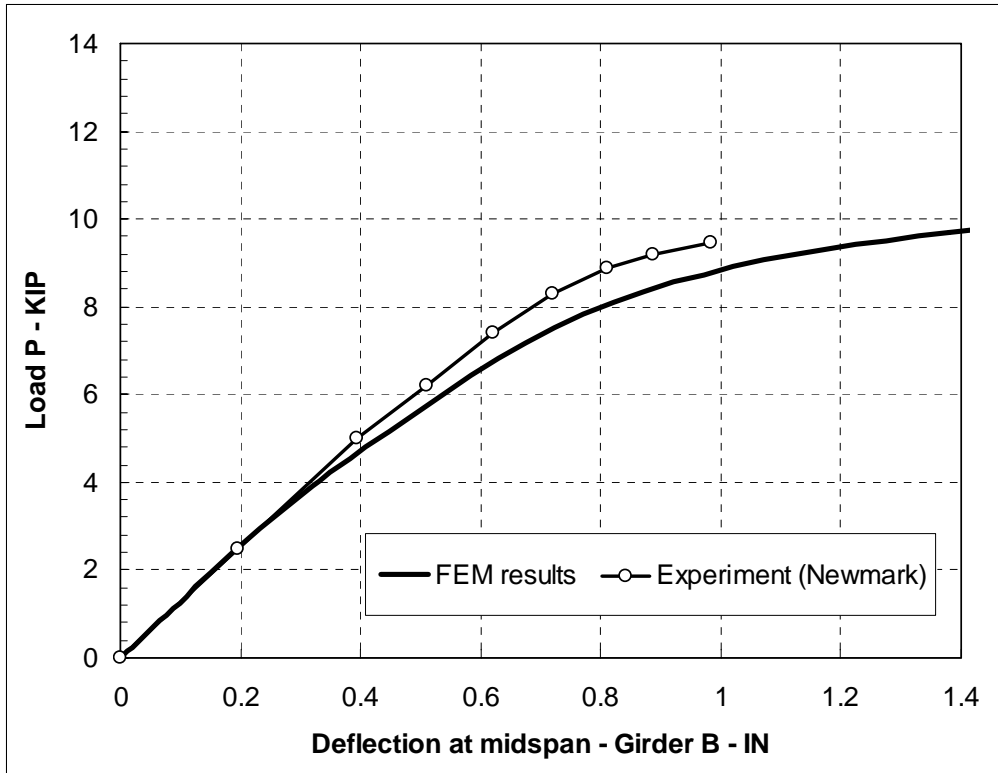


Figure 4.43 Comparison between experimental results and FE results of the Newmark bridge at girder B

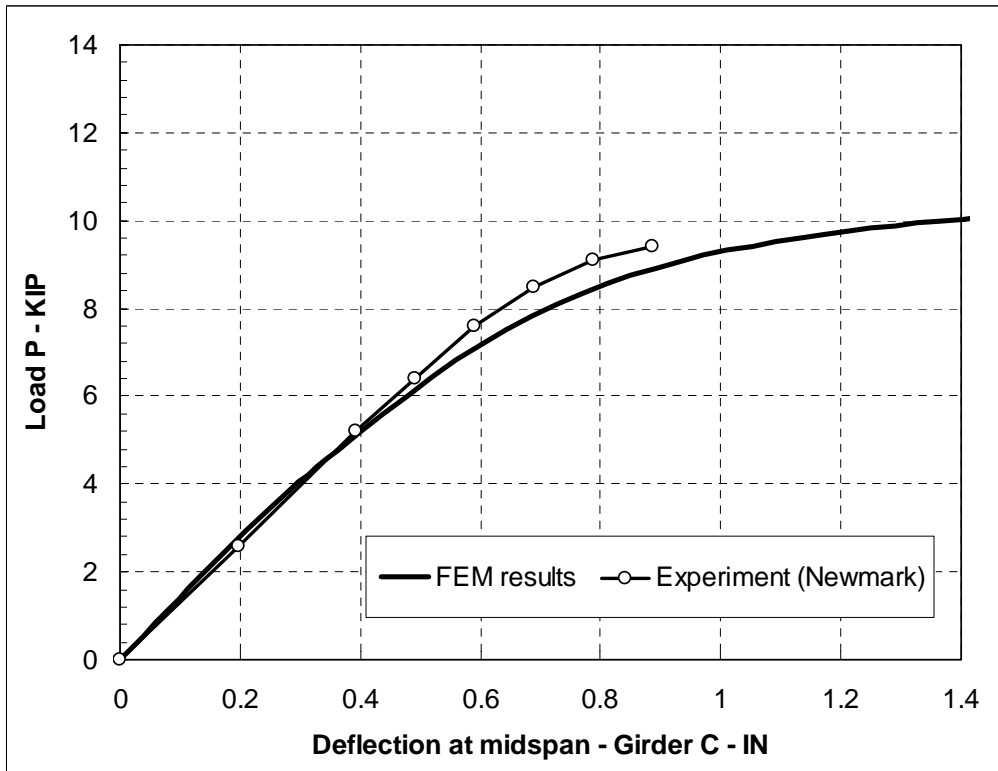


Figure 4.44 Comparison between experimental results and FE results of the Newmark bridge at girder C

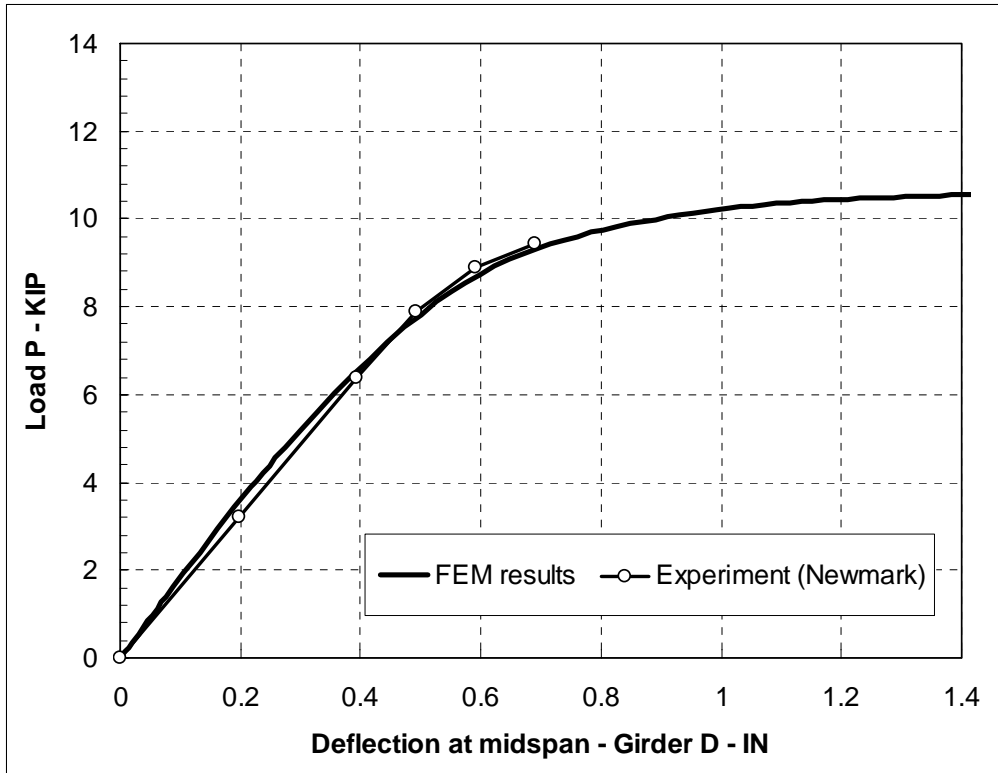


Figure 4.45 Comparison between experimental results and FE results of the Newmark bridge at girder D

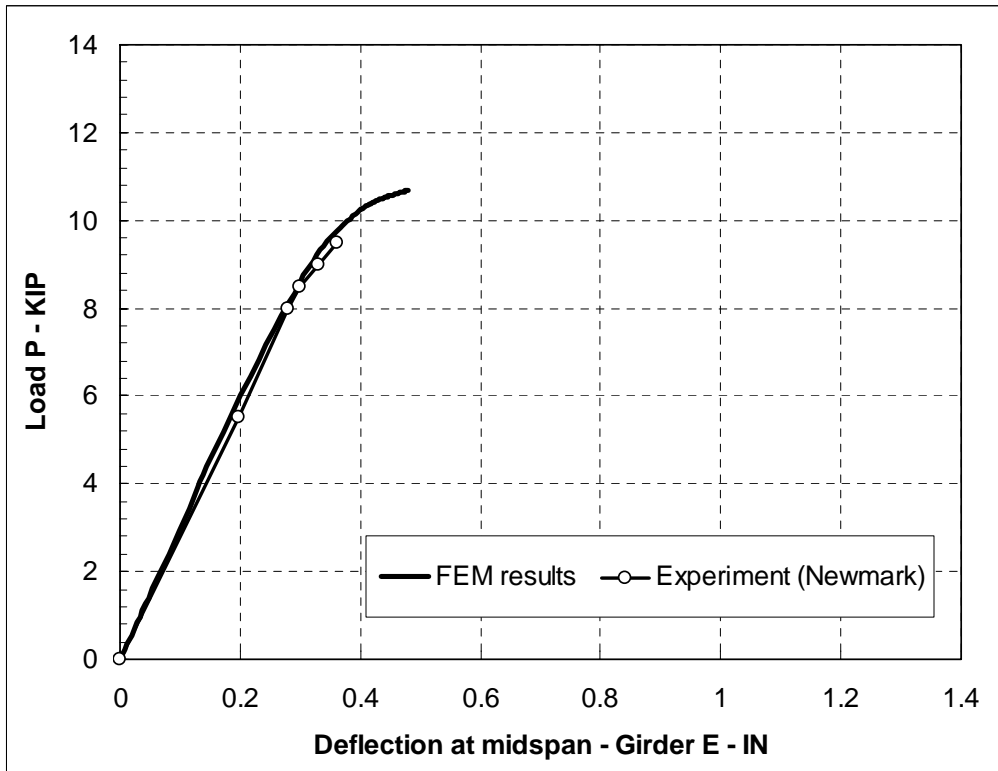


Figure 4.46 Comparison between experimental results and FE results of the Newmark bridge at girder E

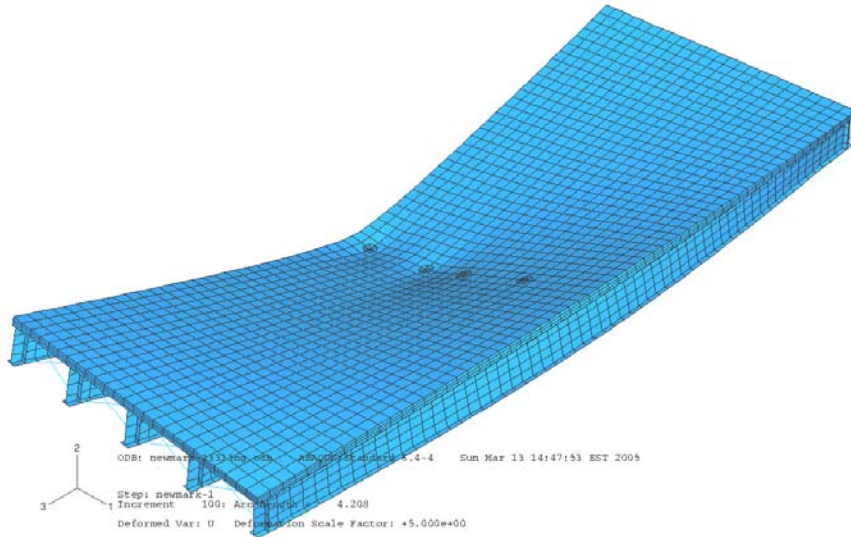


Figure 4.47 View of the deformed shape of the FE Model of the Newmark bridge

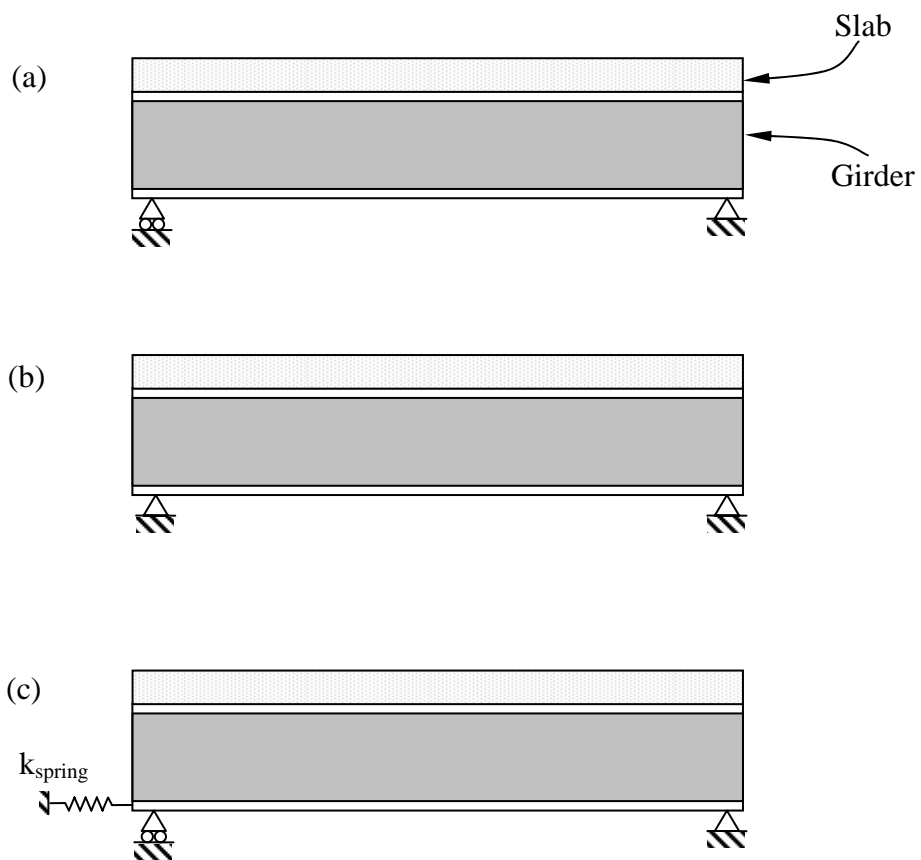


Figure 4.48 Three cases of boundary conditions used in the Finite Element Analysis: (a) Simply supported, hinge-roller; (b) Hinge at both end of the girder, (c) Partially fixed support.

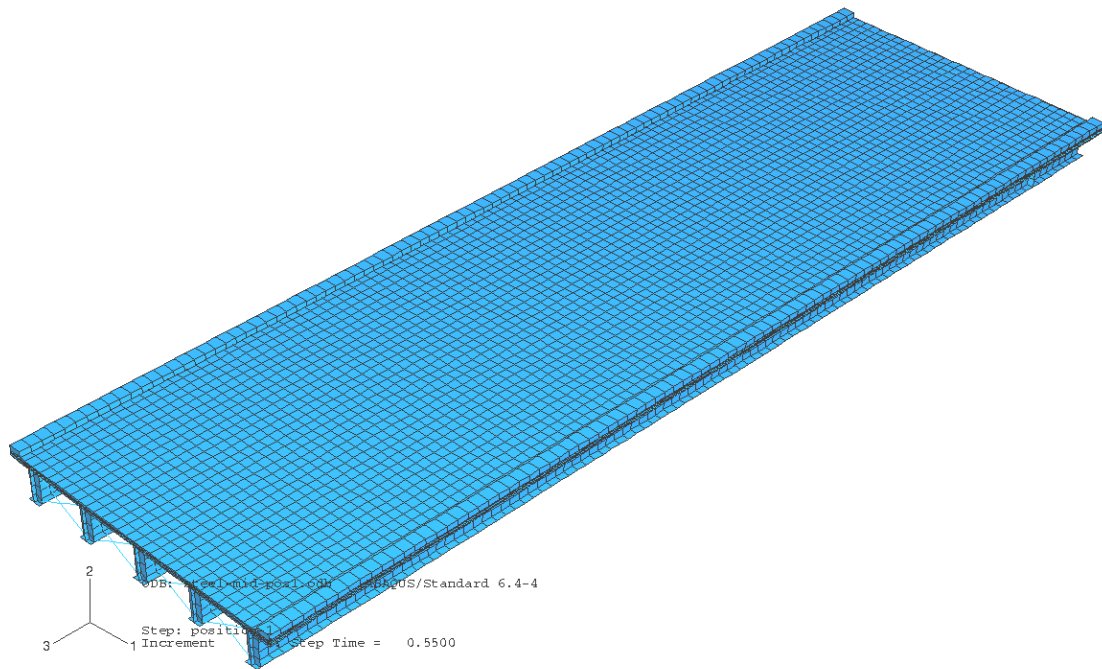


Figure 4.49 General view of the tested bridge FE Model

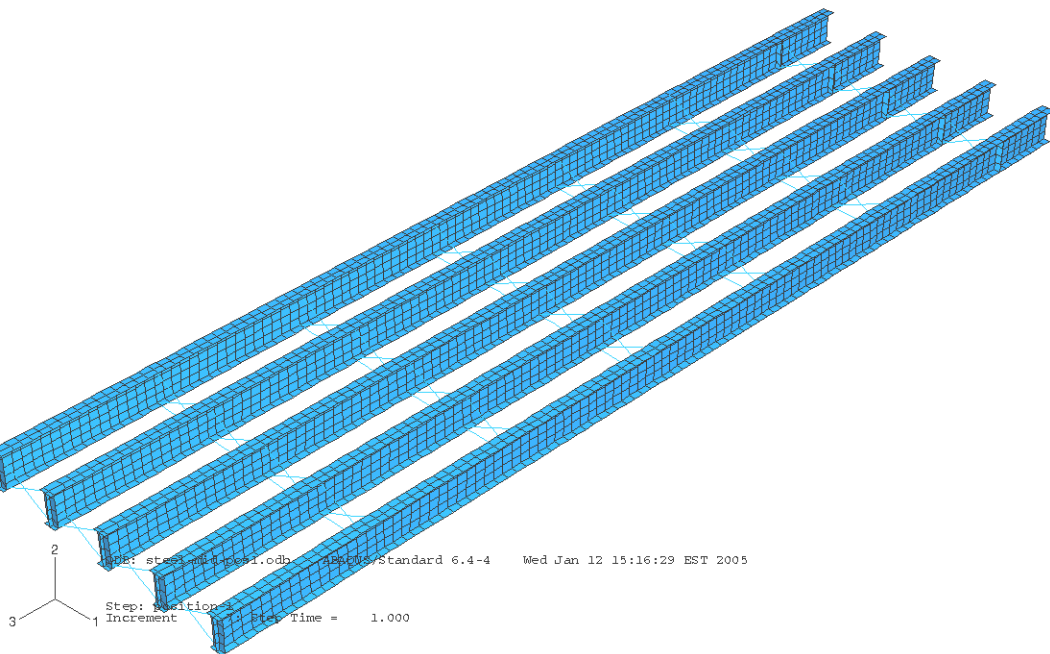


Figure 4.50 View of the girder and cross frame of the FE Model

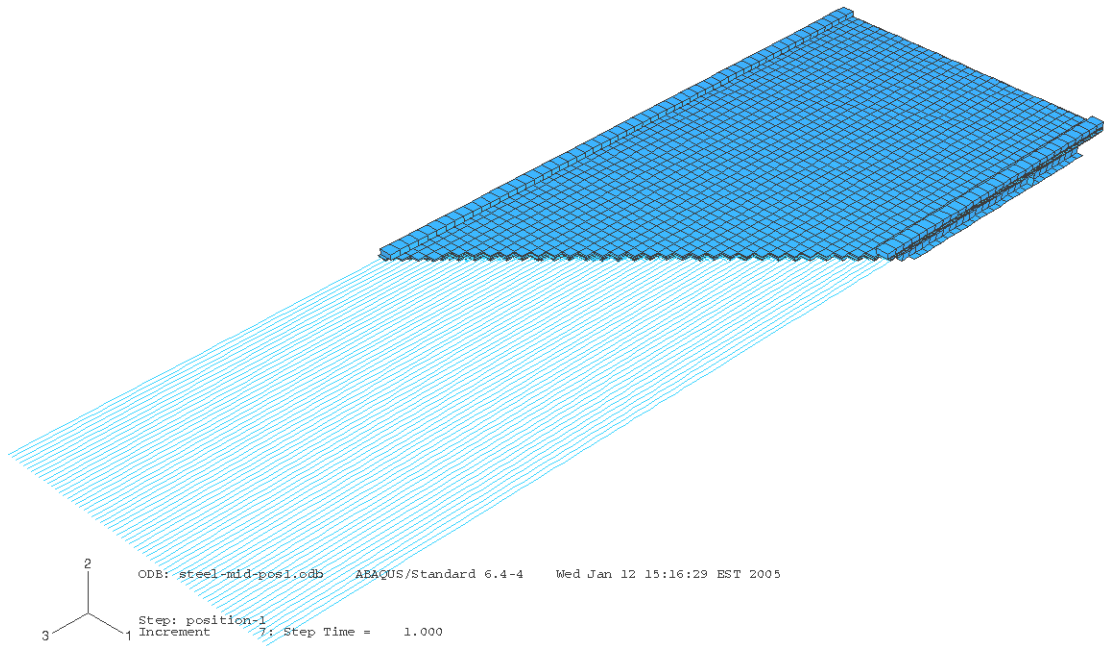


Figure 4.51 View of the bottom longitudinal reinforcement in the FE Model

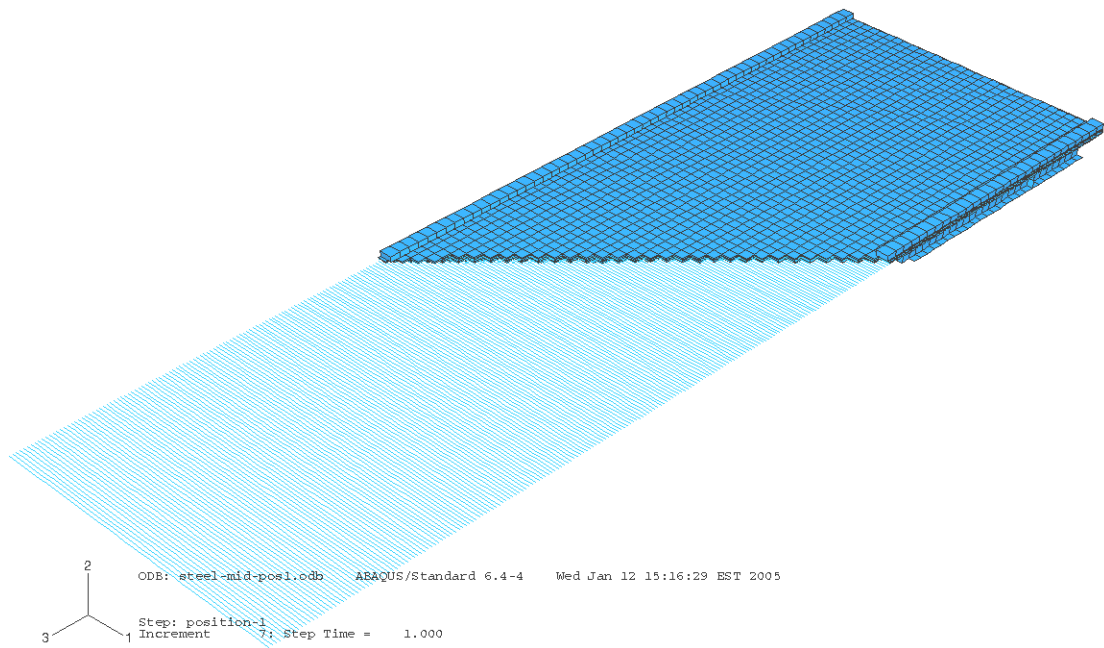


Figure 4.52 View of the bottom transversal reinforcement in the FE Model

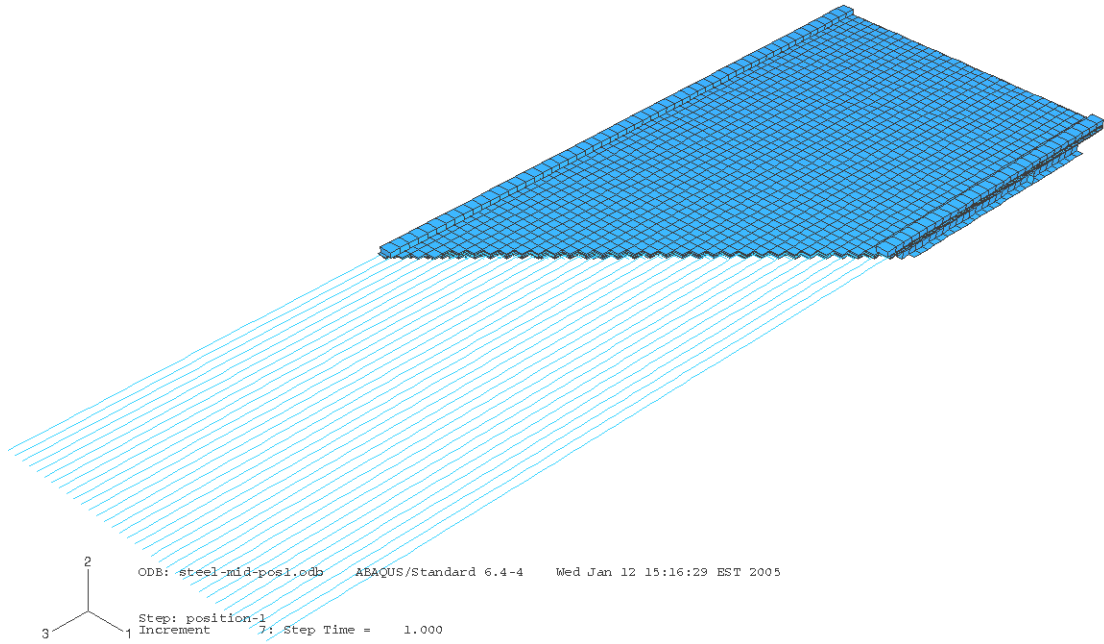


Figure 4.53 View of the top longitudinal reinforcement in the FE Model

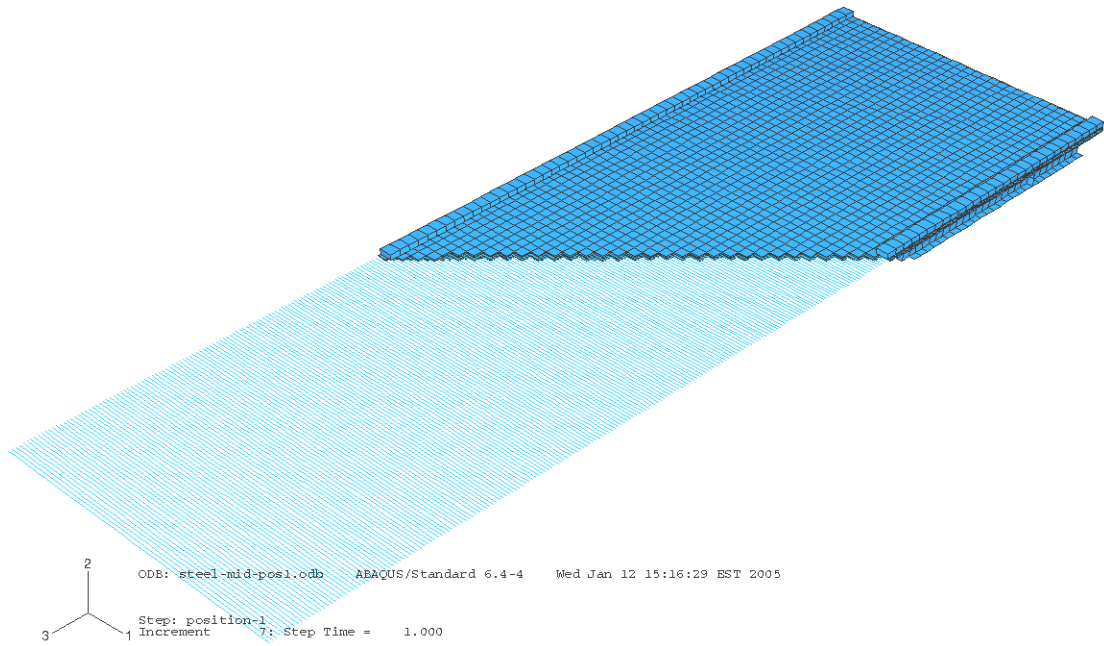


Figure 4.54 View of the top transversal reinforcement in the FE Model

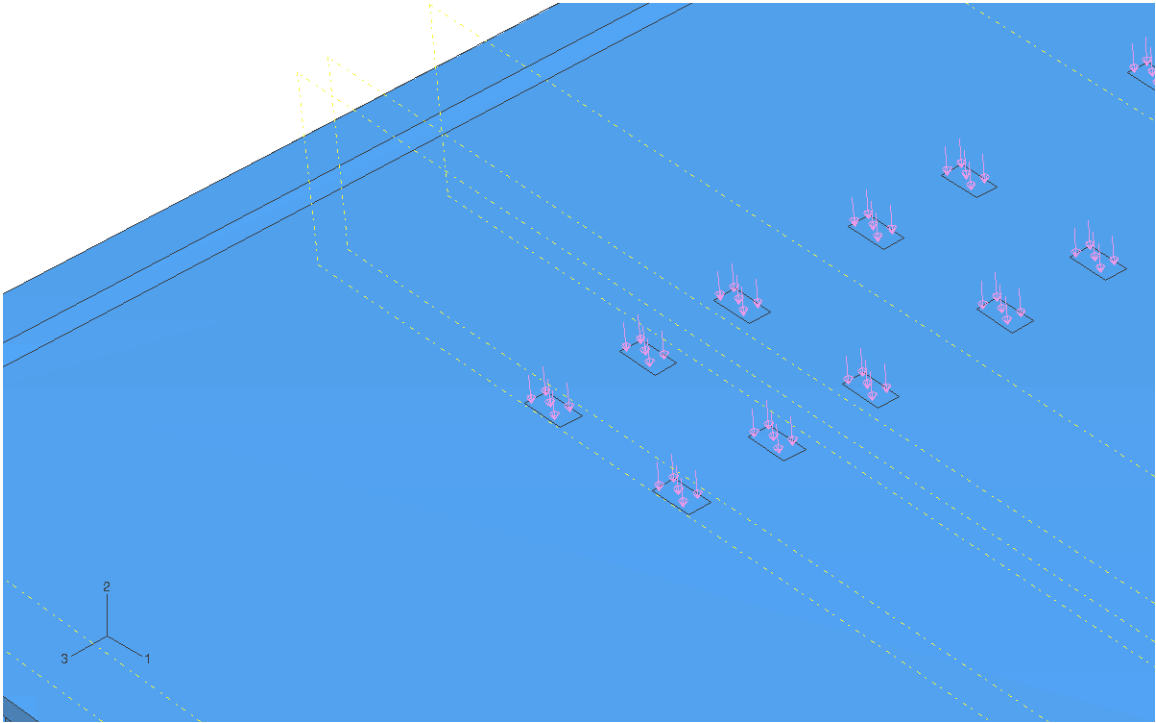


Figure 4.55 Close view of the tire pressure applied on the deck

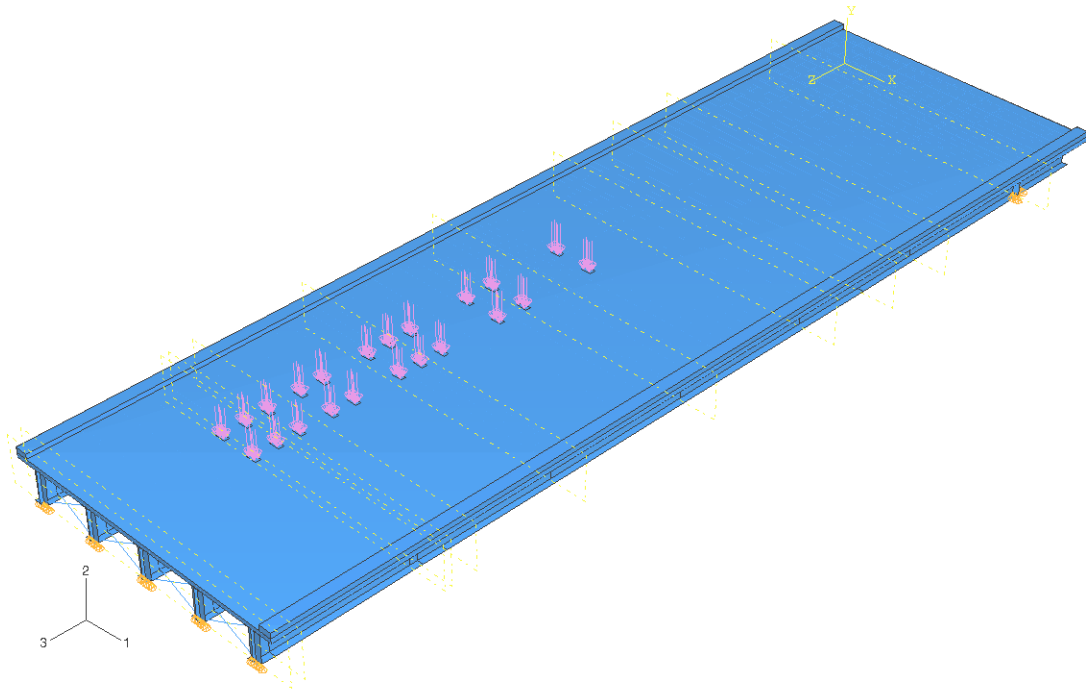


Figure 4.56 General view of the 11-axle truck applied on the FE model

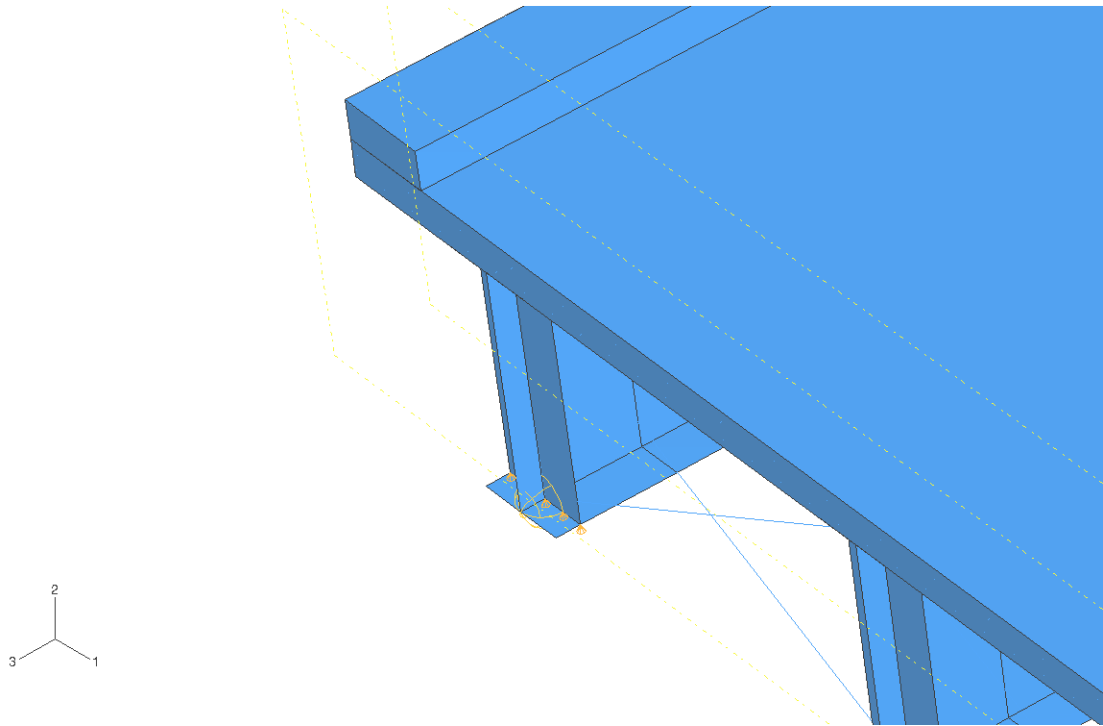


Figure 4.57 View of the spring used in the FE Model to simulate partial fixity

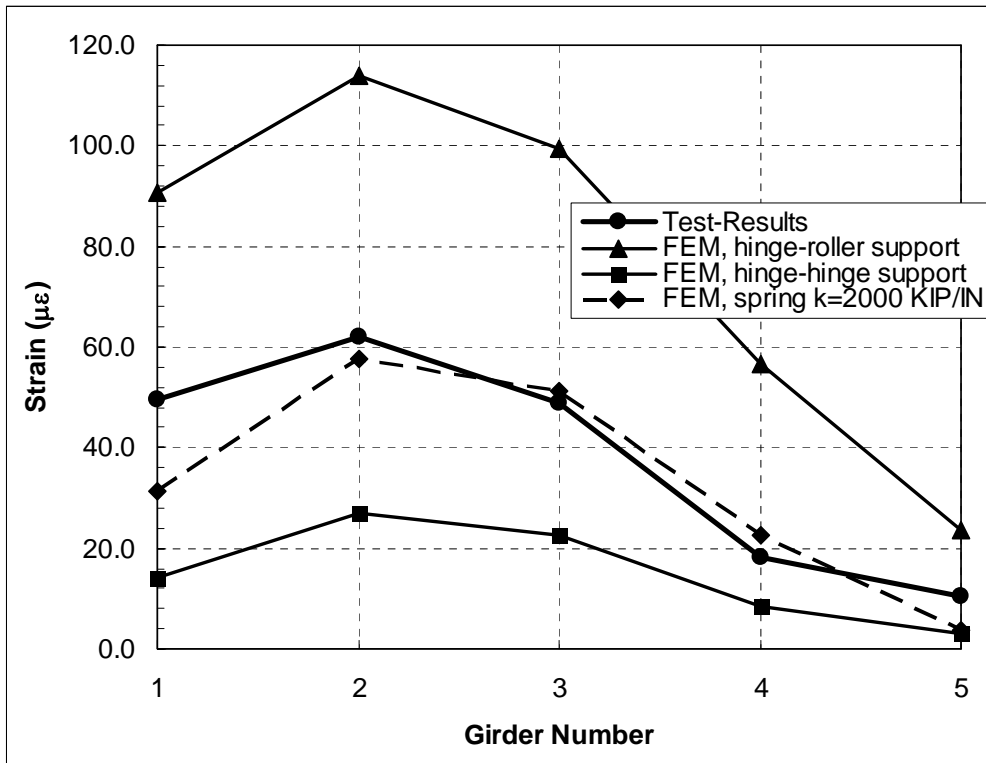


Figure 4.58 Comparison of test results with analytical results at third span – Truck in the center of north lane

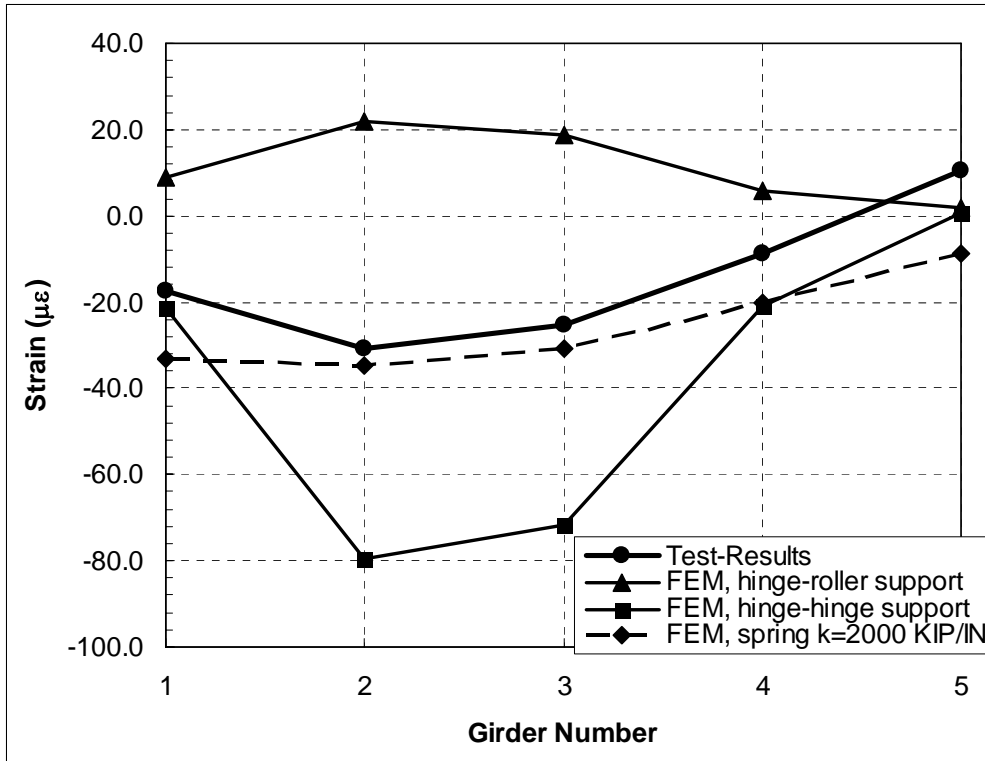


Figure 4.59 Comparison of test results with analytical results near support – Truck in the center of north lane

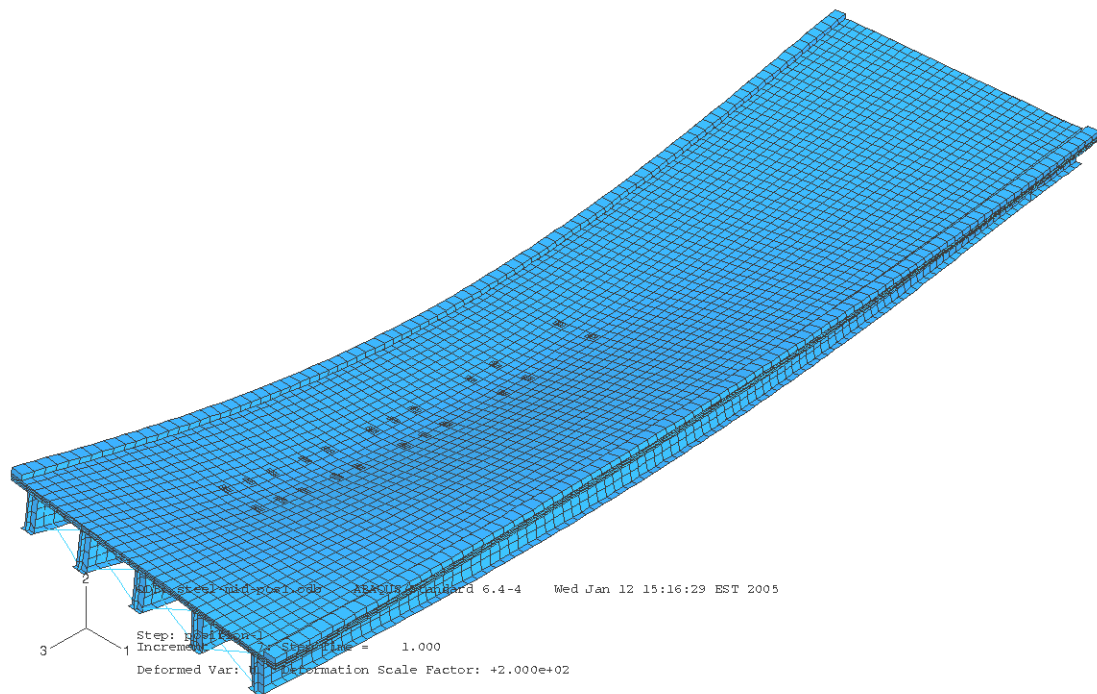


Figure 4.60 Displaced shape of the bridge model – Truck in the center of north lane

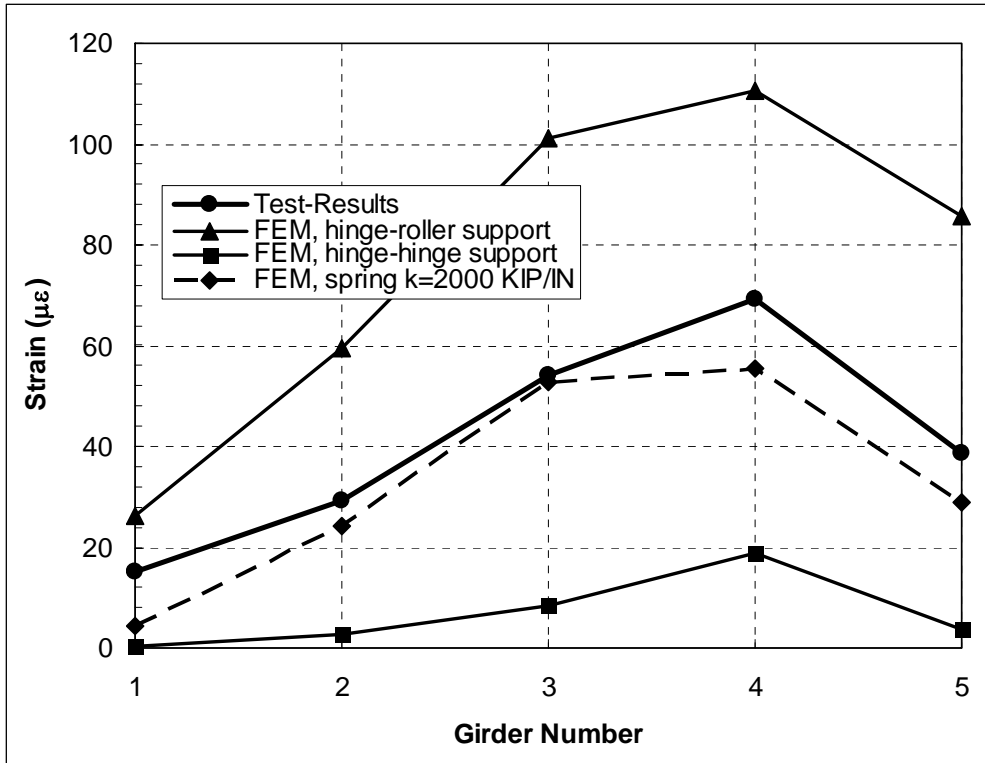


Figure 4.61 Comparison of test results with analytical results at third span – Truck in the center of south lane

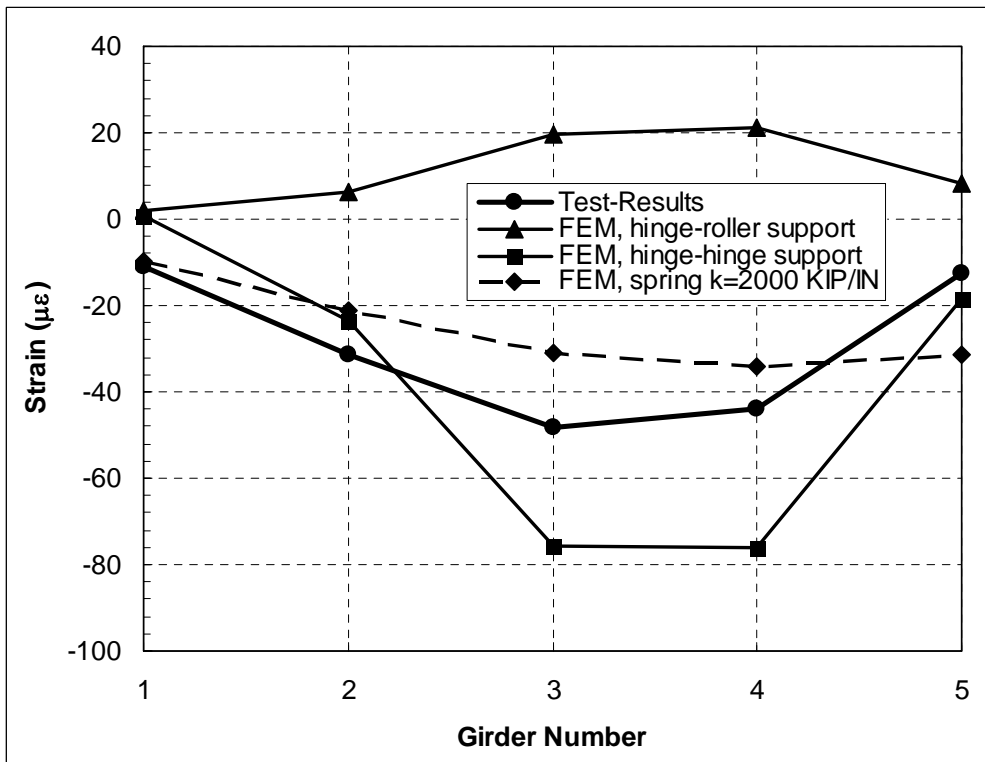


Figure 4.62 Comparison of test results with analytical results near support – Truck in the center of south lane

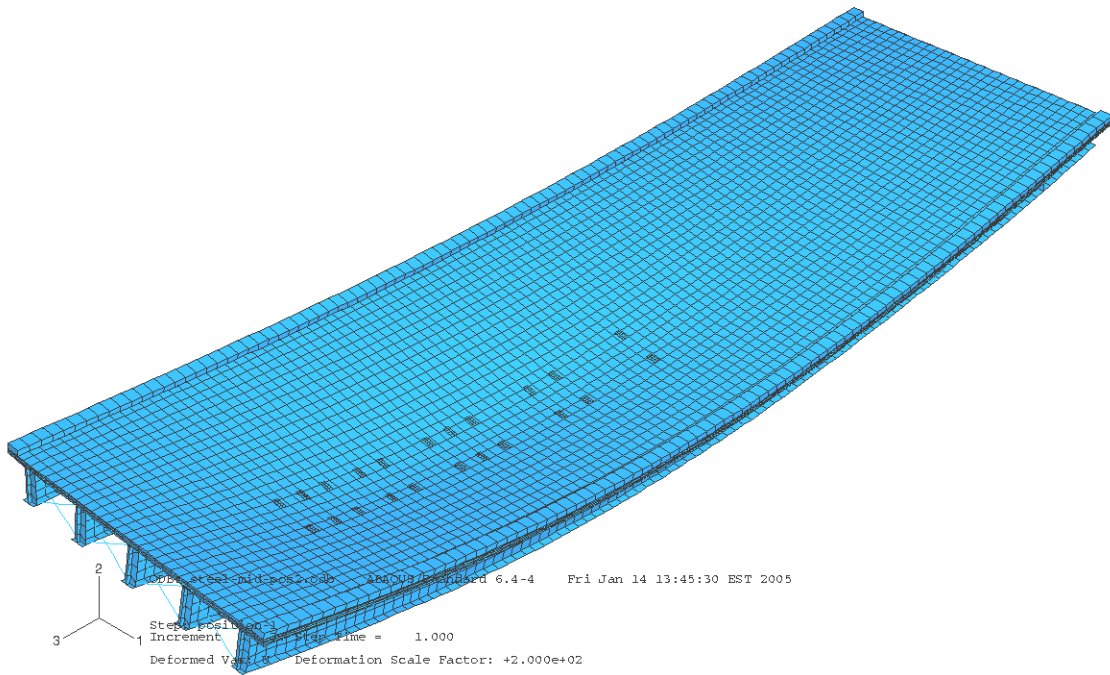


Figure 4.63 Displaced shape of the bridge model – Truck in the center of south lane

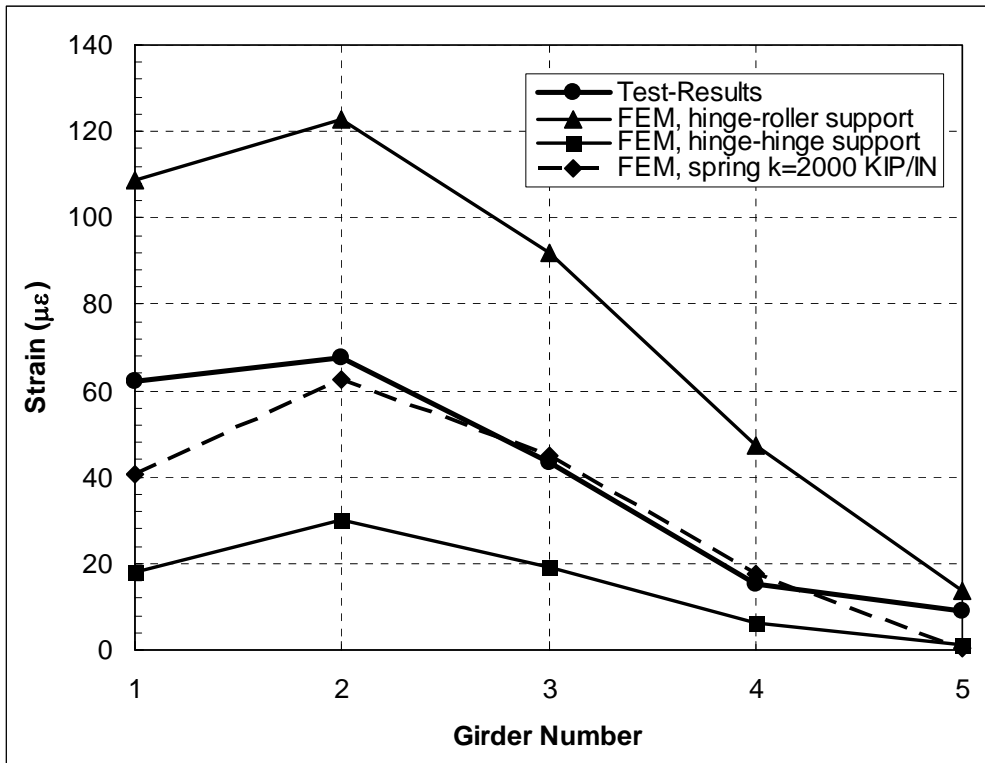


Figure 4.64 Comparison of test results with analytical results at third span – Truck close to the curb of north lane

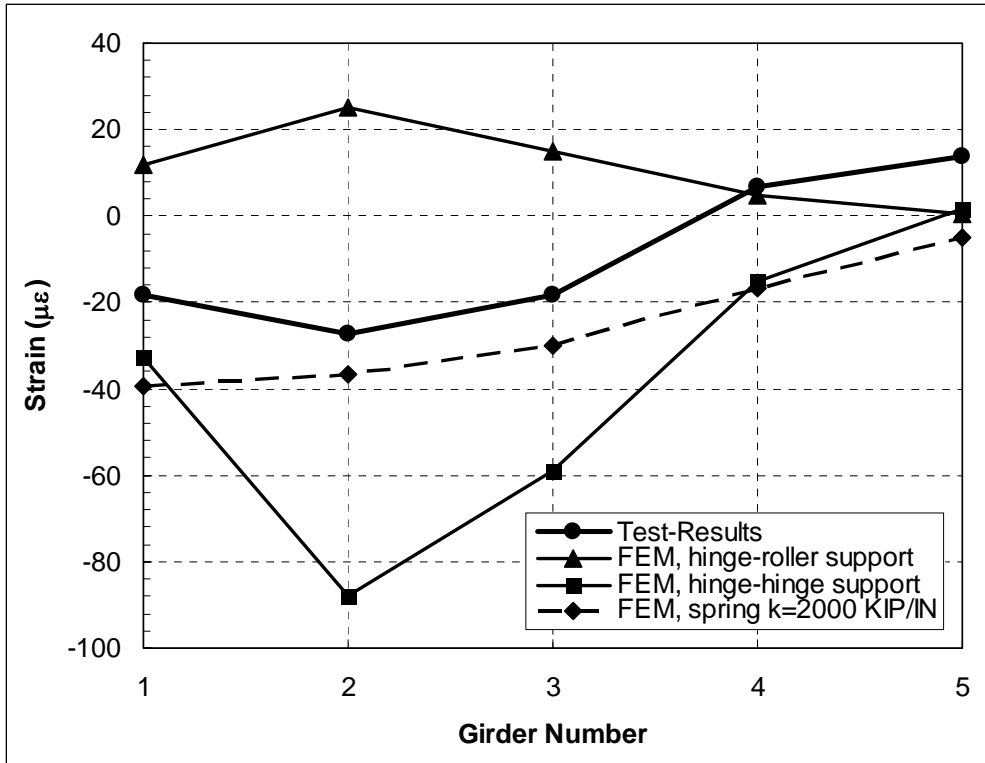


Figure 4.65 Comparison of test results with analytical results near support – Truck close to the curb of north lane

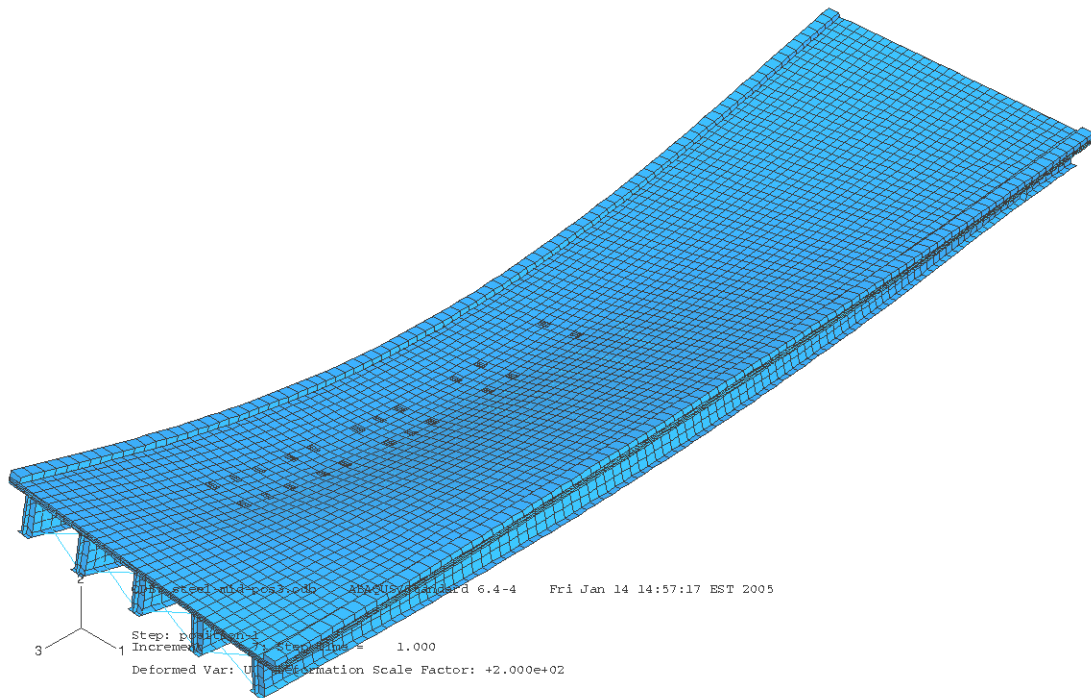


Figure 4.66 Displaced shape of the bridge model – Truck close to curb of north lane

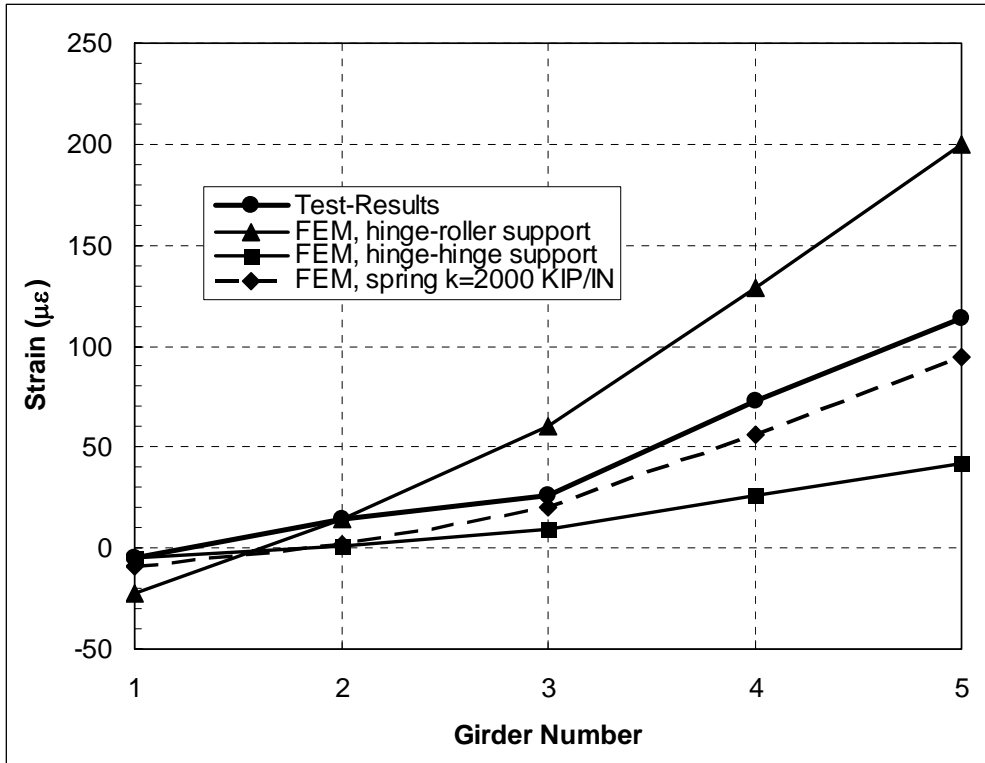


Figure 4.67 Comparison of test results with analytical results at third span – Truck close to the curb of south lane

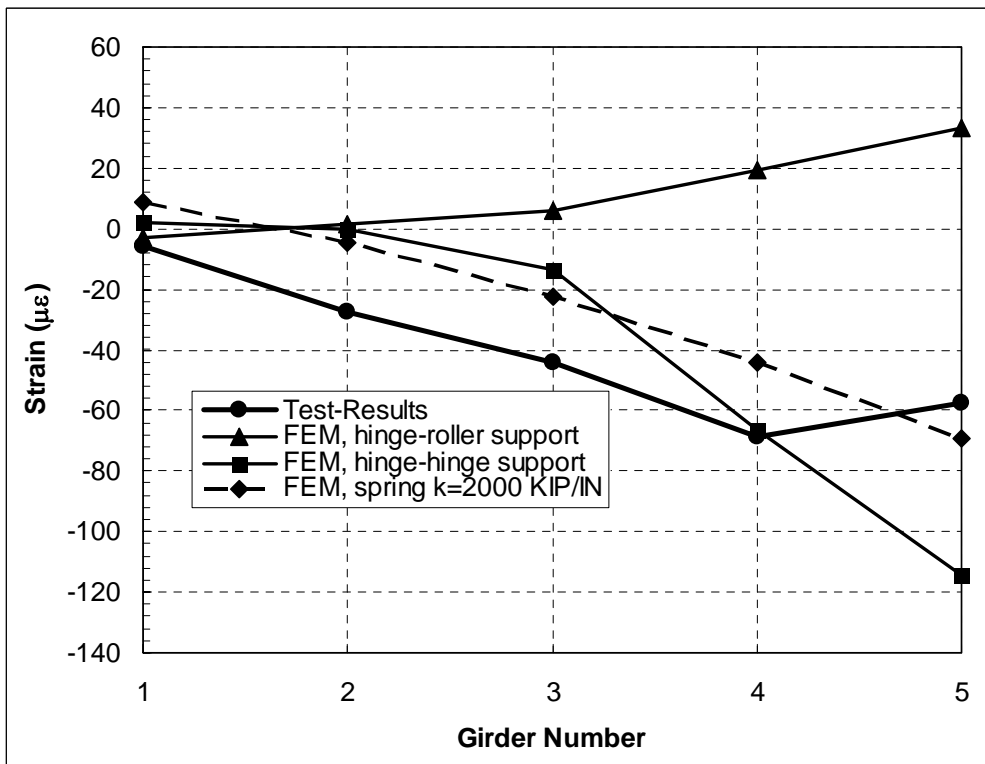


Figure 4.68 Comparison of test results with analytical results near support – Truck close to the curb of south lane

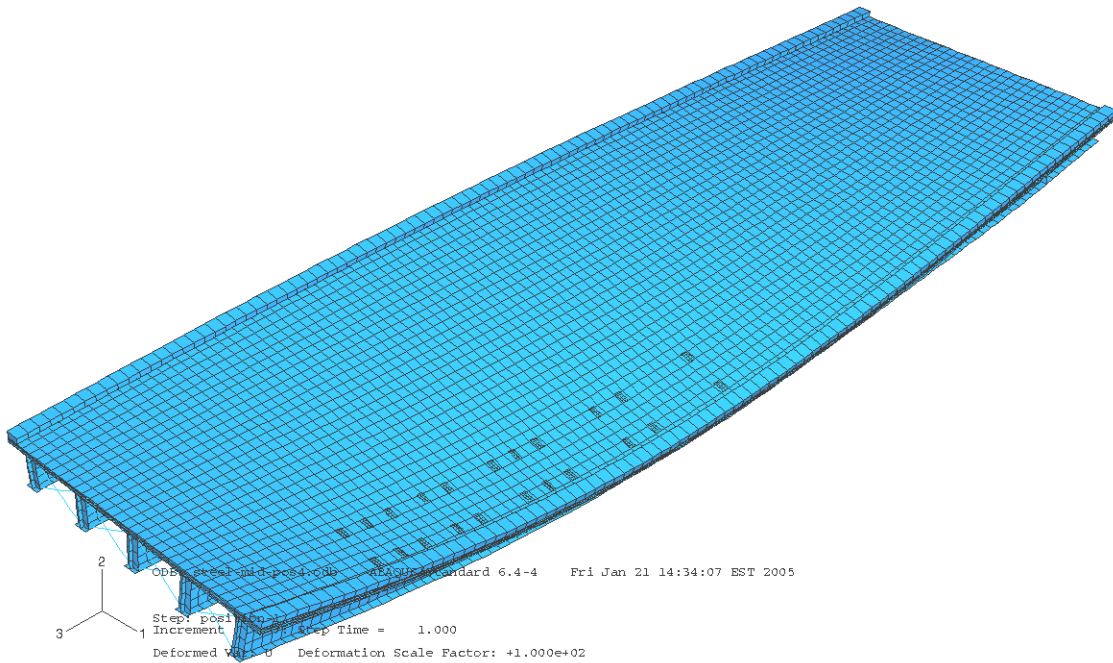


Figure 4.69 Displaced shape of the bridge model – Truck close to the curb of south lane

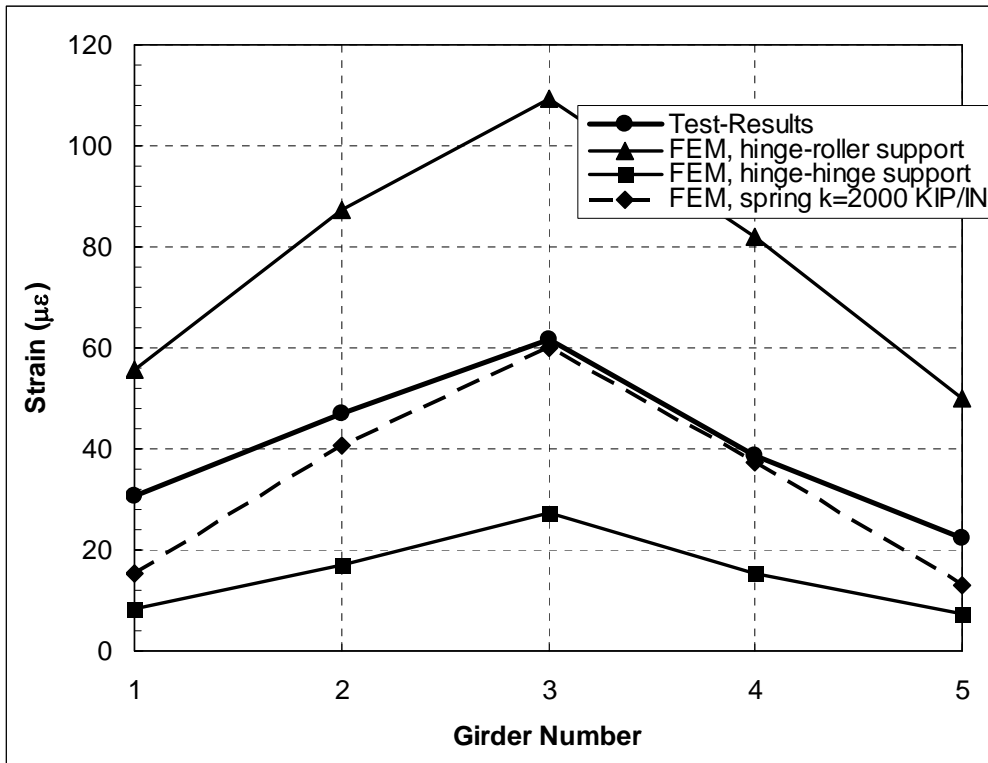


Figure 4.70 Comparison of test results with analytical results at third span – Truck in the center of the bridge

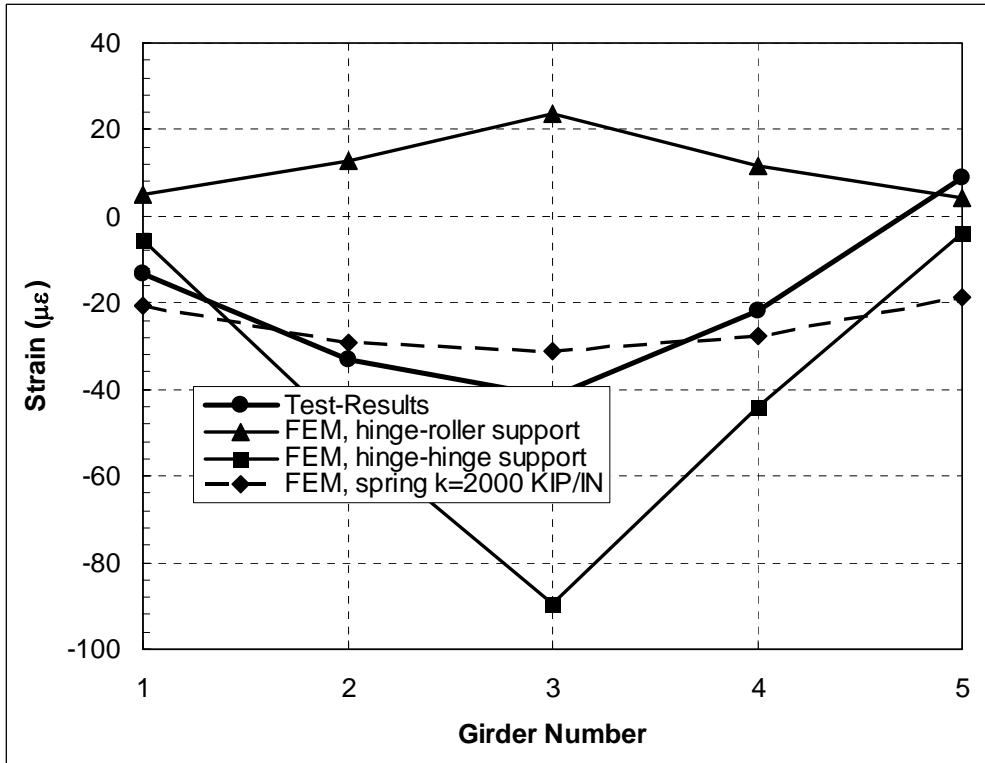


Figure 4.71 Comparison of test results with analytical results near support – Truck in the center of the bridge

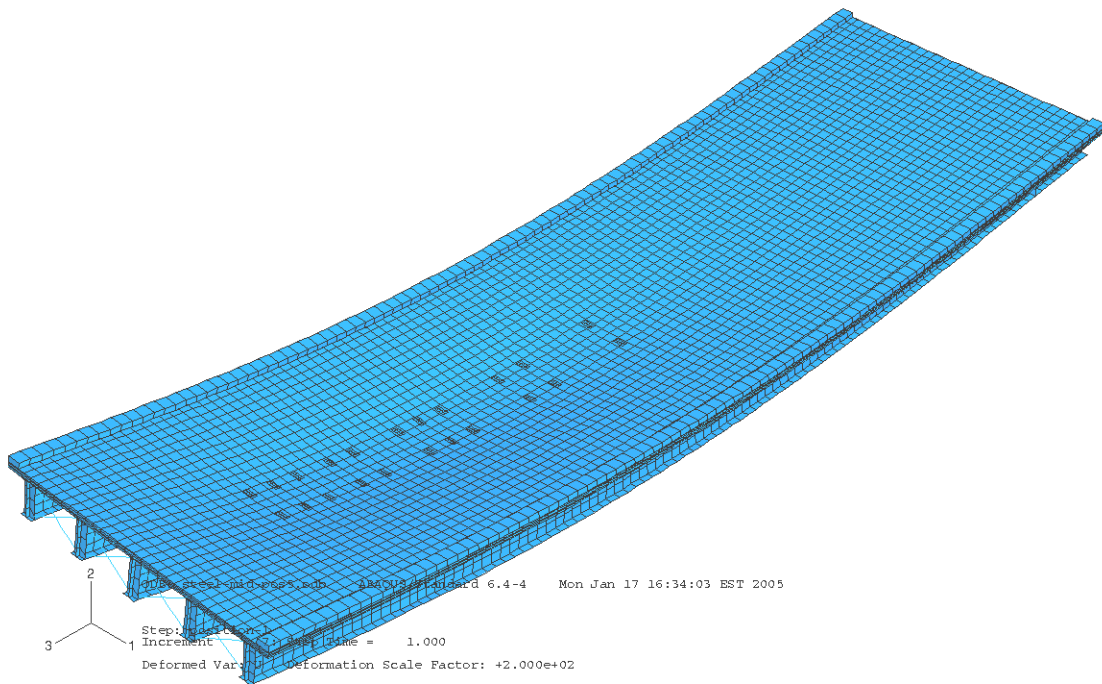


Figure 4.72 Displaced shape of the bridge model – Truck in the center of the bridge

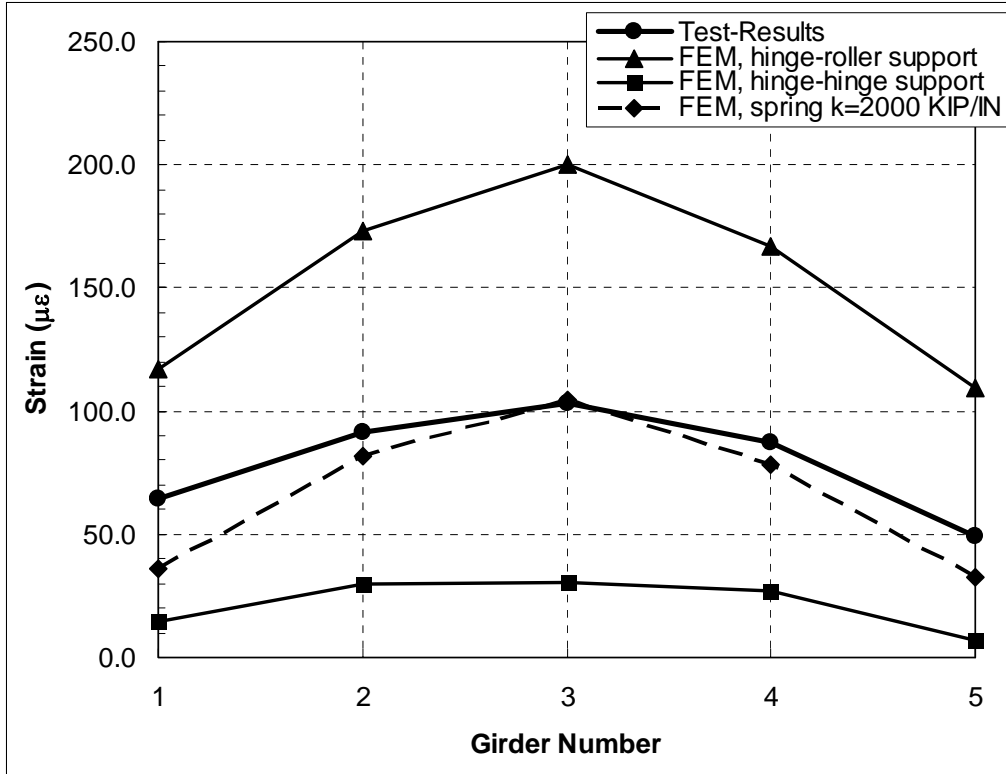


Figure 4.73 Comparison of test results with analytical results at third span – Simulation of two trucks in the center of south and north lane

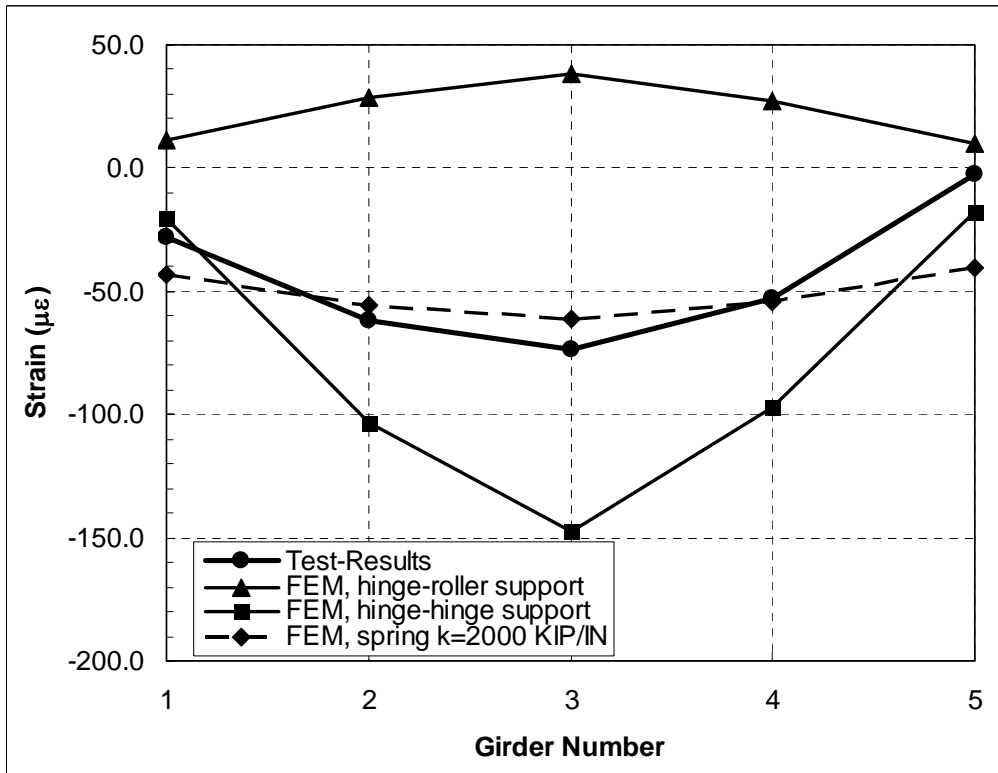


Figure 4.74 Comparison of test results with analytical results near support – Simulation of two trucks in the center of south and north lane

## CHAPTER 5

### STRUCTURAL RELIABILITY

#### 5.1. Introduction

Because of all uncertainties related to material strengths and other characteristics, loads imposed on the structure, and even the analysis methods used for evaluation and design, it is impossible to achieve absolute safety of the structure. Indeed, loads and load-carrying capacities are not perfectly known quantities, they are random variables. Therefore, structural reliability analysis requires the probabilistic modeling of these uncertainties and it provides the method for quantification of the probability that the structure does not satisfy the performance criteria.

#### 5.2. Fundamental Concepts

A random variable is a function that maps events onto intervals on the axis of real numbers. A continuous or discrete random variable is described by its cumulative distribution function (CDF) which basically relates a specific value of the random variable to a probability of realization of that value. For continuous random variables, the probability density function (PDF) is defined as the first derivative of the CDF. The PDF ( $f_x(x)$ ) and the CDF ( $F_x(x)$ ) for a continuous random variable are related as follows:

$$f_x(x) = \frac{d}{dx} F_x(x) \quad (5.1)$$

$$F_x(x) = \int_{-\infty}^x f_x(\xi) d\xi \quad (5.2)$$

In this study only continuous random variables are considered. The most important parameter of random variable is the mean value of  $x$  denoted by  $\mu_x$  also called average value and defined as:

$$\mu_x = \int_{-\infty}^{+\infty} x f_x(x) dx \quad (5.3)$$

Another one is the standard deviation of  $x$ ,  $\sigma_x$ , depends on the degree of distribution of the data around the mean. It is defined as the square root of the variance:

$$\sigma_x = \sqrt{\sigma_x^2} \quad (5.4)$$

where the variance is:

$$\sigma_x^2 = \int_{-\infty}^{+\infty} (x - \mu_x)^2 f_x(x) dx \quad (5.5)$$

Finally a nondimensional coefficient of variation,  $COV_x$ , is defined as the standard deviation divided by the mean:

$$COV_x = \frac{\sigma_x}{\mu_x} \quad (5.6)$$

Although there are many types of distributions of random variables (uniform, Gamma, Poisson, etc.), the most common types of distribution of random variables in the structural reliability theory are normal and lognormal. The PDF of a normal random variable is:

$$f_X(x) = \frac{1}{\sigma_X \sqrt{2\pi}} \exp \left[ -\frac{1}{2} \left( \frac{x - \mu_X}{\sigma_X} \right)^2 \right] \quad (5.7)$$

Where  $\sigma_x$  is the standard deviation of  $x$  and  $\mu_x$  is the mean value of  $x$  as defined earlier in equation (5.3) and equation (5.4). A standard normal variable is a special case of normal variable in which the mean value is equal to zero and the standard deviation is equal to one. The PDF of a standard normal variable  $z$  is designated as  $\phi(z)$ , while the CDF is  $\Phi(z)$ . An example of a PDF and CDF of a standard normal random variable are given in Figure 5.1.

The PDF of a lognormal random variable is:

$$f_X(x) = \frac{1}{x \sigma_{\ln(X)}} \phi \left( \frac{\ln(x) - \mu_{\ln(X)}}{\sigma_{\ln(X)}} \right) \quad (5.8)$$

where:

$$\sigma_{\ln(X)}^2 = \ln(V_X^2 + 1) \quad (5.9)$$

$$\mu_{\ln(X)} = \ln(\mu_X) - \frac{1}{2} \sigma_{\ln(X)}^2 \quad (5.10)$$

### 5.3. Reliability Analysis Method

#### 5.3.1. Limit State

The concept of a limit state is used to help define failure in the context of structure reliability analyses. A limit state is the boundary between the desired and the undesired performance of a structure. For a bridge an undesired performance is loss of ability to carry traffic. The undesired performance can include collapse of the bridge

structure or excessive deflection causing discomfort for pedestrians and drivers. Limit states can be divided into two categories:

Ultimate Limit States (ULS) are mostly related to the loss of load carrying capacity. When an Ultimate Limit State (ULS) is exceeded, a catastrophic failure of the structure occurs, such as collapse or loss of operability. ULSs can be the formation of a plastic hinge, crushing of concrete, buckling or loss of stability. These are the limit state considered in a reliability-based design code.

Serviceability Limit States (SLSs) are related to gradual degradation and user's comfort. These limit states are usually not associated with an immediate structural collapse. SLSs can be an excessive cracking on a bridge deck leading to potholes and spalling of concrete.

The acceptability criteria are often based on engineering judgment (arbitrary decision). For example, consider a beam that fails if the moment due to the loads exceeds the moment carrying capacity. Then the corresponding limit state function can be written as follows:

$$g = g(x_1, x_2, x_3, \dots, x_n) = R - Q \quad (5.11)$$

where R represents the resistance (moment carrying capacity), Q represents the load effect (total moment applied) and  $x_i$  represent the random variables of load and resistance such as dead load, live load, length, depth, etc. The limit state function represents the boundary beyond which the structure no longer functions. The probability of failure,  $P_f$ , is equal to the probability that the undesired performance will occur. Mathematically, this can be expressed in terms of the limit state function as:

$$P_f = P(R - Q < 0) = P(g < 0) \quad (5.12)$$

If both R and Q are continuous random variables, then each has a probability density function (PDF) such as shown in Figure 5.2. Furthermore, R-Q is also a random variable with its own PDF. This is also shown in Figure 5.2. The probability of failure corresponds to the shaded area in Figure 5.2. Specifically the probability of failure is:

$$P_f = \int_{-\infty}^{+\infty} F_R(x_i) f_Q(x_i) dx_i \quad (5.13)$$

where  $F_R(x)$  is the CDF of resistance R and  $f_Q(x)$  is the PDF of the load Q.

Because there are often multiple random variables that determine R and Q, the evaluation of equation 5.13 cannot be calculated as this would require complex and time consuming numerical techniques. Moreover, there is often insufficient data to fully define the basic variables needed for this numerical procedure in order to obtain acceptable accuracy. Therefore, it is convenient to measure structural safety in terms of a reliability index.

### 5.3.2. Reliability Index

A formal definition of the reliability index is that it represents the shortest distance from the origin of standard space (reduced variable space) to the limit state line  $g(Z_R, Z_Q) = 0$ , in the reduced variables space, as shown in Figure 5.3, where  $Z_R$  is the reduced random variable for resistance and  $Z_Q$  is the reduced variable for load. The reduced form of a random variable, X, is given by:

$$Z_X = \frac{X - \mu_X}{\sigma_X} \quad (5.14)$$

There are various procedures available for calculation of  $\beta$ . These procedures vary with regard to accuracy and required input data.

The reliability index,  $\beta$ , is related to the probability of failure,  $P_f$ , by:

$$\beta = -\Phi^{-1}(P_f) \quad (5.15)$$

where  $\Phi^{-1}$  is the inverse standard normal distribution function. A comparison of the reliability index to probability of failure according the equation 5.15 is given in Table 5.1. The value of 3.5 in Table 5.1 represents the target reliability index for bridges of the AASHTO LRFD Code. However, this value is used for calibration only, and as it will be shown in this study, the actual components can have significantly different values of  $\beta$ .

### 5.3.3. First Order Second Moment Methods (FOSM)

The First Order Second Moment method is one the simplest procedures for calculating the reliability indices. First order implies that this method considers only linear limit state functions or linear approximation of them, while second moment refers to the fact that the first two moments of a random variable, the mean value and the standard deviation, are considered. The third and fourth moments are skewness and kurtosis, respectively, but these parameters are often unavailable and are rarely used. If both R and Q are independent normal random variables, then the reliability index,  $\beta$ , as originally defined by Cornell (1969) is expressed as:

$$\beta = \frac{\mu_R - \mu_Q}{\sqrt{\sigma_R^2 + \sigma_Q^2}} \quad (5.16)$$

Where  $\mu_R$  and  $\mu_Q$  are the means of R and Q, respectively, and  $\sigma_R$ ,  $\sigma_Q$  are the standard deviations of R and Q, respectively. If both R and Q are lognormal variables, then,  $\beta$  can be derived equal to:

$$\beta = \frac{\ln\left(\frac{\mu_R}{\mu_Q} \sqrt{\frac{COV_Q^2 + 1}{COV_R^2 + 1}}\right)}{\sqrt{\ln((COV_R^2 + 1)(COV_Q^2 + 1))}} \quad (5.17)$$

using equation 5.18 and 5.19,

$$\sigma_{\ln(X)}^2 = \ln(COV_X^2 + 1) \quad (5.18)$$

$$\mu_{\ln(X)} = \ln(\mu_x) - \frac{1}{2} \sigma_{\ln(X)}^2 \quad (5.19)$$

where  $COV_R$ ,  $COV_Q$  are the coefficients of variation of R and Q respectively. If  $COV_R$  and  $COV_Q$  are less or equal to 0.20, the value of  $\beta$  can be approximated by the following expression (Rosenblueth and Esteva 1972):

$$\beta = \frac{\ln(\mu_R / \mu_Q)}{\sqrt{COV_R^2 + COV_Q^2}} \quad (5.20)$$

using the following equations

$$\sigma_{\ln(X)}^2 \approx V_X^2 \quad (5.21)$$

$$\mu_{\ln(X)} \approx \ln(\mu_X) \quad (5.22)$$

where  $\mu_R$  and  $\mu_Q$  are the means of R and Q, respectively, and  $COV_R$ ,  $COV_Q$  are the standard deviations of R and Q, respectively.

When the limit state function is a *linear* combination of  $n$  uncorrelated random variables  $X_1, X_2, \dots, X_n$ , of the form

$$g(X_1, X_2, \dots, X_n) = a_0 + a_1 X_1 + a_2 X_2 + \dots + a_n X_n = a_0 + \sum_{i=1}^n a_i X_i \quad (5.24)$$

where  $a_i$  are constants, the reliability can be calculated using the following expression

$$\beta = \frac{a_0 + \sum_{i=1}^n a_i \mu_{X_i}}{\sqrt{\sum_{i=1}^n (a_i \sigma_{X_i})^2}} \quad (5.25)$$

where  $\mu_{X_i}$  and  $\sigma_{X_i}$  are the means and standard deviations respectively of the normal random variables  $X_i$ .

The First Order Second Moment method can also be used to compute the reliability index in case of nonlinear limit state functions. In this case, the limit state function is linearized using a Taylor series expansion about the mean values of the random variables (Madsen, Krenk and Lind 1986):

$$g(X_1, X_2, \dots, X_n) \approx g(\mu_{X_1}, \mu_{X_2}, \dots, \mu_{X_n}) + \sum_{i=1}^n (X_i - \mu_{X_i}) \left. \frac{\partial g}{\partial X_i} \right|_{\text{evaluated at mean values}} \quad (5.26)$$

Reliability index can then be computed as:

$$\beta = \frac{g(\mu_{X_1}, \mu_{X_2}, \dots, \mu_{X_n})}{\sqrt{\sum_{i=1}^n (a_i \sigma_{X_i})^2}} \quad \text{where } a_i = \left. \frac{\partial g}{\partial X_i} \right|_{\text{evaluated at mean values}} \quad (5.27)$$

The reliability index calculated by this method is called the First Order Second Moment (FOSM) mean value reliability index, as the Taylor series expansion is carried out about the mean values of the random variables.

Because the FOSM mean value method is based on the approximation of non-normal CDF's of the state variables by normal variables, the method presents advantages as well as disadvantages. The main advantage of the method is its simplicity; only the first two moments of each random variable are needed and the calculations are trivial. Moreover, knowledge of the distribution of the random variable is not needed.

However this can be considered as a disadvantage. If the knowledge of the distribution of the random variable is not needed, it means that this method does not account for it. Indeed, if the random variables are other than normally distributed, the method is not as accurate. This is particularly true if the upper tail of the load distribution and the lower tail of the resistance distribution cannot be correctly approximated by normal distributions. Another problem is that the reliability index depends on the formulation of the limit state function. This is referred in the literature as the invariance problem of the mean value FOSM method.

#### **5.3.4. Hasofer-Lind Reliability Index**

To overcome the invariance problem of the FOSM method, Hasofer and Lind (1974) proposed a modified reliability index formulation, the Advanced First Order Second Moment reliability moment (AFSOM). In this method, the limit state function is evaluated at a point known as the “design point” instead of the mean values. The design point is located on failure surface,  $g = 0$ , and since this point is a priori unknown, an iteration technique must be used to solve for the reliability index. As it was done in the FOSM method, the Hasofer-Lind method consists by first transforming each of the random variables into standard normal space, using equation 5.15. As before, the

Hasofer-Lind reliability index is defined as the shortest distance from the origin of the reduced variable space to the limit state function or failure surface  $g = 0$  as presented in Figure 5.4. Therefore, in the case of a linear limit state, equation 5.25 can be used.

However, for a nonlinear limit state function, the iterative method mentioned earlier must be used.

The iterative method requires a simultaneous solution of  $2n + 1$  equations with  $2n + 1$  unknowns, where  $n$  is equal to the number of random variables. The process is repeated until values of  $\beta$  and  $\alpha_i$  converge:

$$\alpha_i = \frac{-\left. \frac{\partial g}{\partial Z_i} \right|_{\text{evaluated at design point}}}{\sqrt{\sum_{k=1}^n \left( \left. \frac{\partial g}{\partial Z_k} \right|_{\text{evaluated at design point}} \right)^2}} \quad (5.28)$$

$$\frac{\partial g}{\partial Z_i} = \frac{\partial g}{\partial X_i} \frac{\partial X_i}{\partial Z_i} = \frac{\partial g}{\partial X_i} \sigma_{X_i}$$

$$\sum_{i=1}^n (\alpha_i)^2 = 1$$

$$z_i^* = \beta \alpha_i$$

$$g(z_1^*, z_2^*, \dots, z_n^*) = 0$$

Although it takes into account the nonlinearity of the limit state function, the Hasofer-Lind method, as for the FOSM method, does not take into account the distribution type of the random variables, and therefore is not accurate when used with distributions other than normal.

### 5.3.5. Rackwitz-Fiessler Procedure

Rackwitz and Fiessler (1978) developed an iterative procedure to calculate reliability indices that this time can take into account the distribution of the random variables for both linear and nonlinear limit states. Each non normal random variable is converted at the design point into “equivalent normal” distribution. This is achieved by equating the CDF and the PDF of the actual function to the normal CDF and normal PDF at the value of the variable  $x^*$  on the failure boundary ( $g = 0$ ) as described in equation 5.29 and 5.30.

$$F_X(x^*) = \Phi\left(\frac{x^* - \mu_X^e}{\sigma_X^e}\right) \quad (5.29)$$

$$f_X(x^*) = \frac{1}{\sigma_X^e} \phi\left(\frac{x^* - \mu_X^e}{\sigma_X^e}\right) \quad (5.30)$$

where  $\Phi$  is the CDF for the standard normal distribution and  $\phi$  is the PDF for the standard normal distribution. The initial design point  $\{x_i^*\}$  is obtained by assuming values for  $n-1$  of the random variables  $X_i$ , the mean values often being a reasonable choice, then, the remaining random variable is calculated using the limit state function  $g=0$ . By doing so, it is ensured that the design point is on the failure boundary. Then the process works the following way:

1. From equation 5.29 and 5.30 we can obtain the expression for the equivalent normal mean and equivalent normal standard deviation for each random variable.

$$\mu_X^e = x^* - \sigma_X^e \left[ \Phi^{-1}(F_X(x^*)) \right] \quad (5.31)$$

$$\sigma_X^e = \frac{1}{f_X(x^*)} \phi\left(\frac{x^* - \mu_X^e}{\sigma_X^e}\right) = \frac{1}{f_X(x^*)} \phi\left[\Phi^{-1}(F_X(x^*))\right] \quad (5.32)$$

2. As in the previous method, the reduced variates are determined using equation 5.33.

$$z_i^* = \frac{x_i^* - \mu_{X_i}^e}{\sigma_{X_i}^e} \quad (5.33)$$

3. Next, the partial derivative of the limit state function  $g$  is evaluated for each random variable  $X_i$ , and presented in a vector form as follow:

$$\{G\} = \begin{Bmatrix} G_1 \\ G_2 \\ \vdots \\ G_n \end{Bmatrix} \quad \text{where} \quad G_i = - \left. \frac{\partial g}{\partial Z_i} \right|_{\text{evaluated at design point}} \quad (5.34)$$

4. Then  $\beta$  is calculated using the following formula:

$$\beta = \frac{\{G\}^T \{z^*\}}{\sqrt{\{G\}^T \{G\}}} \quad \text{where} \quad \{z^*\} = \begin{Bmatrix} z_1^* \\ z_2^* \\ \vdots \\ z_n^* \end{Bmatrix} \quad (5.35)$$

5. The sensitivity factors are calculated in a column vector as follows:

$$\{\alpha\} = \frac{\{G\}}{\sqrt{\{G\}^T \{G\}}} \quad (5.36)$$

6. A new design point is determined in the original coordinates for  $n-1$  values using

$$x_i^* = \mu_{X_i}^e + \alpha_i \beta \sigma_{X_i}^e \quad (5.37)$$

7. The value of remaining random variable is calculated using the limit state function  $g = 0$ .

8. Steps 1-7 are repeated until reliability index converges.

Typically, the Rackwitz-Fiessler procedure converges very quickly, and in most cases, after only a few iterations. In this research, since both the load and the resistance were assumed to have a lognormal distribution, the reliability indices calculated by the Rackwitz-Fiessler method and the reliability indices calculated by the FOSM method using equation 5.19 were found almost the same, therefore, the FOSM method, which is easier to apply, was chosen.

#### **5.4. Simulation Techniques**

In certain cases, the methods for the computation of reliability explained above can become very complicated. This happens especially when the limit state function is very complex or cannot be expressed in a closed form, as, for example in this study, the orthotropic plate equations governing the behavior of a bridge deck slab. In these situations, simulation methods are used.

##### **5.4.1. Monte Carlo Simulation**

The Monte Carlo technique is based on the generating of values for given distribution functions. For example let's have the load effect  $Q$ , and the resistance  $R$ , as functions of random variables,  $R = f(x_1, x_2, \dots, x_n)$  and  $Q = f(y_1, y_2, \dots, y_n)$ . By generating a large number of specific values for the random variables  $x_i$  and  $y_i$ ,  $R$  and  $Q$  can then be evaluated, and their statistical parameters (mean and standard deviation) can be computed. With these statistical parameters, the reliability index can now be calculated using one of the methods described earlier, regardless of how complex the original limit state function is, as now it can be reduced to  $g = R - Q$ . Moreover, the

distribution of the random parameters affecting the load and the resistance ( $x_i$  and  $y_i$ ) is included in the simulation process so that the generated values reflect the actual distributions of the random variables. For each random variable, the generation of values by the Monte Carlo simulation is done the following way.

The first step is to generate random numbers,  $u_i$ , that are uniformly distributed between 0 and 1 (there is an equal chance for any number within that range to be generated)

Then for each random variable,  $X$ , the generated value is calculated using the equation:

$$x_i = F_x^{-1}(u_i) \quad (5.38)$$

where  $F_x^{-1}$  is the CDF of the random variable. For a standard normal variable, equation 5.38 becomes:

$$x_i = \Phi^{-1}(u_i) \quad (5.39)$$

where  $\Phi^{-1}$  is the inverse of the standard normal cumulative distribution function. For any normally distributed random variable,

$$x_i = \mu_x + \Phi^{-1}(u_i) \sigma_x \quad (5.40)$$

Where  $\mu_x$  and  $\sigma_x$  are the mean and standard deviation of the random variable being generated.

For a lognormal random variable,

$$x_i = \exp\left[\mu_{\ln X} + \Phi^{-1}(u_i) \sigma_{\ln X}\right] \quad (5.41)$$

where

$$\begin{aligned}\sigma_{\ln X}^2 &= \ln(V_X^2 + 1) \\ &\approx V_X^2 \quad (\text{for } V_X < 0.20)\end{aligned}\tag{5.42}$$

$$\begin{aligned}\mu_{\ln X} &= \ln(\mu_X) - \frac{1}{2}\sigma_{\ln X}^2 \\ &\approx \ln(\mu_X) \quad (\text{for } V_X < 0.20)\end{aligned}$$

Finally, the limit state function can be evaluated directly for each generated set of variables, and after repeating the process many times, the probability of failure can be obtained. For example, if the limit state function is  $g = R - Q$ , the probability of failure can be estimated by:

$$P_f = \frac{n}{N}\tag{5.43}$$

where  $n$  is the number of times that  $g \leq 0$  and  $N$  is the total number of simulations. As the number of simulations increases, the obtained probability of failure is closer to the real value of the probability of failure. In order to estimate how many simulations are needed to achieve the acceptable accuracy, Soong and Grigoriu (1993) showed that the estimated probability of failure itself can be treated as a random variable with its own mean, standard deviation and coefficient of variation as shown in equation 5.44:

$$\begin{aligned}\sigma_{P_f}^2 &= \frac{P_f(1-P_f)}{N} \\ COV_{P_f} &= \sqrt{\frac{1-P_f}{N \times P_f}}\end{aligned}\tag{5.44}$$

These relationships provide a way to determine how many simulations are required to estimate a probability and limit the uncertainty in the estimate. It is clear that the smaller the expected probability of failure, the larger the number of required simulations.

#### **5.4.2. Rosenblueth's 2K + 1 Point Estimate Method**

In order to reduce the number of required simulations, several simulation techniques have been developed: The Latin Hypercube method, described by Iman and Conover (1980) is one of them. In this method, the range of possible values of each random variable is divided into strata, and a value from each stratum is randomly selected as a representative value. The representative values for each random variable are then combined so that each representative value is considered once and only once in the simulation process. However, in order to further reduce the number of required simulations, point estimation methods can be used.

The point estimate method is very similar to the Monte Carlo simulation, but instead of generating a large number of random values to be used for the simulation, the function of random variables is evaluated at only a few pre-determined key points. The results obtained at these key points are then used to estimate the mean and variance (or coefficient of variation) of the function. These key point values have been derived to give a good accuracy. The 2K + 1 method developed by Rosenblueth (1975, 1981) has been widely used and proved to be accurate; however, the CDF of the function cannot be obtained by this method. Let's consider a limit state function Y described by

$$Y = f(X_1, X_2, \dots, X_i, \dots, X_k) \quad (5.45)$$

where  $f$  is some deterministic function, but not necessarily known in closed form, and  $X_1, X_2, \dots, X_i, \dots, X_k$  are random input variables. The Rosenblueth's  $2K + 1$  point estimate method works the following way:

1. Determine the mean value,  $\mu_{X_i}$ , and standard deviation  $\sigma_{X_i}$  for each of the  $K$  input random variables.

2. Define  $y_0$  as the value obtained from Equation 5.45 when all input variables are equal to their mean values.

$$y_0 = f(\mu_{X_1}, \mu_{X_2}, \dots, \mu_{X_i}, \dots, \mu_{X_K}) \quad (5.46)$$

3. For each random variable  $X_i$ , evaluate the function at two values of  $X_i$  which are shifted from the mean value  $\mu_{X_i}$  by  $\pm \sigma_{X_i}$  while all other variables are assumed to be equal to their mean values. The function  $Y$  will be then evaluated at  $2K$  additional points. These values of the function will be referred to as  $y_i^+$  and  $y_i^-$ . The subscript denotes the variable which is shifted, and the superscript indicates the direction of the shift. In mathematical notation,

$$y_i^+ = f(\mu_{X_1}, \mu_{X_2}, \dots, \mu_{X_i} + \sigma_{X_i}, \dots, \mu_{X_K}) \quad (5.47)$$

$$y_i^- = f(\mu_{X_1}, \mu_{X_2}, \dots, \mu_{X_i} - \sigma_{X_i}, \dots, \mu_{X_K})$$

4. For each random variable, calculate the following two quantities based on  $y_i^+$  and  $y_i^-$ .

$$\bar{y}_i = \frac{y_i^+ + y_i^-}{2} \quad (5.48)$$

$$V_{y_i} = \frac{y_i^+ - y_i^-}{y_i^+ + y_i^-}$$

5. Calculate the estimated mean and coefficient of variation of Y as follows:

$$\bar{Y} = y_0 \prod_{i=1}^K \left( \frac{\bar{y}_i}{y_0} \right) \quad (5.49)$$

$$V_Y = \sqrt{\left\{ \prod_{i=1}^K (1 + V_{y_i}^2) \right\} - 1}$$

The two main advantages of this method are that first, there is no need to know the distribution of the input random variables, only two first moments are needed. Second, the number of simulations is relatively small compared to the Latin hypercube sampling or Monte Carlo simulation; for K random input variables, only  $2K + 1$  simulations are needed.

In this study the Rosenblueth's  $2K + 1$  point estimate method is used and the Y function is evaluated at the  $2K + 1$  points using the Finite Element model presented in chapter 4.

## 5.5. Bridge Load Model

### 5.5.1. Introduction

The load component of highway bridges can be divided into several groups, such as dead, live load, (static and dynamic), environmental loads (temperature, wind, earthquake, earth pressure, ice) and other loads (collision, braking load). Load components are treated as random variables, their variation is described by a cumulative distribution function (CDF), a mean value and a coefficient of variation.

The basic load combination for highway bridges considered in this study is the combination of dead load, live load and dynamic load. The time period considered in this study for reliability calculation is one year.

### **5.5.2. Dead Load**

Dead load, usually denoted  $D$ , is the gravity load due to the self weight of the structural elements permanently attached to the bridge. The statistical parameters of dead load are summarized in Table 5.2.

Because of different degree of variation it is recommended (Nowak 1993) to consider the following components of  $D$ :

$D_1$  = weight of factory made elements (steel, precast concrete)

$D_2$  = weight of cast in place concrete

$D_3$  = weight of wearing surface (asphalt)

$D_4$  = weight of miscellaneous weight (e.g. railing, luminaries)

All component of dead load are typically treated as normal random variables. Usually, it is assumed that the total dead load remains constant throughout the life of the structure.

### **5.5.3. Live Load**

Live load,  $L$ , covers a range of forces produced by vehicles moving on the bridge. Live load effect can be divided into two components, the static portion,  $L$ , and the dynamic portion,  $I$ . The effect of live load depends on many parameters (Nowak 1993) such as the span length, truck weight, axle loads, axle configuration, position of the vehicle on the bridge (longitudinal and transversal), traffic volume (ADTT) numbers of

vehicle on the bridge (multiple presence), girder spacing, and stiffness of structural members.

Live Load model for AASHTO LRFD 1998 is interpreted from recent research related to the development of LRFD codes (Agarwal and Wolkowicz 1976, Nowak 1993). The LRFD live loads are modeled on the basis of the available truck survey data (Nowak 1993) and are shown in Figure 5.5 and Figure 5.6.

The available statistical parameters of bridge live load have been determined from truck surveys and simulation. Several sources of truck load data exist. Weigh-in-Motion (WIM) reported in the literature include studies done by the University of Colorado for the Federal Highway Administration (FHWA) and Michigan Department Of Transportation (MDOT) (Goble 1991, Nowak and Nassif, 1991, Nowak and Kim 1996). The WIM system records truck weight and configuration as the vehicles pass over the bridge and is almost invisible to driver. One advantage of the database obtained from WIM is that all truck will be recorded, unlike data obtained from weigh station that heavy vehicle tend to avoid. Examples of recorded vehicle information recorded by Kim et al. are shown in Figure 5.7 and Figure 5.8.

Based on further field observations, Nowak (1999) made the following observation and conclusions: with both lane loaded, every 15<sup>th</sup> truck on the bridge is accompanied by another truck side-by-side. With this occurrence, it is assumed that every 10<sup>th</sup> time the truck weight is partially correlated and every 30<sup>th</sup> time the truck weight is fully correlated. By simulating this pattern, it was determined that over the 75 year assumed lifespan, for interior bridge girders the two lane loaded, fully correlated case governs, with each truck equal to the maximum two month truck.

Live load effect is considered in terms of moment in the study. Live load is a time varying load and the truck occurrence and weight are random variables that require special procedures to predict extreme values for given time intervals. In this study

citation data are used to determine the maximum expected load effect for the evaluation time period of one year as detailed in the next chapter.

#### **5.5.4. Dynamic Live Load**

The dynamic load is a function of three major parameters: road surface roughness, bridge dynamics (natural period of vibration), and vehicle dynamics (type and condition of suspension system). Dynamic load effect,  $I$ , is considered as an equivalent static load effect added to the live load,  $L$ . The derivation of the statistical model for the dynamic behavior of bridges is presented by Hwang and Nowak (1991) and Nassif and Nowak (1995). The simulations and tests indicate that the dynamic load decreases for heavier truck (as a percentage of static live load). Therefore, the dynamic load factor, (DLF) is lower for two trucks than one truck. The dynamic load corresponding to an extremely heavy truck is close to the mean of dynamic load factor. In this study we assumed a dynamic coefficient of 0.1 for all configurations. The coefficient of variation of dynamic load is 0.80. The coefficient of variation of a joint effect of live load and dynamic load is 0.18.

### **5.6. Bridge Resistance Model**

The capacity of a bridge depends on the resistance of its component and connections. The component,  $R$ , is determined mostly by material strength and dimensions. Although in design these quantities are often considered deterministic, in reality there is some uncertainty associated with each quantity. Therefore  $R$  is considered as a random variable. The causes of uncertainty can be put into three categories:

1. Material properties: uncertainty in the strength of material, the modulus of elasticity, cracking stresses, and chemical composition.

2. Fabrication: uncertainty in the overall dimensions of the component which can affect the cross section area, moment of inertia, and section modulus.

3. Analysis: uncertainty resulting from approximate methods of analysis and idealized stress/strain distribution models.

The resulting variation has been modeled by test, observation of existing structures and by engineering judgment. The resistance models can be developed using the available material test data. However structural members are often made of several materials like for instance reinforced concrete is a combination of concrete and steel. Therefore special methods of analysis are required. Since information on the variability of the resistance of such members is not always available, it is often necessary to develop resistance models using the available material test data and numerical simulations (Nowak 1993, Tabsh and Nowak 1991). In reliability analysis one popular way to model the resistance  $R$  is to consider the resistance as a product of the nominal resistance,  $R_n$ , used in design and three parameters that account for some of the sources of uncertainty mentioned above as expressed in the following equation:

$$R = R_n M F P \quad (5.50)$$

Where  $M$  is the parameter reflecting variation in the strength of the material,  $F$  is the parameter reflecting uncertainties in fabrication (dimensions), and  $P$  is an analysis factor (also known as professional factor) which accounts for uncertainties due to the analysis method used. The mean value of  $R$ ,  $\mu_R$ , and the coefficient of variation,  $V_R$ , is computed as follows:

$$\mu_R = R_n \mu_M \mu_F \mu_P \quad (5.51)$$

$$V_R = \sqrt{(V_M)^2 + (V_F)^2 + (V_P)^2} \quad (5.52)$$

Where  $\mu_M$ ,  $\mu_F$ , and  $\mu_P$  are the means of M, F, and P, and  $V_M$ ,  $V_F$ , and  $V_P$  are the coefficient of variation of M, F, and P, respectively.

The statistical parameters are developed for steel girders (composite and non-composite), reinforced concrete T-beams, and prestressed concrete AASHTO-type girders by Nowak (1993), and Tabsh and Nowak (1991). The statistical parameters of resistance for steel girdes, reinforced concrete T-beams and prestressed concrete girders are shown in Table 5.3. Factors M and F are combined. The parameters R are calculated as follows:

$$\lambda_R = \lambda_{FM} \lambda_P \quad (5.53)$$

$$V_R = \sqrt{(V_{FM})^2 + (V_P)^2} \quad (5.54)$$

Where  $\lambda_R$  is the bias factor of R,  $\lambda_{FM}$  is the bias factor of FM, and  $\lambda_P$  is the bias factor of P.  $V_R$  is the coefficient of variation of R,  $V_{FM}$  is the coefficient of variation of FM, and  $V_P$  is the coefficient of variation of P.

In this study Rosenblueth's 2K + 1 point estimate simulation method is used with the results of the finite element analysis to generate resistance parameter for the reinforced concrete deck slab as detailed in the next chapter.

Table 5.1 Reliability index versus probability of failure

Reliability index, $\beta$	Probability of failure	
0.0	$0.500 \times 10^0$	1/2
1.0	$0.159 \times 10^0$	1/6
2.0	$0.228 \times 10^{-1}$	1/35
3.0	$0.135 \times 10^{-2}$	1/720
3.5	$0.233 \times 10^{-3}$	1/4350
4.0	$0.317 \times 10^{-4}$	$1/3.1 \times 10^4$
5.0	$0.287 \times 10^{-6}$	$1/3.5 \times 10^6$
6.0	$0.987 \times 10^{-9}$	$1/1.0 \times 10^9$
7.0	$0.128 \times 10^{-11}$	$1/7.7 \times 10^{11}$

Table 5.2 Statistical parameters of dead load

Component	Bias factor	Coefficient of variation
Factory-made members, $D_1$	1.03	0.08
Cast-in-place members, $D_2$	1.05	0.10
Asphalt, $D_3$	3.5 IN (mean thickness)	0.25
Miscellaneous, $D_4$	1.03-1.05	0.08-0.10

Table 5.3 Statistical parameters of resistance

Type of structure	FM		P		R	
	$\lambda$	V	$\lambda$	V	$\lambda$	V
Non-composite steel girders						
Moment (compact)	1.095	0.075	1.02	0.06	1.12	0.1
Moment (non-compact)	1.085	0.075	1.03	0.06	1.12	0.1
Shear	1.12	0.08	1.02	0.07	1.14	0.105
Composite steel girders						
Moment	1.07	0.08	1.05	0.06	1.12	0.1
Shear	1.12	0.08	1.02	0.07	1.14	0.105
Reinforced concrete						
Moment	1.12	0.12	1.02	0.06	1.14	0.13
Shear w/steel	1.13	0.12	1.075	0.1	1.2	0.155
Shear no steel	1.165	0.135	1.20	0.1	1.4	0.17
Prestressed concrete						
Moment	1.04	0.045	1.01	0.06	1.05	0.075
Shear w/steel	1.07	0.1	1.075	0.1	1.15	0.14

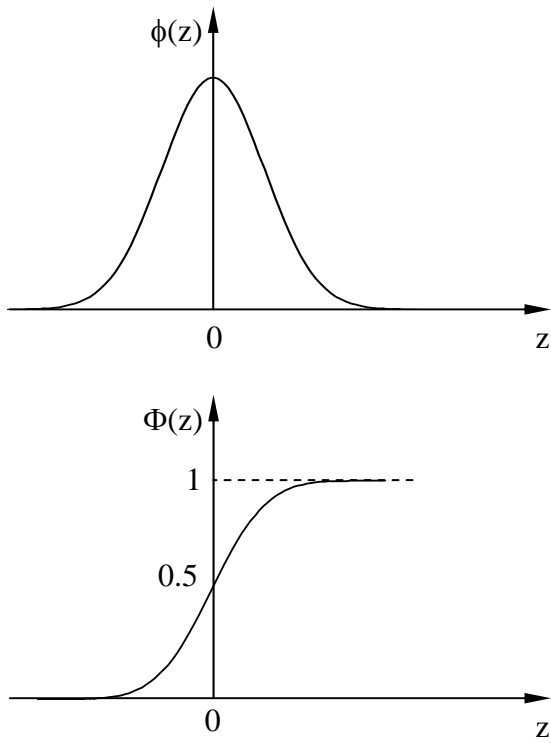


Figure 5.1 PDF  $\phi(z)$  and CDF  $\Phi(z)$  for a standard normal random variable

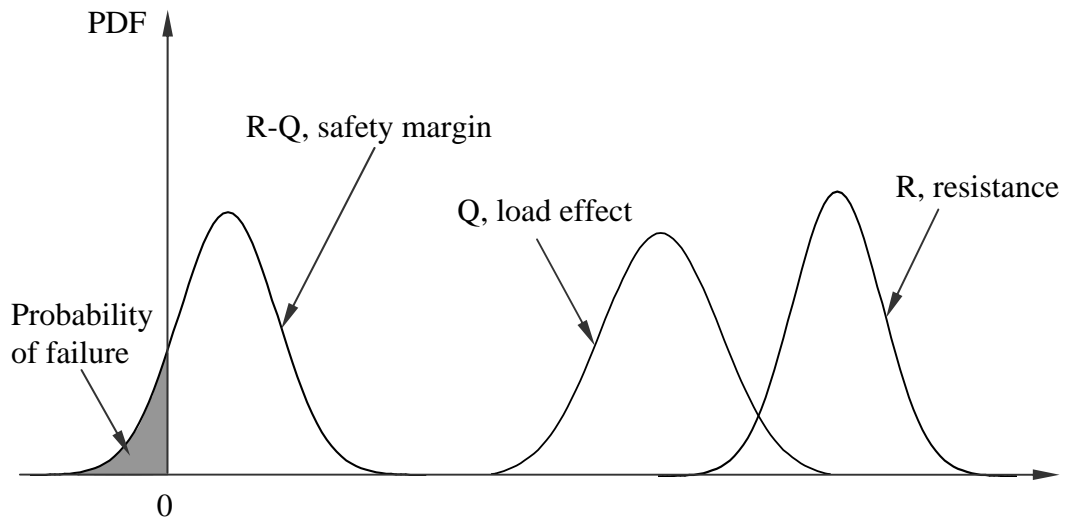


Figure 5.2 Probability Density Function of load, resistance, and safety margin (Nowak & Collins 2000)

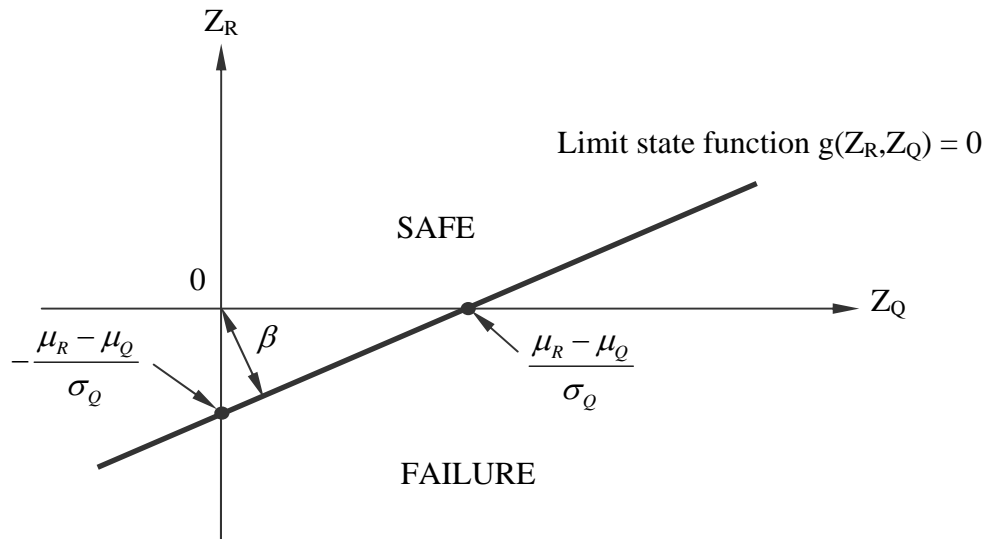


Figure 5.3 Reliability index as shortest distance to origin

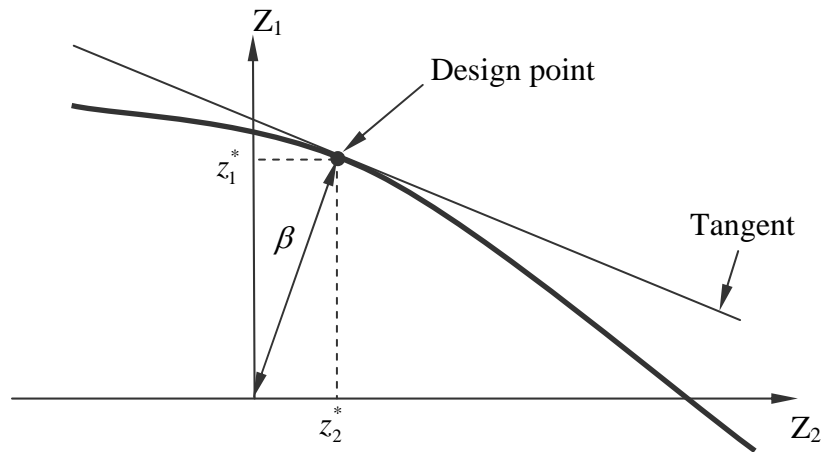


Figure 5.4 Hasofer-Lind reliability index

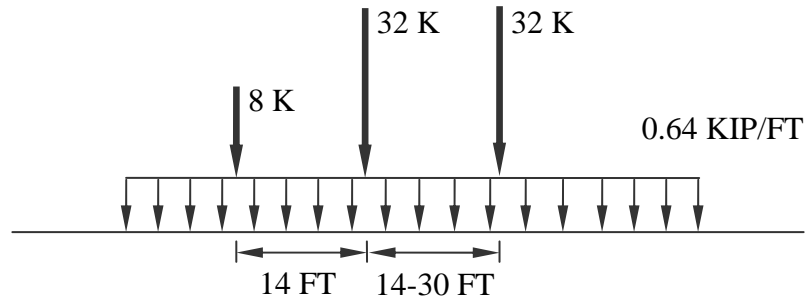


Figure 5.5 HL-93 loading specified by AASHTO LRFD 2005 – Truck and uniform load

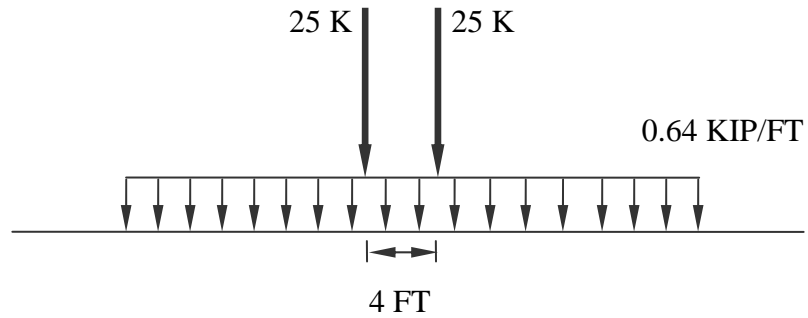


Figure 5.6 HL-93 loading specified by AASHTO LRFD 2005 – Tandem and uniform load

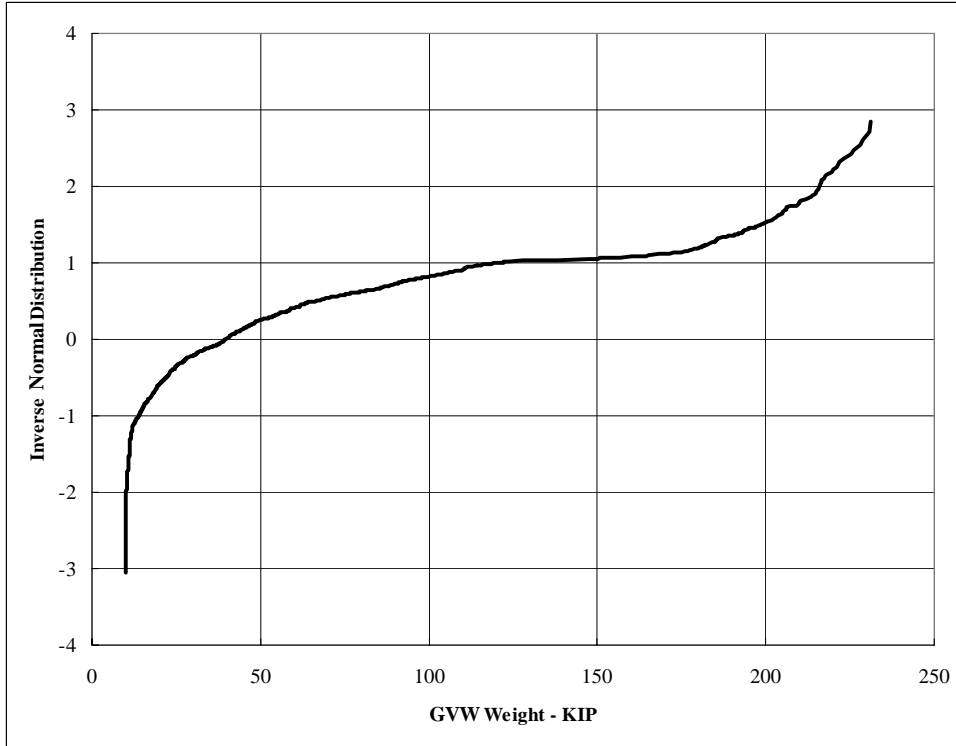


Figure 5.7 Gross vehicle weight (GVW) of trucks surveyed on I-94 over M-10 in the Greater Detroit area (Michigan)

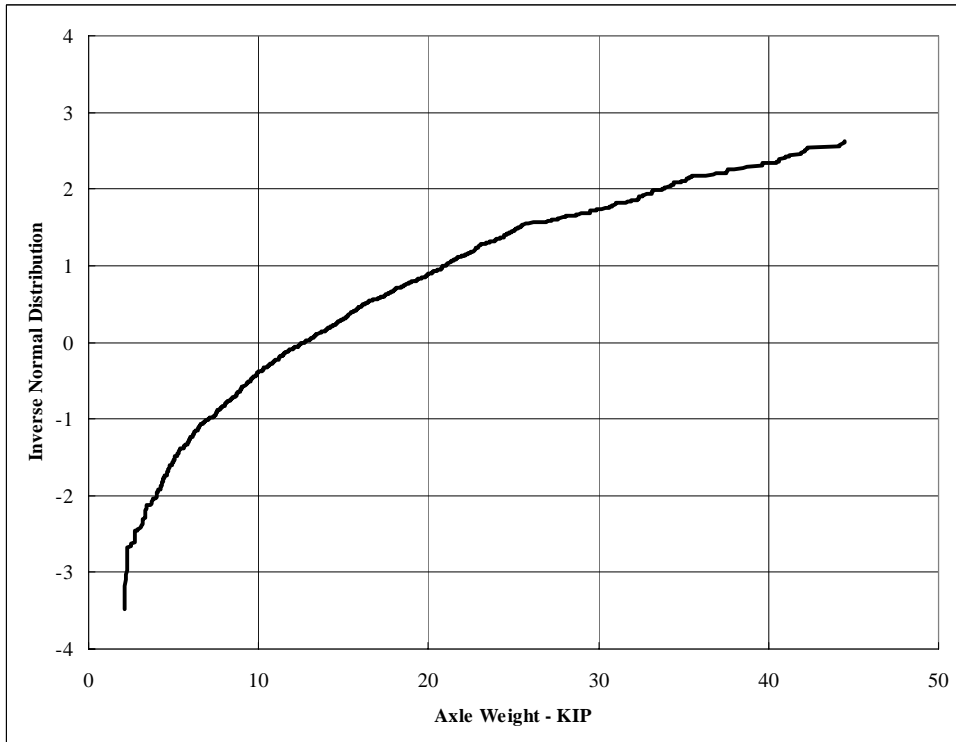


Figure 5.8 Axle weight (GVW) of trucks surveyed on I-94 over M-10 in the Greater Detroit area (Michigan)

## **CHAPTER 6**

### **RESULTS OF RELIABILITY ANALYSIS**

Reliability analysis involves formulation of limit states and development of the load and resistance models. Two limit states are considered in this study: Initiation of the first crack and the crack opening. The load parameters calculated from live load data obtained in previous work by Nowak and Kim (1997) are also explained. In the case of resistance parameters, a significant amount of time (more than 24 hours in some cases) is usually needed for nonlinear finite element computation of a bridge superstructure. Therefore, Rosenblueth's 2K+1 point estimate method is used, which requires a minimum numbers of simulations to obtain the resistance parameters. Configurations of the considered bridges and the results of FEM computations which served in the calculation of resistance parameters are explained in details. Ultimately, results from the reliability analysis for each studied limit state are discussed and reliability indices obtained for each case are reported.

#### **6.1. Considered Parameters and Configuration of the Studied Bridges**

One of the objectives of this research is to evaluate the code provision with respect to serviceability and durability of deck slabs; therefore the two different design methods available in the AASHTO LRFD 2005 edition (traditional and empirical methods) were investigated for three different girder spacings (6 FT, 8 FT and 10 FT), two different span lengths (60 FT and 120 FT), two different boundary conditions (hinge-roller and partially-fixed), and three different positions of the live load. Details of the considered parameters are explained as follows:

### 6.1.1. Empirical and Traditional Design Method for Bridge Decks

The traditional (analytical) method is based on linear elastic theory to calculate the width of slab strip that must satisfy the specified strength and service limit states. On the other hand, the empirical approach requires that the designer has to satisfy a few simple requirements regarding the deck thickness and reinforcement details, and strength and serviceability limit states are assumed to be automatically satisfied without further design validations.

Both methods may be used to design the slab. Even though, they yield different results, both methods are generally viable and reasonable.

#### 6.1.1.1 Traditional (analytical) Method Approach

A deck slab can be considered as a one-way slab system because its aspect ratio (panel length divided by the panel width) is large. For example, a typical panel width (girder spacing) is 8-11 FT and a typical girder length is from 30 to 200 FT. The associated aspect ratios vary from 3.75 to 10. Deck panels with aspect ratios of 1.5 or larger can be considered as one-way systems. Such systems are assumed to carry the load effects in the short panel direction, that is, a beamlike manner. Assuming the load is carried to the girder by one-way action, the primary issue is the width of a strip (slab width) used in the analysis and subsequent design. Guidance is provided in the AASHTO Code.

The strip width for a cast in place section is (IN)

$$\text{Positive Moment: Strip Width} = 26.0 + 6.6S \quad (6.1)$$

$$\text{Negative Moment: Strip Width} = 48.0 + 3.0S \quad (6.2)$$

where S is the girder spacing in FT. A model of the strip on top of supporting girders is shown in Figure 6.1(a). A design truck is shown positioned for the near critical positive moment. The displacement of the slab-girder system is shown in Figure 6.1(b). This

displacement can be considered as a superposition of the displacements associated with the local load effects [Figure 6.1(c)] and the global load effects [Figure 6.1(d)]. The global effects consist of bending of the strip due to the displacement of the girders. A small change in load position does not significantly affect these displacements; hence this is a global effect. The local effect is principally attributed to the bending of the strip due to the application of the wheel loads on this strip. A small transverse movement significantly affects the local response. For decks, the local effect can be significantly greater than the global effect. The global effects can be neglected and the strip can be analyzed using the classical beam theory assuming that the girders provide a rigid support. To account for the stiffening effect of the support (girder) width, the design shears and moments can be taken as critical at the face of the support for monolithic construction and at one quarter flange width for steel girders.

A complete example of the deck design using the traditional approach can be found in Appendix B.

#### 6.1.1.2 Empirical Method

Empirical method is based on observation that the primary structural action of a concrete deck is not flexure, but internal arching. The arching creates an internal compressive dome. Only a minimum amount of isotropic reinforcement is required for local flexure resistance and global arching effects.

To use the Empirical method, the following conditions must be satisfied

##### Conditions to satisfy

- The supporting components (girders) are made of steel or concrete.
- The deck is fully cast-in-place and water cured.

-The deck is of uniform depth, except for haunches at girder flanges and other local thickening.

-The ratio of effective length to design depth does not exceed 18 and is not less than 6.

-Core depth of the slab is not less than 4 IN.

-The effective length does not exceed 13.5 FT.

-The minimum depth of the slab is not less than 7 IN, excluding a sacrificial wearing surface where applicable.

-There is an overhang beyond the centerline of the outside girder of at least 5 times the depth of the slab; this condition is satisfied if the overhang is at least 3 times the depth of the slab and a structurally continuous concrete barrier is made composite with the overhang.

-The specified 28-day strength of the deck concrete is not less than 4000 PSI

-The deck is made composite with the supporting structural components

#### Reinforcement requirements

-4 layers of isotropic reinforcement shall be provided.

-Reinforcement shall be located as close to the outside surfaces as permitted by the cover requirements.

-Reinforcement shall be provided in each face of the slab with the outermost layers placed in the direction of the effective length.

-The minimum amount of reinforcement shall be  $0.27 \text{ IN}^2/\text{FT}$  ( $0.0225 \text{ IN}^2/\text{IN}$ ) of steel for each bottom layer and  $0.18 \text{ IN}^2/\text{FT}$  ( $0.015 \text{ IN}^2/\text{IN}$ ) of steel for each top layer.

-Spacing of steel shall not exceed 18 IN.

-Reinforcing steel shall be Grade 60 or better.

-All reinforcement shall be straight bars, except that hooks may be provided where required.

A complete example of the deck design using the empirical design is shown in Appendix B.

### **6.1.2. Girder Spacing**

As mentioned earlier, three girder-spacings were investigated in this research; namely 6, 8, 10 FT; for both the empirical method and the traditional method. The objective was to assess and compare the serviceability behavior of these two design methods when increasing the spacing between girders.

In case of traditional method, the factored moment used for the three considered spacings are presented in Table 6.1 and Figure 6.2 shows the layout of the reinforcement corresponding to different girder spacings. Table 6.2 summarizes the reinforcement quantity for each of the four rebar layers for each configuration.

In case of empirical method, since this method does not take into account the girder spacings, only one layout for the three different girder spacings is needed as shown in Figure 6.3. Table 6.3 summarizes the reinforcement quantity for each of the four rebar layers.

As mentioned earlier, the responses of these bridges obtained from FEM program were used in the calculation of resistance parameters. Figure 6.4 and Figure 6.5 show the reinforcement layout modeled in the Finite Element Model for the Empirical and the Traditional design method, respectively. A view of the 60 FT span Finite Element Model is shown in Figure 6.6, Figure 6.7 and Figure 6.8 for 6 FT, 8 FT and 10 FT spacing, respectively.

### **6.1.3. Span Length**

As it is explained earlier in this chapter, the global effect in deck behavior, i.e. bending of the slab due to deflection of the girder, is not directly taken into account

during the design for any of the two methods. The traditional method considers only the bending of the strip due to application of the wheel loads on this strip. Since the global effect is controlled by the girder deflection, it was decided to investigate the behavior of the reinforced concrete deck slab for two different span lengths, 60 FT and 120 FT. The 60 FT span bridge was designed for the three different girder spacings (6 FT, 8 FT, 10 FT) while the 120 FT span bridge was only designed for the 10 FT girder spacing. Both deck design methods detailed earlier were investigated for the two different spans as well. Table 6.4 and Table 6.5 show the factored moment and factored shear in the girders computed in the design of the bridges according the AASHTO LRFD 2005 edition. A summary of the girder sections used in this research is presented in Table 6.6. A view of the 120 FT span Finite Element Model with 10 FT spacing between the girders is shown in Figure 6.9. A complete bridge design example is shown in Appendix A.

#### **6.1.4. Boundary Conditions**

Since it has been reported in the literature that the boundary conditions have great influence on bridge behavior, two different boundary conditions were investigated to estimate if these observations were also valid for the bridge deck behavior. The first configuration was the hinge-roller boundary conditions as shown in Figure 6.10(a). This is a boundary condition assumed in the design. The second configuration simulates partial fixity by adding a longitudinal spring to partially restrained longitudinal displacement as shown in Figure 6.10(b). The stiffness of the spring,  $K=2000$  KIP/IN, used in the reliability analysis is the value found during the calibration process of the Finite Element Model with the field test data detailed in Chapter 4.

### 6.1.5. Live Load Position

The code specified live load, the HS-20 truck shown in Figure 6.11, was the load applied live load on the finite element. The spacing between two rear axles was 14 FT. As explained earlier, instead of using concentrated load for the axle, each tire contact area is modeled by a rectangle of 20 IN by 10 IN as shown in Figure 6.12 and the load due to each axle is modeled as a pressure, applied on the contact area, and equal to the axle load divided by two, to obtain the wheel load, and then divided by the area of the contact area ( $200 \text{ IN}^2$ ). By using this method, stress concentrations, which were a recurrent problem when using concentrated load are avoided. A general view of the truck load applied to the model is shown in Figure 6.12. The spacing between tires on the same axle was set to 6 FT as recommended in the code.

Three different Truck positions were investigated to check the serviceability of the deck at critical locations. First, the truck was placed such that it would produce the maximum negative moment over the first interior girder; longitudinally, the rear axle was right over the support, and transversally the truck was located right above the girder (3 FT on each side) as seen in Figure 6.13. This position was intended to investigate a longitudinal crack over the girder at the top of the deck as shown in Figure 6.14. For the second position, the truck was placed so that it would produce the maximum positive moment between the first two girders; longitudinally the rear axle was right over the support again, and transversally the left row of wheel was placed at 40% of the distance between the girders which is approximately the location of the maximum positive moment as seen in Figure 6.15. This position intended to investigate a longitudinal crack between the girders at the bottom of the deck as shown in Figure 6.16. Finally a third position was investigated, similar to the second position but this time the truck was placed longitudinally so that it would produce the maximum longitudinal moment as seen

in Figure 6.17. This position was intended to investigate longitudinal and transverse cracks at midspan, between girders, at the bottom of the deck as shown in Figure 6.18.

Configurations of bridges constructed from combinations of the studied parameters described above are analyzed by FEM program and the results from FEM program which served in calculation of the resistance parameters are explained in details in section 6.4. Table 6.7 shows a summary of all the bridge deck configurations considered in this study.

## 6.2. Limit state function

The concept of limit state function, as related to the structural reliability, is discussed fully in chapter 5.

The two limit states considered in this study are 1) the cracking of concrete and 2) the crack opening under live load. In this research, the first considered limit state, cracking of concrete, is defined as the exact moment when the tensile stress exceeds the modulus of rupture of concrete,  $\sigma_{t0}$ . The nominal value of  $\sigma_{t0}$  was taken as  $0.24\sqrt{f'_c}$ ; as recommended in the AASHTO LRFD 2005 for normal weight concrete. Note that even though this equation does not always represent the actual value of modulus of rupture of concrete; however, it is adopted in the code and therefore is used as a nominal value in this research. Figure 6.24 shows a sample curve taken from the FEM results of the tensile stress in concrete versus the load applied. As seen from the figure, cracking occurred when the tensile stress in concrete reached its maximum tensile strength and started to decrease as the applied load increased.

The second considered limit state is the opening of the crack. According to the AASHTO LRFD 1998 code provisions, reinforced concrete structure members shall be designed in such a way that the tensile stress in the steel reinforcement at the service limit state,  $f_{sa}$ , does not exceed:

$$f_{sa} = \frac{Z}{(d_c A)^{1/3}} \leq 0.6 f_y \quad (6.3)$$

where  $d_c$  is the concrete cover measured from the extreme tension fiber to the center of the closest bar, but not to be taken greater than 2 IN;  $A$  is the area of concrete having the same centroid as the principal tensile reinforcement, divided by the numbers of bars; and  $Z$  is a crack width parameter taken as 130 KIP/IN for members in severe exposure, as considered in this research. This value of  $Z$  corresponds to a crack width of approximately 0.012 IN. The different values of  $f_{sa}$  used in each studied bridge configuration are shown in Table 6.8 for negative moment section and in Table 6.9 for positive moment section.

### 6.3. Load Model

Conventional bridge load models for structural reliability calculation are discussed fully in chapter 5.

One possible source of information regarding the weight and configuration of highways trucks is the citation data of overweight vehicles. This data was provided by the Michigan State Police Motor Carrier Division. The survey covered 2511 citations in the calendar year 1985. Citation data are very accurate and include only the heaviest trucks in the load model.

The frequency histogram for the number of axles of citation trucks is shown in Figure 6.19. The traffic is dominated by 5 and 6 axle trucks. The third most frequent number of axles is 11.

The frequency histogram for the gross vehicle weight (GVW) of all citations trucks is shown in Figure 6.20. Most of GVW's are between 70 and 90 KIP.

The axle weight, which is the most important value for this research, is also represented as by cumulative distribution function (CDF), as shown in Figure 6.21. The

distribution functions are plotted using normal probability paper. The vertical scale corresponds to the probability and the actual numbers are equal to the inverse normal probability. The maximum recorded axle weight of 41 KIP was taken as the axle creating the annual mean maximum moment. A dynamic live load of 10% was added. The coefficient of variation for the maximum axle moment can be calculated by transformation of the cumulative distribution function (CDF). The function can be raised to a certain power, so that the earlier mean maximum axle moment becomes the mean after the transformation. The slope of the transformed CDF determines the coefficient of variation. In this study the coefficient of variation was assumed to be 18% including the dynamic effect. It is important to note that even if dead loads are included into the Finite Element Model, only live loads are included into the reliability calculations. Indeed, this analysis intend to estimate reliability indices at serviceability level under live load, dead load is included into the Finite Element Model only to accurately reproduce the stress distribution state in the deck slab before application of the live load. Moreover, resistance of the deck slab was derived from the value of live load; therefore only live load parameters are included in the reliability calculation.

#### **6.4. Resistance Model**

Various conventional bridge resistance models for structural reliability calculation are discussed fully in chapter 5. In this study the Rosenblueth's 2K+1 point estimate method used in combination with the Finite Element Analysis is used to determine the resistance parameters.

##### **6.4.1. Parameters Used in Finite Element Model**

Each bridge configuration investigated was modeled using exactly the same material model as described in Chapter 4. It is very important that in all Finite Element

Models, the same parameters are used in order to be able to compare the obtained results. For all cases, the Young modulus was computed according to the compressive strength,  $f'_c$ , considered using the following equation:

$$E = 57,000\sqrt{f'_c} \text{ (PSI)} \quad (6.4)$$

The nominal value of  $f'_c$  considered in this study was 4000 PSI since it is the standard value used in the design of deck slab. The Poisson coefficient was set to 0.15 and the density to 150 PCF in each case. All programs used the same tension stiffening as shown in Figure 6.22. The nominal value of yield strength for all rebars was set to 60 KSI, and the bilinear model described in chapter 4 was used with a Young modulus equal to 29,000 KSI.

As described earlier, 4-nodes linear shell element for the girders and 4 layers of 8-nodes linear brick element for the deck were used for all models. Full composite action was assumed. Reinforcement was included in the model, as described earlier, for the empirical reinforcement and the traditional reinforcement as shown in Figure 6.4 and Figure 6.5 using truss elements. Each rebar layer was precisely placed at the correct depth. Perfect bond is assumed between the rebars and concrete.

#### **6.4.2. Procedure to Obtain Resistance Parameters**

The Rosenblueth's 2K+1 point estimate method, detailed in chapter 5, was used in this study to obtain the resistance parameters.

The parameters used as random variables in the Rosenblueth's 2K+1 point estimate method were 1) yield strength,  $f_y$ , of the steel rebars #4, 2) yield strength,  $f_y$ , of the steel rebars #5, 3) compressive strength,  $f'_c$ , of concrete, 4) modulus of rupture,  $f_r$ , of

concrete and 5) thickness,  $t$ , of the slab. The mean and standard deviation of these five random variables are shown in Table 6.10.

Based on the Rosenblueth's  $2K+1$  point estimate method explained in chapter 5, for each studied bridge configuration, a total of  $(2 \times K + 1)$  simulations are required to obtain resistance parameters where  $K$  is the number of random variables considered. Therefore; in this study, a total of 11 simulations were run for each studied bridge configuration. The 11 simulations comprised of 1 run with each of the five considered random variables equal to their mean value and 10 runs each of the five considered random variables equal to their mean value shifted by + and – one standard deviation. Ultimately, a set of 11 simulations was carried out repeatedly for all studied bridge configurations listed in Table 6.7.

To clarify the process of obtaining the resistance parameters, a procedure for a particular bridge configuration is explained in details as follows:

The compressive stress-strain curve of concrete is plotted using three curves, the middle one corresponds to the mean and the other two represent one standard deviation below and above the mean in Figure 6.23. Let's consider an FEM run corresponding to the mean value of this compressive stress-strain curve of concrete. The results obtained from this FEM run are shown in Figure 6.24 and Figure 6.25 where Figure 6.24 shows the tensile stress in concrete versus the applied load and Figure 6.25 shows the tensile stress in the reinforcement versus the applied load. From these two curves, the load corresponding to the limit state of cracking of concrete and the load corresponding to the limit state of the maximum allowable stress in reinforcement (crack opening), were obtained. These loads were then converted into moments depending on the considered bridge configuration as shown in Table 6.11. As a result, these moments represent the moment carrying capacity or resistance parameters of the considered bridge deck configuration.

This process was then repeated for each simulation of the studied random variables and for all bridge configurations considered in this research.

It is important to note that the obtained moment carrying capacity is for live load only. Once all the moment carrying capacities are obtained, the mean and standard deviation for resistance are calculated using equation 5.49 presented in the previous chapter. It is also noted that by using this method, uncertainties originating from material properties, fabrication tolerances and analysis factor are taken into account. The reliability analysis procedure carried out in this study is explained in details in the following section.

## 6.5. Reliability Analysis Procedure and Results

### 6.5.1. Reliability Analysis Procedure

The statistical parameters of load and resistance are now determined for each bridge configuration. Assuming that the load and resistance are lognormal random variables, the formula for reliability index can be expressed in terms of the given data ( $\mu_R$ ,  $\mu_Q$ ,  $COV_R$ ,  $COV_Q$ ) as follows:

$$\beta = \frac{\ln\left(\frac{\mu_R \sqrt{COV_Q^2 + 1}}{\mu_Q \sqrt{COV_R^2 + 1}}\right)}{\sqrt{\ln((COV_R^2 + 1)(COV_Q^2 + 1))}} \quad (6.5)$$

where  $\mu_R$  is the mean resistance,  $\mu_Q$  is the mean load,  $COV_R$  is the coefficient of variation of resistance, and  $COV_Q$  is the coefficient of variation of load. Equation 6.5 is derived from Equation 6.6, which expresses the reliability index for normal random variables, using the relations expressed in equation 6.7 and 6.8

$$\beta = \frac{\mu_R - \mu_Q}{\sqrt{\sigma_R^2 + \sigma_Q^2}} \quad (6.6)$$

where  $\mu_R$  is the mean resistance,  $\mu_Q$  is the mean of load,  $\sigma_R$  is the standard deviation of resistance, and  $\sigma_Q$  is the standard deviation of load.

$$\sigma_{\ln(X)}^2 = \ln(COV_X^2 + 1) \quad (6.7)$$

$$\mu_{\ln(X)} = \ln(\mu_x) - \frac{1}{2} \sigma_{\ln(X)}^2 \quad (6.8)$$

where  $\mu_{\ln(X)}$  is the mean value of  $\ln(X)$ , and  $\sigma_{\ln(X)}$  is the standard deviation of  $\ln(X)$ .

An detailed example of the calculations is shown in Table 6.12 and Table 6.13 for the empirical design method with a 60 FT span bridge, 10 FT girder spacing, negative moment (top of the slab) for the cracking limit state and the crack opening limit state respectively.

### 6.5.2. Results of the Reliability Analysis

Table 6.14 and Table 6.15 summarize the calculated reliability indices for all configurations investigated for the cracking limit state and the crack opening limit state, respectively.

#### 6.5.2.1 Discussion and Results for the Cracking Limit State

The comparison of reliability indices between the two design methods as a function of the girder spacing is shown in Figure 6.26, Figure 6.27, and Figure 6.28 for the longitudinal cracking at the top of the deck close to support (negative moment), the longitudinal cracking at the bottom of the deck close to support (positive moment), and the longitudinal cracking at the bottom of the deck at midspan (positive moment), respectively.

The comparison of reliability indices between the two design methods as a function of the span length is shown in Figure 6.29, Figure 6.30, and Figure 6.31 for the longitudinal cracking at the top of the deck close to support (negative moment), the longitudinal cracking at the bottom of the deck close to support (positive moment), and the longitudinal cracking at the bottom of the deck at midspan (positive moment), respectively.

Finally, the comparison of reliability indices between the two boundary conditions investigated, for the empirical design, as a function of girder spacing is shown in Figure 6.32, Figure 6.33, and Figure 6.34 for the longitudinal cracking at the top of the deck close to support (negative moment), the longitudinal cracking at the bottom of the deck at midspan (positive moment), and the transverse cracking at the bottom of the deck at midspan (positive moment), respectively.

It was observed that for the longitudinal cracking, the reliability indices are very low, ranging from 0 to 2, for all deck configurations studied. Since we used annual mean maximum for the load, a reliability index of zero corresponds to a probability of 50% for the deck to crack within a year. Figure 6.26, Figure 6.27, and Figure 6.28 show that the reliability index slightly decreases when the girder spacing increases which indicates a slightly higher probability for deck supported on widely spaced girders to crack. Both design methods show similar reliability level at the cracking limit state, with traditional design showing just slightly higher values for wider girder spacing. It can be concluded that the ratio of reinforcement has a minimal influence on the cracking moment of decks with girder spacing ranging from 6 FT to 10 FT. Finally, no significant differences were noticed between crack at the top or bottom of the deck, as well as between the crack close to support and at midspan.

Figure 6.29, Figure 6.30, and Figure 6.31 show that the reliability index slightly increases, from 0 to 2, when the span increases for both design methods regardless of the location of the crack. This effect is due to the fact that long span bridge decks have a

behavior closer to a beam behavior than a plate behavior. The longitudinal stiffness of a long span bridge relatively to the span length is smaller than the one of a short span. Therefore, the deck in a long span bridge deflects more, creating transverse compression in the deck; hence, decreasing the probability of longitudinal crack to occur. In addition, shorter bridge decks have a higher torsional stiffness than longer bridges. Therefore, shorter bridge decks experience more torsional stress than longer bridge decks, increasing the probability of cracking for shorter spans, especially close to support and in the corner of the deck.

Figure 6.32 and Figure 6.33 show that the partial fixity slightly reduces the probability of longitudinal crack to appear in bridge deck supported on widely spaced girders. However, Figure 6.34 shows that the effect of boundary conditions is more significant for transverse cracking than longitudinal cracking. For the case of transverse cracking at the bottom of the deck at midspan, it is observed that partial fixity significantly increase the reliability indices (see Figure 6.34). These effects can be explained by the fact that partial fixity limits the longitudinal displacement of support and; therefore, increase the longitudinal compressive stresses in the structure. This increase of longitudinal compressive stresses in the deck increases the resistance of the deck to transverse cracks. Moreover, due to Poisson effect, this longitudinal compressive stress also creates, but at a smaller scale, transversal compressive stress. This slight increase in transversal compressive stress explains that the probability of the cracking to occur decreases when partial fixity at the support is applied; this phenomena is enhanced when the spacing between girders increases.

#### 6.5.2.2 Discussion and Results for the Crack Opening Limit State

The comparison of reliability indices between the two design methods as a function of the girder spacing is shown in Figure 6.35, Figure 6.36, and Figure 6.37 for

the longitudinal crack opening at the top of the deck close to support (negative moment), the longitudinal cracking at the bottom of the deck close to support (positive moment), and the longitudinal cracking at the bottom of the deck at midspan (positive moment), respectively.

The comparison of reliability indices between the two design methods as a function of the span length is shown in Figure 6.38, Figure 6.39, and Figure 6.40 for the longitudinal crack opening at the top of the deck close to support (negative moment), the longitudinal cracking at the bottom of the deck close to support (positive moment), and the longitudinal cracking at the bottom of the deck at midspan (positive moment), respectively.

Finally, the comparison of reliability indices between the two boundary conditions investigated, for the empirical design, as a function of girder spacing is shown in Figure 6.41 and Figure 6.42 for the longitudinal cracking at the top of the deck close to support (negative moment), and the longitudinal cracking at the bottom of the deck at midspan (positive moment), respectively.

It was observed that for the longitudinal crack opening limit state, the reliability indices are relatively high, ranging from 3.5 to 7, for all deck configurations studied. It means that the probability of the crack to open at the width recommended by the code is less than the probability of the crack to occur. However, this can also be explained by the fact that only live load was considered in this study. Shrinkage and difference temperature gradient analysis which would reduce the reliability indices were not included.

Figure 6.35, Figure 6.36, and Figure 6.37 show that crack opening is more sensitive to girder spacing than cracking. The reliability index significantly decreases when the girder spacing increases which indicates a higher probability for deck supported on widely spaced girders to crack. Traditional design indicates higher values of reliability indices for wider spacing. It can be concluded that, contrary to cracking, crack opening is

significantly more influenced by the ratio of reinforcement. As a result, in the case of empirical design, because the design yields a constant ratio of reinforcement for all girder spacings (see Table 6.3), thus, the reliability indices decrease significantly as the girder spacing increased. On the contrary, the traditional design method yields the increase of the ratio of reinforcement as girder spacing increases (see Table 6.2); hence, the reliability only slightly decreases as the spacing increases. In addition, no significant differences were noticed between crack at the top or bottom of the deck, as well as between the crack close to support and at midspan.

Similar to the cracking limit state, Figure 6.38, Figure 6.39, and Figure 6.40 show that reliability index for the crack opening limit state slightly increases when the span increases for both design methods, regardless of the location of the crack. Similar to the cracking limit state, this effect is due to the fact that long span bridge decks have a behavior closer to a beam behavior than a plate behavior and the torsional stiffness is greater for shorter bridge than for the longer ones.

Figure 6.41 and Figure 6.42 show that a partial fixity slightly reduces the probability of longitudinal crack to open in bridge deck supported on widely spaced girders. As explained earlier, partial fixity increases longitudinal compressive stresses. Due to Poisson effect this longitudinal compressive stress also creates, but at a smaller scale, transversal compressive stress. This slight increase in transversal compressive stress explains a decrease of the probability of the crack to open at the maximum width recommended by the code when partial fixity at the support is applied.

#### 6.5.2.3 Effect of the annual mean maximum axle weight on reliability indices

Figure 6.43 and Figure 6.44 show the comparison of reliability indices between the two design methods as a function of the annual mean maximum for a 60 FT span

bridge and 10 FT girder spacing at the cracking limit state and the crack opening limit state, respectively.

Figure 6.45 and Figure 6.46 show the same comparison but for a 120 FT span bridge, for the cracking limit state and the crack opening limit state, respectively.

It can be observed that, for all cases, the reliability indices decrease significantly when the annual mean maximum axle weight increases. This emphasizes the importance of an accurate estimation of the real traffic crossing bridges in order to predict their behavior at serviceability and also point out the importance of posting on a bridge.

Table 6.1 Factored moments computed using the traditional method for the three different spacing.

	Girder Spacing		
	6FT	8FT	10FT
Negative Moment exterior (KIP-FT/FT)	-0.78	-0.78	-0.78
Positive Moment (KIP-FT/FT)	8.71	10.61	13.11
Negative Moment (KIP-FT/FT)	-9.05	-11.91	-13.64
Reaction first support (KIP/FT)	11.19	11.30	11.43

Table 6.2 Summary of rebars quantity using the traditional method for the three different spacing

Girder Spacing = 6FT		
Position and Orientation	Repartition	Area (IN <sup>2</sup> /IN)
Bottom Transverse	#4 @ 9 IN	0.0222
Top Tansverse	#4 @ 7 IN	0.0286
Bottom Longitudinal	#4 @ 10 IN	0.02
Top Longitudinal	#4 @ 18 IN	0.0111
	Total	0.0819

Girder Spacing = 8FT		
Position and Orientation	Repartition	Area (IN <sup>2</sup> /IN)
Bottom Transverse	#5 @ 11 IN	0.0282
Top Tansverse	#5 @ 9 IN	0.0344
Bottom Longitudinal	#4 @ 8 IN	0.025
Top Longitudinal	#4 @ 18 IN	0.0111
	Total	0.0987

Girder Spacing = 10FT		
Position and Orientation	Repartition	Area (IN <sup>2</sup> /IN)
Bottom Transverse	#5 @ 9 IN	0.0344
Top Tansverse	#5 @ 7 IN	0.0443
Bottom Longitudinal	#4 @ 6 IN	0.0333
Top Longitudinal	#4 @ 18 IN	0.0111
	Total	0.1231

Table 6.3 Summary of rebars quantity using the empirical method

Position and Orientation	Repartition	Area (IN <sup>2</sup> /IN)
Bottom Transverse	#4 @ 13 IN	0.0154
Top Transverse	#4 @ 13 IN	0.154
Bottom Longitudinal	#5 @ 13 IN	0.0238
Top Longitudinal	#5 @ 13 IN	0.0238
Total		0.0784

Table 6.4 Factored moments computed for the design of the bridge

Span (FT)	Total factored Moment (KIP-FT)		
	6 FT	8 FT	10 FT
60.00	1966.61	2452.64	2936.50
120.00	-	-	9162.02

Table 6.5 Factored shear computed for the design of the bridge

Span (FT)	Total Factored Shear (KIP)		
	6 FT	8 FT	10 FT
60.00	160.71	198.64	236.25
120.00	-	-	366.66

Table 6.6 Summary of the girder section used in this research

Span (FT)	Girder Section		
	6 FT	8 FT	10 FT
60.00	W24 x 94	W27 x 102	W30 x 116
120.00	-	-	W44 x 335

Table 6.7 Summary of the different bridge configuration studied

		Span = 60 FT					
		6 FT	6 FT	8FT	8 FT	10 FT	10 FT
		Trad	Emp	Trad	Emp	Trad	Emp
normal B/C	n.s.	√	√	√	√	√	√
	p.s.	√	√	√	√	√	√
	p.m.	√	√	√	√	√	√
partial fixity B/C	n.s.		√		√		√
	p.s.						
	p.m.		√		√		√

		Span = 120 FT					
		6 FT	6 FT	8FT	8 FT	10 FT	10 FT
		Trad	Emp	Trad	Emp	Trad	Emp
normal B/C	n.s.					√	√
	p.s.					√	√
	p.m.					√	√

n.s: negative moment at the support

p.s: positive moment at the support

p.m: positive moment at midspan

■ Longitudinal crack investigated as well

Table 6.8 Value of  $f_{sa}$  for negative moment section

	Traditional			Empirical
	6 FT	8 FT	10 FT	
Z (IN)	130.00	130.00	130.00	130.00
$d_c$ (IN)	2.25	2.31	2.31	2.25
A (IN <sup>2</sup> )	31.50	41.63	32.38	58.50
$f_{sa}$ (KSI)	31.41	28.37	30.84	25.56

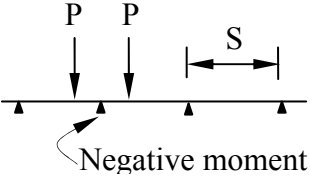
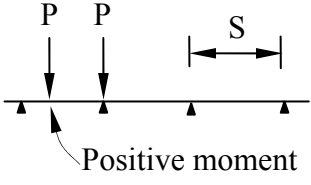
Table 6.9 Value of  $f_{sa}$  for p moment section

	Traditional			Empirical
	6 FT	8 FT	10 FT	
Z (IN)	130.00	130.00	130.00	130.00
$d_c$ (IN)	1.25	1.31	1.31	1.31
A (IN <sup>2</sup> )	22.50	28.88	23.63	34.13
$f_{sa}$ (KSI)	36.84	32.29	34.52	36.61

Table 6.10 Random variables parameters used in the 2K+1 point estimate method

	nominal	bias $\lambda$	COV	Mean $\mu$	Standard dev. $\sigma$	$\mu+\sigma$	$\mu-\sigma$
$f_y$ (#4) (KSI)	60	1.128	0.026	67.68	1.76	69.44	65.92
$f_y$ (#5) (KSI)	60	1.12	0.023	67.20	1.55	68.75	65.65
$f_c$ (PSI)	4000	1.2125	0.154	4850.00	746.90	5596.90	4103.10
thickness (IN)	9	0.92	0.12	8.28	0.99	9.27	7.29
$f_r$ (PSI)	480	1.213	0.2	582.24	116.45	698.69	465.79

Table 6.11 Moment due to live load for different bridge configuration

Girder spacing $S$				
	6 FT	-1.044 x P (KIP-FT)*	1.035 x P (KIP-FT)*	
8 FT	-1.448 x P (KIP-FT)*	1.463 x P (KIP-FT)*		
10 FT	-1.727 x P (KIP-FT)*	2.041 x P (KIP-FT)*		

\* Dynamic effect not included

Table 6.12 Example of calculation of the reliability index for the empirical design, 60 FT span bridge, 10 FT girder spacing, negative moment (top of the slab) – cracking limit state

<b>RESISTANCE (KIP-FT)</b>										
Variable	$y_i^-$	$y_i^+$	$\bar{y}_i = \frac{y_i^+ + y_i^-}{2}$	$V_{y_i} = \frac{y_i^+ - y_i^-}{y_i^+ + y_i^-}$	$y_0$	$\bar{Y} = y_0 \prod_{i=1}^k \left( \frac{\bar{y}_i}{y_0} \right)$	$V_y = \sqrt{\left[ \prod_{i=1}^k (1 + V_{y_i}^2) \right] - 1}$	$\sigma_y$	$\beta$	
F <sub>v</sub> #4	y <sub>1</sub>	46.98	46.98	46.98	0.00				<b>0.07</b>	
F <sub>v</sub> #5	y <sub>2</sub>	46.98	46.98	46.98	0.00					
f <sub>c</sub>	y <sub>3</sub>	46.96	46.98	46.97	2.94E-04	46.99	40.31	0.25		9.97
t	y <sub>4</sub>	35.98	49.69	42.84	0.16					
f <sub>r</sub>	y <sub>5</sub>	35.98	52.46	44.22	0.186					
<b>LOAD (KIP-FT)</b>										
					$\mu_{load}$	$COV_{load}$	$\sigma_{load}$			
					38.96	0.18	6.48			

Table 6.13 Example of calculation of the reliability index for the empirical design, 60 FT span bridge, 10 FT girder spacing, negative moment (top of the slab) – crack opening limit state

<b>RESISTANCE (KIP-FT)</b>									
Variable	$y_i^-$	$y_i^+$	$\bar{y}_i = \frac{y_i^+ + y_i^-}{2}$	$V_{y_i} = \frac{y_i^+ - y_i^-}{y_i^+ + y_i^-}$	$y_0$	$\bar{Y} = y_0 \prod_{i=1}^k \left( \frac{\bar{y}_i}{y_0} \right)$	$V_y = \sqrt{\left[ \prod_{i=1}^k (1 + V_{y_i}^2) \right]^{-1}}$	$\sigma_y$	$\beta$
F <sub>v</sub> #4	y <sub>1</sub>	117.94	117.94	117.93	0				<b>3.51</b>
F <sub>v</sub> #5	y <sub>2</sub>	117.94	117.94	117.93	0				
f <sub>c</sub>	y <sub>3</sub>	115.56	119.26	117.41	0.015	117.93	113.71	0.24	
t	y <sub>4</sub>	91.62	143.17	117.40	0.219				
f <sub>r</sub>	y <sub>5</sub>	102.24	127.25	114.74	0.108				
<b>LOAD (KIP-FT)</b>									
						$\mu_{load}$	$COV_{load}$	$\sigma_{load}$	
						38.96	0.18	6.48	

Table 6.14 Summary of reliability indices for all configurations investigated - cracking

L	S	Design	position	boundary	resistance (KIP-FT)		load (KIP-FT)		$\beta$
					$\mu_{res}$	$\sigma_{res}$	$\mu_{load}$	$\sigma_{load}$	
60	6	empirical	n.s.	roller	38.76	0.24	23.55	0.18	1.62
60	6	empirical	p.s.	roller	42.58	0.25	23.34	0.18	1.9
60	6	empirical	p.m.	roller	45.87	0.3	23.34	0.18	1.86
60	8	empirical	n.s.	roller	43.65	0.23	32.65	0.18	0.59
60	8	empirical	p.s.	roller	41.65	0.28	32.99	0.18	0.63
60	8	empirical	p.m.	roller	56.06	0.33	32.99	0.18	1.34
60	10	empirical	n.s.	roller	40.31	0.24	38.95	0.18	0.07
60	10	empirical	p.s.	roller	45.31	0.37	46.03	0.18	-0.16
60	10	empirical	p.m.	roller	73.23	0.31	46.03	0.18	1.21
120	10	empirical	n.s.	roller	54.11	0.29	35.41	0.18	1.18
120	10	empirical	p.s.	roller	47.13	0.33	41.84	0.18	0.23
120	10	empirical	p.m.	roller	77.96	0.32	41.84	0.18	1.64
60	6	traditional	n.s.	roller	37.36	0.24	23.55	0.18	1.52
60	6	traditional	p.s.	roller	38.42	0.31	23.34	0.18	1.33
60	6	traditional	p.m.	roller	43.39	0.29	23.34	0.18	1.79
60	8	traditional	n.s.	roller	43.49	0.29	32.65	0.18	0.77
60	8	traditional	p.s.	roller	41.62	0.28	32.99	0.18	0.63
60	8	traditional	p.m.	roller	58.19	0.16	32.99	0.18	1.57
60	10	traditional	n.s.	roller	49.64	0.29	38.95	0.18	0.65
60	10	traditional	p.s.	roller	52.54	0.25	46.03	0.18	0.38
60	10	traditional	p.m.	roller	73.06	0.3	46.03	0.18	1.24
120	10	traditional	n.s.	roller	61.69	0.29	35.41	0.18	1.57
120	10	traditional	p.s.	roller	47.92	0.16	41.84	0.18	0.57
120	10	traditional	p.m.	roller	78.36	0.3	41.84	0.18	1.75
60	6	empirical	n.s.	spring	44.07	0.3	23.55	0.18	1.71
60	6	empirical	p.m.	spring	43.11	0.26	23.34	0.18	1.87
60	6	empirical	p.m.*	spring	4545	0.2	1073.05	0.18	5.38
60	8	empirical	n.s.	spring	46.04	0.31	32.65	0.18	0.88
60	8	empirical	p.m.	spring	44.21	0.31	32.99	0.18	1.3
60	8	empirical	p.m.*	spring	3130.1	0.2	1073.05	0.18	4.1
60	10	empirical	n.s.	spring	52.36	0.29	38.95	0.18	0.78
60	10	empirical	p.m.	spring	90.92	0.28	46.03	0.18	1.97
60	10	empirical	p.m.*	spring	2562.63	0.19	1073.05	0.18	3.3

n.s: negative moment at the support

p.s: positive moment at the support

p.m: positive moment at midspan

p.m.\*: positive moment at midspan - longitudinal crack

Table 6.15 Summary of reliability indices for all configurations investigated – crack opening

L	S	Design	position	boundary	Resistance (KIP-FT)		Load (KIP-FT)		$\beta$
					$\mu_{res}$	$\sigma_{res}$	$\mu_{load}$	$\sigma_{load}$	
60	6	empirical	n.s.	roller	113.84	0.15	23.55	0.18	6.76
60	6	empirical	p.s.	roller	128.486	0.22	23.34	0.18	5.98
60	6	empirical	p.m.	roller	96.57	0.11	23.34	0.18	6.88
60	8	empirical	n.s.	roller	112.29	0.22	32.65	0.18	4.35
60	8	empirical	p.s.	roller	110.28	0.22	32.99	0.18	4.21
60	8	empirical	p.m.	roller	114.91	0.16	32.99	0.18	5.17
60	10	empirical	n.s.	roller	113.71	0.24	38.95	0.18	3.51
60	10	empirical	p.s.	roller	147.95	0.32	46.03	0.18	3.09
60	10	empirical	p.m.	roller	137.28	0.18	46.03	0.18	4.28
120	10	empirical	n.s.	roller	132.18	0.21	35.41	0.18	4.7
120	10	empirical	p.s.	roller	112.21	0.11	41.84	0.18	4.76
120	10	empirical	p.m.	roller	127.61	0.16	41.84	0.18	4.63
60	6	traditional	n.s.	roller	125.68	0.15	23.55	0.18	7.19
60	6	traditional	p.s.	roller	126.6	0.19	23.34	0.18	6.44
60	6	traditional	p.m.	roller	97.92	0.11	23.34	0.18	6.82
60	8	traditional	n.s.	roller	121.37	0.21	32.65	0.18	4.7
60	8	traditional	p.s.	roller	105.39	0.22	32.99	0.18	4.01
60	8	traditional	p.m.	roller	116.4	0.16	32.99	0.18	5.22
60	10	traditional	n.s.	roller	131.39	0.21	38.95	0.18	4.34
60	10	traditional	p.s.	roller	130.7	0.2	46.03	0.18	3.84
60	10	traditional	p.m.	roller	147.91	0.17	46.03	0.18	4.79
120	10	traditional	n.s.	roller	149.76	0.2	35.41	0.18	5.31
120	10	traditional	p.s.	roller	141.68	0.19	41.84	0.18	4.7
120	10	traditional	p.m.	roller	146.47	0.14	41.84	0.18	5.51
60	6	empirical	n.s.	spring	115.97	0.19	23.55	0.18	6.13
60	6	empirical	p.m.	spring	116.41	0.15	23.34	0.18	6.79
60	8	empirical	n.s.	spring	114.56	0.22	32.65	0.18	4.33
60	8	empirical	p.m.	spring	123.07	0.18	32.99	0.18	5.18
60	10	empirical	n.s.	spring	121.37	0.23	38.95	0.18	3.91
60	10	empirical	p.m.	spring	143.24	0.18	46.03	0.18	4.5

n.s: negative moment at the support

p.s: positive moment at the support

p.m: positive moment at midspan

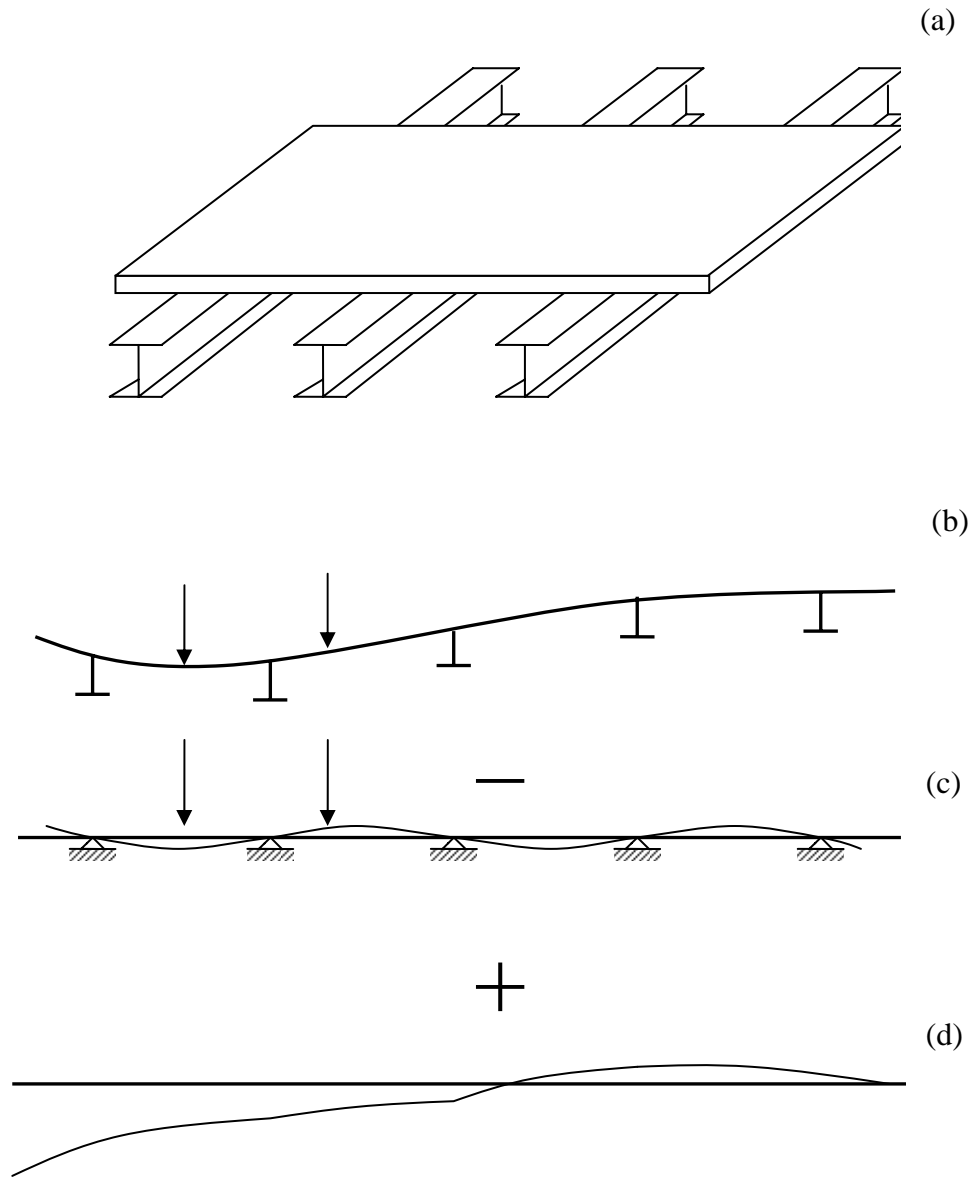


Figure 6.1(a) Idealized strip design, (b) transverse section under load, (c) rigid girder model, and (d) displacement due to girder translation

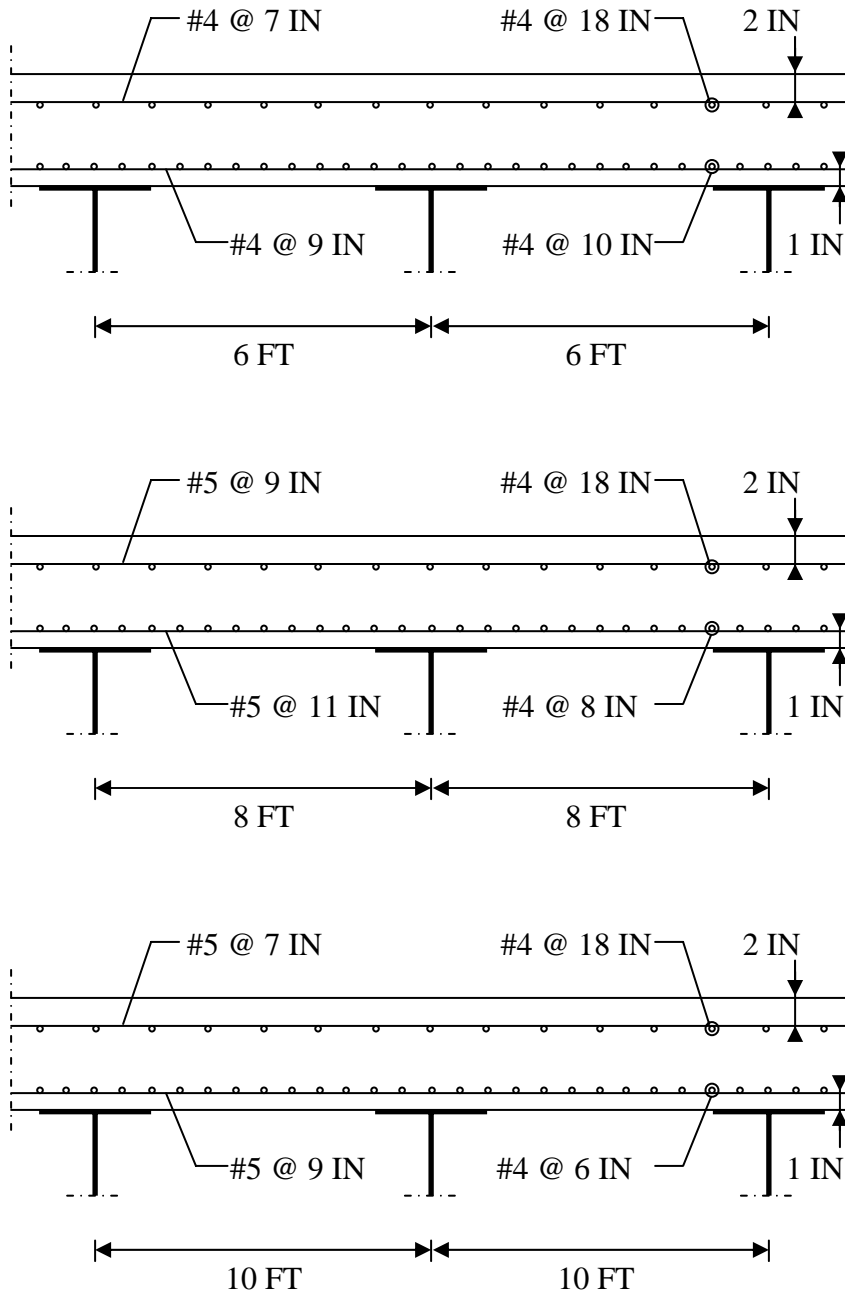


Figure 6.2 Layout of the deck reinforcement for the three girders spacing according the traditional method

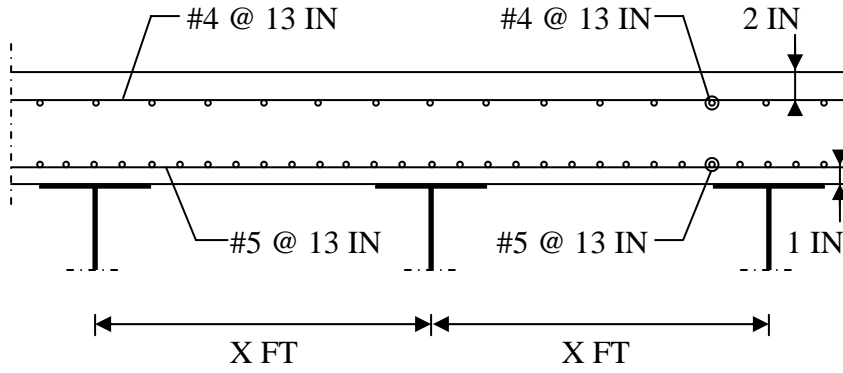


Figure 6.3 Layout of the deck reinforcement according to the empirical method

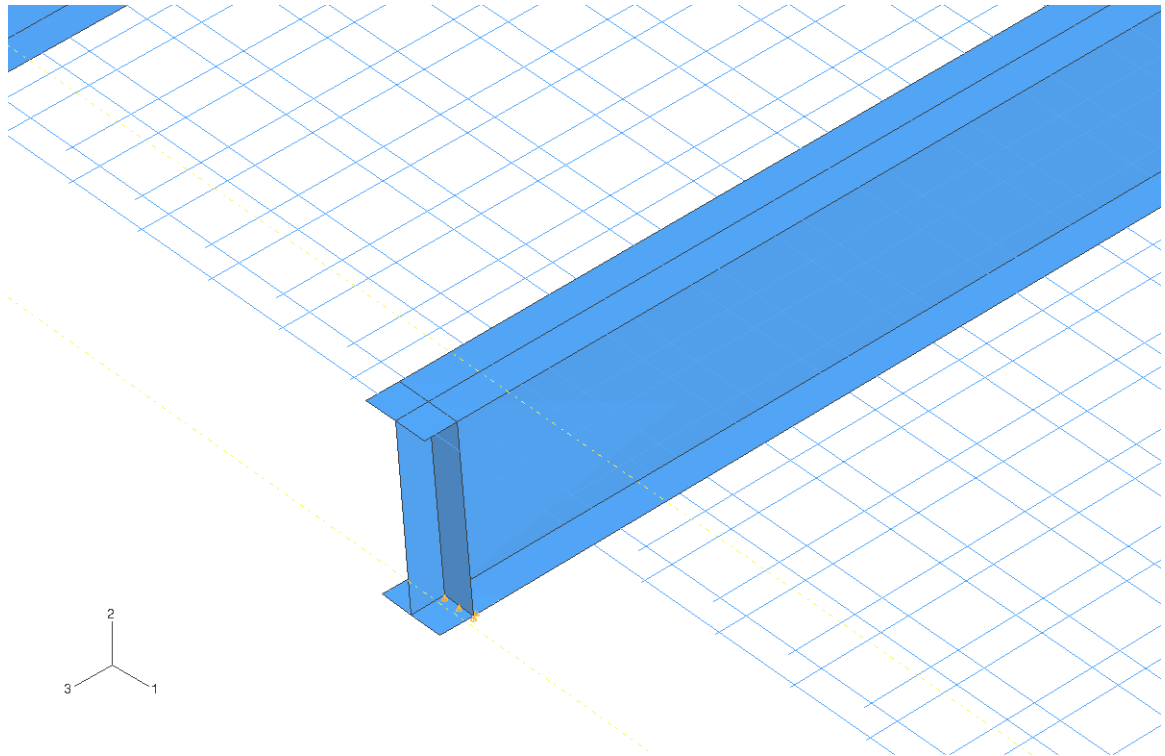


Figure 6.4 View of the Empirical reinforcement modeled in the Finite Element Model

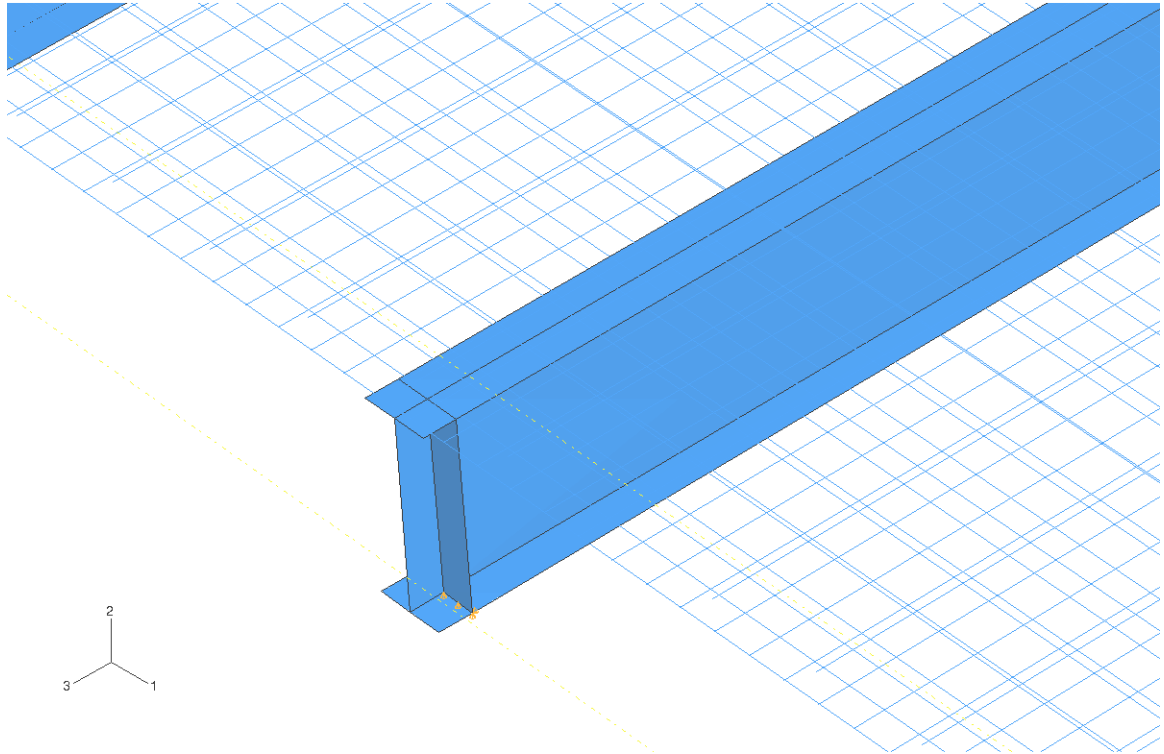


Figure 6.5 View of the Traditional reinforcement modeled in the Finite Element Model

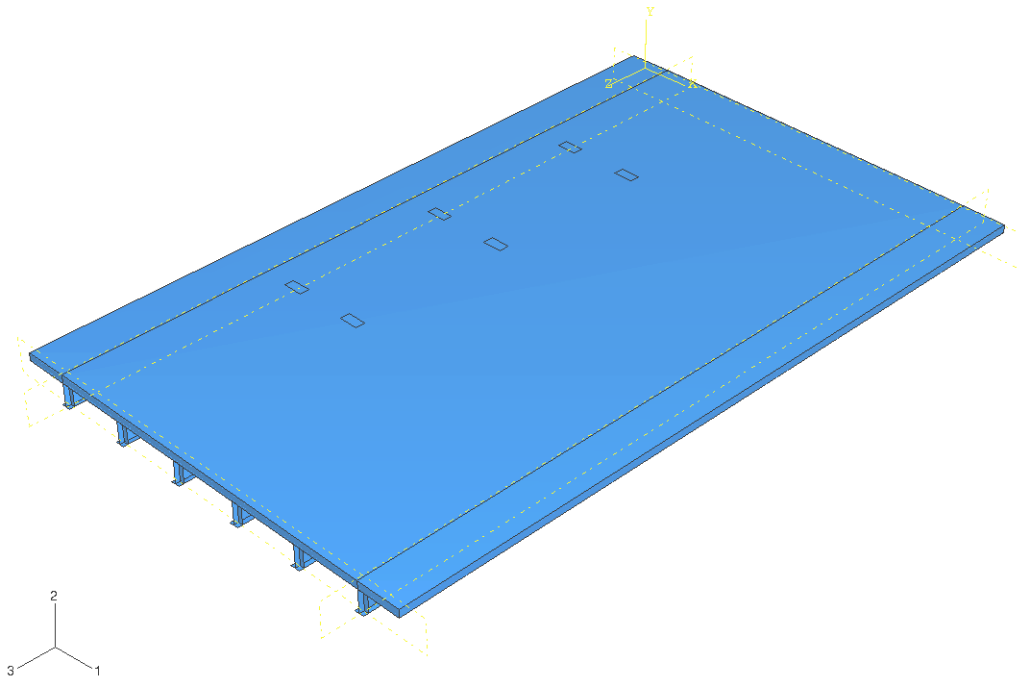


Figure 6.6 View of the 60 FT span Finite Element Model with 6 FT girder spacing.

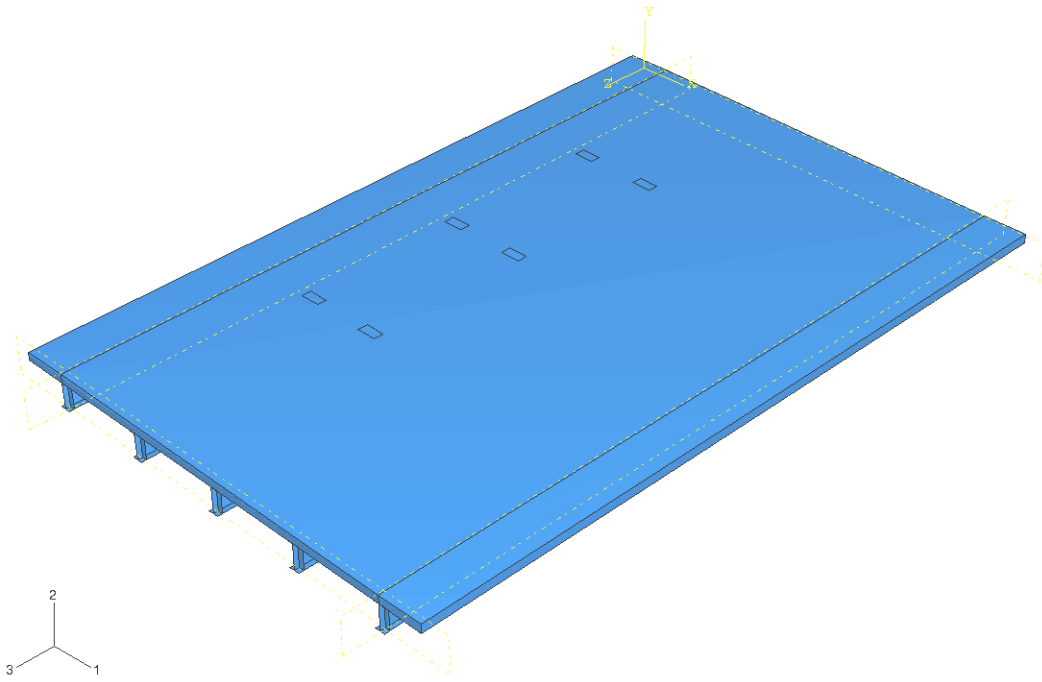


Figure 6.7 View of the 60 FT span Finite Element Model with 6 FT girder spacing.

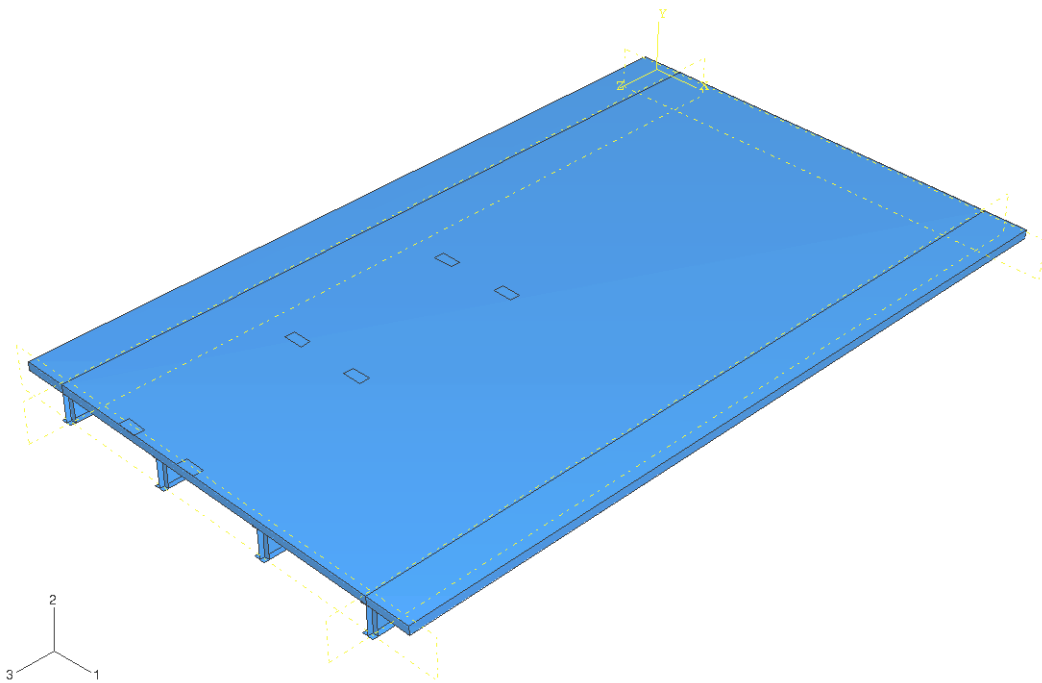


Figure 6.8 View of the 60 FT span Finite Element Model with 10 FT girder spacing.

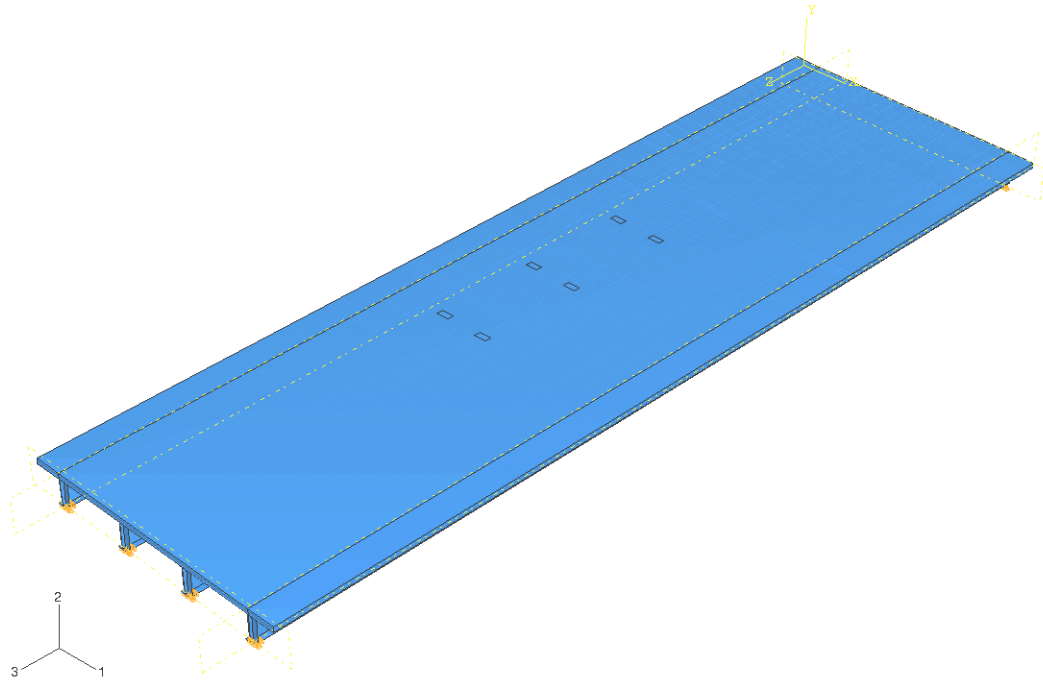


Figure 6.9 View of the 120 FT span Finite Element Model with 10 FT girder spacing.

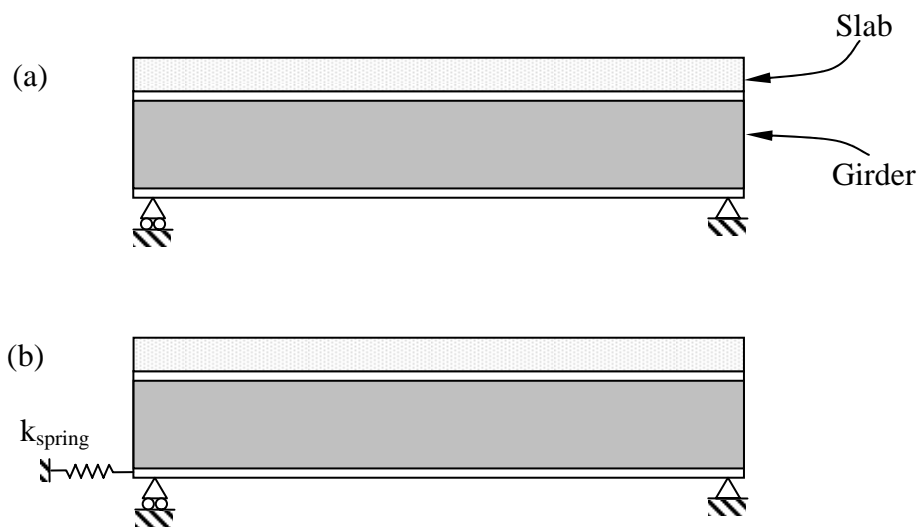


Figure 6.10 Boundary conditions used in the reliability analysis

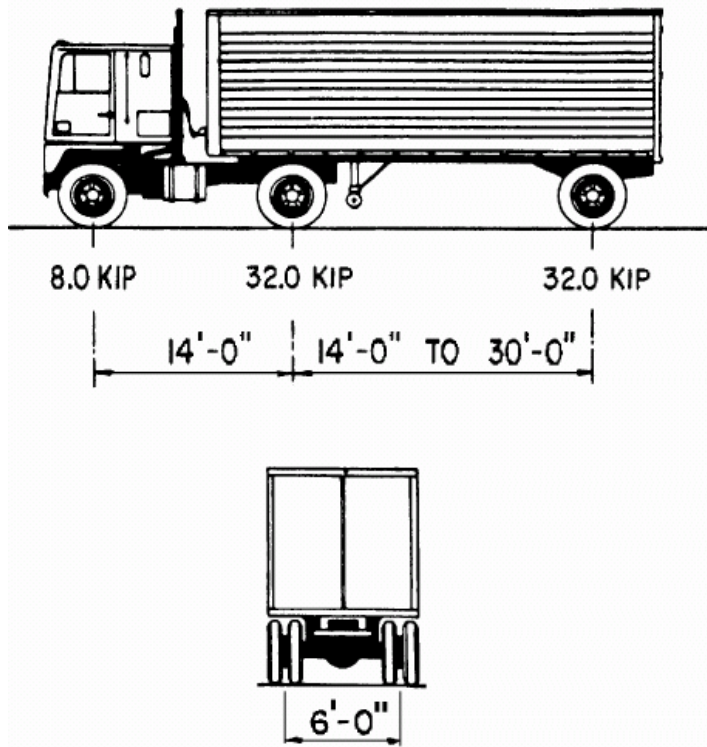


Figure 6.11 Characteristics of the design truck

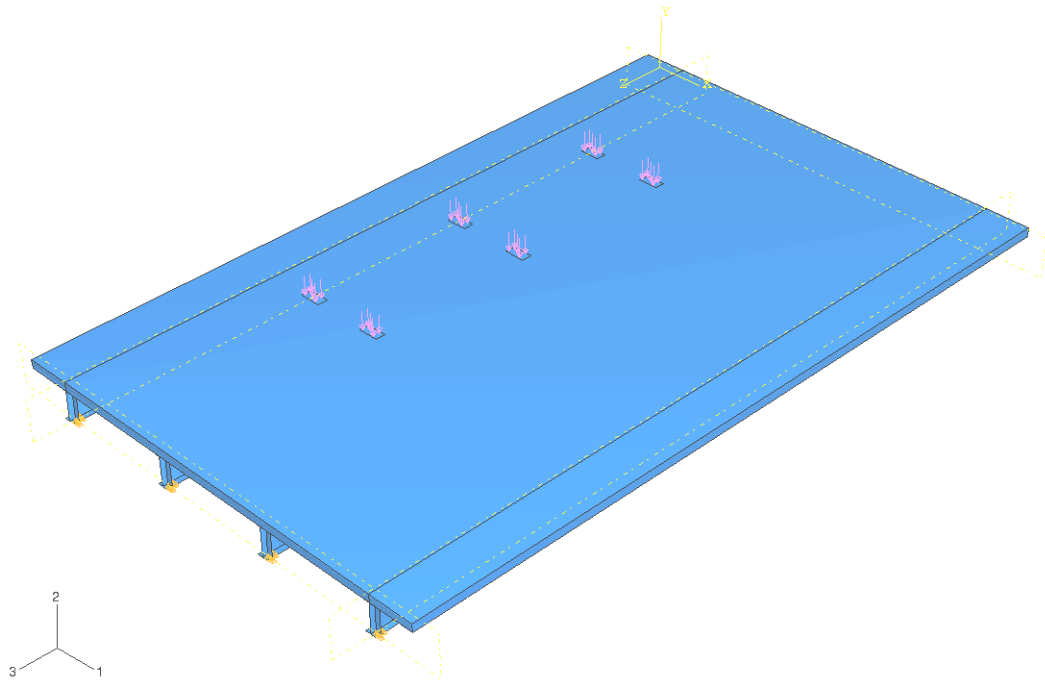


Figure 6.12 General view of the HS-20 load applied on the FE model

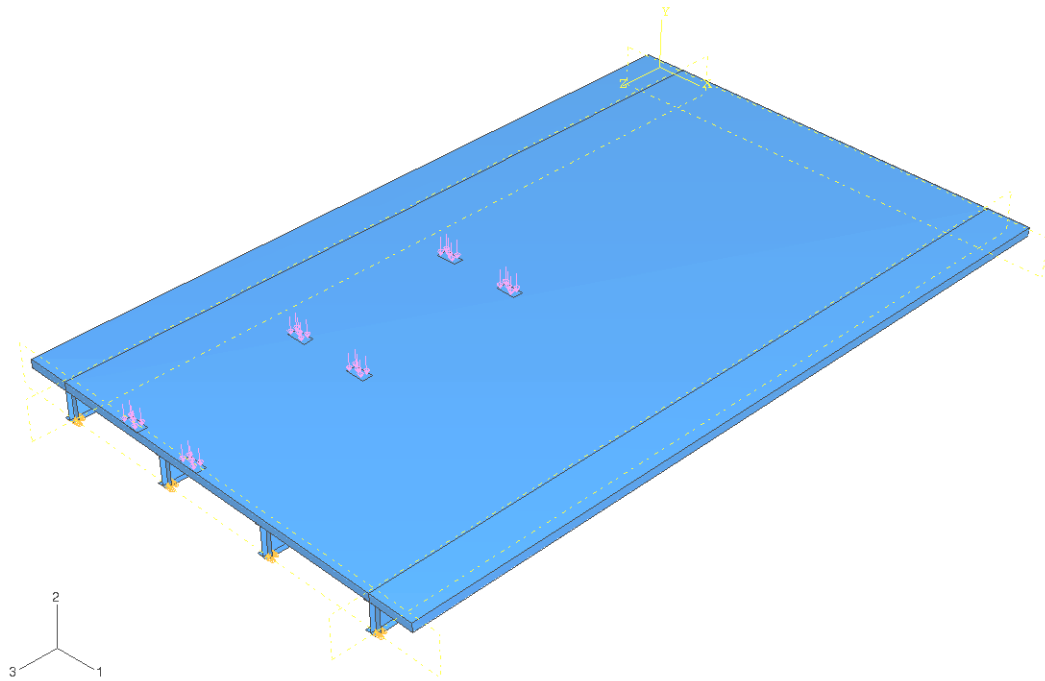


Figure 6.13 First investigated truck position – maximum negative moment

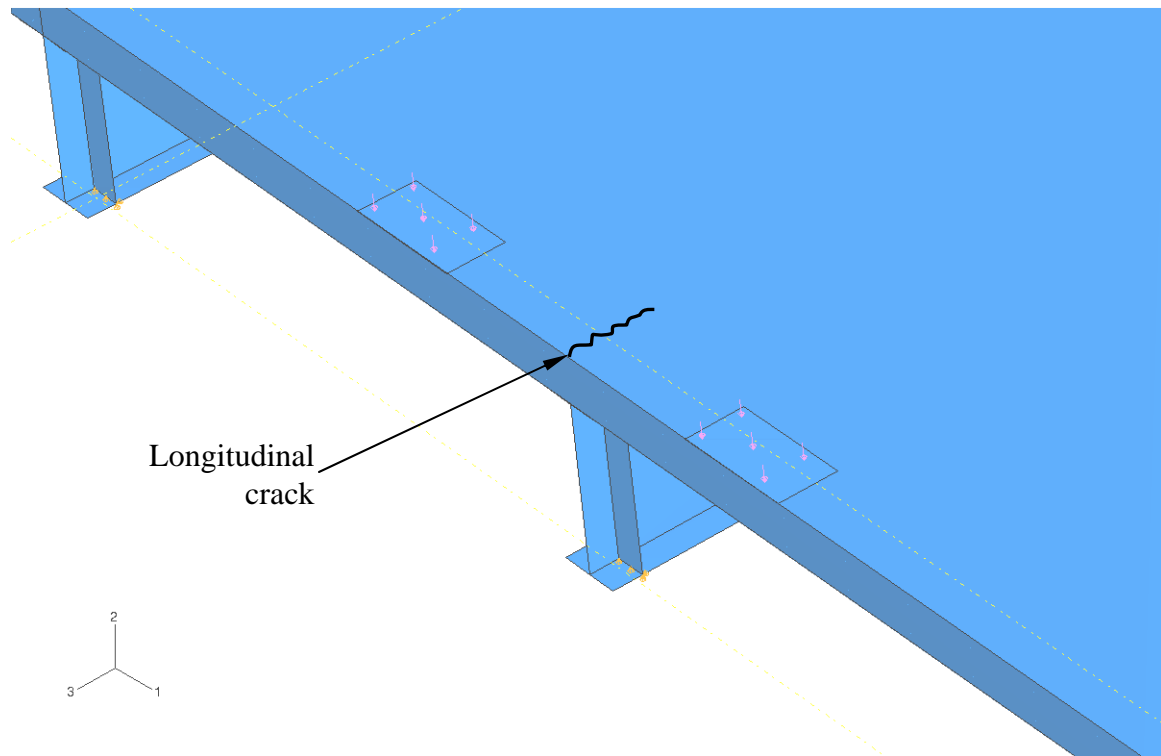


Figure 6.14 Detail of the first investigated position – longitudinal crack at the top of the deck

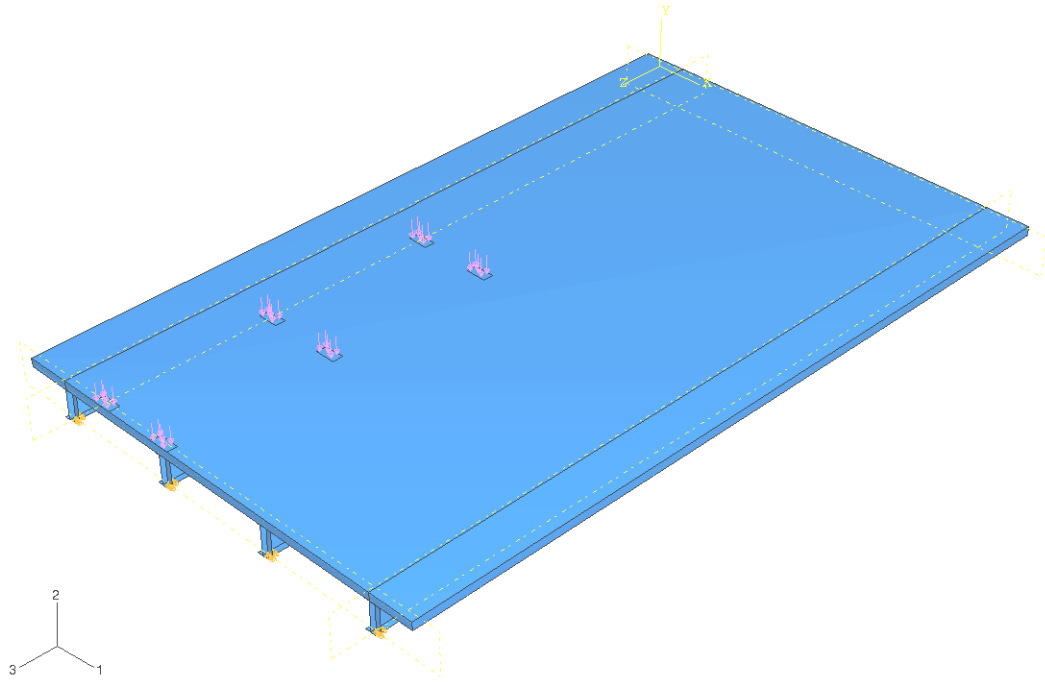


Figure 6.15 Second investigated truck position – maximum positive moment

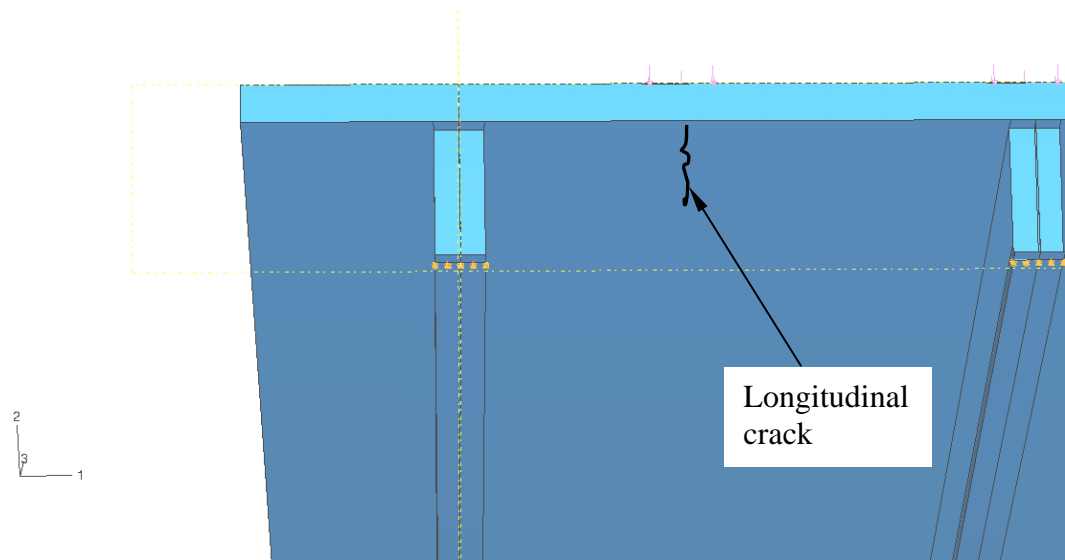


Figure 6.16 Detail of the second investigated position – longitudinal crack at the bottom of the deck

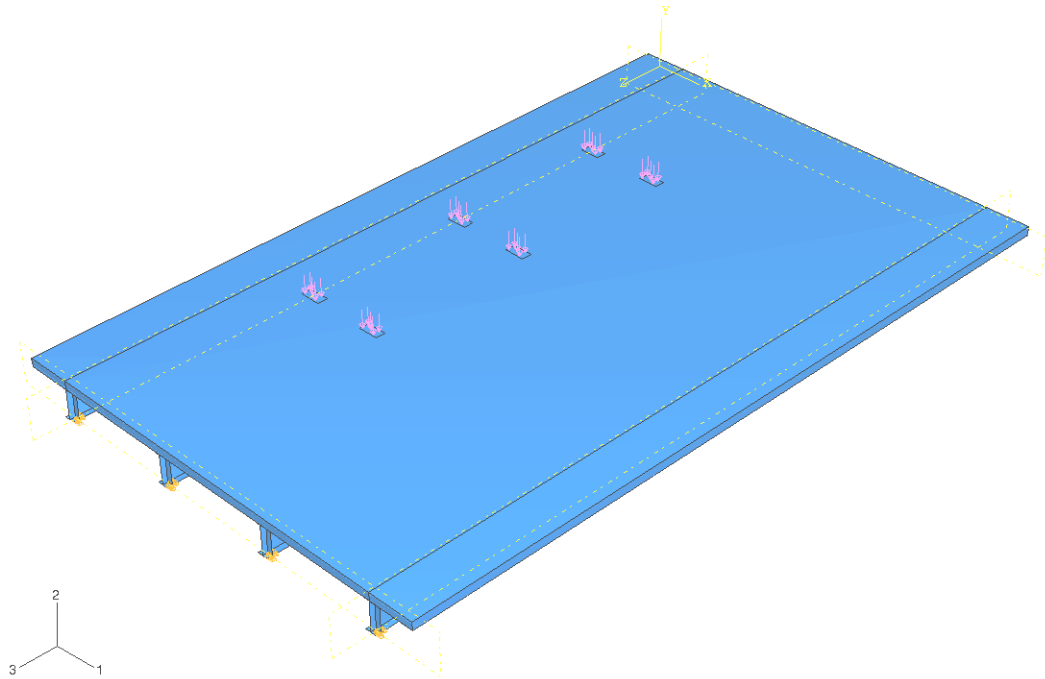


Figure 6.17 Third investigated truck position – maximum positive moment at midspan

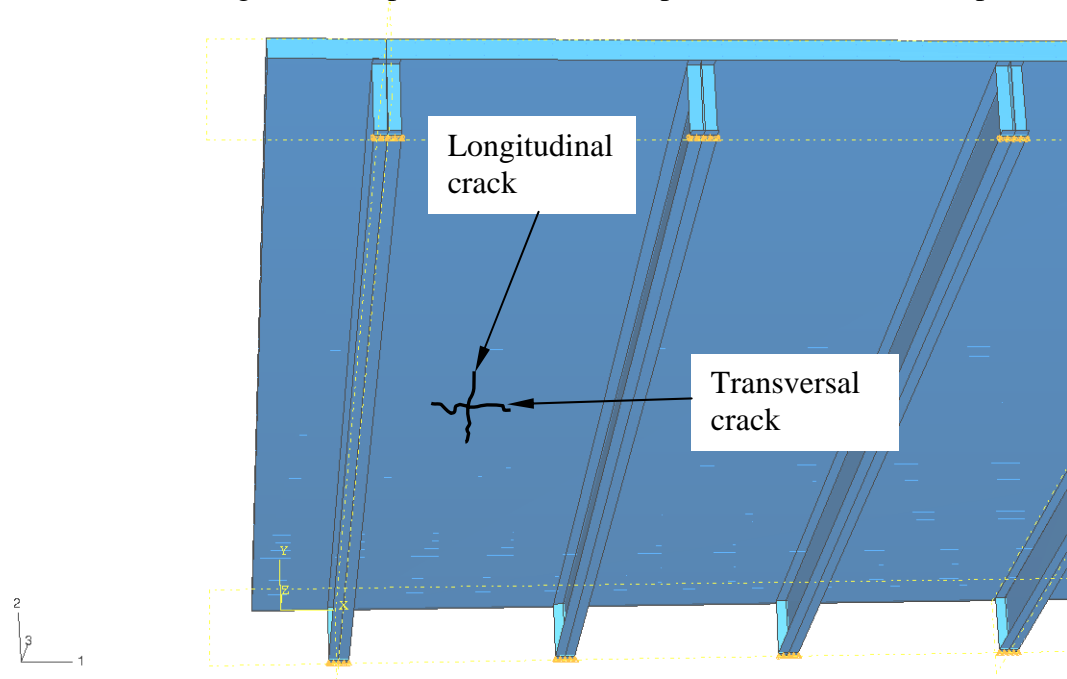


Figure 6.18 Detail of the third investigated position – longitudinal and transversal crack at the bottom of the deck

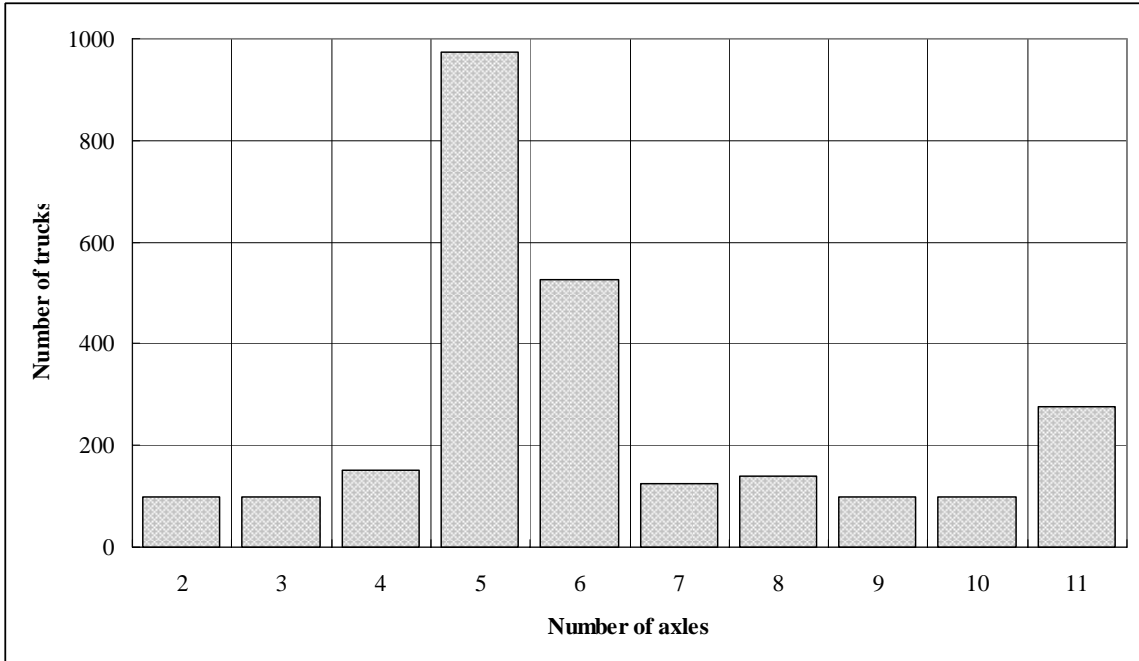


Figure 6.19 Histogram of number of axles for citation trucks

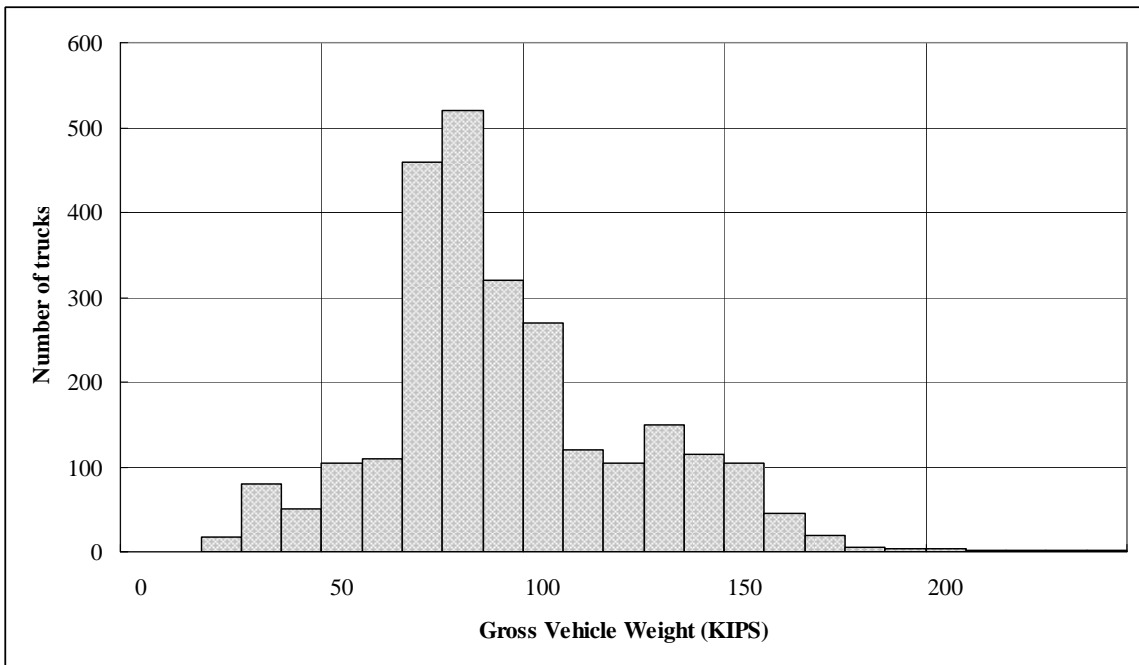


Figure 6.20 Histogram of Gross Vehicle Weight for citation trucks

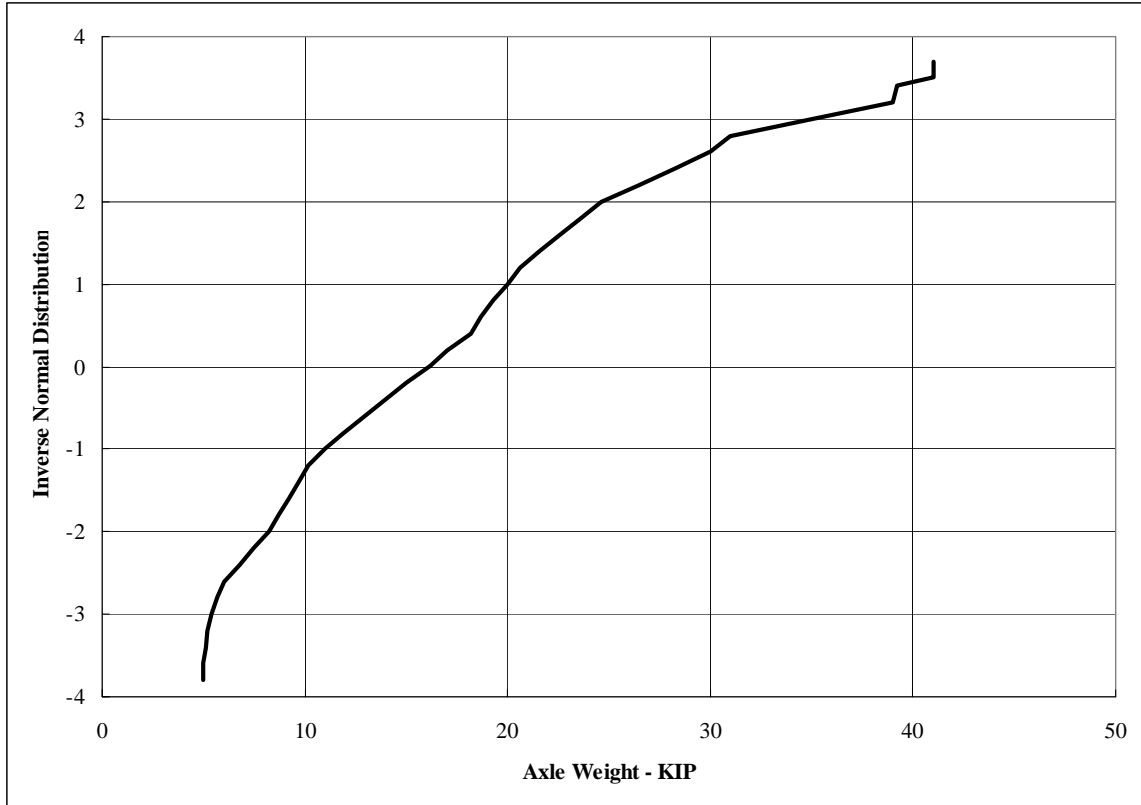


Figure 6.21 Cumulative Distribution Function of axle load for a year, citation data

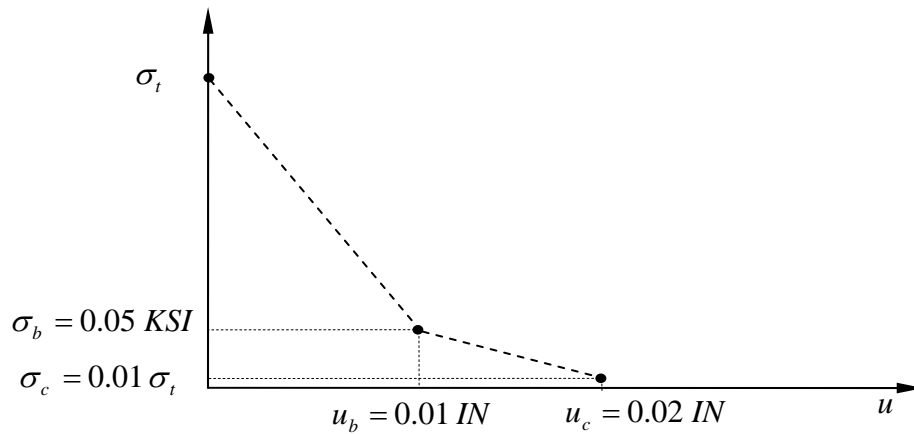


Figure 6.22 Tension stiffening used in the Finite Element Program

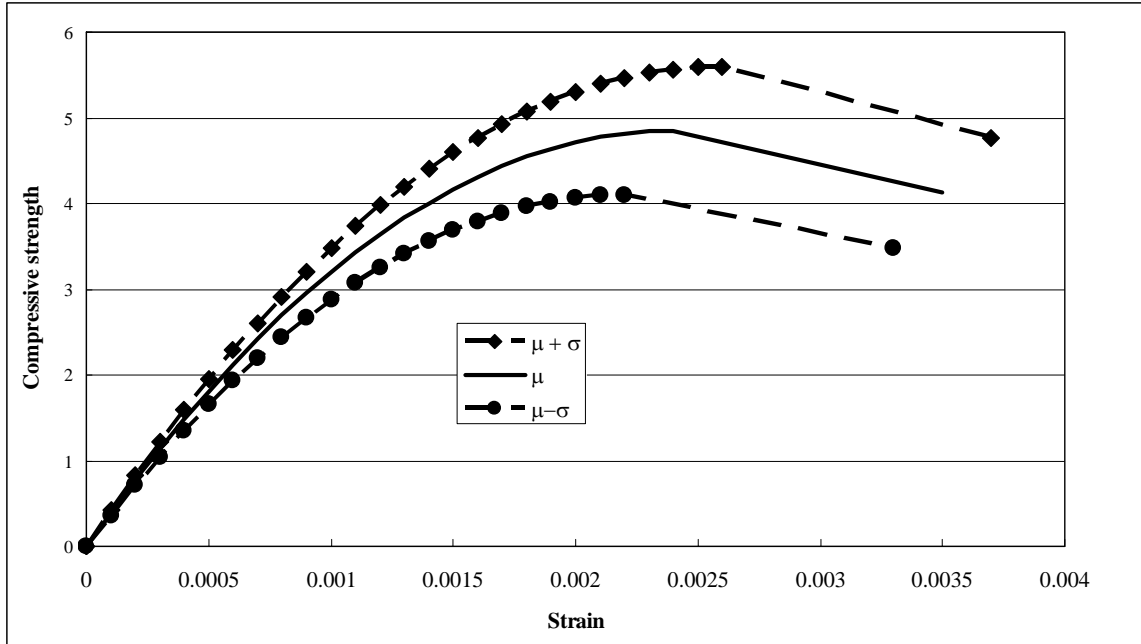


Figure 6.23 Compressive stress-strain of concrete implemented in the FEM

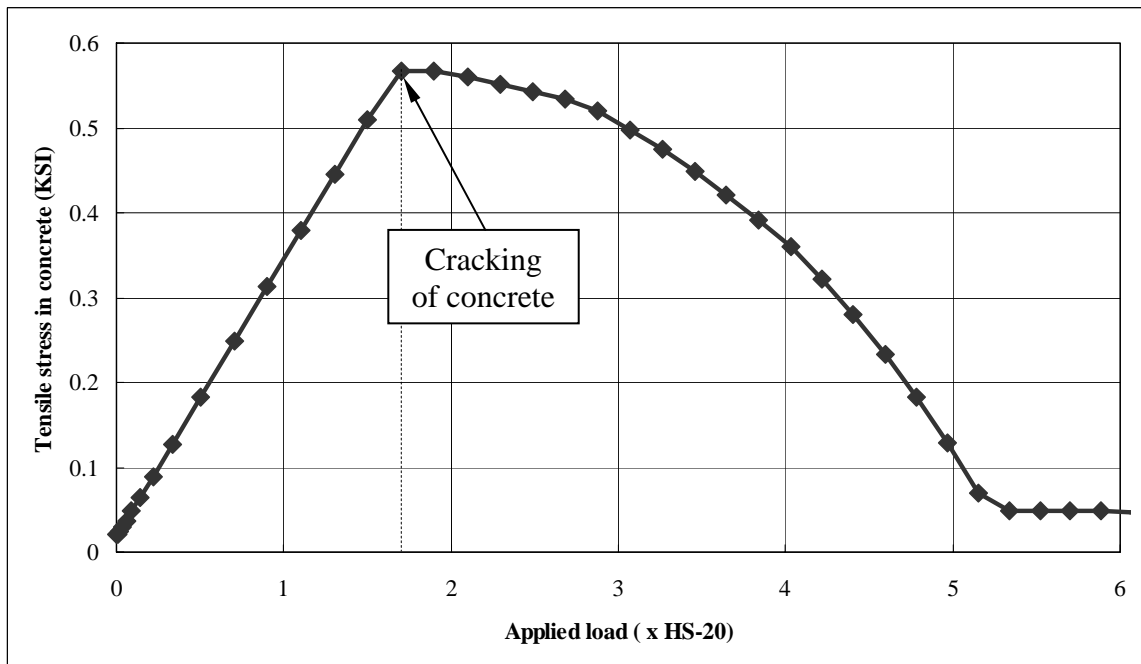
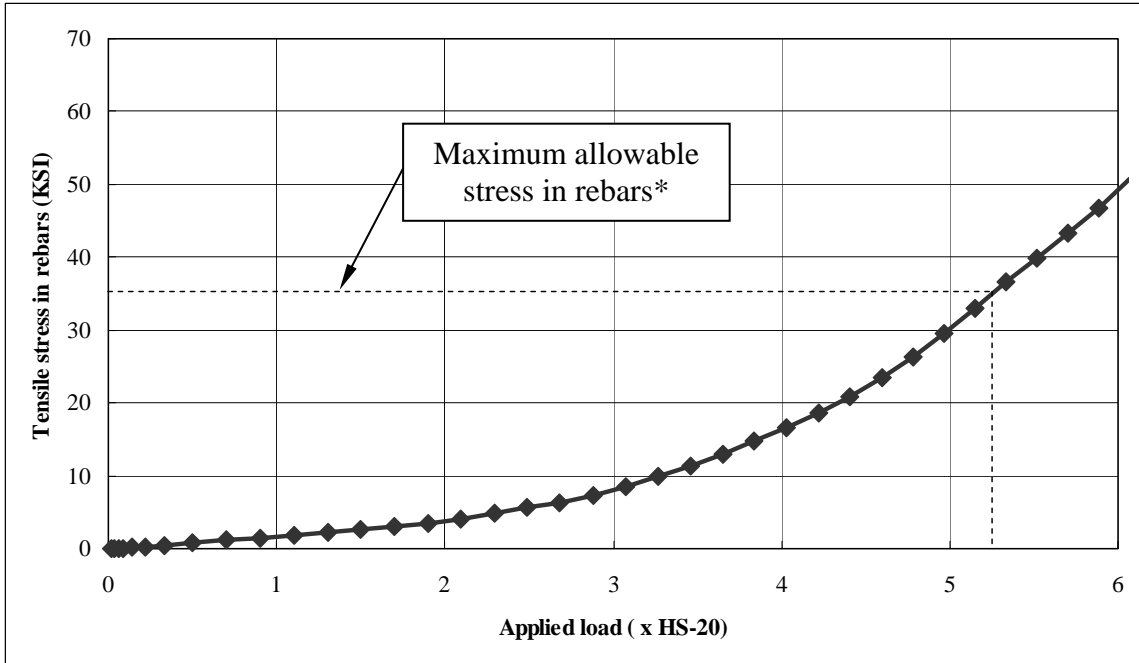


Figure 6.24 Tensile stress in concrete versus applied load



\*Vary depending on bridge configuration considered

Figure 6.25 Tensile stress in reinforcement versus applied load

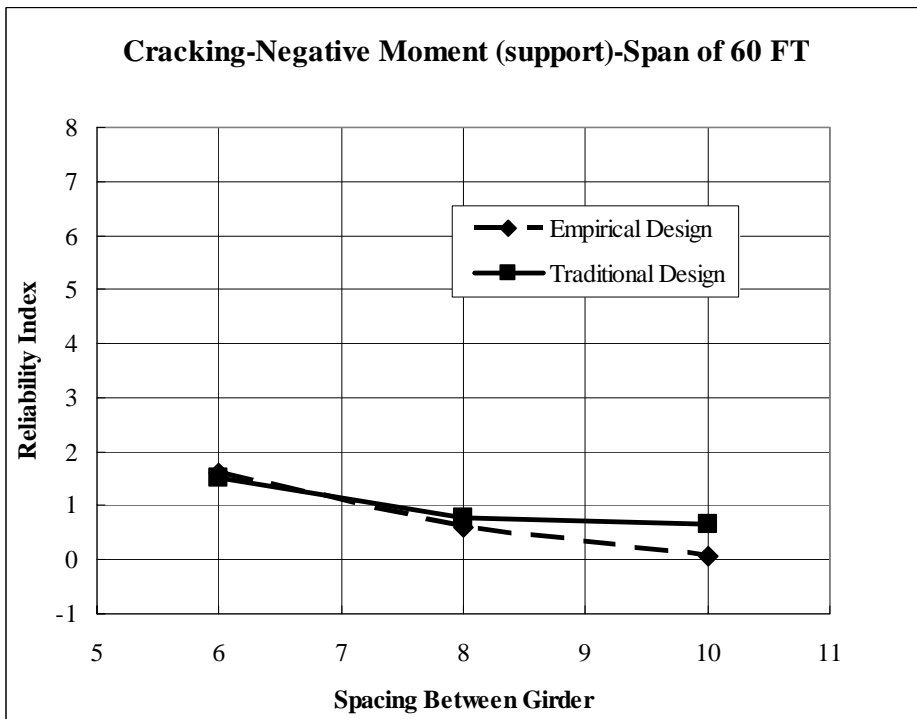


Figure 6.26 Comparison of reliability indices between the two design methods as a function of the girder spacing for the longitudinal cracking, negative moment at the support (top of the slab)

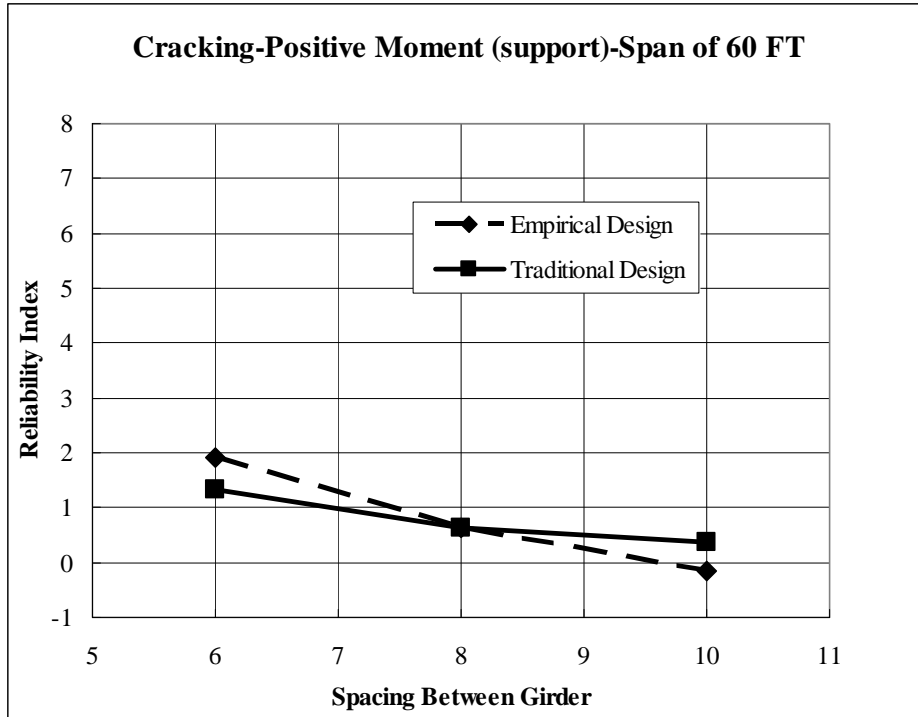


Figure 6.27 Comparison of reliability indices between the two design methods as a function of the girder spacing for the longitudinal cracking, positive moment at the support (bottom of the slab)

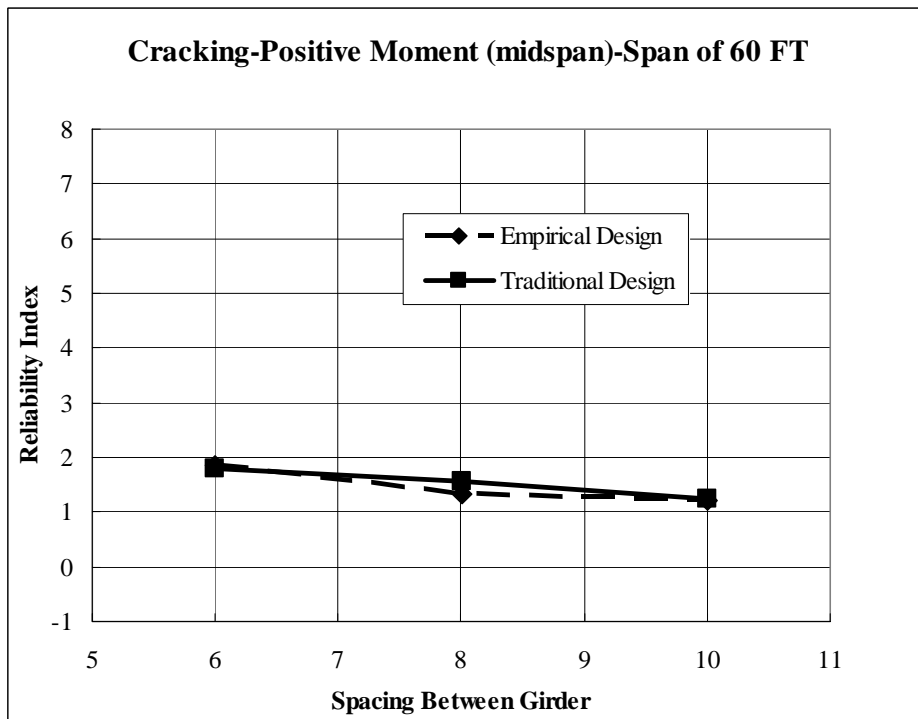


Figure 6.28 Comparison of reliability indices between the two design methods as a function of the girder spacing for the longitudinal cracking, positive moment at midspan (top of the slab)

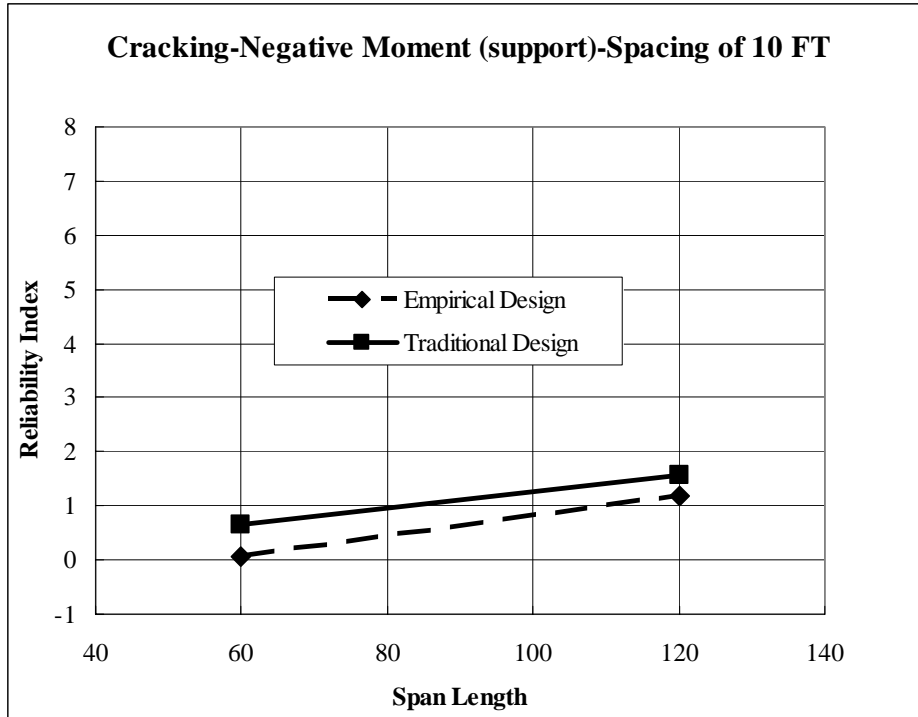


Figure 6.29 Comparison of reliability indices between the two design methods as a function of the span length for the longitudinal cracking, negative moment at the support (top of the slab)

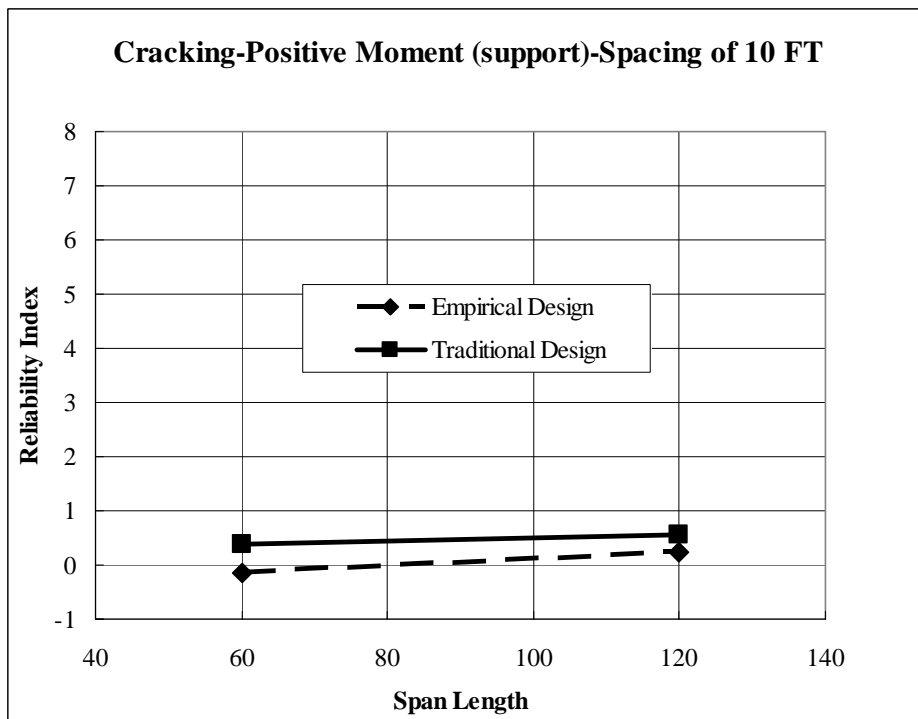


Figure 6.30 Comparison of reliability indices between the two design methods as a function of the span length for the longitudinal cracking, positive moment at the support (bottom of the slab)

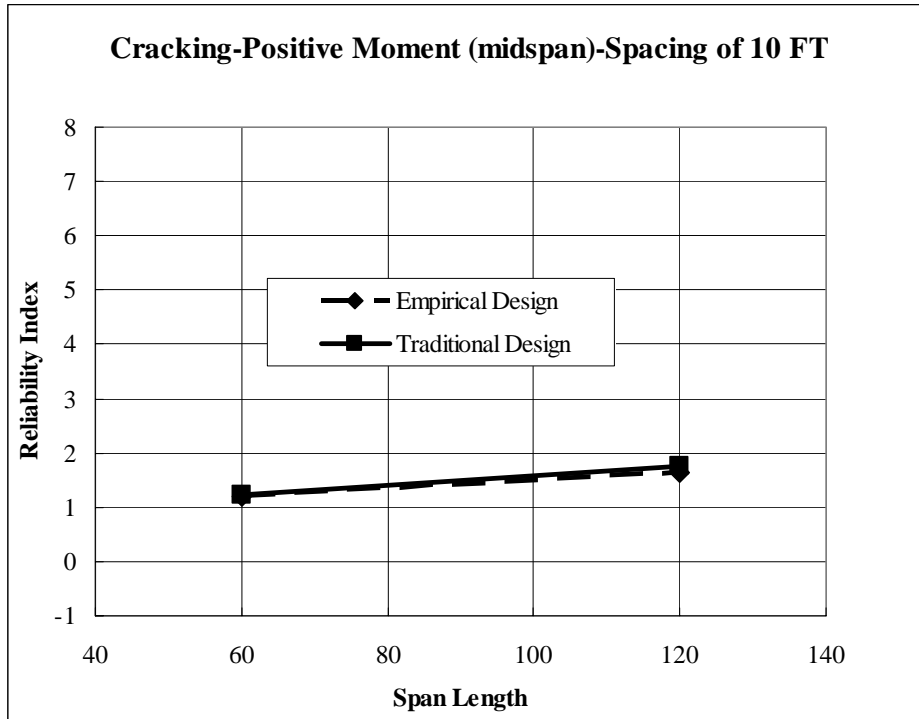


Figure 6.31 Comparison of reliability indices between the two design methods as a function of the span length for the longitudinal cracking, positive moment at midspan (bottom of the slab)

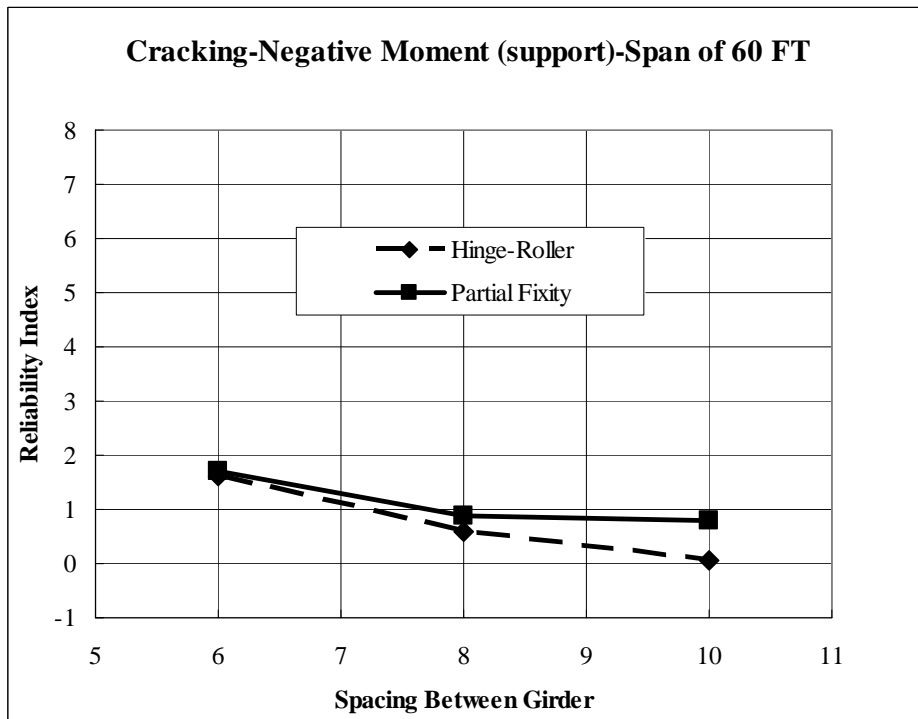


Figure 6.32 Comparison of reliability indices between the two boundary conditions as a function of the girder spacing for the longitudinal cracking, negative moment at support (top of the slab)

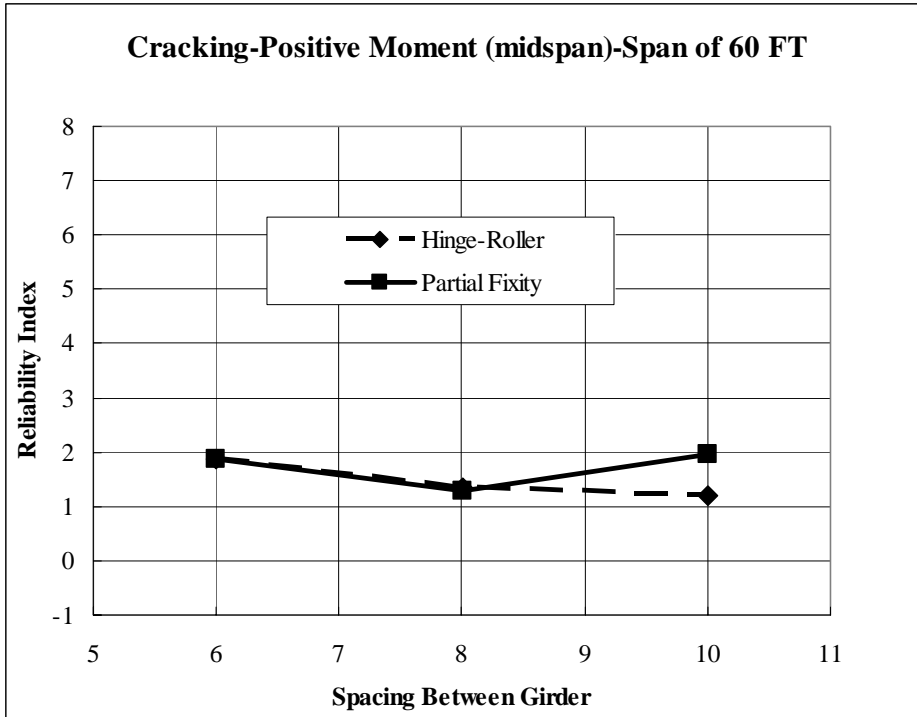


Figure 6.33 Comparison of reliability indices between the two boundary conditions as a function of the girder spacing for the longitudinal cracking, positive moment at midspan (bottom of the slab)

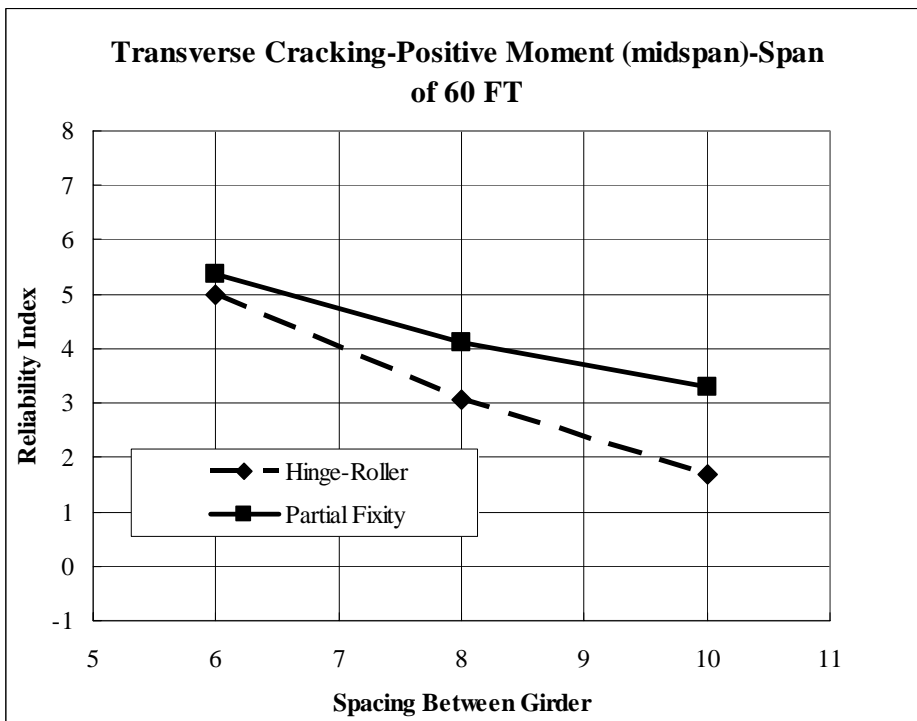


Figure 6.34 Comparison of reliability indices between the two boundary conditions as a function of the girder spacing for the transverse cracking, positive moment at midspan (bottom of the slab)

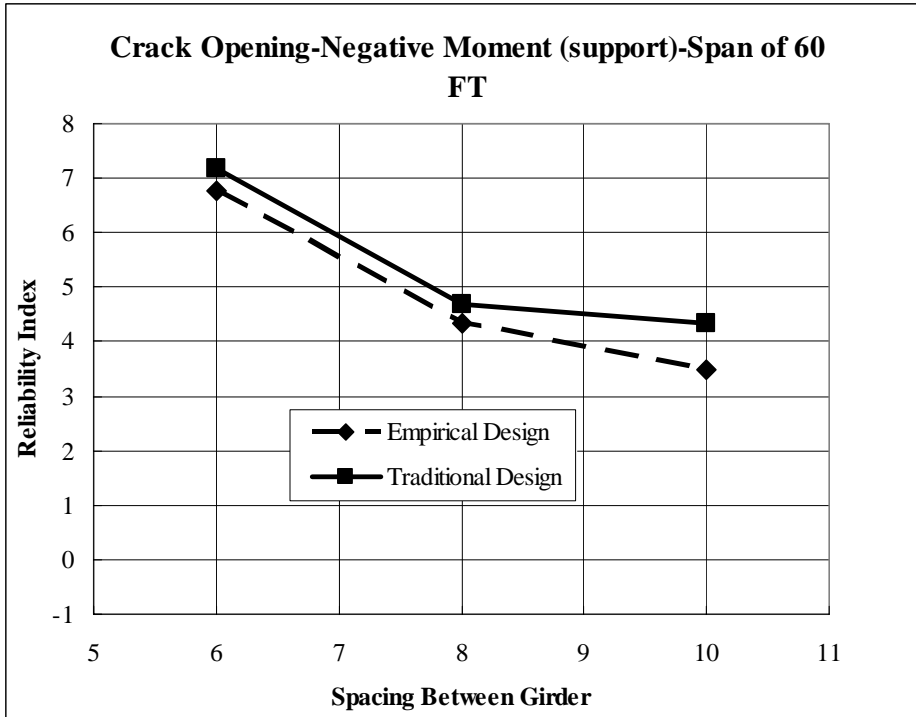


Figure 6.35 Comparison of reliability indices between the two design methods as a function of the girder spacing for the longitudinal crack opening, negative moment at the support (top of the slab)

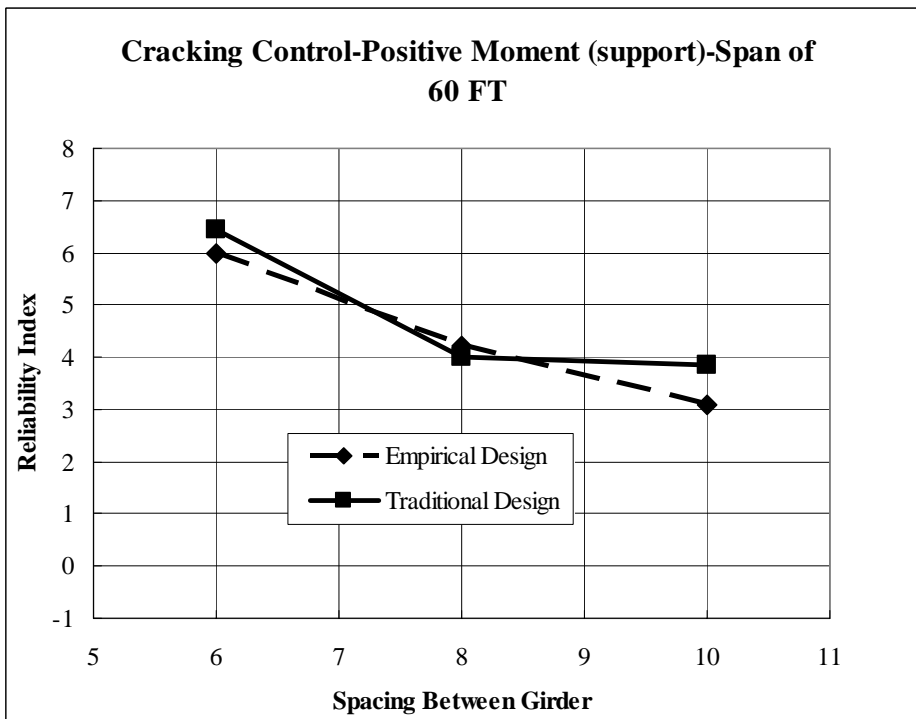


Figure 6.36 Comparison of reliability indices between the two design methods as a function of the girder spacing for the longitudinal crack opening, positive moment at the support (bottom of the slab)

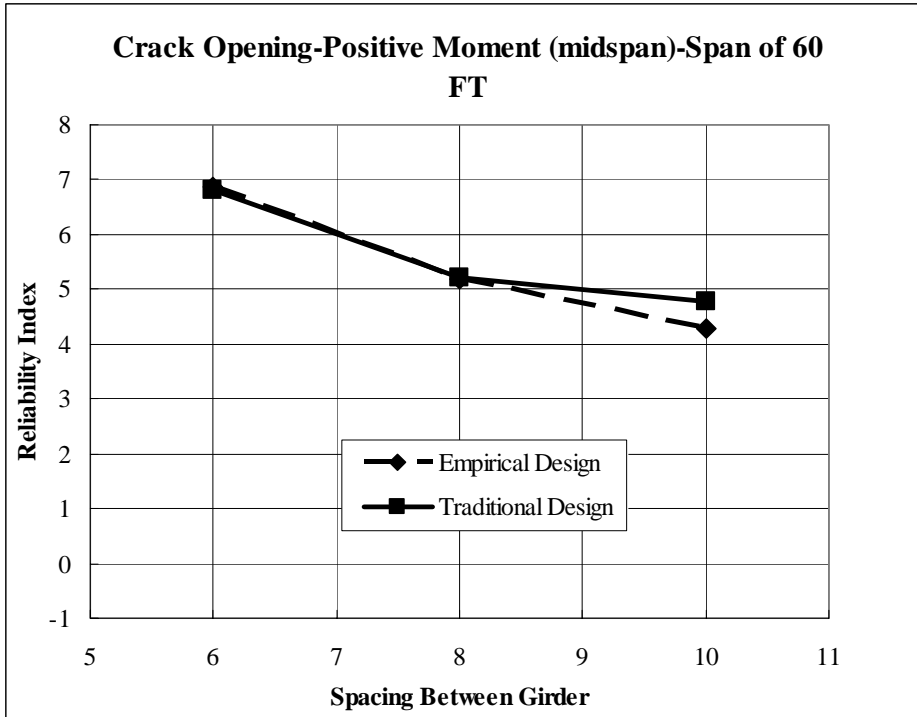


Figure 6.37 Comparison of reliability indices between the two design methods as a function of the girder spacing for the longitudinal crack opening, positive moment at midspan (bottom of the slab)

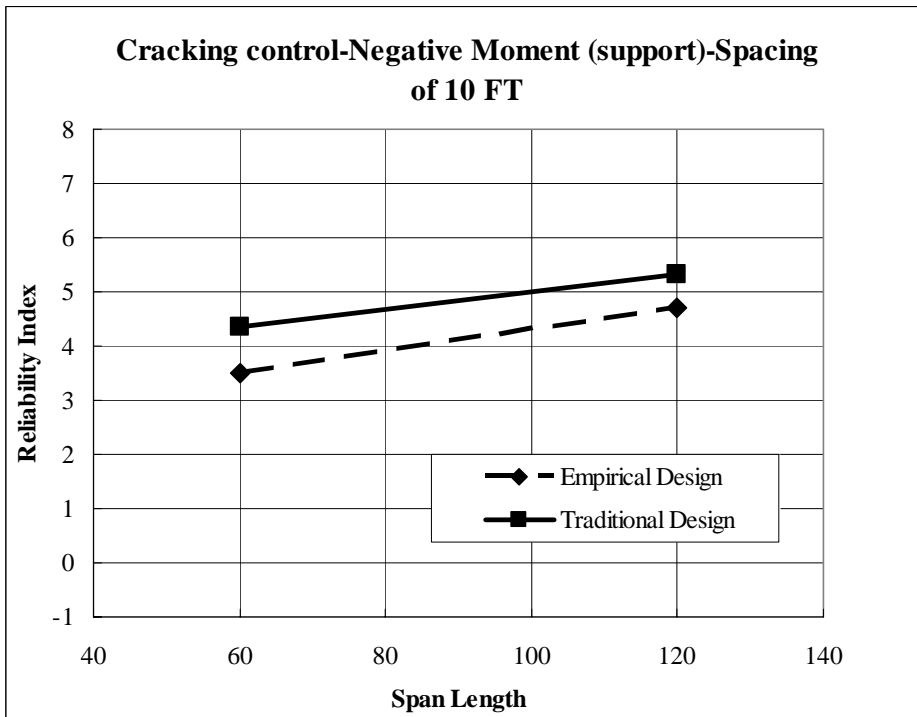


Figure 6.38 Comparison of reliability indices between the two design methods as a function of the span length for the longitudinal crack opening, negative moment at the support (top of the slab)

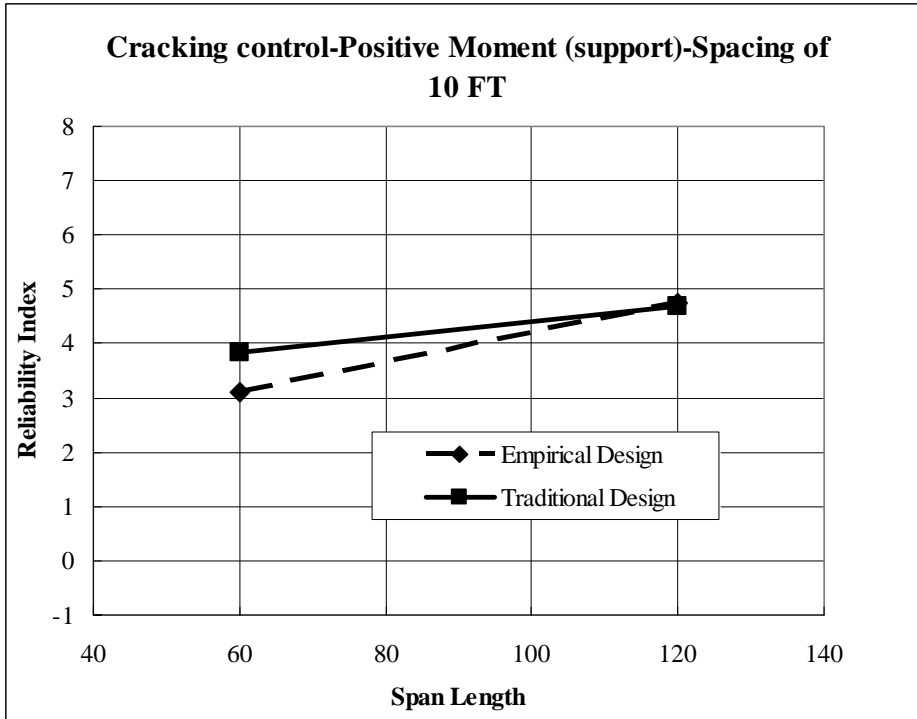


Figure 6.39 Comparison of reliability indices between the two design methods as a function of the span length for the longitudinal crack opening, positive moment at the support (bottom of the slab)

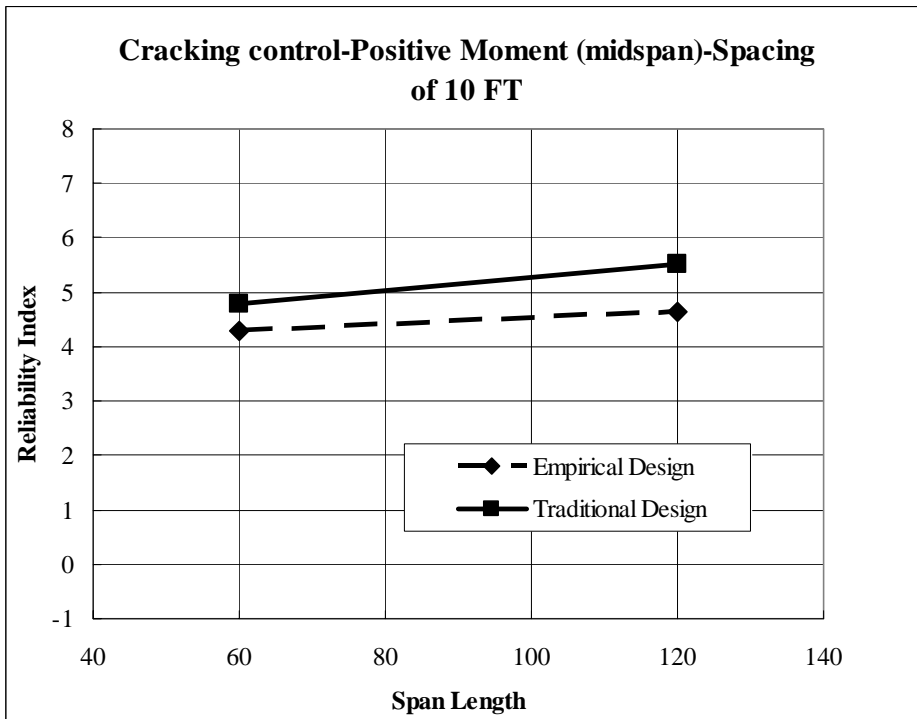


Figure 6.40 Comparison of reliability indices between the two design methods as a function of the span length for the longitudinal crack opening, positive moment at midspan (bottom of the slab)

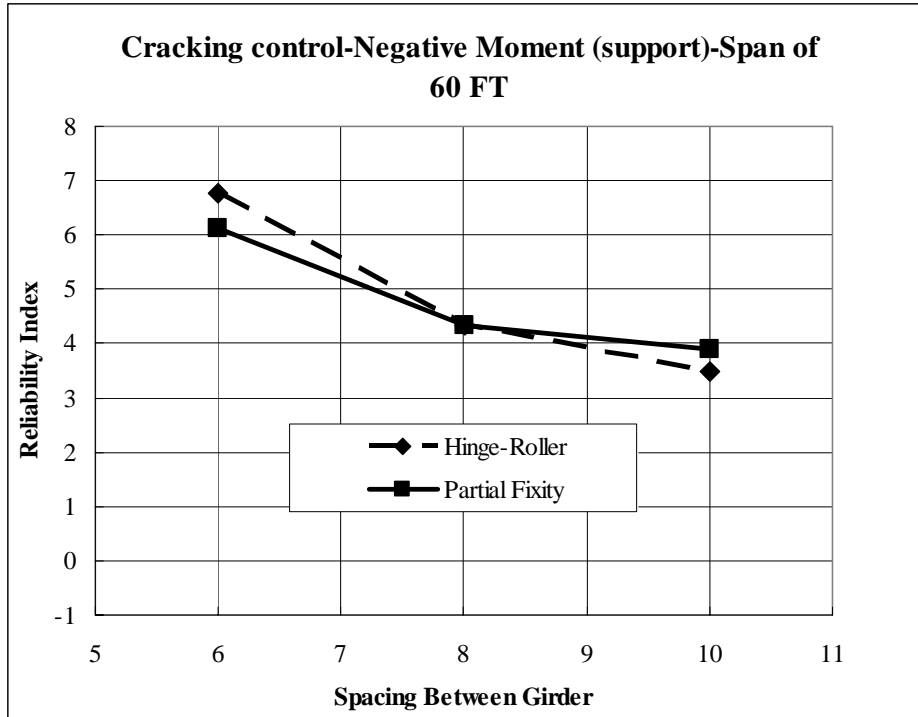


Figure 6.41 Comparison of reliability indices between the two boundary conditions as a function of the girder spacing for the longitudinal crack opening, positive moment at the support (bottom of the slab)

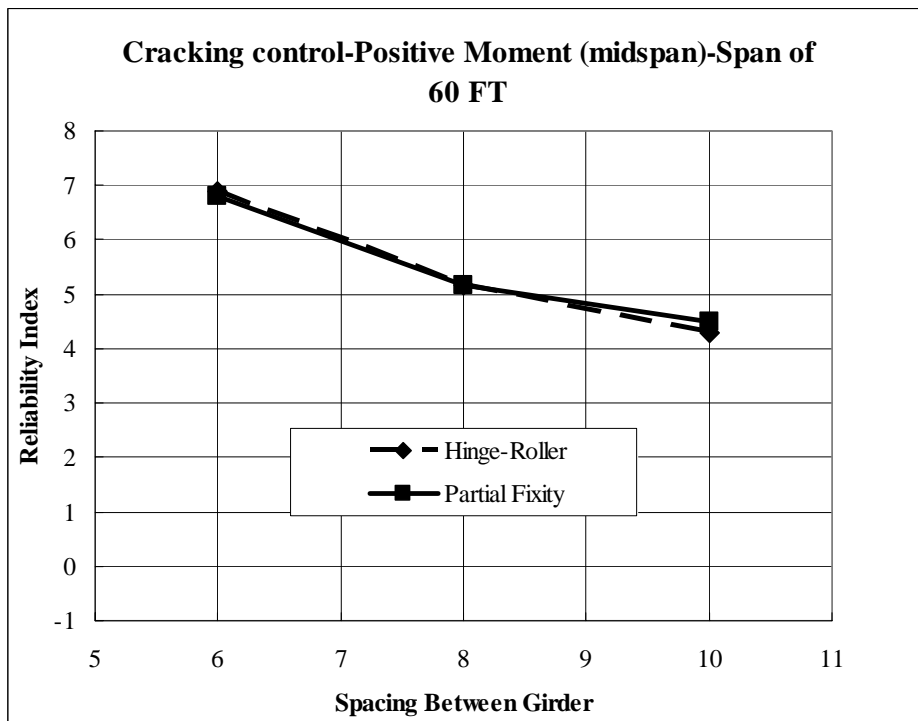


Figure 6.42 Comparison of reliability indices between the two boundary conditions as a function of the girder spacing for the longitudinal crack opening, positive moment at midspan (bottom of the slab)

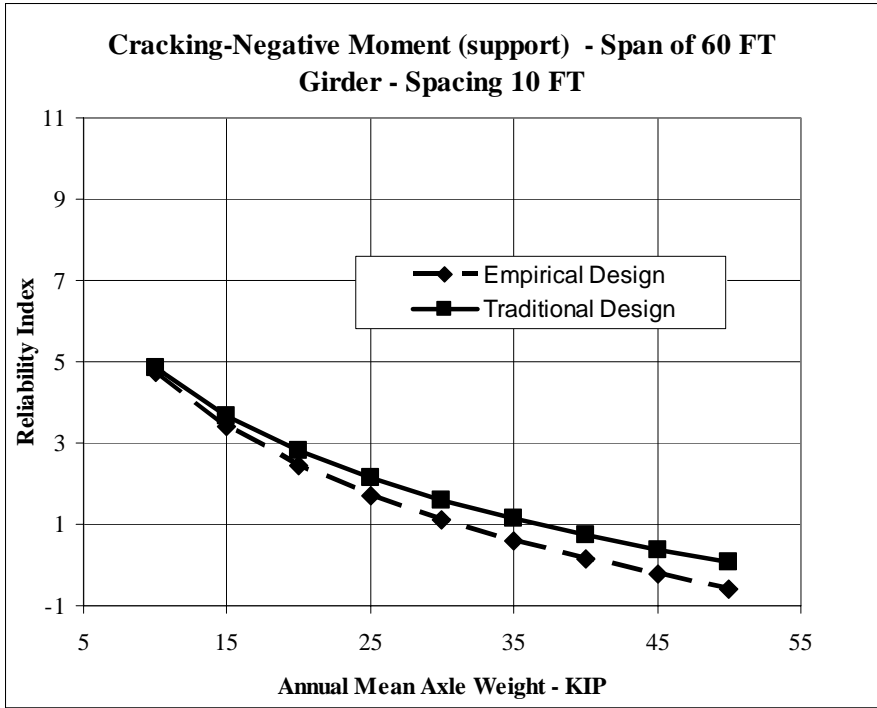


Figure 6.43 Comparison of reliability indices between the two design methods as a function of the annual mean maximum axle weight for the longitudinal cracking, negative moment at midspan (top of the slab) – span = 60 FT, Girder spacing = 10 FT

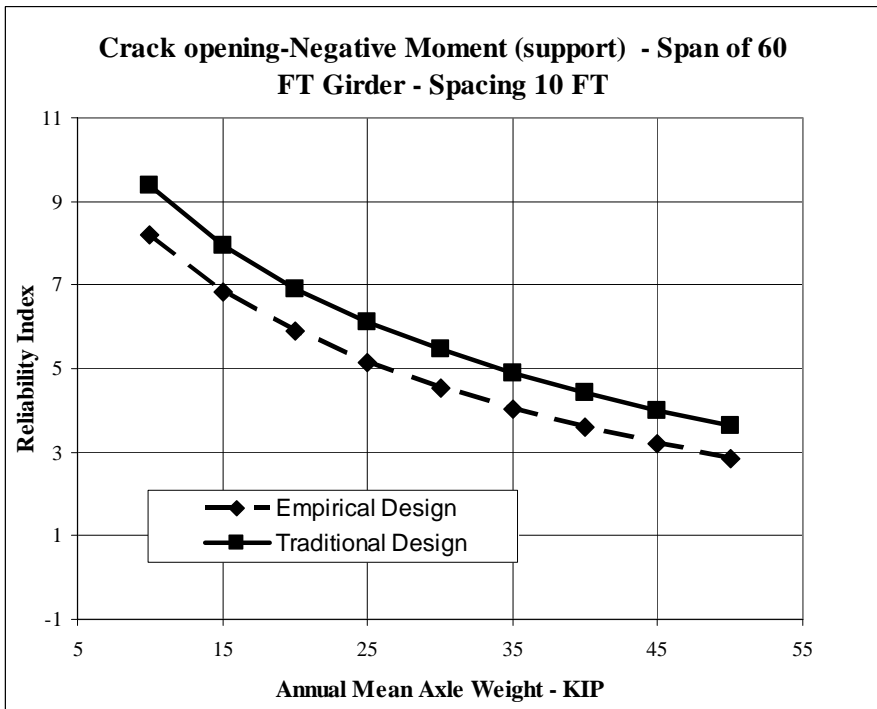


Figure 6.44 Comparison of reliability indices between the two design methods as a function of the annual mean maximum axle weight for the longitudinal crack opening, negative moment at midspan (top of the slab) – span = 60 FT, Girder spacing = 10 FT

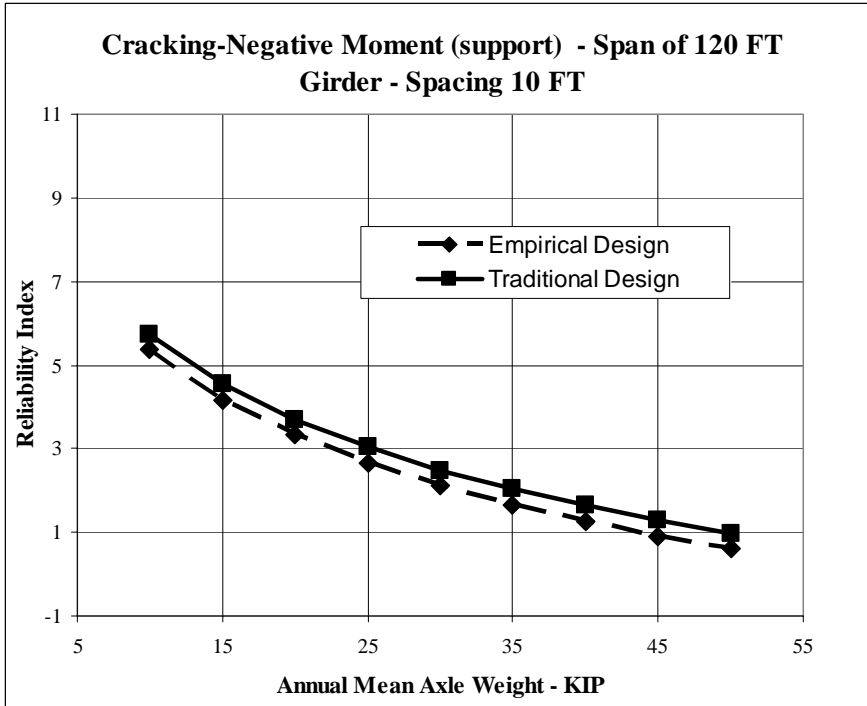


Figure 6.45 Comparison of reliability indices between the two design methods as a function of the annual mean maximum axle weight for the longitudinal cracking, negative moment at midspan (top of the slab) – span = 120 FT, Girder spacing = 10 FT

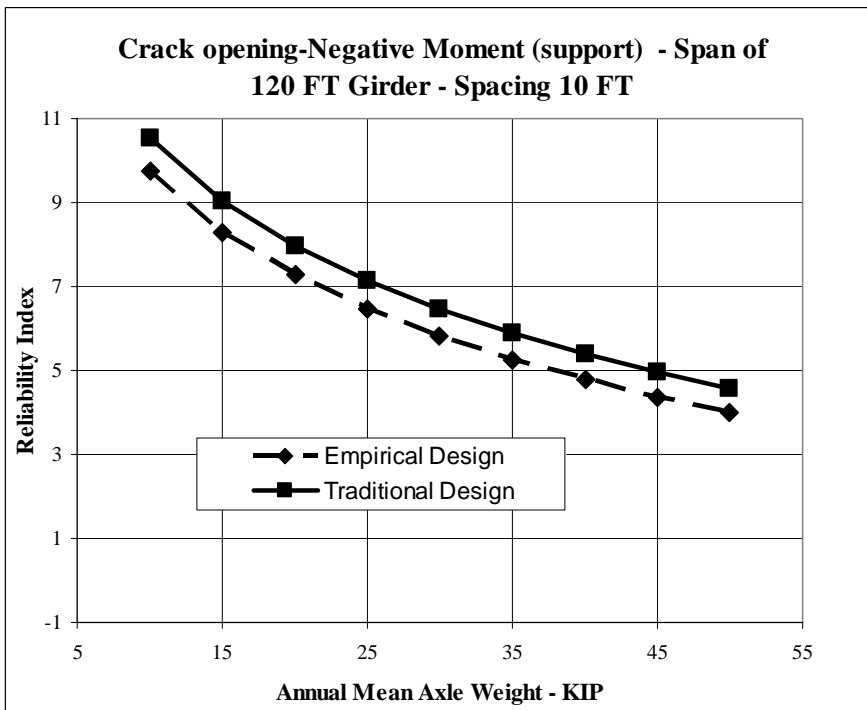


Figure 6.46 Comparison of reliability indices between the two design methods as a function of annual mean maximum axle weight for the longitudinal crack opening, negative moment at midspan (top of the slab) – span = 120 FT, Girder spacing = 10 FT

## **CHAPTER 7**

### **SUMMARY AND CONCLUSIONS**

#### **7.1. Summary**

At present, there is no assessment method available to evaluate the serviceability and durability of bridge decks. In this dissertation, a procedure for bridge decks evaluation is developed, that is focused on evaluation and comparison of performance of reinforced concrete slab-on-girders with girder spacing up to 10 FT, designed according to the two methods specified by the AASHTO LRFD (2005) code (strip method and empirical method). Ultimately, a reliability based method associated with a state of the art non linear finite element analysis, calibrated using field tests, is developed in order to understand the structural behavior of the deck and to assess its performance.

The field tests were carried out on a steel girder bridge, with the girders spaced at 10 FT. The bridge was selected from a list of bridges with large spacing between girders, provided by the Michigan Department of Transportation. The field tests were carried out to determine the actual behavior of bridge superstructure supported by steel girders spaced at more than 10 FT. The results were used to calibrate the Finite Element Model and to analyze the effect of partial fixity of the support on the behavior of reinforced concrete bridge deck. The selected bridge was tested using a three-unit 11-axles truck as live load (the largest live load legally permitted in the State of Michigan) with known gross vehicle weight and axle configuration. The actual axle weights of the test truck were measured at a weigh station prior to the test. The truck was driven over the bridge at different transverse positions at crawling speed to simulate a static loading. For each run,

the strain measurement was recorded simultaneously on all the girders at two locations; close to support and 26 FT from the support.

A non-linear finite element model for reinforced concrete was developed using the commercial software ABAQUS. Eventually, the results from the FEM program for each configuration of the studied bridges served in the calculation of resistance parameters in the reliability analysis.

In the FEM model, a three-dimensional model was selected to investigate the behavior of the bridge decks. The web and flanges of the steel girders were modeled with 4-node shell elements, each node having six degrees of freedom (three in translation and three in rotation). The reinforced concrete deck slab was modeled using 8-node brick elements, each node having three degrees of freedom. Each reinforcing rebar was modeled using truss elements embedded in the deck slab at the exactly determined depth and spacing. Since this study concentrated on stress distribution within the reinforced concrete deck slab, special attention was paid to the meshing process. It was observed that with the type of element selected in this study, a model with four layers of elements was giving good results in terms of stress/strain distribution and load/deflection behavior. The structural effects of the secondary members such as sidewalk and parapet were taken into account in the finite element model of the tested bridge. Transverse bracing and cross framed diaphragm were also modeled using truss elements.

The three materials used in this research were concrete and two types of steel; reinforcing steel for the rebars and structural steel for the girders. Rather than attempting to develop complicated material models with a complete mechanical description of the behavior of concrete and reinforcement and their interaction, the built-in material models available in ABAQUS were used that efficiently represent the main parameters governing the response of structural concrete.

The concrete model available in ABAQUS and used in this study includes inelastic damage behavior. This model is based on the assumptions of isotropic damage

and it is designed for applications with concrete subjected to arbitrary loading conditions. The model takes into consideration a degradation of the elastic stiffness induced by plastic straining both in tension and compression. The Honegstad model was applied to model the compression stress-strain curve of concrete, and a bilinear tension stiffening defined in terms of displacement is used to model post-cracking behavior. Regarding steel, a perfect elastic-plastic idealization of the stress-strain response of reinforcement was used in this study.

Results of three available laboratory experiments on slabs were compared with the analytical results in order to validate the developed material behavior model. The tested bridge was also analyzed using the same material model in order to investigate the effect of partial fixity of the boundary conditions. The FEM results from all three cases considered were in very good agreement with the experimental results in terms of load versus deflection. Therefore, this proves that the modeling technique and the material model used in this study are accurate and efficient enough to accurately predict the reinforced concrete deck slab behavior.

After the FEM model was validated and refined, a reliability analysis at serviceability limit state was carried out. The reliability analysis comprises of three main components: 1) Limit states, 2) Load parameters, and 3) Resistance parameters.

Two limit states considered in this study were the cracking of concrete and the crack opening of concrete.

The load parameters were calculated from live load data obtained from previous studies by Nowak and Kim (1997).

In case of resistance parameters, a significant amount of time (more than 24 hours in some cases) is needed for nonlinear finite element computation of a bridge superstructure; therefore, the Rosenblueth 2K+1 point estimate method, which requires a minimum numbers of simulations, is chosen to obtain the resistance parameters. Several configurations of bridge deck slabs were considered. For bridge deck slabs designed

according to two different design methods specified by the AASHTO LRFD code (the traditional strip method and empirical design), the considered parameters include: three different girder spacings (6 FT, 8 FT and 10 FT); two different span lengths (60 FT and 120 FT); and the effect of partial fixity of the boundary conditions. The random variables used in the Rosenblueth  $2K + 1$  point estimate method were: the compressive strength of concrete ( $f'_c$ ); the modulus of rupture of concrete ( $f_r$ ); the yield strength of steel rebars #4 and #5; and the thickness of the slab.

A total of 11 FEM computations were run for each studied bridge configuration. The 11 simulations comprised of 5 runs at the mean value of each of the five considered random variables, and 10 runs at + and – one standard deviation for each of the five considered random variables. Ultimately, a set of 11 simulations were carried out repeatedly for all studied bridge configurations to obtain the resistance parameters.

The computed resistance parameters were then applied along with live load parameters to obtain reliability indices. Serviceability of bridge decks was then assessed by comparing the calculated reliability indices of all investigated configurations. Finally, conclusions and recommendations were formulated.

## **7.2. Conclusions**

### **7.2.1. General conclusions**

1. The developed and calibrated nonlinear Finite Element Method procedure for the analysis of reinforced concrete slabs can effectively predict the behavior of bridge deck at serviceability level. A material model for concrete and steel is presented along with a modeling method capable of accurately represent reinforcement (rebar diameter, spacing, and depth) in the model.

2. An efficient procedure for evaluation of reinforced concrete deck slab at serviceability limit state is presented and validated. The procedure involves field testing of bridge decks to evaluate partial fixity of supports, development of FEM model for reinforced concrete bridge decks, calibration of FEM model using field tests, and development of the reliability analysis procedure for evaluation of the deck slab performance at serviceability.

### **7.2.2. Conclusions for cracking limit state**

1. For the longitudinal cracking limit state, the reliability indices are very low, ranging from 0 to 2, for all deck configurations studied. Since we used annual mean maximum for the load, a reliability index of zero corresponds to a probability of 50% for the deck to crack within a year. It was observed that the reliability index for cracking slightly decreases when the girder spacing increases which indicates a slightly higher probability of cracking for decks supported on widely spaced girders. Both design methods show a similar reliability level at cracking limit state, with traditional design having just slightly higher values of the reliability for wider spacing.

2. In all investigated cases, the partial fixity reduces the probability of longitudinal cracks to appear in a bridge deck supported on widely spaced girders. However, it was observed that the effect of boundary conditions is more significant for transverse cracking than for longitudinal cracking. In case of transverse cracking at the bottom of the deck at midspan, it is observed that partial fixity significantly increase the reliability indices.

3. Results showed that the reliability indices increase, from 0 to 2, when the span increases for both design methods regardless of the crack location.

4. For all cases, the reliability indices decreases significantly when the annual mean maximum axle weight increases. This emphasizes the importance of an accurate

estimation of the actual traffic on the bridge in order to predict the bridge behavior at serviceability and also point out the importance of bridge posting.

### **7.2.3. Conclusions for crack opening limit state**

5. For the longitudinal crack opening limit state, it was observed that the reliability indices are relatively high, ranging from 3.5 to 7, for all deck configurations studied. It means that the probability of the crack to occur is higher than the probability of the crack to open at the width recommended by the code. However, this can also be explained by the fact that only live load was considered in this study. Shrinkage and differential temperature analysis that can reduce the reliability indices were not included.

6. Results showed that crack opening is more sensitive to girder spacing than cracking; the reliability index significantly decreases when the girder spacing increases which indicates a higher probability of cracking for the deck supported on widely spaced girders. Traditional design results in higher values of the reliability index for wider spacing. Therefore, as expected, crack opening is significantly influenced by the reinforcement ratio. In case of empirical design, because the design yields a constant ratio of reinforcement for all girder spacings, the reliability indices decrease significantly as the girder spacing increases. On the contrary, in case of the traditional design method, the reinforcement ratio increases as girder spacing increases; hence, the reliability only slightly decreases as the spacing increases.

7. The analysis of the cracking limit state indicates that reliability indices slightly increase, from 3 to 5, when the span increases for both design methods regardless of the crack location.

8. The analysis of the cracking limit state indicates that the reliability indices decrease significantly when the annual mean maximum axle weight increases. This, again, emphasizes the importance of an accurate estimation of the actual traffic on the

bridge in order to predict the behavior at serviceability and also points out how important is bridge posting.

### **7.3. Suggestions for future research**

An extensive analytical program has been carried out in this research to understand the behavior of reinforced concrete bridge deck slab at the serviceability level. The following future research work is recommended:

To include restrained plastic shrinkage and temperature changes in the analysis to investigate early age transverse cracking. When these early age transverse cracks meet the longitudinal cracks due to live load as considered in this study, the degradation of the deck slab can be dramatically increased.

To perform a reduced scale laboratory testing on bridge deck slab to validate the finding of the analytical study and to investigate reliability of the deck slab at the ultimate limit state. The actual code provisions are based on bending design but several authors observed a punching shear failure of deck slab. Laboratory testing associated with a nonlinear Finite Element analysis can help to determine the failure mode of a bridge deck slab.

To study the behavior of reinforced concrete deck slab supported on prestressed concrete girders. Recent field tests performed at the University of Michigan showed that the distribution of load on prestressed concrete girders was quite different than that observed for steel girders. According to the current code provisions, these two decks are designed using the same method. Analytical methods and field tests are needed to fully understand the behavior of the deck slab supported on prestressed girders.

To define target reliability indices for bridge deck at serviceability and ultimate limit states. Since the definition of a target reliability index involves a lot of economical

considerations, a system reliability analysis should be performed including a life cost cycle analysis to adequately define the corresponding target reliability index.

## **APPENDICES**

## APPENDIX A

### EXAMPLE OF DESIGN OF A COMPOSITE STEEL BRIDGE

#### A.1. Description

Design a simple span composite steel girder bridge shown in Figure A.1 with the span of 60 FT. Roadway width is 34 FT curb to curb as shown in Figure A.2 and Figure A.3. The deck thickness is 9 IN. Allow for a future concrete wearing surface of 3 IN (125 PCF). Use  $f'_c=4000$  PSI and A60 steel.

#### A.2. General Design

- The bridge is to carry an interstate traffic over a creek.
- The roadway width: 34 FT curb to curb
- Span: Simple span of 34 ft
- Select bridge type: *I*-Girders

#### A.3. Design basis

##### I-Girder

General [A6.10.1]. Design flexural members for

Strength limit state

Service limit state for control of permanent deflections

Fatigue and fracture limit state for details

Fatigue requirements for the webs

Constructibility

Member proportions of flexural components

$$0.1 \leq \frac{I_{yc}}{I_y} \leq 0.9 \quad (\text{A.1})$$

where  $I_y$  is the moment of inertia of the steel section about the vertical axis in the plane of the web ( $\text{IN}^4$ ) and  $I_{yc}$  is the moment of inertia of the compression flange about the vertical axis in the plane of the web ( $\text{IN}^4$ ).

Elastic analysis or Inelastic Analysis [A6.10.2.2] Elastic analysis will be performed. The span is simply supported; thus moment redistribution is not used.

Homogeneous or Hybrid [A6.10.5.4] Rolled beams are homogeneous (flanges and the web are made of the same material). For homogeneous sections, the hybrid factor,  $R_h$  shall be taken as 1.0.

#### **A.4. Design of a Conventionally Reinforced Concrete Deck**

See example of deck design in Appendix B.

#### **A.5. Selection of Resistance Factors**

1. Strength Limit State	$\phi$	[A6.5.4.2]
Flexure	1.00	
Shear	1.00	
2. Other Limit States	1.00	[A1.3.2.1]

### A.6. Selection of Load Modifiers

		<u>Strength</u>	<u>ServiceFatigue</u>	
1. Ductility, $\eta_D$	[A1.3.3]	1.0	1.0	1.0
2. Redundancy, $\eta_R$	[A1.3.4]	1.0	1.0	1.0
3. Importance, $\eta_I$	[A1.3.2.1]	1.0	N/A	N/A
$\eta = \eta_D \eta_R \eta_I$	[A1.3.2.1]	1.0	1.0	1.0

### A.7. Selection of Applicable Load Combinations

Strength I Limit State (detailed in this example)

$$U = \eta[1.25DC + 1.50DW + 1.75(LL + IM)] \quad (A.2)$$

Service I Limit State

$$U = 1.0(DC + DW) + 1.0(LL + IM) \quad (A.3)$$

Fatigue and Fracture limit State

$$U = 0.75(LL + IM): \text{LL calculated for truck with rear axle spacing of 30 FT} \quad (A.4)$$

(A3.6.1.4.1)

### A.8. Calculation of Live Load Force Effects [A3.6.1.1.1]

Select Number of Lanes [A3.6.1.1.1]

$$N_L = INT\left(\frac{w}{12}\right) = INT\left(\frac{34}{12}\right) = 2 \quad (A.5)$$

Multiple Presence factor: [A3.6.1.1.2]

<u>Nb of loaded Lanes</u>	<u>m</u>
1	1.20
2	1.00
3	0.85
>3	0.65

Dynamic Load Allowance: [A3.6.2.1]

<u>Components</u>	<u>IM(%)</u>
Deck joints	75
Fatigue	15
All other	33
Not applied to the design lane load	

Distribution Factors: Cross section type (a), S=8 FT, L=60 FT

For preliminary design, the entire term containing  $K_g$  in the approximate formulas can be taken as 1.0. Although the  $K_g$  term varies slightly along the span, the value at the maximum positive moment section is used to compute the distribution factor for use along the entire span. Other options are to compute  $K_g$  based on the average or a weighted average of the properties along the span, or to use the actual values of  $K_g$  at each change of section to compute a variable distribution along the span. However, the distribution factor is typically not overly sensitive to the value of  $K_g$  that is assumed.

The girders satisfy the limitations defining the range of applicability of the approximate formulas; these limitations are specified in the individual tables containing the formulas. For example, the number of girders in the cross section is greater than or equal to four, the transverse girder spacing is greater than or equal to 3.5 FT and less than

or equal to 16 ft and the span length is greater than or equal to 20 FT and less than or equal to 240 FT. The limitations on the slab thickness are also satisfied. The computation of the factors (in units of lane) is illustrated below

### A.8.1. Interior Beams

The live load distribution factors for an interior girder for checking the strength limit state are determined using the approximate formulas given in the tables. Multiple presence factors (Article 3.6.1.1.2) are not explicit because these factors were included in the derivation of these formulas. Separate factors are given to compute the bending moment and shear.

Distribution factors for moment [Table A4.6.2.2.2b-1]

$$\begin{aligned} \text{One design lane loaded} \quad & 0.06 + \left(\frac{S}{14}\right)^{0.4} \left(\frac{S}{L}\right)^{0.3} \left(\frac{K_g}{12.0Lt_s^3}\right)^{0.1} & (A.6) \\ & 0.06 + \left(\frac{8}{14}\right)^{0.4} \left(\frac{8}{60}\right)^{0.3} (1.0)^{0.1} = 0.497 \end{aligned}$$

$$\begin{aligned} \text{Two design lanes loaded} \quad & 0.075 + \left(\frac{S}{9.5}\right)^{0.6} \left(\frac{S}{L}\right)^{0.2} \left(\frac{K_g}{12.0Lt_s^3}\right)^{0.1} & (A.7) \\ & 0.075 + \left(\frac{8}{9.5}\right)^{0.6} \left(\frac{8}{60}\right)^{0.2} (1.0)^{0.1} = 0.68 \text{ (governs)} \end{aligned}$$

Distribution factor for shear [Table A4.6.2.2.3a-1]

$$\begin{aligned} \text{One design lane loaded} \quad & 0.36 + \left(\frac{S}{25}\right) & (A.8) \\ & 0.36 + \left(\frac{8}{25}\right) = 0.68 \end{aligned}$$

$$\begin{aligned}
 \text{Two design lanes loaded} \quad & 0.2 + \left(\frac{S}{12}\right) - \left(\frac{S}{35}\right)^2 & (A.9) \\
 & 0.2 + \left(\frac{8}{12}\right) - \left(\frac{8}{35}\right)^2 = 0.81 \quad (\text{governs})
 \end{aligned}$$

### A.8.2. Exterior Beams: Lever Rule

The live-load distribution factors for an exterior girder for checking the strength limit state are determined as the governing factors calculated using the lever rule assuming that the entire cross section deflects and rotates as a rigid body. The method is illustrated below. As stated in Article 3.6.1.1.2, multiple presence factors are applicable when the lever rule is used. Separate factors are computed for bending moment and shear.

The lever rule involves the use of static to determine the lateral distribution of live load to the exterior girder. Wheel-load reaction at the exterior girder is calculated assuming the concrete deck is hinged at the interior girder (Figure A.4). A wheel cannot be closer than 2 FT from the curb (Article 3.6.1.3.1). For the specified transverse wheel spacing of 6 FT, the wheel-load distribution to the exterior girder is computed as:

Distribution factor for moment [Table A4.6.2.2.2d-1]

$$R = \frac{P}{2} \left( \frac{1+7}{8} \right) = 0.5P \quad (A.10)$$

$$\text{One design lane loaded} \quad 1.2 \times 0.5 = 0.6 \quad (\text{governs})$$

Two or more design lanes loaded      Modify interior-girder factor by  $e$  (Table 4.6.2.2.2d-1)

$$d_e = 1 \text{ FT}$$

The factor  $e$  is computed using the distance  $d_e$ , where  $d_e$  is the distance from the exterior girder to the edge of the curb or traffic barrier (less than or equal to 5.5 FT).  $d_e$  is negative if the girder web is outboard of the curb or traffic barrier.

$$e = 0.77 + \frac{1}{9.1} = 0.88$$

$$0.88 \times 0.68 = 0.598$$



Distribution factor of the  
corresponding interior girder

Distribution factor for shear [Table A4.6.2.2.3b-1]

$$R = \frac{P}{2} \left( \frac{1+7}{8} \right) = 0.5P \quad (\text{A.11})$$

One design lane loaded       $1.2 \times 0.5 = 0.6$  *governs*

Two or more design lanes Loaded      Modify interior-girder factor by  $e$  (Table 4.6.2.2.3b-1)

$$d_e = 1 \text{ ft}$$

$$e = 0.6 + \frac{1}{10} = 0.7$$

$$0.7 \times 0.81 = 0.57$$



Distribution factor of the  
corresponding interior girder

## A.9. Distributed Live Load Moments

### A.9.1. Moment due to Truck and Lane Load

The live load is a superposition of the old HS20 truck and of the old uniformly distributed lane loading (without the concentrated load) as shown in Figure A.5.

Moments and shears can be calculated separately for the truck and lane load and added.

The impact coefficient of 33% is applied only to the truck loading. (Equations developed by Naaman et al.).

$$\alpha = \frac{(32-8) \times 14}{2 \times (32+32+8) + 0.64 \times L} = \frac{336}{144 + 0.64 \times 60} = 1.842 \quad (\text{A.12})$$

$$M_{truck} = P \left( \frac{9}{8} L + \frac{\alpha}{L} (21 - 4.5\alpha) - 17.5 \right)$$

$$M_{truck} = 16 \left( \frac{9}{8} \times 60 + \frac{1.842}{60} (21 - 4.5 \times 1.842) - 17.5 \right) = 806.2 \text{ KIP-FT, governs}$$

$$M_{lane} = 0.08 (L^2 - 4\alpha^2) = 286.9 \text{ KIP-FT}$$

P = 16 kips (wheel load)

### A.9.2. Moment Due to a Tandem and Lane Load

The design Tandem Loading is similar as in the AASHTO Standard, with 25 KIPS per axle (as shown Figure A.6) compared to 24 KIPS per axle in AASHTO Standard. Dynamic load allowance applies to tandem loading.

$$\beta = \frac{4 \times 25}{4 \times 25 + 0.64 \times L} = \frac{100}{100 + 0.64 \times 60} = 0.723$$

$$M_{\text{tan}} = 50 \left( \frac{L}{4} + \frac{\beta}{L} (2 - \beta) - 1 \right) \quad (\text{A.13})$$

$$M_{\text{tan}} = 50 \left( \frac{60}{4} + \frac{0.723}{60} (2 - 0.723) - 1 \right) = 700.77 \text{ KIP} - \text{FT},$$

$$M_{\text{lane}} = 0.08 (L^2 - 4\beta^2) = 287.83 \text{ KIP} - \text{FT}$$

### A.9.3. Moment for an Interior Beam

$$M_{LL+IM} = 0.68 (806.2 \times 1.33 + 286.9) = 921.29 \text{ kip} - \text{ft} \quad (\text{A.14})$$

### A.9.4. Moment for an Exterior Beam

$$M_{LL+IM} = 0.6 (806.2 \times 1.33 + 286.9) = 815.5 \text{ KIP} - \text{FT} \quad (\text{A.15})$$

## A.10. Distributed Shear Due to Live Load.

### A.10.1. Shear Due to a Design Truck

The placement of the truck for maximum shear is shown in Figure A.7

$$V_{\text{truck}} = P \left( 4.5 - \frac{42}{L} \right) \quad (\text{A.16})$$

$$V_{\text{truck}} = 16 \left( 4.5 - \frac{42}{60} \right) = 60.8 \text{ KIPS} \text{ governs}$$

### A.10.2. Shear Due to a Tandem

The placement of the tandem for maximum shear is shown in Figure A.8

$$V_{\text{tan}} = 50 \left( 1 - \frac{2}{L} \right)$$

$$V_{\text{tan}} = 50 \left( 1 - \frac{2}{60} \right) = 48.33 \text{ KIPS} \quad (\text{A.17})$$

### A.10.3. Shear Due to a Lane Load

Lane loading is shown in Figure A.9

$$V_{\text{lane}} = \frac{0.64 \times L}{2}$$

$$V_{\text{lane}} = \frac{0.64 \times 60}{2} = 19.2 \text{ KIPS} \quad (\text{A.18})$$

### A.10.4. Shear For an Interior Beam

$$V_{LL+IM} = 0.81(60.8 \times 1.33 + 19.2) = 81.49 \text{ KIPS} \quad (\text{A.19})$$

### A.10.5. Shear for an Exterior Beam

$$V_{LL+IM} = 0.6(60.8 \times 1.33 + 19.2) = 60.25 \text{ KIPS} \quad (\text{A.20})$$

## A.11. Calculate the Effect of Other Loads

As specified in the AASHTO Table 3.4.1-2, the Dead Load includes the weight of all components of the structure and utility loads.

$DC_1$ =Dead load of structural components and their attachments, acting on the non-composite section

DW=Future wearing surface

DC<sub>2</sub>=barriers that have a cross sectional area of 3.2 FT<sup>2</sup> (acting on the composite section)

Let's assume a W27 X 102 steel beam.

### A.11.1. Interior Girders

$$\begin{array}{rclcl}
 \text{DC}_1: & \text{Deck Slab} & (150)(8)(9/12) & = & 900 \text{ lb/ft} \\
 & \text{Girder} & & = & 102 \text{ lb/ft} \\
 & & & & \hline
 & & & = & 1002 \text{ lb/ft}
 \end{array}$$

$$\text{DW: } 3 \text{ IN concrete wearing pavement} \quad (125)(3/12)(8) = 250 \text{ lb/ft}$$

$$\text{DC}_2: \text{ Barrier, per girder} \quad (2/5)(150)(3.2) = 192 \text{ lb/ft}$$

The unfactored moments and shears at critical section for an interior girder is summarized in Table A.1.

### A.11.2. Exterior Girders

$$\begin{array}{rclcl}
 \text{DC}_1: & \text{Deck Slab} & (150)(4 + 3.75)(9/12) & = & 872 \text{ lb/ft} \\
 & \text{Girder} & & = & 102 \text{ lb/ft} \\
 & & & & \hline
 & & & = & 974 \text{ lb/ft}
 \end{array}$$

$$\text{DW: } 3 \text{ IN concrete wearing} \quad (125)(3/12)(4+3.75-1.75) = 187.5 \text{ lb/ft}$$

$$DC_2: \text{Barrier, one sixth share } (2/5)(150)(3.2) = 192 \text{ lb/ft}$$

The unfactored moments and shears at critical section for an interior girder is summarized in Table A.2.

## A.12. Design of the Required Sections

### A.12.1. Strength Limit State

Interior beam – factored shear and moment

$$U = \eta[1.25DC_1 + 1.5DW + 1.25DC_2 + 1.75(LL + IM)]$$

$$M_U = 1[1.25(450.9) + 1.5(112.5) + 1.25(86.4) + 1.75(921.29)] = 2452.64 \text{ KIP-FT (A.21)}$$

$$V_u = 1[1.25(30.06) + 1.5(7.5) + 1.25(5.76) + 1.75(81.49)] = 198.64 \text{ KIPS}$$

Exterior beam – factored shear and moment

$$U = \eta[1.25DC_1 + 1.5DW + 1.25DC_2 + 1.75(LL + IM)]$$

$$M_U = 1[1.25(438.3) + 1.5(84.375) + 1.25(86.4) + 1.75(815.5)] = 2209.56 \text{ KIP-FT (A.22)}$$

$$V_u = 1[1.25(29.22) + 1.5(5.625) + 1.25(5.76) + 1.75(60.25)] = 157.6 \text{ KIPS}$$

Consider loading and concrete placement sequence [A6.10.5.1.1.a]

- Case 1: Weight of girder and slab ( $DC_1$ ) supported by steel girder alone.
- Case 2: Superimposed dead load (wearing surface, curbs and railing)( $DW$  and  $DC_2$ ) supported by long term composite section.
- Case 3: Live load plus dynamic load ( $LL+IM$ ) supported by short term composite section.

Determine effective flange width [A4.6.2.6] for interior girders. The effective flange width is the least of:

- a) One quarter of the average span length
- b) 12 times the average thickness of the slab, plus the greater of the web thickness or one-half the width of the top flange of the girder
- c) Average spacing of adjacent girders

Assume the girder top flange is 8 IN wide

$$b_i = \min \begin{cases} (60)(12/4) = 180 \text{ IN} \\ (12)(9) + (8/2) = 112 \text{ IN} \\ (8)(12) = 96 \text{ IN} \end{cases} \quad (\text{A.23})$$

Therefore  $b_i = 96$  IN

For an exterior girder, the effective flange width is one half the effective flange width of the adjacent interior girder plus the least of:

- a) One-eighth of the effective span length
- b) 6 times the average thickness of the slab, plus the greater of one half of the web thickness or one quarter of the width of the top flange of the girder
- c) The width of the overhang

$$b_e = \frac{b_i}{2} + \min \begin{cases} (60)(12/8) = 90 \text{ IN} \\ (6)(9) + (8/2) = 58 \text{ IN} \\ (3.75)(12) = 45 \text{ IN} \end{cases} \quad (\text{A.24})$$

Therefore  $b_e = \frac{b_i}{2} + 45 = 48 + 45 = 93$  IN

Modular ratio

For  $f'_c = 4000$  PSI ,  $n=8$

Steel section at midspan

Try W27 x 102. Properties of W24 x 68 are taken from AISC Manual. The steel section is shown in Figure A.10.

$$t_f = 0.83 \text{ IN}$$

$$t_w = 0.515 \text{ IN}$$

$$I_{NA} = 3620 \text{ IN}^4$$

Figure 11 shows the composite section with a net slab thickness of 9 IN, and an effective width of 96 IN. The calculations of composite section properties are summarized in Table A.3.

$$\bar{y} = \frac{Ay}{A} = \frac{1162.35}{138} = 8.42 \text{ IN} \quad (\text{A.25})$$

$$I_{NA} = 21784.31 - (1162.35 \times 8.42) = 11997.32 \text{ IN}^4$$

**A.12.2. Plastic Moment Capacity**

Determine the plastic-moment capacity,  $M_p$ , of the composite section. The reinforcement of the deck according the traditional design is given as follows (see appendix B):

- number of bars in the top of slab within the effective width = 5 #4 (0.2 IN<sup>2</sup>)
- number of bars in the bottom of slab within effective width = 12 #4 (0.2 IN<sup>2</sup>)

Calculate  $M_p$  using the equations provided in Appendix A to Section 6 of the specification [Appendix A6.1]. See Figure A.12.

Use case V; neutral axis is in the slab above bottom bars ( $c < 6$  IN)

$$\begin{aligned}
 P_{rt} &= F_{yr} A_{rt} = (60)(5)(0.2) = 60 \text{ KIPS} \\
 P_s &= 0.85 f'_c b_{eff} t_s = (0.85)(4)(96)(9) = 2937.6 \text{ KIPS} \\
 P_{rb} &= F_{yr} A_{rb} = (60)(12)(0.2) = 144 \text{ KIPS} \\
 P_c &= A_{tf} F_y = (0.83)(10.015)(50) = 415.62 \text{ KIPS} \\
 P_w &= A_w F_y = (0.515)(25.43)(50) = 654.82 \text{ KIPS} \\
 P_t &= A_{bf} F_y = (0.83)(10.015)(50) = 415.62 \text{ KIPS}
 \end{aligned} \tag{A.26}$$

Calculate  $M_p$  using the equations provided in Appendix A to Section 6 of the specification [Article A6.1]:

We use Case V since

$$\begin{aligned}
 P_t + P_w + P_c + P_{rb} &\geq \left( \frac{C_{rt}}{t_s} \right) P_s + P_{rt} \\
 415.62 + 654.82 + 415.62 + 144 &= 1630.06 \text{ KIPS} \\
 \frac{2.875}{9} \times 2937.6 + 60 &= 998.4 \text{ KIPS } \textit{ok}
 \end{aligned} \tag{A.27}$$

$$\begin{aligned}
 \bar{y} &= (t_s) \left[ \frac{P_{rb} + P_c + P_w + P_t - P_{rt}}{P_s} \right] = 4.85 \text{ IN} < 6 \text{ IN} \\
 M_p &= \left( \frac{\bar{y}^2 P_s}{2 t_s} \right) + \left[ P_{rt} d_{rt} + P_{rb} d_{rb} + T_{cp} d_{cp} + P_c d_c + P_w d_w + P_t d_t \right] \\
 M_p &= \left( \frac{4.85^2 \times 2937.6}{2 \times 9} \right) + \left[ 60 \times 1.98 + 144 \times 2.27 + 415.62 \times 4.56 + \right. \\
 &\quad \left. 654.82 \times 17.69 + 415.62 \times 30.82 \right] \\
 M_p &= 2568.96 \text{ KIP-FT}
 \end{aligned} \tag{A.28}$$

$$\phi M_p = 1.0(2568.96) = 2568.96 \text{ KIP-FT} > M_u = 2452.64 \text{ KIP-FT, } \textit{ok}$$

**A.12.3. Member Proportions [A6.10.2.1]**

$$\begin{aligned}
 0.1 &\leq \frac{I_{yc}}{I_y} \leq 0.9 \\
 I_y &= 139 \text{ IN}^4 \\
 I_{yc} &= \frac{1}{12} (0.83)(10.015)^3 = 69.48 \text{ IN}^4 \\
 0.1 &\leq \frac{69.48}{139} = 0.499 < 0.9 \text{ ok}
 \end{aligned}
 \tag{A.29}$$

where  $I_{yc}$  is the moment of inertia of the compression flange about the vertical axis.

**A.12.4. Compactness of the Section**

Web Slenderness: because the neutral axis is not in the web,  $D_{cp}$  is taken equal to 0, the web slenderness requirement is satisfied [A6.10.5.1.4b], the section is classified as a compact section and  $M_n = M_p$ .

Compression flange slenderness [A6.10.5.2.2c]: No requirement at strength limit state for compact I-sections in positive flexure.

Compression flange bracing: No requirement at strength limit state for compact composite I-sections in positive flexure.

Calculate flexural resistance [A6.10.5.2.2a]:

For simple spans, the nominal flexural resistance is taken as

$$\begin{aligned}
 M_n &= M_p = 2568.96 \text{ KIP-FT} \\
 M_r &= \phi M_n = 1.0 (2754.9) \\
 M_r &= 2568.96 \text{ KIP-FT} > 2452.64 \text{ KIP-FT} \text{ ok}
 \end{aligned}
 \tag{A.30}$$

Check positive flexure ductility:

The section must satisfy

$$D_p \leq \frac{d + t_s + t_h}{7.5} \quad (\text{A.31})$$

where:

$D_p$  = distance from the top of the slab to the neutral axis at the plastic moment =  
4.85 IN

$d$  = depth of the steel section = 27.09 IN

$t_s$  = thickness of the concrete slab = 9 IN

$t_h$  = thickness of the concrete haunch = 0 IN

$$\frac{d + t_s + t_h}{7.5} = \frac{27.09 + 9}{7.5} = 4.94 \text{ IN} > D_p = 4.85 \text{ IN} \text{ ok}$$

All the requirements for flexure have been satisfied.

### A.13. Shear Design

#### A.13.1. Beam with Unstiffened Web [A6.10.7.2]

Figure A.17 shows a flow chart for the calculation of shear resistance of unstiffened webs.

$$\begin{aligned} V_r &= \phi_v V_n = 1.0 V_n \\ \frac{D}{t_w} &= \frac{d - 2t_f}{t_w} = \frac{27.09 - 2 \times 0.83}{0.515} = 49.38 \\ 2.46 \sqrt{\frac{E}{F_{yw}}} &= 2.46 \sqrt{\frac{29000}{50}} = 59.24 > 49.38 \\ \frac{D}{t_w} &\leq 2.46 \sqrt{\frac{E}{F_{yw}}} \end{aligned} \quad (\text{A.32})$$

therefore,

$$\begin{aligned} V_n &= 0.58F_{yw}Dt_w = 0.58(50)(25.43)(0.515) = 379.79 \text{ KIP} \\ V_r &= 1.0V_n = 379.79 \text{ KIP} > V_u = 198.64 \text{ ok} \end{aligned} \quad (\text{A.33})$$

### A.13.2. Bearing Stiffener Design

$$0.75\phi_b V_n = 0.75(1.0)(379.79) = 284.85 \text{ kip} > V_u = 198.64 \text{ KIP} \quad (\text{A.34})$$

The bearing stiffeners are not required.

### A.14. Constructability

General proportions: ok

Flexure: the section must satisfy compression flange slenderness, web slenderness and compression flange bracing requirements: ok

### A.15. Dimension and Detail Requirements

Material thickness: Bracing and cross frames shall not be less than 0.3 in in thickness, web thickness of rolled beams shall not be less than 0.28 in.

Optimal deflection control: allowable service load (recommended)

$$\text{Deflection} \leq \frac{1}{800} \text{span} = \frac{60 \times 12}{800} = 0.9 \text{ IN} \quad (\text{A.35})$$

From [A3.6.1.3.2] deflection is taken as the larger of

- (a) that resulting from the design truck alone
- (b) that resulting from 25% of the design truck taken together with the design lane load

The distribution factor for deflection can be taken as the number of lanes divided by the number of beams [C2.5.2.6.2], because all design lanes should be loaded, and all supporting components should be assumed to deflect equally.

$$DF = \frac{nb \text{ of lanes}}{nb \text{ of girders}} = \frac{2}{5} = 0.4 \quad (\text{A.36})$$

#### A.15.1. Deflection: Design Truck Alone

$$\begin{aligned} P_1 = P_2 &= 0.4(32)(1.33) = 17.024 \text{ KIP} \\ P_3 &= 0.4(8)(1.33) = 4.256 \text{ KIP} \end{aligned} \quad (\text{A.37})$$

The maximum deflection (at the center) of a simply supported span due to a concentrated load at the center of the span, is equal to

$$\Delta_{cl} = \frac{PL^3}{48EI} \quad (\text{A.38})$$

The deflection at any point,  $\Delta_x$ , due to point load P as shown in Figure A.13 can be found from AISC Manual.

$$\Delta_x = \frac{Pbx}{6EIL}(L^2 - b^2 - x^2), \quad x < a. \quad (\text{A.39})$$

The position of the truck is shown in Figure A.14

$$\begin{aligned}\Delta_{tr} &= \Delta_{p1} + \Delta_{p2} + \Delta_{p3} \\ \Delta_{tr} &= \frac{(P1 + P3)(16 \times 12)(60 \times 12 / 2)}{6(29000)(11997.32)(60 \times 12)} \times ((60 \times 12)^2 - (16 \times 12)^2 - (60 \times 12 / 2)^2) \quad (\text{A.40}) \\ &+ \frac{P2(60 \times 12)^3}{48(29000)(11997.32)} = 0.725 \text{ IN}\end{aligned}$$

### A.15.2. Deflection: 25% of the Design Truck Plus the Design Lane Load

The deflection due to the lane load can be found from:

$$\Delta_{\max} = \frac{5wL^4}{384EI} = \frac{5 \times 0.4 \times 0.64 / 12 \times (60 \times 12)^4}{384(29000)(11997.32)} = 0.215 \text{ IN} \quad (\text{A.41})$$

$0.25(0.725) + 0.215 = 0.39 \text{ IN}$ , therefore truck deflection = 0.725 IN controls

$0.725 \text{ IN} < 0.9 \text{ IN}$  OK.

Table A.1 Unfactored moments and shears for an interior girder

Load type	W (LB/FT)	Moment (KIP-FT)	Shear (KIP)
DC <sub>1</sub>	1002	450.9	30.06
DW	250	112.5	7.5
DC <sub>2</sub>	192	86.4	5.76
LL+IM	N/A	921.29	81.49

Table A.2 Unfactored moments and shears for an exterior girder

Load type	W (LB/FT)	Moment (KIP-FT)	Shear (KIP)
DC <sub>1</sub>	974	438.3	29.22
DW	187.5	84.375	5.625
DC <sub>2</sub>	192	86.4	5.76
LL+IM	N/A	815.5	60.25

Table A.3 Composite section properties

Component	A	y	Ay	Ay <sup>2</sup>	<i>I</i> <sub>o</sub>	I
concrete	108	4.5	486	2187	729	2916
steel	30	22.545	676.35	15248.31	3620	18868.31
Σ	138		1162.35			21784.31

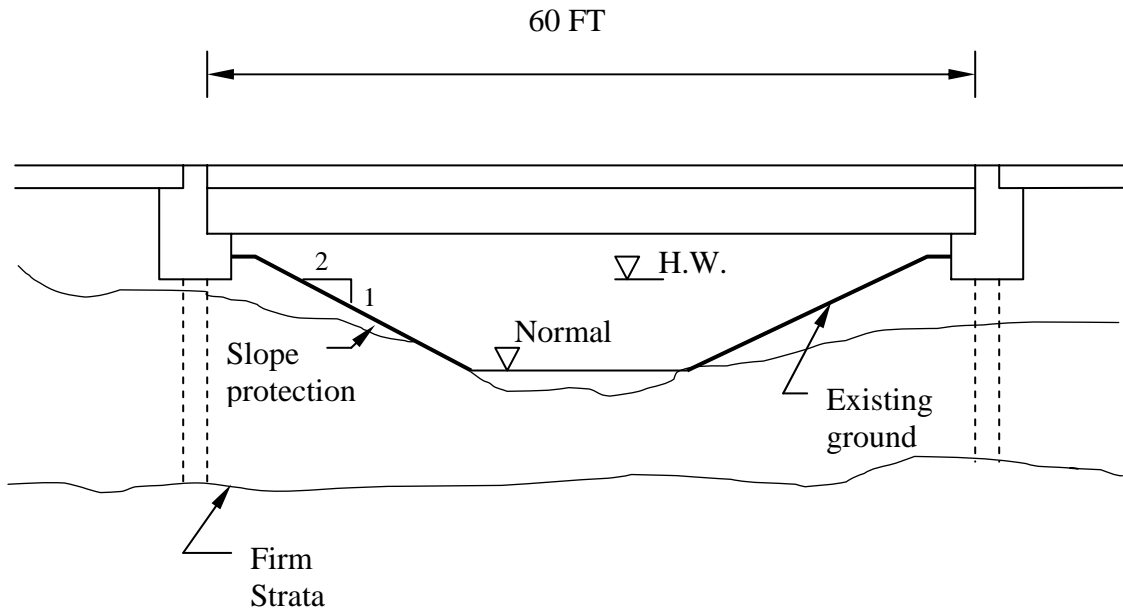


Figure A.1 Elevation of the bridge

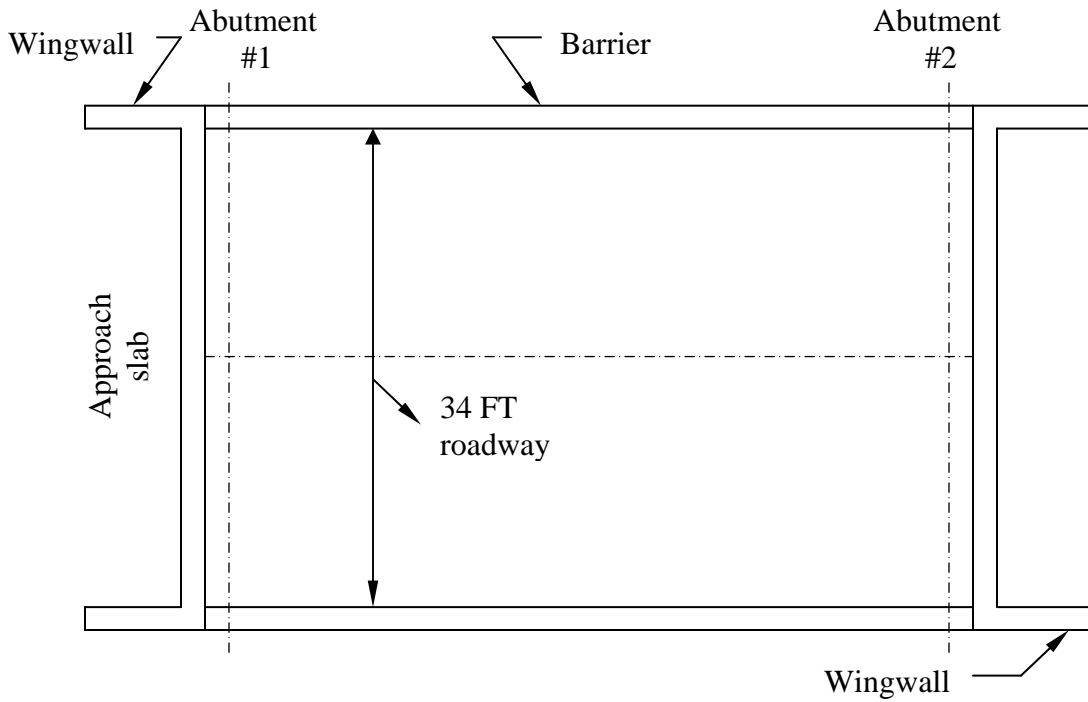


Figure A.2 Plan view of the bridge

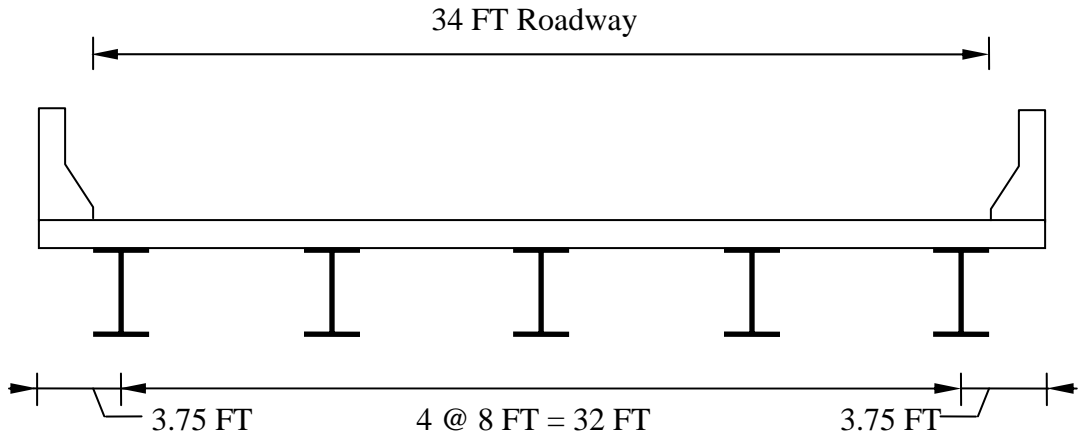


Figure A.3 Cross section of the bridge

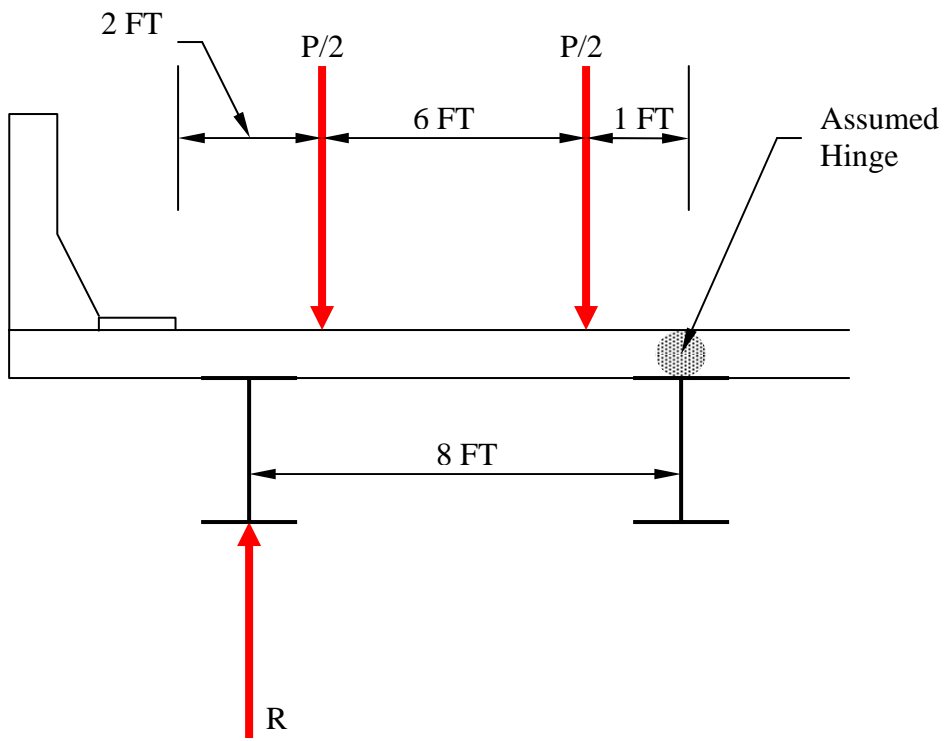


Figure A.4 Lever rule

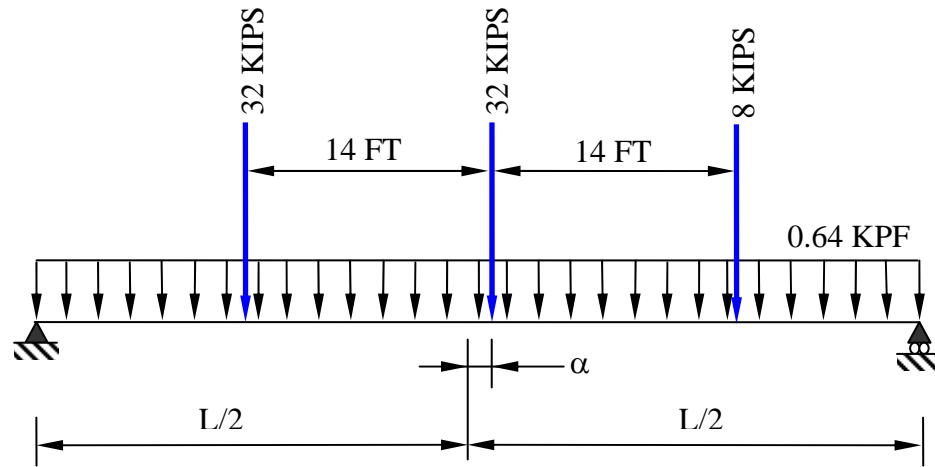


Figure A.5 Truck placement for maximum moment plus lane load

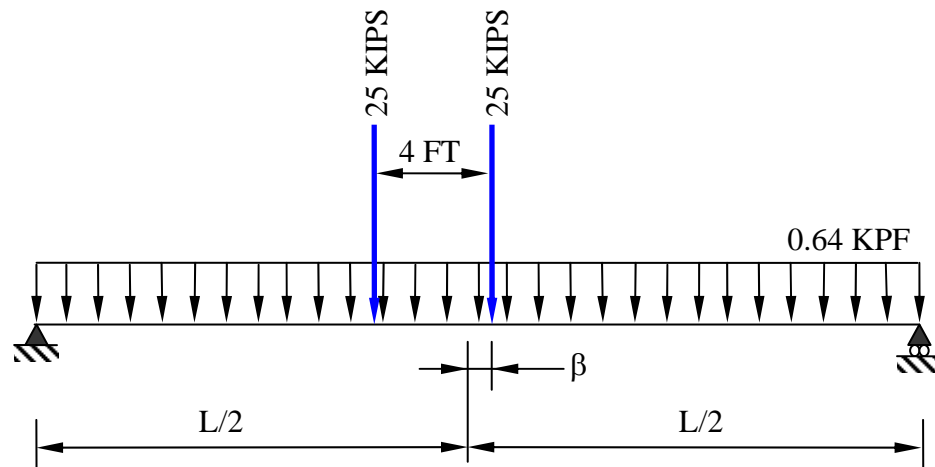


Figure A.6 Tandem placement for maximum moment plus lane load

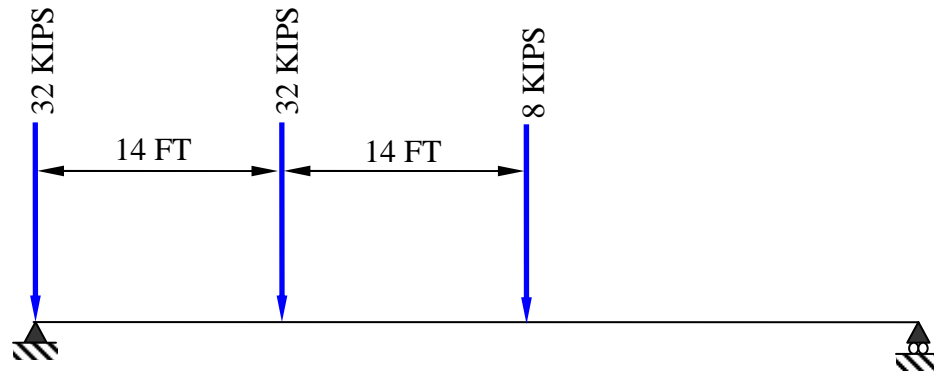


Figure A.7 Truck placement for the maximum shear



Figure A.8 Tandem placement for the maximum shear

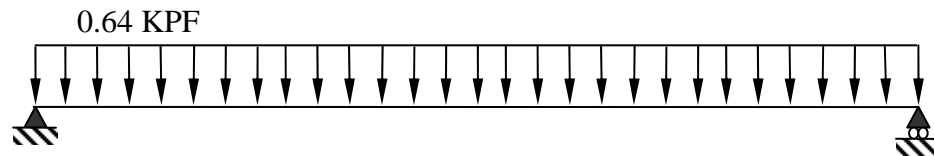


Figure A.9 Lane loading

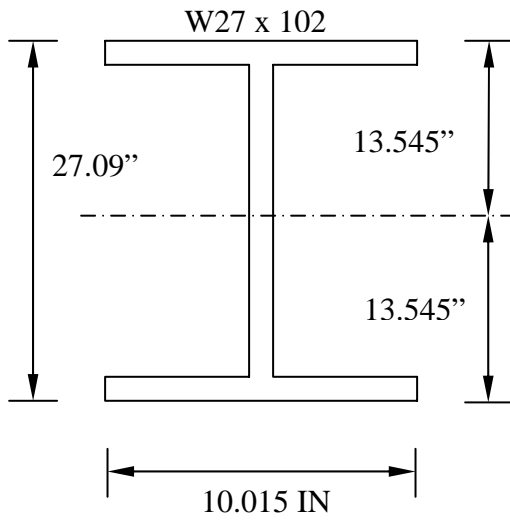


Figure A.10 Steel section at midspan

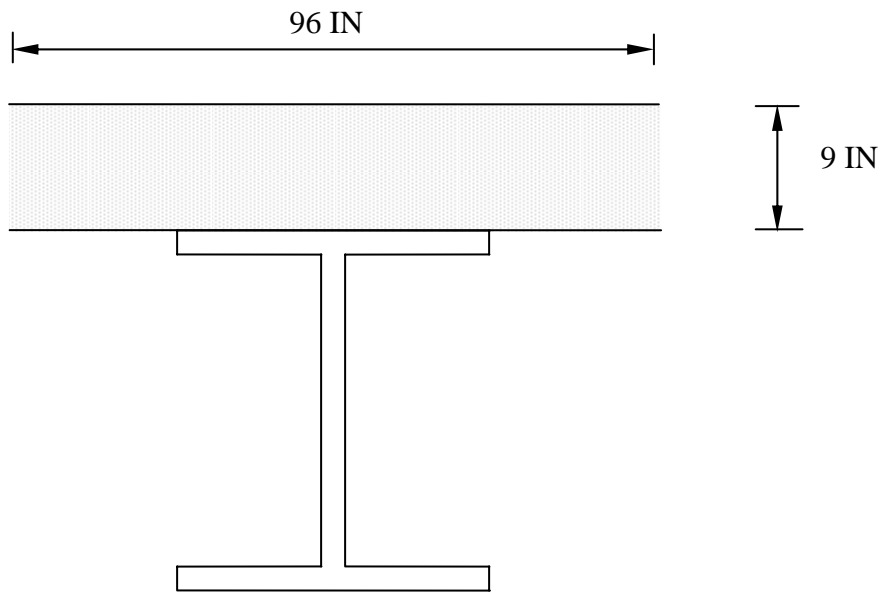


Figure A.11 Composite section at midspan

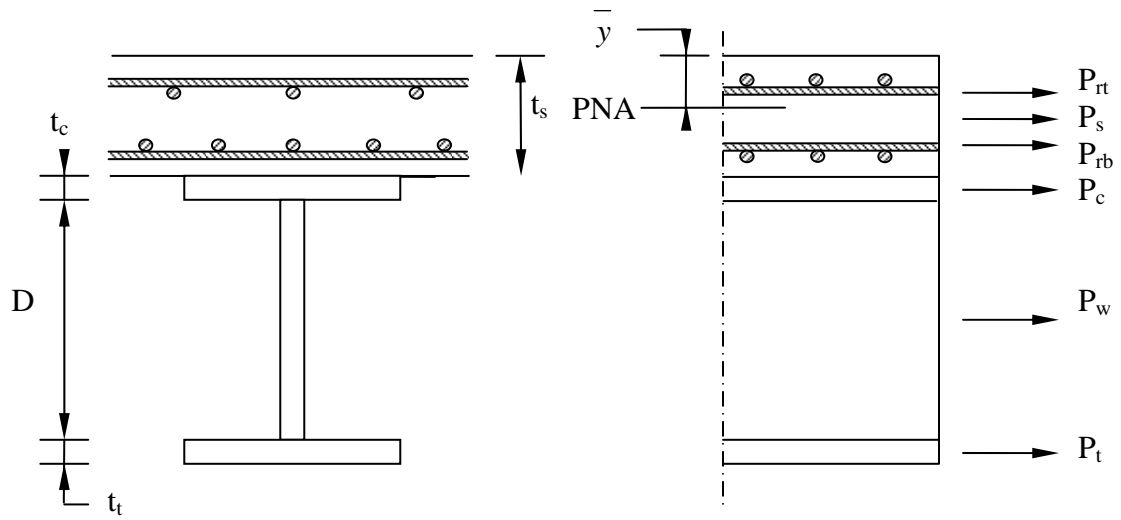
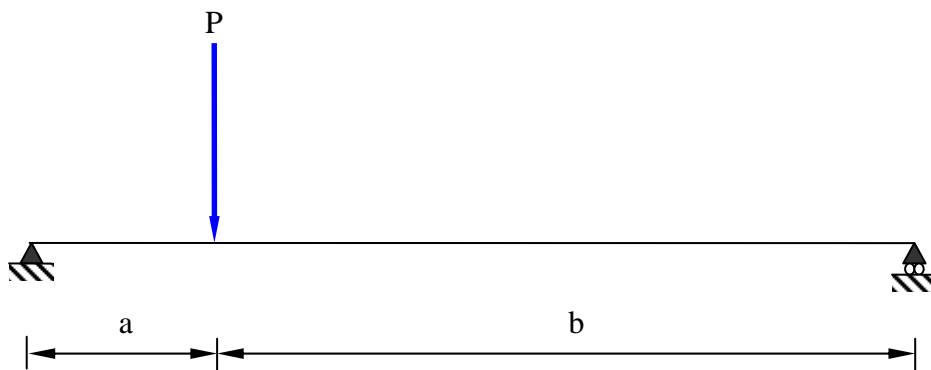


Figure A.12 Computation of plastic moment

Figure A.13 Deflection due to load  $P$

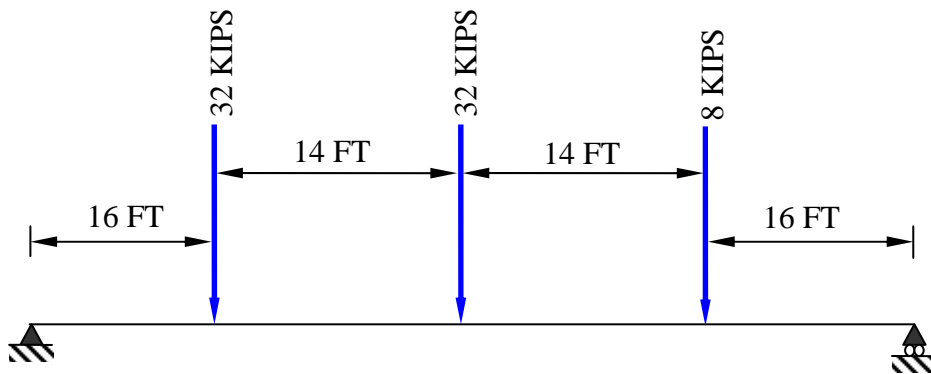


Figure A.14 Truck placement for the maximum deflection

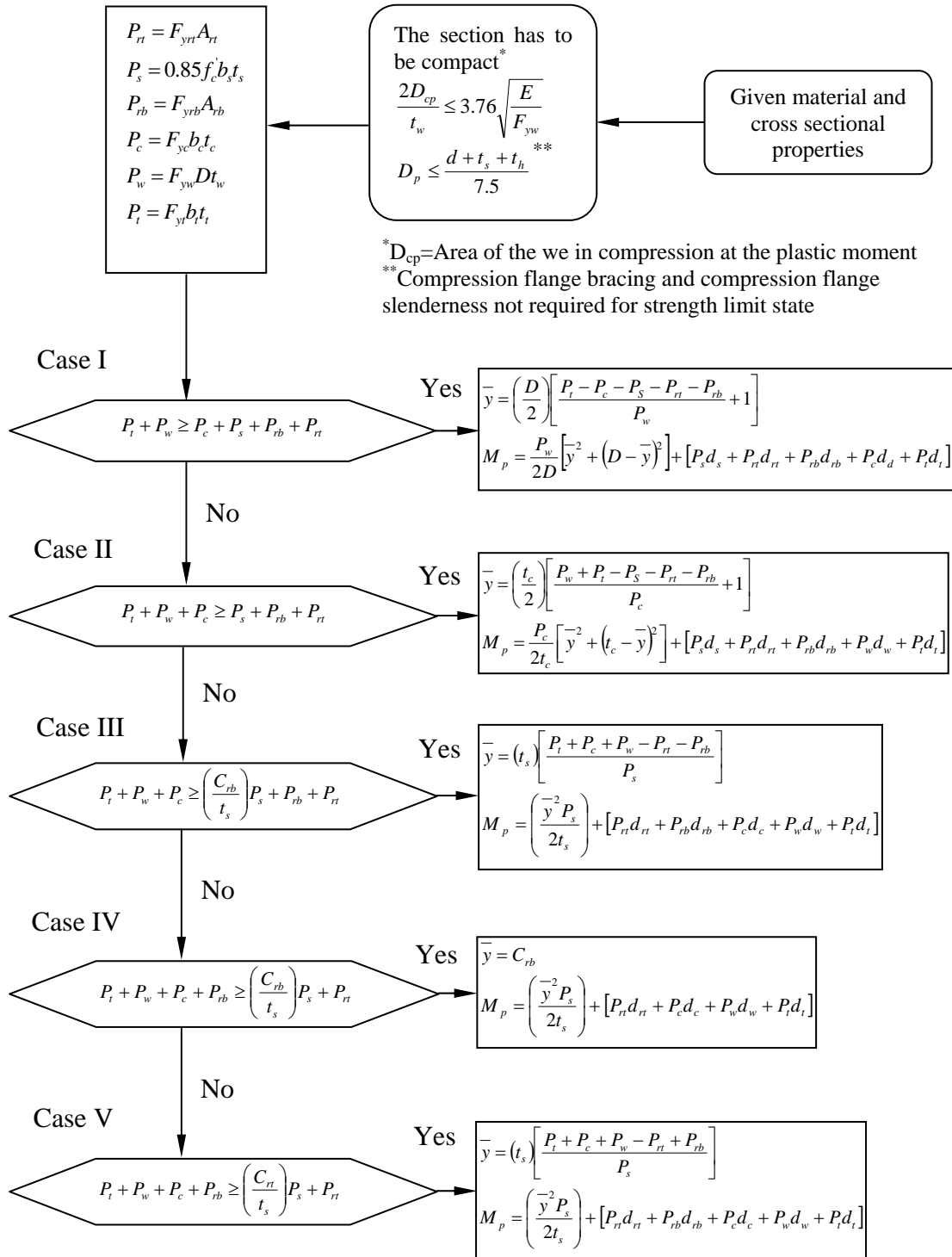


Figure A.15 Flow chart for the plastic moment of compact section for flexural members, computation of  $\bar{y}$  and  $M_p$  for positive bending sections

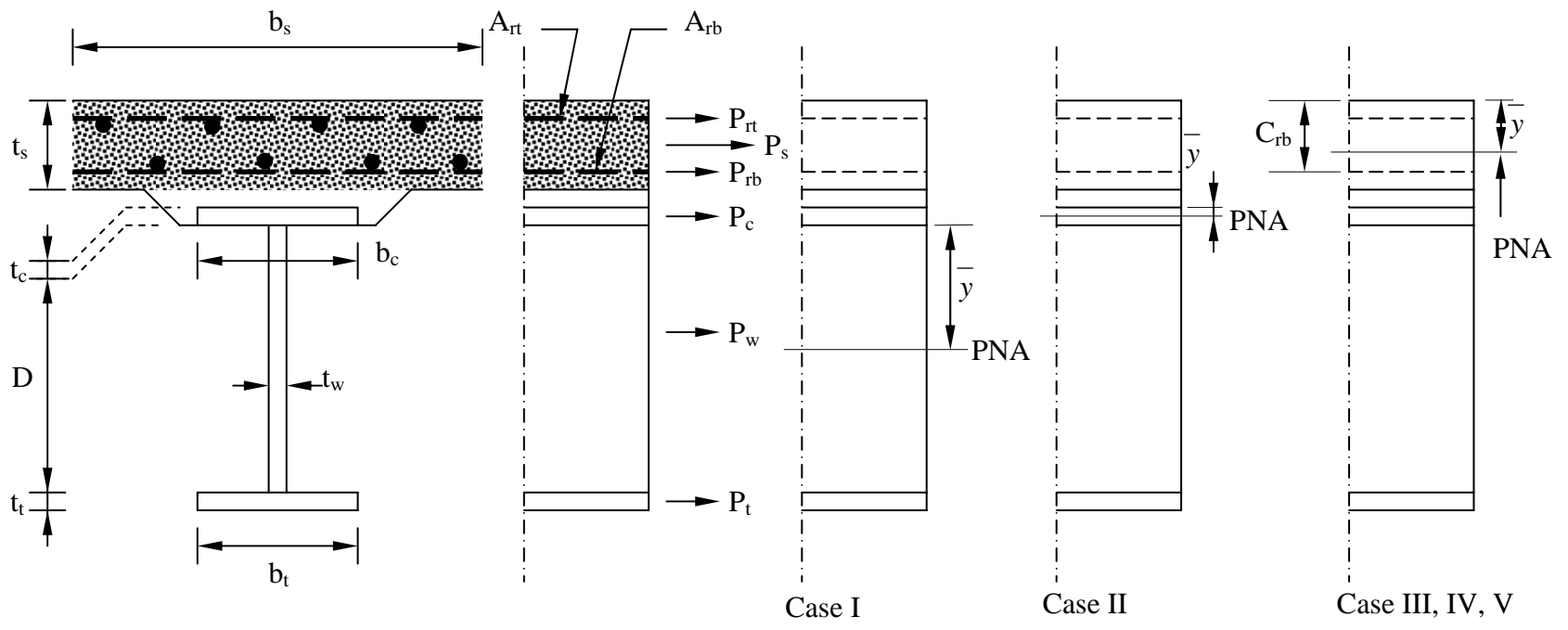
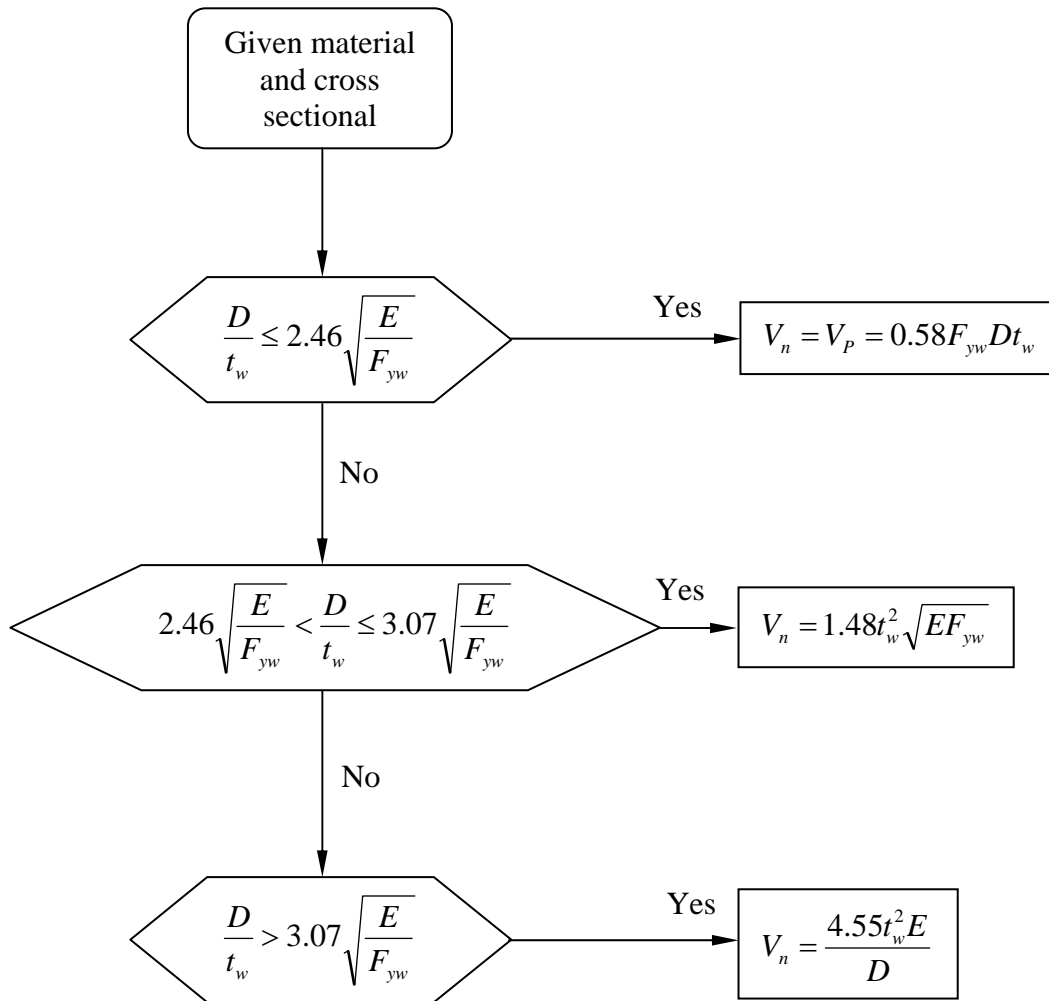


Figure A.16 Position of the neutral axis for the five different cases



where:

$F_{yw}$  = specified minimum yield strength of the web (KSI)

$D$  = web depth (IN)

$t_w$  = Thickness of the web (IN)

Figure A.17 Flow chart for the computation of shear resistance, nominal resistance of unstiffened webs

## APPENDIX B

### EXAMPLE OF DECK SLAB DESIGN

#### B.1. Description

Both design method (traditional and empirical) are used to design the deck slab of the steel-beam bridge whose section is shown in Figure B.1. The live load considered is the HL-93. The steel-beams supporting the deck are spaced at 8 FT on centers. The deck thickness is 9 IN. Allow for a future wearing surface of 3 IN thick bituminous overlay. Use  $f'_c = 4000$  PSI,  $f_y = 60$  KSI.

#### B.2. Traditional Method

##### B.2.1. Deck Thickness

The minimum thickness for concrete deck slab is 7 IN [A9.7.1.1]. Traditional minimum depths of slab are based on the deck span length  $S$  to control deflection to give [Table A2.5.2.6.3-1]

$$h_{\min} = \frac{1.2(S + 10)}{30} = \frac{1.2(96 + 10)}{30} = 4.24 \text{ IN} \quad (\text{B.1})$$

So we use  $h_s = 9$  IN for the structural thickness of the deck.

##### B.2.2. Weight of Components

For 1 FT width of a transverse strip

Barrier (Area = 3.2 FT<sup>2</sup>)

$$P_b = 0.150 \times 3.2 = 0.48 \quad KIPS / FT \quad (B.2)$$

Future wearing surface

$$W_{DW} = 0.125 \times \frac{3}{12} = 0.3125 \quad KIPS / FT^2 \quad (B.3)$$

Slab 9 IN thick

$$W_s = 0.150 \times \frac{9}{12} = 0.1125 \quad KIPS / FT^2 \quad (B.4)$$

Cantilever overhang 10 IN thick

$$0.150 \times \frac{10}{12} = 0.125 \quad KIPS / FT^2 \quad (B.5)$$

### **B.2.3. Bending Moments Force Effects**

An approximate analysis of strips perpendicular to girders is considered acceptable [A9.6.1]. The extreme positive moment in any deck panel between girders shall be taken to apply to all positive moment regions. Similarly, the extreme negative moment over any girder shall be taken to apply to all negative moment regions [A4.6.2.1.1].

The strips shall be treated as continuous beams with span length equal to the center-to-center distance between girders. The girders shall be assumed to be rigid [A4.6.2.1.6].

For ease in applying load factors, the moment will be determined separately for the deck slab, overhang, barrier, future wearing surface, and vehicle live load.

A structural software was used to precisely determine those moments.

#### Deck slab

Placement of the deck slab dead load is shown in Figure B.2

$M_s(+)$  = 0.55 KIPS-FT/FT at 3.2 ft right of the exterior girder

$M_s(-)$  = -0.77 KIPS-FT/FT over the second girder

$R_{1st\ support}$  = 0.35 KIPS/FT

#### Overhang

Placement of the overhang dead load is shown in Figure B.3

$M_o(-)$  = -0.879 KIPS-FT/FT over the exterior girder

$M_o(-)$  = -0.427 KIPS-FT/FT at 3.2 ft right of the exterior girder

$M_o(+)$  = 0.251 KIPS-FT/FT over the second girder

$R_{1st\ support}$  = 0.61 KIPS/FT

#### Barrier

Placement of the barrier dead load is shown Figure B.4

$M_b(-)$  = -1.206 KIPS-FT/FT over the exterior support

$M_b(-)$  = -0.586 KIPS-FT/FT at 3.2 ft right of the exterior girder

$M_b(+)$  = 0.345 KIPS-FT/FT over the second girder

$R_{1st\ support}$  = 0.674 KIPS/FT

#### Future Wearing Surface

Placement of the future wearing surface dead load (curb to curb) in Figure B.5

$M_w(-) = 0$  KIPS-FT/FT over the exterior girder

$M_w(+)$  = 0.15 KIPS-FT/FT at 3.2 ft right of the exterior girder

$M_w(-)$  = -0.21 KIPS-FT/FT over the second girder

$R_{1st\ support} = 0.10$  KIPS/FT

#### **B.2.4. Vehicular Live Load**

When decks are designed using the approximate strip method and the strip are transverse, they shall be designed for the 32 KIPS axle of the design truck [A3.6.1.3.3]. Wheel loads on an axle are assumed to be equal and spaced at 6 FT apart. The design truck shall be positioned transversely to produce maximum force effect such that the center of any wheel load is not closer than 1 FT from the face of the curb for the design of the deck overhang and 2 FT from the edge of the 12 FT wide design lane for the design of all other component. Tire contact area shall be assumed as a rectangle, but when calculating the force effect, wheel loads may be modeled as concentrated loads.

The width of equivalent interior transverse strips (IN) over which the wheel loads can be considered distributed longitudinally in cast in place concrete decks is given as [Table A4.6.2.1.3-1]

Overhang	$45+10x$	
Positive moment	$26+6.6S$	(B.6)
Negative moment	$48+3S$	

Where S is the spacing of supporting components and x the distance from load to point of support, (both in FT).

The number of design lanes NL to be considered across a transverse strip is the integer value of the roadway width divided by 12 ft [A3.6.1.1.1].

For this example

$$N_L = \text{int}\left(\frac{34}{12}\right) = 2 \quad (\text{B.7})$$

The multiple presence factor m is 1.2 for one loaded lane, 1.0 for two loaded lane, and 0.85 for three loaded lanes

#### Overhang Negative Live Load Moment.

Because of the presence of a sidewalk, the live load cannot be put such it would create a negative moment over the first girder, therefore  
 $M_o(-) = 0/4.58 = 0 \text{ KIP-FT/FT}$  over the exterior support.

#### Maximum Positive Live Load Moment

For repeating equal spans, the maximum positive, the maximum positive bending moment occurs near the 0.4 point of the first interior span. In the following figures, the placement of wheel loads is given for one or two loaded lanes. For both cases, the equivalent width of a transverse strip is  $26+6.6(8) = 78.8 \text{ IN} = 6.56 \text{ FT}$

For one lane loaded

$$M(+)= 1.2(23.41)/6.56 = 4.28 \text{ KIPS-FT/FT}$$

$$R_{1\text{st support}} = 1.2(7.32)/6.56 = 1.34 \text{ KIPS/FT}$$

For two lane loaded

$$M(+)=1.0(24.40)/6.56=3.72 \text{ kips-ft/ft}$$

$$R_{1\text{st support}}=1.0(7.59)/6.56=1.16 \text{ kips/ft}$$

Thus the one lane loaded case governs.

#### Maximum Interior Negative Live Load moment

The critical placement of live load for maximum negative moment is at the first interior deck support with one loaded lane ( $m = 1.2$ ) as shown in the following figure.

The equivalent transverse width strip is  $48 + 3(8) = 72 \text{ IN} = 6 \text{ FT}$ .

$$M(-)=1.2(-23.17)/6=-4.63 \text{ KIPS-FT/FT over the first interior support.}$$

Note that the small increase due to a second truck is less than 20% ( $m = 1.00$ ) required to control. Only the one lane case is investigated.

#### **B.2.5. Strength Limit State**

The gravity load combination can be stated as [Table A3.4.1-1]

$$\eta \sum \gamma_i Q_i = \eta (\gamma_p DC + \gamma_p DW + 1.75(LL + IM))$$

where (B.8)

$$\eta = 1$$

The factor for permanent loads  $\gamma_p$  is taken at its maximum value if the force effects are additive and at its minimum value if it subtracts from the dominant force effect [Table A3.4.1-2]. The dead load DW is for the future wearing surface and DC represents all the other dead loads. The dynamic load allowance IM [A3.6.2.1] is 33% of the live load force effect.

#### Positive moment in the first interior span

$$\begin{aligned}
 M(+) &= 1.25(0.55) + 0.9(-0.427 - 0.586) + 1.5(0.15) + 1.75(1.33)(4.28) \\
 &= 9.96 \text{ KIPS} - FT / FT
 \end{aligned}$$

Negative moment over the first interior support

$$\begin{aligned}
 M(-) &= 1.25(-0.77) + 0.9(0.251 + 0.345) + 1.5(-0.21) + 1.75(1.33)(-4.63) \\
 &= -11.51 \text{ KIPS} - FT / FT
 \end{aligned}$$

For selection of reinforcement, these moments could be reduced to their value at the face of the support [A4.6.2.1.6] but it was decided to not do it to on the conservative side.

### **B.2.6. Selection of Reinforcement**

The material strengths are  $f'_c = 4000$  psi and  $f_y = 60$  ksi. Epoxy-coated reinforcement is used in the deck. The effective concrete depths for positive and negative bending will be different because of different cover requirements (see Figure B.9).

Concrete cover [Table A5.12.3-1]

Deck surfaces subject to wear            2 IN

Bottom of CIP slabs                        1 IN

Assuming #5 rebars,  $d_b = 0.625$  IN  $A_b = 0.31$  IN<sup>2</sup>

$$d_{\text{pos}} = 9 - 1 - 5/16 = 7.69 \text{ IN}$$

$$d_{\text{neg}} = 9 - 2 - 5/16 = 6.69 \text{ IN}$$

A simplified expression for the required area of steel can be developed by neglecting the compressive reinforcement in the resisting moment to give [A5.7.3.2].

$$\phi M_n = \phi A_s f_y \left( d - \frac{a}{2} \right)$$

where (B.9)

$$a = \frac{A_s f_y}{0.85 f'_c b}$$

assuming that the lever arm  $(d-a/2)$  is independent of  $A_s$ , we can replace it by  $jd$  and solve for an approximate  $A_s$ , required to resist  $\phi M_n = M_u$ .

$$A_s \approx \frac{M_u / \phi}{f_y (jd)}$$
(B.10)

If we substitute  $f_y = 60$  ksi,  $\phi = 0.9$  [A5.5.4.2.1], and assume that for lightly sections  $j = 0.92$ , a trial steel area can be expressed as

$$\text{trial } A_s \approx \frac{M_u}{49.68d}$$
(B.11)

Because it is an approximate expression, it will be necessary to verify the moment capacity of the selected reinforcement.

Maximum reinforcement [A5.7.3.3.1] is limited by the ductility requirement of  $c < 0.42d$  or  $a < 0.42 \beta_1 d$ . For our example,  $\beta_1 = 0.85$ , so

$$a \leq 0.357d$$
(B.12)

Minimum reinforcement [A5.7.3.3.2] for components containing no prestressing steel is satisfied if:

$$\rho = \frac{A_s}{(bd)} \geq 0.03 \frac{f'_c}{f_y}$$
(B.13)

For the given material properties, the minimum area of steel per unit width of slab is

$$\min A_s = \frac{0.03(4)}{60}(1)d = 0.002d \quad \text{IN}^2 / \text{IN} \quad (\text{B.14})$$

Maximum spacing of primary reinforcement [A5.10.3.2] for slab is 1.5 times the thickness of the member or 18 in. By using the structural slab thickness of 9 in,

$$S_{\max} = 1.5 \times 9 = 13.5 \quad \text{IN} \quad (\text{B.15})$$

#### Positive reinforcement

$$M_u = 9.96 \quad \text{KIPS} - \text{FT} / \text{FT}$$

$$d_{\text{pos}} = 7.69 \quad \text{IN}$$

$$\text{trial } A_s \approx \frac{M_u}{49.68d} = \frac{9.96}{49.68(7.69)} = 0.026 \quad \text{IN}^2 / \text{IN}$$

$$\min A_s = 0.002d = 0.002 \times 7.69 = 0.0154 \quad \text{IN}^2 / \text{IN}, \quad \text{ok}$$

We try #5 @ 11 IN, provided  $A_s = 0.31/11 = 0.0282 \text{ IN}^2/\text{IN}$

$$a = \frac{A_s f_y}{0.85 f_c' b} = \frac{0.0282(60)}{0.85(4)} = 0.5 \quad \text{IN}$$

check ductility

$$a \leq 0.357d = 0.357(7.69) = 2.75 \quad \text{IN}, \quad \text{ok}$$

check moment strength

$$\phi M_n = \phi A_s f_y \left( d - \frac{a}{2} \right)$$

$$\phi M_n = 0.9(0.0282)(60) \left( 7.69 - \frac{0.5}{2} \right) = 11.33 \text{ KIPS} - \text{IN} / \text{IN}$$

$$\phi M_n = 11.33 \text{ kips} - \text{FT} / \text{FT} > 10.08 \text{ kips} - \text{FT} / \text{FT}, \text{ ok}$$

For transverse bottom bars, Use #5 @ 11 IN

### Negative moment reinforcement

$$M_u = -11.51 \text{ kips} - \text{ft} / \text{ft}$$

$$d_{pos} = 6.69 \text{ in}$$

$$\text{trial } A_s \approx \frac{M_u}{49.68d} = \frac{11.51}{49.68(6.69)} = 0.0346 \text{ IN}^2 / \text{IN}$$

$$\text{min } A_s = 0.002d = 0.002 \times 7.19 = 0.0144 \text{ IN}^2 / \text{IN}, \text{ ok}$$

We try #5 @ 9 IN, provided  $A_s = 0.31/9 = 0.034 \text{ IN}^2/\text{IN}$

$$a = \frac{A_s f_y}{0.85 f'_c b} = \frac{0.0344(60)}{0.85(4)} = 0.6 \text{ IN}$$

check ductility

$$a \leq 0.357d = 0.357(6.69) = 2.39 \text{ IN}, \text{ ok}$$

check moment strength

$$\phi M_n = \phi A_s f_y \left( d - \frac{a}{2} \right)$$

$$\phi M_n = 0.9(0.0344)(60) \left( 6.69 - \frac{0.6}{2} \right) = 11.87 \text{ KIPS} - FT / FT$$

$$\phi M_n = 11.87 \text{ KIPS} - FT / FT > 11.51 \text{ KIPS} - FT / FT, \text{ ok}$$

For transverse top bars, Use #5 @ 9 IN

### Distribution Reinforcement

Secondary reinforcement is placed in the bottom of the slab to distribute wheel loads in the longitudinal direction of the bridge to the primary reinforcement in the transverse direction. The required area is a percentage of the primary positive moment reinforcement. For primary reinforcement perpendicular to traffic [A9.7.3.2]

$$percentage = \frac{220}{\sqrt{S_e}} \leq 67\% \quad (\text{B.16})$$

where  $S_e$  is the effective span length [A9.7.2.3]. For steel I-beams,  $S_e$  is the distance web to web, that is,  $S_e = 8 \text{ FT}$ , and

$$percentage = \frac{220}{\sqrt{8}} = 77\%, \text{ use } 67\%$$

$$\text{dist } A_s = 0.67(\text{pos } A_s) = 0.67(0.0282) = 0.019 \text{ in}^2/\text{in}$$

For longitudinal bottom bars, Use #4 @ 8 IN,  $A_s = 0.025 \text{ IN}^2/\text{IN}$

### Shrinkage and Temperature Reinforcement

The minimum amount of reinforcement in each direction shall be [A5.10.8.2]

$$\text{temp } A_s \geq 0.11 \frac{A_g}{f_y} \quad (\text{B.17})$$

where  $A_g$  is the gross area of the section. For the full 9 IN thickness,

$$\text{temp } A_s \geq 0.11 \frac{9}{60} = 0.0165 \text{ IN}^2 / \text{IN}$$

The primary and secondary reinforcement already selected provide more than this amount, however, for members greater than 6 IN in thickness, the shrinkage and temperature reinforcement is to be distributed equally in both faces. The maximum spacing of this reinforcement is 3 times the slab thickness or 18 in. For the top longitudinal bars,

$$\frac{1}{2}(\text{temp } A_s) = 0.00825 \text{ IN}^2 / \text{IN}$$

Use #4 @ 18 in,  $A_s = 0.0111 \text{ IN}^2 / \text{IN}$

### **B.3. Empirical Design of Concrete Deck Slabs**

Research has shown that the primary structural action of concrete deck is not flexure, but internal arching. The arching creates an internal compressive dome. Only a minimum amount of isotropic reinforcement is required for local flexural resistance and global arching effects [C9.7.2.1]

Design conditions [A9.7.2.4]

Design depth excludes the loss due to wear,  $h = 9$  in. The following conditions must be satisfied:

-Supporting components are made of steel and/or concrete	YES
-The deck is fully CIP and water cured	YES
$-6 < S_e/h = 96/9 = 10.66 < 18$	OK
-Core depth = $9 - 2 - 1 = 6$ IN $> 4$ IN	OK
-Effective length [A9.7.2.3] = 96 IN $< 162$ IN	OK
-Minimum slab depth = 7 IN $< 9$ IN	OK
-Overhang = 45 IN $\geq 5h = 45$ IN	OK
$-f'_c = 4000$ PSI (minimum value)	OK
-Deck must be made composite with the girders	YES

Reinforcement requirements [A9.7.2.5]

- Four layer of isotropic reinforcement,  $f_y \geq 60$  KSI
- Outer layers placed in direction of effective length
- Bottom layers:  $\text{Min } A_S = 0.27 \text{ IN}^2/\text{FT} = 0.0225 \text{ IN}^2/\text{IN}$ , Use #5 @ 13 IN
- Top layers:  $\text{Min } A_S = 0.18 \text{ IN}^2/\text{FT} = 0.015 \text{ IN}^2/\text{IN}$ , Use #4 @ 13 IN
- Maximum spacing = 18 IN
- Straight bars only, hooks allowed, no truss bars
- Only lap splices, no welded or mechanical splices permitted

The layout of the reinforcement according the traditional design is shown in Figure B.10 and the layout of the reinforcement according the empirical design is shown in Figure B.11.

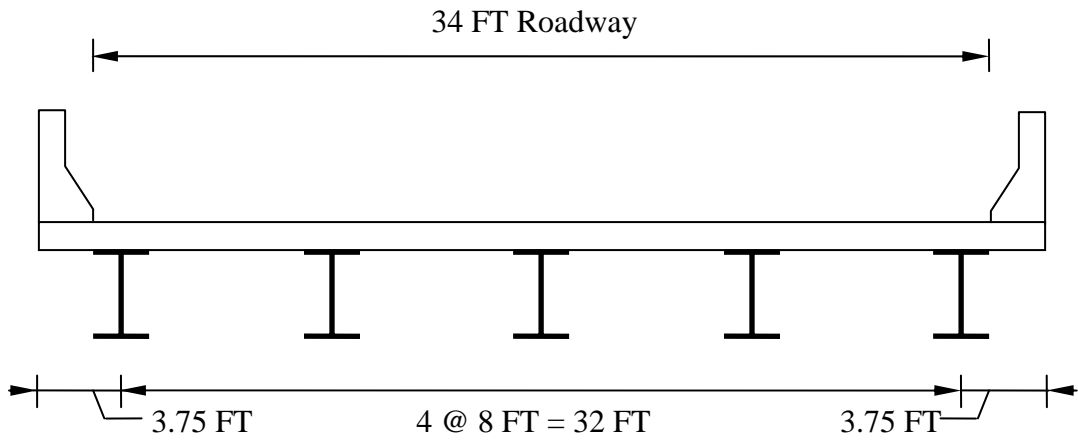


Figure B.1 Bridge deck cross section

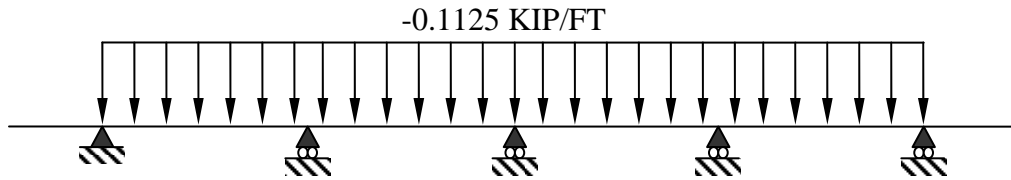


Figure B.2 Deck slab dead load

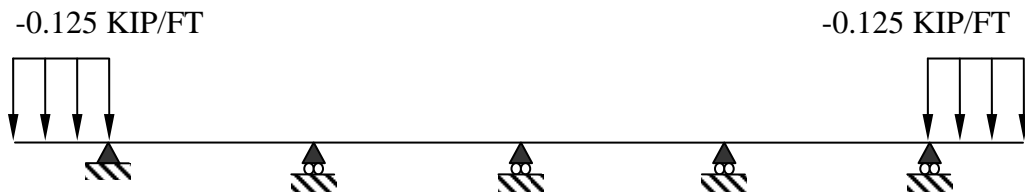


Figure B.3 Overhang dead load

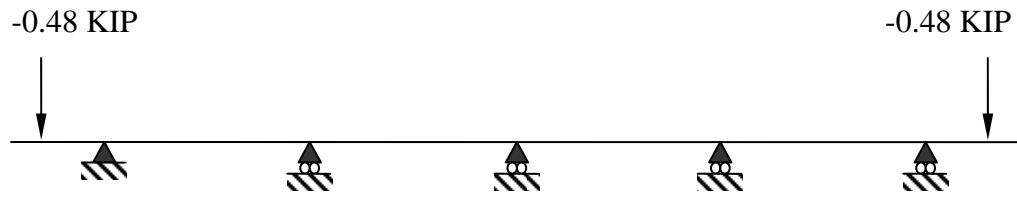


Figure B.4 Barrier dead load (15 IN from the edge of the bridge)

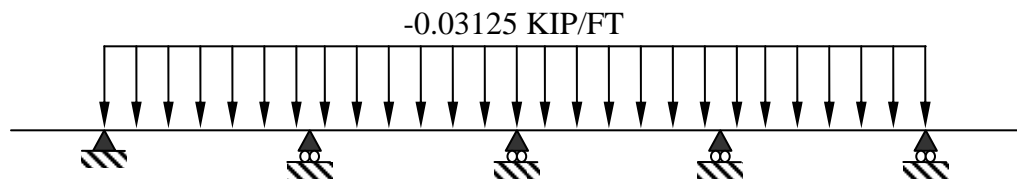


Figure B.5 Wearing surface dead load

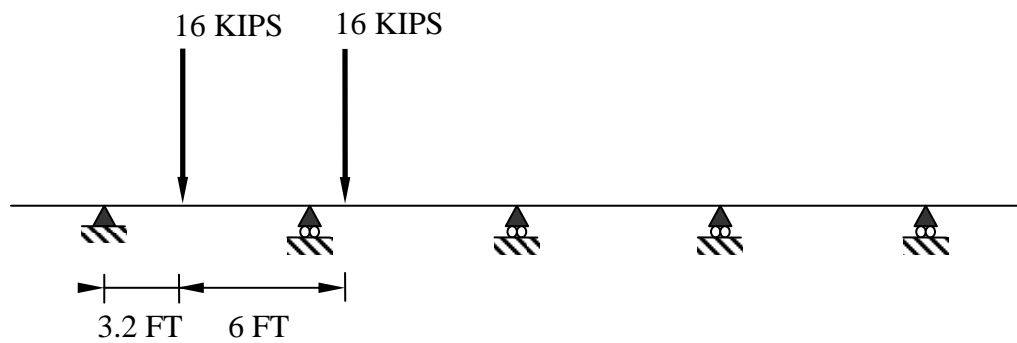


Figure B.6 Live load, maximum positive moment one lane loaded

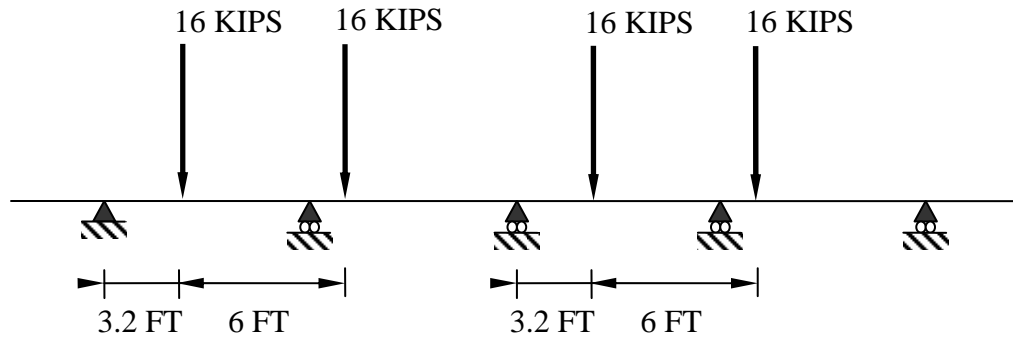


Figure B.7 Live load, maximum positive moment two lanes loaded

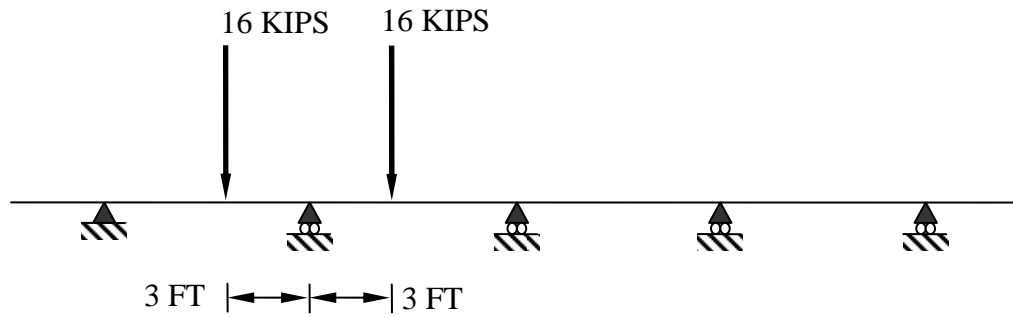


Figure B.8 Live load, maximum negative moment

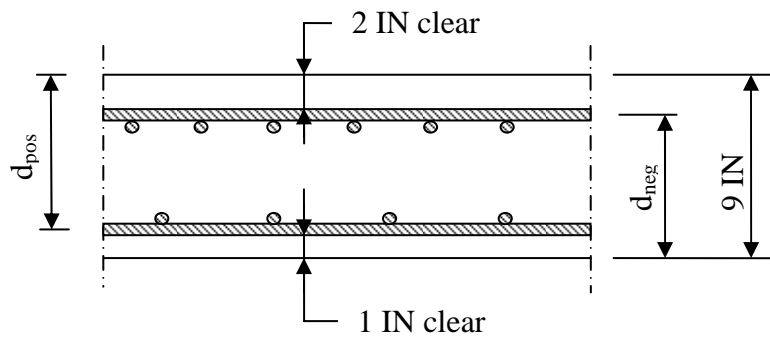


Figure B.9 Concrete cover

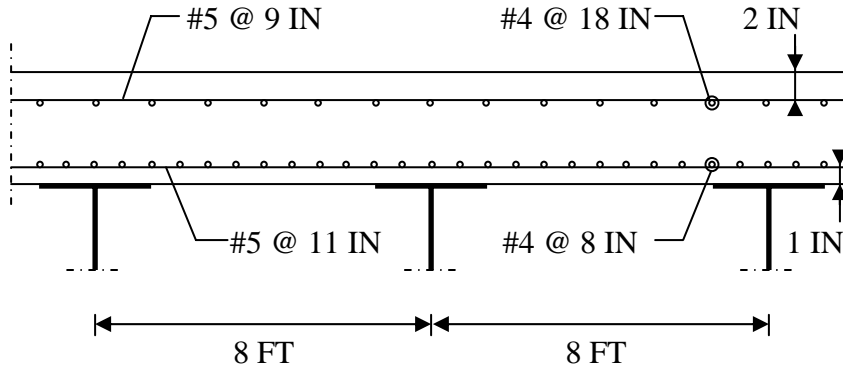


Figure B.10 Deck slab reinforcement according to the Traditional Method

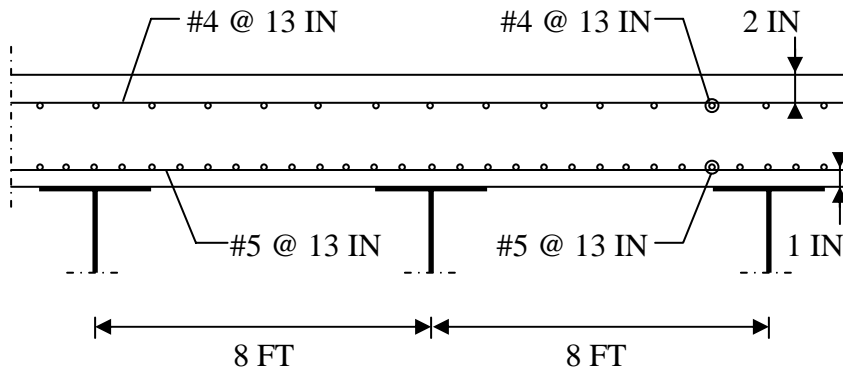


Figure B.11 Deck slab reinforcement according to the Empirical Method

## **BIBLIOGRAPHY**

## BIBLIOGRAPHY

- AASHTO *Guide Specification for Strength Evaluation of Existing Steel and Concrete Bridges*. American Association of State Highway and Transportation Officials, Washington, D.C., 1989.
- AASHTO *LRFD Bridge Design Specifications*. American Association of State Highway and Transportation Officials, Washington, D.C., 2005.
- AASHTO *Manual for Condition Evaluation of Bridges*. American Association of State Highway and Transportation Officials, Washington, D.C., 1994.
- ABAQUS *User's Manual-version 6.4.*, Hibbit, Karlsson & Sorenson, Inc., Pawtucket, Rhode Island, 1996.
- Agarwal, A.C. and Wolkowicz, M. (1976) “*Interim Report on 1975 Commercial Vehicle Survey*” Research and Development Division, Ministry of Transportation, Downsview, Ontario, Canada
- Alaylioglu H., Alaylioglu A. (1997) “*Static behavior simulation of a bridge structure by an FE-PC model.*” *Simulation Practice and Theory* Vol.5, pp. 49-63.
- Allen, J.H., (1991) “*Serviceability, and Strength of Concrete Bridge Decks*” *Transportation Research Record* 1290, Washington, D.C.
- Azizinamini, A., Kathol, S., and Beacham, M. W. (1995), “*Influence of Cross Frames on Load Resisting Capacity of Steel Girder Bridges.*” *Engineering Journal*, AISC, Vol. 33, No.2, pp. 107-116.
- Bakht, B. (1981). “*Testing of the Manitou Bridge To Determine Its Safe Load Carrying Capacity.*” *Canadian Journal of Civil Engineering*, Vol. 8, pp. 218-229.
- Bakht, B., and Jaeger, L. G. (1988). “*Bearing Restraint in Slab-on-Girder Bridges.*” *Journal of Structural Engineering*, ASCE, Vol. 114, No. 12, pp. 2724-2740.
- Bakht, B., and Jaeger, L. G. (1990). “*Bridge Testing-A Surprise Every time.*” *Journal of Structural Engineering*, ASCE, Vol. 116, No. 5, pp. 1370-1383.
- Bakht, B., and Jaeger, L.G. (1992), “*Ultimate Load Test of Slab-on-Girder Bridge.*” *Journal of Structural Engineering*, ASCE, Vol. 118, No 6, pp. 1608-1624
- Bakht, B., and Moses, F. (1988). “*Lateral Distribution Factors for Highway Bridges.*” *Journal of Structural Engineering*, ASCE, Vol. 114, No. 8, pp. 1785-1803

- Bakht, B., and Pinjarkar, S.G. (1989). “*Dynamic Testing of Highway Bridges-A Review.*” Transportation Research Record 1223, Transportation Research Board, National Research Council, Washington, D.C., pp. 93-100.
- Barker, M., Puckett, Jay A. (1997). “*Design of Highway Bridges based on AASHTO LRFD Bridge Design Specifications.*”. John Wiley & Sons, INC.
- Beal, D. B., (1982). “*Load Capacity of Concrete Bridge Decks*”. Journal of the Structural Division, Proceedings of the American Society of Civil Engineers, Vol. 108,.
- Bishara, A.G., Liu, M.C., El-Ali, N.D. (1993). “*Wheel Load Distribution on Simply Supported Skew I-Beam Composite Bridges.*” Journal of Structural Engineering, ASCE, Vol. 119, No. 2, pp. 399-419, February.
- Brozzetti, J. (2000) “*Design Development of Steel-Concrete Composite Bridges in France*”. Journal of Constructional Steel Research.
- Burdette, E.G., and Goodpasture, D.W. (1988). “*Correlation of Bridge Load Capacity Estimates with Test.*” Rep. No.306 National Cooperative Highway Research Program, Transportation Research Board, Washington, D.C.
- Burns N-H, Fang I-K and Worley, J-A. (1986). “*Behavior of Ontario-type bridges deck on steel girders*”, Center for Transportation Research, The University of Texas at Austin, Report 350-1.
- Cao, L., Allen, J. H., Shing, P. B., Woodham, D. (1996). “*Behavior of RC Bridge Decks with Flexible Girders.*” Journal of Structural Engineering.
- Cao, L., Shing, P. (1999). “*Simplified Analysis Method for Slab-on-Girder Highway Bridge Decks.*” Journal of Structural Engineering.
- CEB-FIP *Model Code, Comite Euro – International Du Beton, Design Code*, Thomas Telford 1993.
- Cornell, C.A. (1969). “*A Probability Based Structural Code.*” ACI Journal, Vol. 66, pp. 974-985.
- Csagoly, P.F., and Dorton, R.A., (1978) “*The development of the Ontario Highway Design Bridge Code*” Transportation Research Record, No. 665, pp. 1-12.
- Cussens, A.R. (1975) *Bridge Deck Analysis*. John Wiley & Sons, NY.
- Dagher, H.J., and, Hamilton, W. (1990) “*Durability of Concrete Bridge Deck with Reduced Reinforcement*” First year report, Region One University Transportation Center, Massachusetts Institute of Technology.

- Eamon, C.D. (2000). “*Reliability-Based Resistance Model for Bridge Structural Systems.*” Ph.D. dissertation, Department of Civil Engineering, University of Michigan, Ann Arbor, Michigan.
- Ebeido, T, and Kennedy, J.B. (1996). “*Girder Moments in Simply Supported Skew Composite Bridges.*” Canadian Journal of Civil Engineering, Vol. 23, pp. 904-916.
- Ellingwood, B., Galambos, T. V., MacGregor, J. G., and Cornell, C. A. (1980). *Development of a Probability Based Load Criterion for American National Standard A58.* National Bureau of Standards, NBS Special Publication 577, Washington, D.C.
- Eom J., (2001) Ph.D. *Verification of the Bridge Reliability Based on field testing.* Ph.D dissertation, Department of Civil Engineering, University of Michigan, Ann Arbor, Michigan.
- Fang I-K, Lee J-H and Chen C-R. (1994). “*Behavior of partially restrained slabs under concentrated load*”, Department of Civil Engineering, National Cheng Kung University, Taiwan, Republic of China, ACI Structural Journal, Vol. 91, No. 2.
- Fang, I.-K., Worley, J., Burns, N. H., Klingner, R. E. (1988). “*Behavior of Isotropic R/C Bridge decks on Steel Girders*”. Journal of Structural Engineering.
- Frangopol, D.M., and Goble, G.G. (1987). “*Development of a Redundancy Measure for Existing Bridges.*” Bridge Evaluation, Repair, and Rehabilitation, Ernst & Sohn, Berlin, pp. 365-376.
- Fu, C.C., Elhelbawey, M., Sahin, M.A., and Schilling, D.R. (1996). “*Lateral Distribution Factor from Bridge Field Testing.*” Journal of Structural Engineering, ASCE, Vol. 122, No. 9, pp. 2150-2168, September.
- Ghosn, M., and Moses, F. (1992). “*Evaluation of the Redundancy of Highway Bridges.*” Bridge Evaluation, Repair, and Rehabilitation, Ernst & Sohn, Berlin, pp. 581-590.
- Ghosn, M., Moses, F., and Gobieski, J. (1986). “*Evaluation of Steel Bridges Using In-Service Testing.*” Transportation Research Record 1072, Transportation Research Board, National Research Council, Washington, D.C., pp. 71-78.
- Girolami, A.G., Sozen, M.A., and Gamble, W.L., (1970) “*Flexural Strength of Reinforced Concrete Slabs with Externally Applied In-Plane Forces*” Report to the Defense Office of the Secretary of the Army and Office of Civil Defense
- Grigoriu M.D., and Soong, T.T., (1986) “*Time-Delay Linear System with Gaussian White Noise Input*” Conference on Probabilistics Mechanics and Structural Reliability, pp. 422-425
- Guyon, Y., (1962) *Prestressed Concrete*, Vol. 2, New York, John Wiley & Sons, NY.

- Hambly, E.C. *“Bridge deck Behavior”* John Wiley & Sons, NY.
- Hasofer, A.M, and Lind, N.C. (1974) *“Exact and Invariant Second-Moment Code Format”* Journal of the Engineering Mechanics Division, Vol. 100, No. 1, pp. 111-121.
- Hayes, C.O., Sessions, L.M., and Berry, A.J. (1986), *“Further Studies on Lateral Load Distribution using FEA.”* Transportation Research Record 1072, Transportation Research Board, Washington, D.C.
- Hillerborg, A., Mooder, M., and Petersson, P.E. (1976) *“Analysis of Crack Growth in Concrete by Means of Fracture Mechanics and Finite Elements”* Cement and Concrete Research, Vol. 6, pp. 773-782.
- Hognestad, E., *“A Study of Combined Bending and Axial Load in Reinforced Concrete Members”*, Bulletin 399, University of Illinois Engineering Experiment Station, Urbana, Ill., November 1951, 128 pp.
- Holowka, M., (1979) *“Testing of a Trapezoidal Box Girder Bridge”* Structural Research Report RR221, Ontario Ministry of Transportation and Communications.
- Huria, V., Lee, K., and Aktan, A.E. (1993) *“Nonlinear Finite Element Analysis of R/C Slab Bridges”* Journal of Structural Engineering, N.Y. Vol. 119, No. 1, pp. 88-108.
- Imbson, R.A., and Nutt, R.V. (1978). *“Load Distribution Study on Highway Bridges using STRUDL FEA Fatigue-Load Models for Girder Bridges.”* Journal of Structural Engineering, ASCE, Vol. 122, No. 7, pp. 726-733, July.
- Jain, C.S., and Kennedy J.B. (1974) *“Yield Criterion for Reinforced Concrete Slabs”* Journal of the Structural Division, Vol. 100, No. ST3, pp. 631-644.
- Jofriet J.C., and McNeice G.M. (1971) *“Finite Element Analysis of Reinforced Concrete Deck Slabs”* Journal of the Structural Division, Vol. 97, No. ST3, pp. 785-807.
- Kennedy, L. D. J., Baker, K. A., (1984) *“Resistance Factors for Steel Highway Bridges”*, Canadian Journal of Civil Engineering, Vol.11, No.2, pp. 324-334.
- Keogh D-L, and O’Brien E-J, *“Recommendation on the use of a 3-D grillage model for bridge deck analysis”*, Department of Civil, Structural and Environmental Engineering, Trinity College, Dublin, Ireland, Structural Engineering Review, Vol. 8, No. 4, pp.357-366.
- Kim, S. (1997). *Bridge Evaluation Based on Field Testing*. Ph.D. dissertation, Department of Civil Engineering, University of Michigan, Ann Arbor, Michigan.

- Kim, S., Sokolik, A.F., and Nowak, A.S. (1996). "*Measurement of Truck Load on Bridges in the Detroit Area.*" Transportation Research Record 1541, TRB, National Research Council, Washington, D.C., pp. 58-63.
- LabView User Manual for Windows. National Instrument Corporation, Austin, TX, 1994.
- Laman, J.A., and Nowak, A.S. (1996). "*Fatigue-Load Models for Girder Bridges.*" Journal of Structural Engineering, ASCE, Vol. 122, No. 7, pp. 726-733, July.
- Laman, Jeffrey A. (1995). *Fatigue Load Models for Girder Bridges*. Ph.D. dissertation, Department of Civil Engineering, University of Michigan, Ann Arbor, Michigan.
- Lichtenstein, A.G. (1993) "Bridge Rating Through Nondestructive Load Testing," NCHRP report No. 12-28(13)A, June
- Lublinter J., Oliver J., and Onate, E. (1989) "*A Plastic-Damage Model for Concrete*" International Journal of Solids and Structures, Vol. 25, pp. 299-329.
- Mabsout M-E, Tarhini K-M, Frederic G-R and Kesserwan A (1999). "*Effect of multilanes on wheel load distribution in steel girder bridges*" Department of Civil and Environmental Engineering, American University of Beirut, Lebanon, Journal of Bridge Engineering, Vol. 4, No. 2.
- Mabsout, M.E., Tarhini, K.M., Frederick, G.R., and Kobrosly, M. (1997) "*Influence of Sidewalks and Railings on Wheel Load Distribution in Steel Girder Bridges.*" Journal of Bridge Engineering. Vol 2, No 3, pp. 88-96.
- Mabsout, M.E., Tarhini, K.M., Frederick, G.R., and Tayar, C. (1997) "*Finite Element Analysis of Steel Girder Highway Bridges.*" Journal of Bridge Engineering. Vol 2, No 3, pp83-86.
- McDonald D. (1972). "*An experimental study of multiaxial creep in concrete*". concrete for Nuclear Reactors, ACI SP-34, Detroit, pp. 732-768.
- MDOT *Michigan Bridge Analysis Guide*. Michigan Department of Transportation, Lansing, Michigan, December 1983.
- Melchers, R.E. (1987). *Structural Reliability Analysis and Prediction*. Ellis Horwood Limited, Chichester, England.
- Mohsen, A. Issa. (1999). "*Investigation of Cracking in Concrete Bridge Decks at Early Ages.*" Journal of Bridge Engineering.
- Moses, F., and Ghosn, M., and Gobieski, J. (1985). "*Weigh-in-Motion Applied to Bridge Evaluation.*" Final Report FHWA/OH-85/012, September.

- Moses, F., and Ghosn, M. (1983). "Instrumentation for Weighing Trucks-in-Motion for Highway Bridge Loads." Final Report FHWA/OH-83/001, August.
- Moses, F., and Verma, D. (1990). *Load Capacity Evaluation of Existing Bridges*. Final Report NCHRP 12-28(1).
- Mufti, A. A., Newhook, J. P. (1999). "On the use of Steel Free Concrete Bridge decks in Continuous Span Bridges". Canadian Journal of Civil Engineer.
- Nassif, H.H. (1993). *Live Load Spectra for Girder Bridges*. Ph.D. dissertation, University of Michigan, Ann Arbor, Michigan.
- Nassif, H.H. and Nowak, A.S. (1995). "Dynamic Load Spectra for Girder Bridges." Transportation Research Record 1476, Transportation Research Board, National Research Council, Washington, D.C., pp. 69-83.
- Newmark, N.M. (1948). "Design of I-beam Bridges." Highway Bridge Floor Symposium, Journal of Structures Division, ASCE, Vol. 24, No. 2, pp. 141-161.
- Nowak A.S., (1999) "Calibration of LRFD Bridge Design Code" ational Cooperative Highway Research Program Report 12-26/1, Transportation Research Board, Washington, D.C.
- Nowak A-S and Kim S-J. (1998). *Development of a Guide for Evaluation of existing Bridges*, Part I and II, Department of Civil and Environmental Engineering, University of Michigan, MDOT Report.
- Nowak A-S, Eamon C and Szerszen M-M. (1998). *Bridge Engineering (Synthesis of planning, design, construction, maintenance, materials and research)*, Department of Civil and Environmental Engineering, University of Michigan, MDOT report.
- Nowak, A. S. (1993). *Calibration of LRFD Bridge Design Code*. Report to NCHRP 12-33, December.
- Nowak, A. S. and Tharmabala, T. (1987), "Mathematical Models for Bridge Reliability", Canadian Journal of Civil Engineering, Vol. 14, No. 2, April, pp. 152-162.
- Nowak, A.S. (1995). "Calibration of LRFD Bridge Code." Journal of Structural Engineering, ASCE, Vol. 121, No. 8, pp. 1245-1251, August.
- Nowak, A.S. and Eom, J. "Verification of Girder Distribution Factors for Existing Bridges." UMCEE 00-10, Department of Civil and Environmental Engineering, University of Michigan, Ann Arbor, MI.
- Nowak, A.S. and Kim, S. "Development of a Guide for Evaluation of Existing Bridges, Part I." UMCEE 98-12, Department of Civil and Environmental Engineering, University of Michigan, Ann Arbor, MI.

- Nowak, A.S. and Sanli, A, and Eom, J. "*Development of a Guide for Evaluation of Existing Bridges, Part II.*" UMCEE 98-13, Department of Civil and Environmental Engineering, University of Michigan, Ann Arbor, MI.
- Nowak, A.S. and Sanli, A, and Eom, J. "*Development of a Guide for Evaluation of Existing Bridges, Phase II.*" UMCEE 99-13, Department of Civil and Environmental Engineering, University of Michigan, Ann Arbor, MI.
- Nowak, A.S., and Saraf, V. K. (1996). "*Target Safety Level for Bridges.*" Proceedings of the 14th Structures Congress. Part 2. ASCE, Chicago, IL.
- Nowak, A.S., Kim, S., Laman, J.A., Saraf, V., and Sokolik, A.F. (1994). "*Truck Loads on Selected Bridges in the Detroit area*". Research Report UMCE 94-34, Dept. of Civil and Environmental Engineering, University of Michigan, Ann Arbor, Michigan.
- Nowak, A.S., Laman, J.A., and Nassif H. (1994). *Effect of Truck Loading on Bridges.* Report UMCE 94-22. Department of Civil and Environmental Engineering, University of Michigan, Ann Arbor, Michigan.
- Nowak, A.S., Nassif, H., and DeFrain, L. (1993). "*Effect of Truck Load on Bridges.*" Journal of Transpiration Engineering, ASCE, Vol. 119, No. 6, pp. 853-867.
- Nowak, A.S., Szerszen, M.M., and Ferrand, D. (2003) "*Analytical Design Procedures and Load Rating for isotropic Bridge Decks*" UMCEE 03-09, Department of Civil and Environmental Engineering, University of Michigan, Ann Arbor, MI.
- Nutt, R.V., Schamber, R.A., and Zokaie, T., (1988). "*Distribution of Wheel Loads on Highway Bridges.*" Final Rep. No.83 National Cooperative Highway Research Program Report 12-26, Transportation Research Board, Washington, D.C.
- Ockleston, A.J., (1955) "*Load Test on a Three Story Concrete Building in Johannesburg*", The Structural Engineer, Vol. 33, No. 10, pp. 304-322.
- Ockleston, A.J., (1958) "*Arching Action in Reinforced Concrete Deck Slabs*", The Structural Engineer, Vol. 36, No. 6, pp. 197-201.
- O'Connor, C., Pritchard, R.W. (1985). "*Impact Studies on Small Composite Girder Bridge.*" Journal of Structural Engineering, ASCE, Vol. 111, No. 3, pp. 641-653.
- Park, C. (1998). *Time Dependent Reliability Models for Steel Girder Bridges.* Ph.D. dissertation, Department of Civil Engineering, University of Michigan, Ann Arbor, Michigan.
- Paultre, P., Chaallal, O., and Proulx, J. (1992). "*Bridge Dynamics and Dynamic Amplification Factors-A Review of Analytical and Experimental Findings.*" Canadian Journal of Civil Engineering, Vol. 19, pp. 260-278.

- Petrou, M.F., Perdikaris, P.C., and Duan M. (1996) “*Static behavior of Noncomposite Concrete Bridge Decks Under Concentrated Loads*” Journal of Bridge Engineering, Vol. 1, No. 4, pp.143-154.
- Rackwitz, R., and Fiessler, B. (1978). “*Structural Reliability under Combined Random Load Sequences.*” Computer and Structures, Vol. 9, pp. 489-494.
- Riley, O., *Heading the Call for Better Bridge Decks: A Success Story*, ACI Seminars on Repairing Concrete Bridges, Seminar Background Materials, SCM-27 (93), Second Edition.
- Rosenblueth, E. and Esteva, L. (1981) “*Two-Point Estimates in Probabilities*” Journal of Applied Mathematical Modeling, May, pp.327-333.
- Rosenblueth, E., and Esteva, L. (1972) “*Reliability Basic for Some Mexican Codes*” ACI publication SP-31, The American Concrete Institute.
- Sanders, W.W., and Elleby, H.A. (1970). *Distributions of Wheel loads on Highway Bridges*. National Cooperative Highway Research Program Report 83, Transportation Research Board, Washington, D.C.
- Sargent, Dennis D., Ventura, Carlos E., Mufti, Aftab A., Bakht, Baidar. (1999). “*Testing of Steel-Free Bridge Decks.*” Concrete International.
- Schilling, C.G.. (1982). “*Impact Factors for Fatigue Design.*” Journal of Structural Engineering, ASCE, Vol. 108, No. 9, pp. 2034-2044.
- Schrader, E.K., *Mistakes, Misconceptions, and Controversial Issues Concerning Concrete and Concrete Repairs*, ACI Seminars on Repairing Concrete Bridges, Seminar Background Materials, SCM-27 (93), Second Edition.
- Schultz J.L., Commander B., Goble G.G., Frangpol D.M. (1995), “*Efficient Field Testing and Load Rating of Short and Medium Span Bridges,*” Structural Engineering Review, Vol. 7, No 3, pp. 181-194.
- Sebastian, W.M., and McConnel R.E. (2000) “*Nonlinear FE Analysis of Steel-Concrete Composite Structures*” Journal of Structural Engineering, Vol. 126, No. 6, pp. 662-674.
- Smith, K.N., and Mikelstein, I.Paultre, (1988). “*Load Distribution in Edge Stiffeneing Slab and Slab-on-Girder Bridge decks.*” Canadian Journal of Civil Engineering, Vol. 15, pp. 977-983.
- Stallings, J.M., and Cousins, T.E., and Stafford, T.E. (1999). “*Removal of Diaphragms from Three-Span Steel Girder Bridge.*” Journal of Bridge Engineering, ASCE, Vol. 4, No. 1, pp. 63-70, February.

- Stallings, J.M., and Yoo, C.H. (1993). “*Tests and Ratings of Short-Span Steel Bridges.*” Journal of Structural Engineering, ASCE, Vol. 119, No. 7, pp. 2150-2168, July.
- Tabsh, S.W., and Nowak, A.S. (1991). “*Reliability of Highway Girder Bridges.*” Journal of Structural Engineering, ASCE, Vol. 117, No. 8, pp. 2373-2388, August.
- Tantawi, H.M. (1986). *Ultimate Strength of Highway Girder Bridges*. Ph.D. dissertation, Department of Civil Engineering, University of Michigan, Ann Arbor, Michigan.
- Tarhini K-M and Frederic G-R. (1992). “*Wheel load distribution in I-girder Highway bridges*”, Department of Civil Engineering, Valparaiso University, USA, Journal of Civil Engineering, Vol. 118, No. 5.
- Tarhini K-M and Frederic G-R. (1995). “*Lateral load distribution in I-girder bridges*”, Department of Civil Engineering, Valparaiso University, USA, Computers & Structures, Vol. 54, No. 2, pp.351-354.
- Tarhini K-M. (1995). “*Experimental evaluation of wheel load distribution on steel I-girder bridges*”, Department of Civil Engineering, Valparaiso University, USA, 10<sup>th</sup> Conf. Eng. Mech. Boulder ASCE pp.593-596.
- Timoshenko, S., and Goodier J.N., (1970) *Theory of Elasticity*, 3<sup>rd</sup> Edition McGraw-Hill Company, Inc., New York
- Timoshenko, S., and Woinowsky-Krieger, S., (1959) *Theory of Plates and Shells*, 2<sup>nd</sup> Edition, McGraw-Hill Company, Inc., New York
- Walker, W.H. (1987), “*Lateral Load Distribution in Multi-Girder Bridges.*” Engineering Journal, First Quarter, pp. 21-28.
- Wegmuller, A.W., and Amer, H.N. (1975) “*Nonlinear Response of Composite Steel-Concrete Bridges*” Computers and Structures, Vol. 7, pp. 161-169.
- Yamani, A.S. (1992). “*Reliability Evaluation of Shear Strength in Highway Girder Bridges*” Ph.D. Dissertation, Department of Civil Engineering, University of Michigan.
- Zhang Z., Aktan A.E., (1997) “*Different Levels of Modeling for the Purpose of Bridge Evaluation*”, Applied Acoustics, Vol. 50, No 3, pp.189-204.
- Zhou, D.C., and Petrou M.F. (2004) “*Effects of Superstructure Flexibility on Strength of reinforced Concrete Bridge Decks*” Journal of Computers and Structures, Vol. 82, pp. 13-23.
- Zokaie, T., Osterkamp, T.A., and Imbsen, R.A. (1991). “*Distribution of Wheel Loads on Highway Bridges.*” National Cooperative Highway Research Program Report 12-26/1, Transportation Research Board, Washington, D.C.